10-13-2020 2:30 PM

Molecular identification and characterization of viral pathogens infecting sweet cherry

Aaron J. Simkovich, *The University of Western Ontario*

Supervisor: Wang, Aiming, *Agriculture and Agri-Food Canada*
Co-Supervisor: Kohalmi, Susanne E, *The University of Western Ontario*
A thesis submitted in partial fulfillment of the requirements for the Doctor of Philosophy degree
in Biology
© Aaron J. Simkovich 2020

Abstract

Stone fruits are a valuable crop grown worldwide, however pathogens such as viruses threaten fruit production by reducing tree health and fruit yield. In an orchard within the Niagara region of Ontario, symptoms typical of viral infection such as chlorosis and leaf deformation were seen on sweet cherry (*Prunus avium L.*) trees. Next generation sequencing was performed on symptomatic and asymptomatic leaves and four viruses were identified. On the tree displaying the most severe symptoms, *Prune dwarf virus* (PDV), was the only virus detected. A survey conducted during this work showed 42% of cherry trees on a single orchard plot are infected by PDV. The first infectious clone of PDV was developed for molecular characterization of this virus. Introduction of the infectious clone into cherry revealed PDV caused dwarfing symptoms but did not induce the foliar symptoms found on orchard grown trees. A mass spectrometry (MS)-based label-free quantitative proteomic analysis was performed to identify host proteins affected by PDV infection. The results show in PDV infected cherry many defense related proteins are upregulated, and many photosynthesis-related proteins are downregulated. In the model plant cucumber (*Cucumis sativus L*.) infected by PDV, significant accumulation changes of proteins related to translation and photosynthesis were identified using proteomics, suggesting a possible role of these proteins in the viral infection cycle of PDV. Two proteins identified through proteomic analysis of cucumber were further studied. These proteins are predicted to be important in the infection cycle of PDV as both co-localized with the viral coat protein (CP) of PDV when visualized using confocal microscopy. Finally, to further understand the intra-host spread of PDV, the movement protein (MP) of PDV was characterized. In plant cells, MP expressed alone formed tubules, a typical structure for virus movement. Additionally, domains of MP crucial for tubule formation and subcellular localization were identified. Taken together, this work advances knowledge in the molecular biology of PDV and host impact caused by PDV infection. In the long run, these findings will assist the development of novel strategies against PDV for the sustainable production of cherry and related *Prunus* fruits.

Keywords

Fruit tree virus, host factor, *Ilarvirus,* infectious clone, label free quantitation, movement protein, next generation sequencing, *Prune dwarf virus,* virus proteomics, plant virus interaction.

Summary for Lay Audience

Stone fruits such as cherries are a valuable crop grown worldwide, when they are infected by viruses, both fruit yield and quality are reduced. In severe cases, infected trees die off. Many sweet cherry trees grown on an orchard in the Niagara region show typical viral symptoms on their leaves. Sequencing of the genetic material isolated from leaves of these trees identified four viruses as possible causes of these symptoms. The strongest symptoms were associated with a virus called prune dwarf virus (PDV). All the trees of a cherry plot were analyzed and almost half were infected by PDV. To study PDV in the laboratory, a copy of this virus was made, and young cherry trees were infected to see if the same leaf symptoms occurred. PDV infection caused the cherry seedlings to grow slower and smaller than healthy seedlings, but PDV didn't cause any leaf symptoms. Another technique was used to study proteins in orchard grown cherries to see if the levels of proteins were different between sick and healthy leaves. The results suggest many proteins and their associated biological pathways are altered, that may contribute to the development of symptoms. In the laboratory, protein changes were studied in PDV infected cucumber plants which are easier to study compared to cherry plants. Some proteins were identified which are likely important in PDV infection. For example, two proteins were identified that might interact with proteins made by the virus. To understand how PDV moves in plants, the movement protein (MP) was studied. It was found that MP can make hollow tubules acting as tunnels for virus movement. Moreover, the beginning of the protein sequence was shown to be important for making tubules whereas the middle of the protein sequence was found to be essential for the MP to find its target in plant cells. We now have a better understanding of how PDV moves inside plants and what plant proteins are important for PDV infection. Protein studies also provided a list of proteins for researchers to study and in the future might be useful to breed PDV resistant plants.

Co-Authorship Statement

This thesis contains information which has been accepted for publication and the permission of use can be found in **Appendix 1**.

Simkovich A, Kohalmi SE, Wang A (2020) Ilarviruses. Encyclopedia of Virology 4th, edition, Elsevier. In press. DOI: https://doi.org/10.1016/B978-0-12-809633-8.21301-0

My contribution to this review chapter included writing the original manuscript and generation of tables and figures. Co-authors SEK and AW proof-read, provided feedback and aided in editing the manuscript before final submission to the publisher. A modified version of this chapter is used as a general introduction (**Section 1**).

Acknowledgments

I would like to express my sincere gratitude to my supervisor Dr. Aiming Wang for the unwavering encouragement, support and patience throughout my studies. I am very thankful for the excellent training I received in the lab where I learned new techniques and developed a strong work ethic and became a critical thinker. Under the guidance of Dr. Wang, I have grown in a professional sense, but have also matured as an individual. I have no doubts that skills learned in the Wang lab will help me daily for the rest of my life.

I would like to thank my co-supervisor Dr. Susanne Kohalmi for the endless support, sound advice, feedback on my written work and always making sure I had placed the horse before the cart. I must also acknowledge my committee members Dr. Christopher Brandl and Dr. Richard Gardiner for helpful feedback during my committee meetings and teaching me to use the transmission electron microscope. I must thank Dr. Mark Sumarah and Dr. Justin Renaud for the opportunity to perform my proteomics research and their mentorship. Thanks to all members of the UWO Biology department and staff at the London Research and Development Centre for providing me with excellent facilities to perform my research, and friendly people to work with.

Thanks to current and former members of the Wang lab for creating a motivational working environment, encouraging hard work. Thanks to Dr. Xiaofei Cheng for his mentorship both in and outside of the lab. Thanks to Dr. Hongguang Cui for teaching me valuable skills related to fruit tree virology. Thanks to Dr. Yinzi Li, Jamie McNeil and Brian Weselowski for making sure the lab ran smoothly every day. To current and former students: thank you for creating an enjoyable working environment.

I must thank my parents Ted and Mindy Simkovich for the infinite supply of love, support and pretending to understand exactly what I study. Lastly, I must thank my wife Dr. Sara Glazer, thank you for your love, support and being an inspiration to me.

Table of Contents

List of Tables

List of Figures

List of Appendices

List of Abbreviations

NOTE: SI units are not listed.

2Fe-2S	Rieske domain-containing protein
aa	Amino acid
ACY1	Aminoacylase-1
ADH1	Alcohol dehydrogenase 1
ADL	AMP dependent ligase
AGC	Automatic gain control
ALP	Aleurain-like protease
ALV	*Ageratum latent virus*
AMT	Aminomethyltransferase
AMV	*Alfalfa mosaic virus*
AO	L-ascorbate oxidase
APLPV	*American plum line pattern virus*
ApMV	*Apple mosaic virus*
ASNS	Asparagine synthetase
at	*Arabidopsis thaliana*
ATPsyn	ATP synthase
ATPsynβ/δ	ATP synthase beta/delta-subunit
AV-2	*Asparagus virus 2*
BCB	Blue copper binding protein
BCRSV	*Blackberry chlorotic ringspot virus*
βGluc	β-1,3-glucanase 3
βGluco	β-glucosidase 44-like
BiFC	Bimolecular fluorescence complementation
BlShV	*Blueberry shock virus*
BMV	*Brome mosaic virus*
BSA	Bovine serum albumin
BSMV	*Barley stripe mosaic virus*

BYDV	*Barley yellow dwarf virus*
CA1	Carbonic anhydrase 1
CaMV	*Cauliflower mosaic virus*
CAT	Catalase
CAT2	Catalase 2
CBG	Cyanogenic beta-glucosidase-like
CCMV	*Cowpea chlorotic mottle virus*
CdhA1	Acetyl-CoA decarbonylase/synthase complex subunit alpha 1
cDNA	Complementary DNA
CFP	Cyan fluorescent protein
CHIT	Chitinase
CHITA	Chitinase A
CHLL	Magnesium-chelatase subunit ChlI
CiLRV	*Citrus leaf rugose virus*
CMV	*Cucumber mosaic virus*
CP	Coat protein
CPm	Minor coat protein
CPMV	*Cowpea mosaic virus*
CS	Citrate synthase
CTAB	Hexadecyltrimethylammonium bromide
CTV	*Citrus tristeza virus*
CVA	*Cherry virus A*
CVV	*Citrus variegation virus*
CVYV	*Cucumber vein yellowing virus*
d35s	Double 35s promoters derived from *Cauliflower mosaic virus*
DEPC	Diethyl pyrocarbonate
DIR1	Bifunctional inhibitor/lipid-transfer /seed-storage 2S albumin protein
DLST	Dihydrolipoamide succinyltransferase
DMSO	Dimethyl sulfoxide

DNA	Deoxy ribonucleic acid
dpa	Days post agroinfiltration
dpi	Days post inoculation
ds	Double stranded
DTT	Dithiothreitol
DUF247	Plant protein of unknown function
ECPP44	Phosphoprotein ECPP44
EDTA	Ethylene diamine tetracetic acid
eEF1B	Eukaryotic translation elongation factor 1B
eEF1D	Eukaryotic translation elongation factor D1
eEFG2	Eukaryotic translation elongation factor G2
Ef-Tu	Eukaryotic translation elongation factor Tu
eIF	Eukaryotic translation initiation factor
eIF(iso)4E	Eukaryotic elongation initiation factor 4 subunit E isoform
eIF(iso)4G	Eukaryotic elongation initiation factor 4 subunit G isoform
eIF2C	Eukaryotic translation initiation factor 2c
eIF4F	Eukaryotic initiation factor 4 subunit F
eIF4G	Eukaryotic translation initiation factor 4 subunit G
ELISA	Enzyme linked immunosorbent assay
EM	Electron microscopy
EMoV	*Elm mottle virus*
ER	Endoplasmic reticulum
FCiLV	*Fragaria chiloensis latent virus*
FDR	False discovery rate
FTSHI5	Inactive ATP-dependent zinc metalloprotease FTSHI 5
GDR	Genome database for *Rosaceae*
GLU	Beta-1,3-glucanase 3
GLXI	Lactoylglutathione lyase/glyoxalase I
GO	Gene ontology

GST	Glutathione S-transferase
HB1	Hemoglobin 1
Hel	Helicase
HJLV	*Humulus japonicus latent virus*
HK1	Histidine kinase 1
HMA	Heavy metal associated domain-containing protein
HMGCS1	3-hydroxy-3-methylglutaryl coenzyme A synthase
hpa	Hours post agroinfiltration
hpt	Hours post transfection
HR	Hypersensitive response
HSP	Heat shock protein
HSP70	Heat shock protein 70
HSP90β1	Heat shock protein 90kDa β member 1
iBAQ	Intensity-based absolute quantification
IT	Injection time
ITHF	Inhibitor of trypsin and Hageman factor
LCD	Little cherry disease
LChV1	*Little cherry virus 1*
LChV2	*Little cherry virus 2*
LFQ	Label-free quantitative/quantification
LHC6	Photosystem I light harvesting complex subunit 6
LHCB	Chlorophyll A/B binding protein 1
LiRMoV	*Lilac ring mottle virus*
LLCV	*Lilac leaf chlorosis virus*
MCF	Mitochondrial substrate carrier family protein C
MDMV	*Maize dwarf mosaic virus*
MES	Morpholinoethanesulfonic acid
Met	Methyltransferase
miRNA	Micro RNA

MLP	Major latex protein
MP	Movement protein
NAD	Nicotinamide adenine dinucleotide
NAD-ME	NAD-dependent malic enzymes
NADP	Nicotinamide adenine dinucleotide phosphate
NADP-ME	NADP-dependent malic enzymes
nb	*Nicotiana benthamiana*
NEP1	Nepenthesin-1
NGS	Next generation sequencing
NHLRC2	NHL repeat-containing protein 2 isoform X1
NOST	Nopaline synthase terminator
NRX1	Nucleoredoxin1
nt	Nucleotide
OD_{600}	Optical density measured at a wavelength of 600 nanometers
OEC	Oxygen evolving complex
OGDH	2-oxoglutarate dehydrogenase
ORF	Open reading frame
OSM34	Osmotin 34
P1	First protein of PDV containing Met and Hel domains
P2	RdRp of PDV
PAG1	20S proteasome subunit G1
PCA	Principal component analysis
PCR	Polymerase chain reaction
PD	Plasmodesmata
PDI	Protein disulfide isomerase
PDLPV	Plasmodesmata localization protein V
PDV	*Prune dwarf virus*
PITP	Phosphatidylglycerol/phosphatidylinositol transfer protein DDB
PLS	Plasmodesmata localization signal

PME3	Pectin methylesterase 3
PMMoV	*Pepper mild mottle virus*
PMoV	*Parietaria mottle virus*
PNRSV	*Prunus necrotic ringspot virus*
poly-A	Polyadenylated
PPI	Peptidyl-prolyl cis-trans isomerase 1
PPV	*Plum pox virus*
PR1	Basic pathogenesis related protein 1
Prot	Protease
PrRSV	*Privet ringspot virus*
PRSV-W	*Papaya ring spot mosaic virus-W*
PRX1	Peroxidase 1
PsbC	Photosystem II reaction center protein C
PsbP	Photosystem II reaction center protein P
PTGS	Post transcriptional gene silencing
PVP-40	Polyvinylpyrrolidone molecular weight 40
PVX	*Potato virus X*
PVY	*Potato virus Y*
PYMV	*Pepper yellow mosaic virus*
PYROXD	Pyridine nucleotide-disulphide oxidoreductase
RACE	Rapid amplification of cDNA ends
Raf1	RuBisCO accumulation factor 1
RBCA	RuBisCO activase
RBCA2	RuBisCO activase isoform X2
RBD	RNA binding domain
RdRp	RNA dependent RNA polymerase
Rep	Replicase
RF	Radio frequency
RGEN	RNA guided endonuclease

RH3	DEAD box RNA helicase 3
RHON1	rho-N domain-containing protein 1
RNA	Ribonucleic acid
RNA(-)	Negative (antisense) stranded RNA
RNA(+)	Positive (sense) stranded RNA
RNAse	Ribonuclease
RNC1	Ribonuclease III domain-containing protein
RNP	Ribonucleoprotein complex
ROS	Reactive oxygen species
RPL4	50S ribosomal protein L4
RPS7	Ribosomal S7 domain-containing protein
RSS	RNA silencing suppressor
RTLNB2	Reticulon-like protein B2
RT-PCR	Reverse transcription PCR
RuBisCO	Ribulose bisphosphate carboxylase
RuBisCO_SC	RuBisCO small chain
RuBisCOlα/β	RuBisCO large subunit binding protein α/β
RYMV	*Rice yellow mottle virus*
RZ	Hammerhead ribozyme derived from TRSV
SAR	Systemic acquired resistance
SCMV	*Sugarcane mosaic virus*
SEL	Size exclusion limit
sgRNA	Sub-genomic RNA
siRNA	Small interfering RNA
SNSV	*Strawberry necrotic shock virus*
SPFMV	*Sweet potato feathery mottle virus*
SpLV	*Spinach latent virus*
sRNA	Small RNA
ssRNA	Single stranded RNA

SUCLA	Succinate co-enzyme A ligase
SUFE1	sufE-like protein 1
SYNV	*Sonchus yellow net virus*
TAMV	*Tulare apple mosaic virus*
TBSV	*Tomato bushy stunt virus*
TCTP1	Translationally-controlled tumor protein 1
T-DNA	Transfer DNA
TGBp1	Triple gene block protein 1
TLP	Thaumatin superfamily protein
TLS	Transfer RNA-like structures
TMV	*Tobacco mosaic virus*
TomNSV	*Tomato necrotic streak virus*
TRSV	*Tobacco ringspot virus*
TRZ2	tRNAse Z
TSPAN8	Tetraspanin 8
TSV	*Tobacco streak virus*
TuMV	*Turnip mosaic virus*
UPRT	Uracil phosphoribosyltransferase
USP	Universal stress protein
UTR	Untranslated region
vATPsynC	Vacuolar ATP synthase subunit C
VIGS	Virus induced gene silencing
VLN2	Villin-2
VPg	Genome linked protein
VRC	Virus replication complex
vRNA	Viral RNA
WD40	Topless-like WD40 repeat containing protein
YFP	Yellow fluorescent protein
ZYMV	*Zucchini yellow mosaic virus*

1.   Introduction

1.1   Stone fruits in Canada

A stone fruit is an edible fruit (drupe) consisting of a soft fleshy layer (mesocarp) with a thin skin (exocarp). This drupe surrounds a hardened layer (the endocarp) which in turn protects the contained seed. The hardened endocarp is commonly described as a stone, giving this type of fruit its name (**Figure 1A**). Stone fruits are a valuable crop in Canada, with recent annual farm gate value estimates of $155 million (Statistics-Canada, 2018). The true value of this crop is likely much higher, as stone fruits are not only sold as fresh produce but are also sold as processed goods such as jams, preserves, health products, juices and alcoholic beverages (Taylor, 1996). Employment opportunities in fruit production, harvest and processing adds to the economic importance of stone fruits. One of the greatest economic problems for growers of stone fruits is the dilemma of delayed return of initial investment. This is due to the long perennial life cycle of stone fruit trees, which must grow for several years before a marketable harvest is obtained. For example, the average orchard of sweet cherry (*Prunus avium* L.) requires eight years of maintenance before being productive, and a total of fifteen years of production to recover initial costs (Seavert and Long, 2007). To balance the large initial investment and delay of harvest after initial planting, maintenance of orchards for 15-30 years or longer is not uncommon (**Figure 1B**; Fridlund, 1963). The extended period over which trees are maintained allows for many opportunities for pathogens, such as viruses, to attack and infect these trees (Németh, 1986; Pallas et al., 2012). Plant viruses are an important agricultural pathogen and conservatively estimated to account for half of known crop diseases, leading to widespread yield losses in food and forage crops (Wei et al., 2010; Schreinemachers et al., 2015; Bernardo et al., 2018). Viruses impact the fruit tree industry in several important ways including yield reduction, graft incompatibilities, and death of planted trees (Hadidi et al., 2011). Once viral infection is established and identified, the most common practice is removal and destruction of infected trees due to a limited number of less invasive options for virus infection management. Currently, the most successful antiviral strategies are those focusing on prevention and early detection.

Figure 1 Cherry grown in Ontario

Cherry is an important stone fruit crop grown on cherry, due to its extended life cycle, cherry can be infected by a variety of agriculturally important pathogens.

A   A cross-section of a drupe from cherry.

i The exocarp is a thin skin surrounding the drupe.

ii The mesocarp is the thick fleshy layer of the drupe.

iii The hard endocarp resembles a stone is surrounded by the mesocarp.

iv The seed is surrounded by the hard endocarp.

B   A healthy cherry tree (planted in 1985) currently grown on a research farm in Jordan, Ontario.

C   A healthy, asymptomatic leaf from cherry showing an even distribution of green colouring, absence of damage or other deformations.

D, E, F Symptomatic leaves from cherry showing symptoms commonly associated with viral infection including chlorosis (yellowing) and uneven distribution of green colouring (**D**), vein suturing (sunken veins; **E**), cupping (upward curling of leaf edges; **E**) and ring spotting (**D,F**).
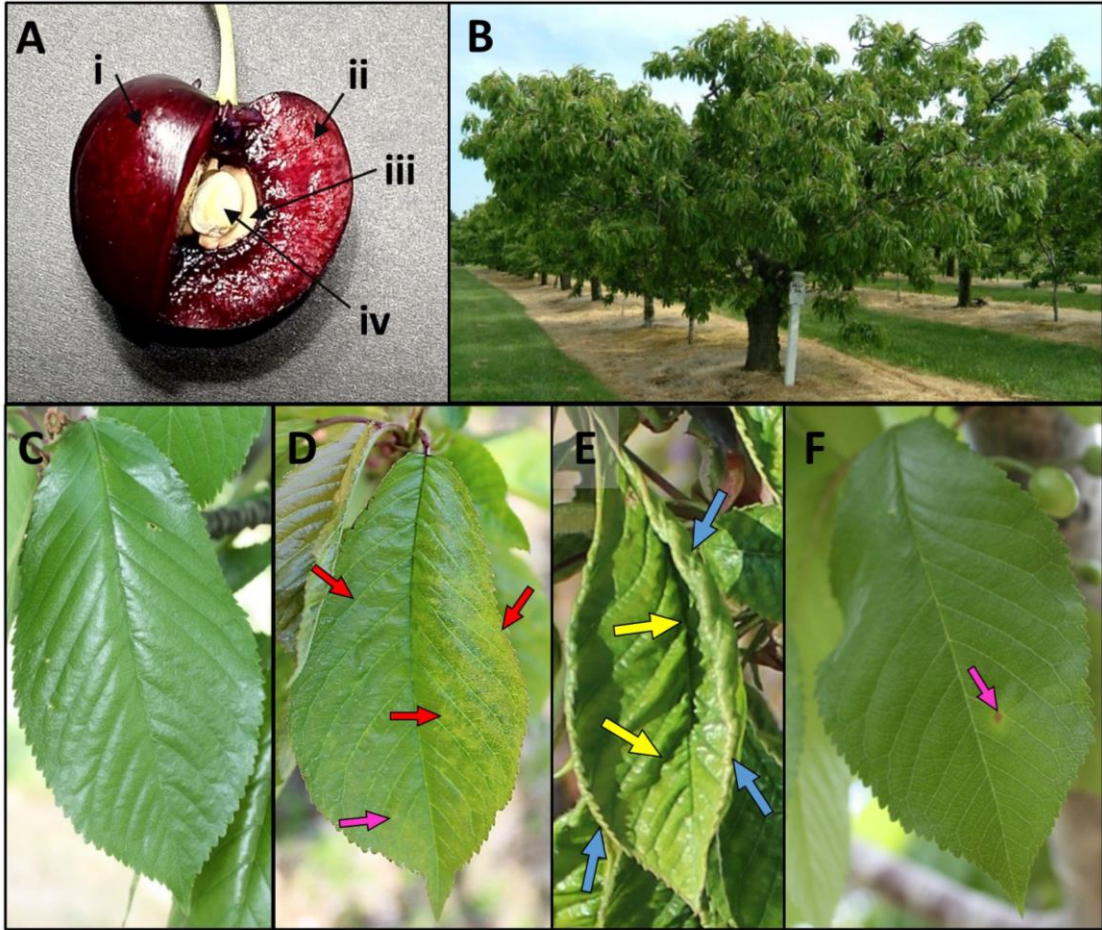
Chlorosis → Vein suturing → Leaf cupping → Ringspot

1.2   Positive-sense plant RNA viruses

Plant viruses are infectious, intracellular, obligate parasites which recruit host cellular machinery (host factors) for replication of their own genome and translation of viral proteins (Sanfaçon, 2015). The viral genome is comprised of either DNA or RNA and is enveloped by either oligomerized viral encoded coat protein(s) (CP) or a membranous structure (Lucas, 2010). The largest group of viruses infecting plants are those with genomes comprised of single-stranded positive-sense RNA (ssRNA(+) ; Pallas and García, 2011). Of the ten viruses with the greatest impact on the global food supply, six are of the ssRNA(+) group, including *Barley yellow dwarf virus* (BYDV), *Cucumber mosaic virus* (CMV), *Maize dwarf mosaic virus* (MDMV), *Sugarcane mosaic virus* (SCMV), *Rice yellow mottle virus* (RYMV) and *Sweet potato feathery mottle* (SPFMV) (Rybicki, 2015). Genomes of ssRNA(+) viruses are relatively small, often between 4 and 17 KB (Sanfaçon, 2005). Due to their small genome size, protein encoding capacity is limited. However, the following viral proteins are typically encoded:

1) An RNA-dependent RNA polymerase (RdRp) required for genome replication.
2) A movement protein (MP) to facilitate intercellular spread of the virus.
3) A structural CP to envelope the viral genome.

A plant virus must overcome many obstacles to establish a compatible infection. Plant cells are surrounded by rigid cell walls which the invading virus must penetrate through to initiate infection (Wu et al., 2019). Herbivorous insects and human activities are common vectors which facilitate virus entry by wounding (**Section 1.4.1**; Barba et al., 2015; Kaiser et al., 1982). Once inside the host cell, viral proteins are translated using host cellular machinery which is described in detail below (**Section 1.4.2**; Sanfaçon, 2015). In addition to acting as a template for translation of viral proteins, viral ssRNA(+) also serves as a template for replication of the viral genome (**Section 1.4.2**). Viral protein translation and RNA replication are tightly regulated and often occur simultaneously (Wang, 2015). After replication, the virus moves to adjacent cells through the plasmodesmata (PD), gated channels connecting adjacent plant cells (Heinlein, 2015). Eventually, to facilitate long distance or systemic movement, the virus enters the phloem and travels through the

vascular tissues throughout the host plant (Carrington et al., 1996; Seo and Kim, 2016).

1.3 Prune dwarf virus

1.3.1 Classification

The species *Prune dwarf virus* is a member of the *Ilarvirus* genus which along with five other genera including *Alfamo-, Anulav-, Bromo-, Cucumo-* and *Oleaviruses*, belongs to the family *Bromoviridae* (Bujarski et al., 2019). Ilarviruses are most closely related to the single member of the *Alfamovirus* genus, *Alfalfa mosaic virus* (AMV). The name "ilarvirus" is in fact a siglum derived from **i**sometric **la**bile **r**ingspot viruses, describing several characteristics of ilarviruses: the isometric shape of virions, the fragility or labile nature of viral particles and lastly, the frequently observed ring spotting symptom on some infected hosts (Bujarski et al., 2019). Currently, the genus *Ilarvirus* consists of 22 recognized members that are further classified into four subgroups based on available sequence data and serological properties determined with antibodies against the CP (**Table 1**).

1.3.2 Host range, disease symptoms and economic importance

The natural host range of PDV is mostly limited to woody fruit trees such as members of the *Prunus* genus: sweet cherry, sour cherry (*Prunus cerasus* L.), peach (*Prunus persica* L.), almond (*Prunus dulcis* L.), and plum (*Prunus domestica* L). PDV also infects commonly traded ornamental plants of various genera such as flowering plum (*Prunus mume* L.), east Asian cherry (*Prunus serrulata* L.) and lilac (*Syringa yunnanensis* L.) (Caglayan et al., 2011). Herbaceous plants including cucumber (*Cucumis sativus* L.), squash (*Cucurbita maxima* L.) and tobacco (*Nicotiana benthamiana* L.) are all readily infected by PDV and are often used as herbaceous hosts. Symptoms caused by infection with PDV vary and are influenced by many factors such as host species and cultivars, plant age and virus isolates (Cui et al., 2013; Fulton, 1959, 1982; Kamenova et al., 2019; Ozturk and Cevik, 2015). A common symptom of PDV infection is the smaller stature (stunting or

Table 1 Currently recognized members of the *Ilarvirus* genus

Subgroup	Species	Abbreviation
Subgroup 1	*Ageratum latent virus*	ALV
	Parietaria mottle virus	PMoV
	Blackberry chlorotic ringspot virus	BCRSV
	Privet ringspot virus	PrRSV
	Strawberry necrotic shock virus	SNSV
	Tobacco streak virus	TSV
Subgroup 2	*Asparagus virus 2*	AV-2
	Citrus leaf rugose virus	CiLRV
	Citrus variegation virus	CVV
	Elm mottle virus	EMoV
	Lilac ring mottle virus	LiRMoV
	Spinach latent virus	SpLV
	Tomato necrotic streak virus	TomNSV
	Tulare apple mosaic virus	TAMV
Subgroup 3	*Apple mosaic virus*	ApMV
	Blueberry shock virus	BlShV
	Lilac leaf chlorosis virus	LLCV
	Prunus necrotic ringspot virus	PNRSV
Subgroup 4	*Fragaria chiloensis latent virus*	FCiLV
	Prune dwarf virus	PDV
Unassigned	*Humulus japonicus latent virus*	HJLV
	American plum line pattern virus	APLPV

dwarfing) which is a consequence of reduced growth and vigor (Gilmer et al., 1976). Additionally, various foliar symptoms are associated with this virus. Narrowed leaves or those appearing cup shaped are sometimes found in PDV infected trees. Clearing (absence of colour), or chlorosis (yellowing) of leaf veins is also associated with PDV (Gilmer et al., 1976). Another symptom found on the leaves of PDV infected trees is the formation of a deep groove following the veins of a leaf, termed deep suturing (Millikan, 1955; Németh, 1986; Pallas et al., 2012, 2013). General foliar chlorosis is also associated with PDV. The disease "sour cherry yellows" describes foliar chlorosis found on *P. cerasus* infected with a particularly severe isolate of PDV (Gilmer et al., 1976).

Known as one of the most damaging and widespread ilarviruses, PDV is distributed globally and found wherever *Prunus* spp. are cultivated (Martelli and Savino, 2008). Infection by PDV impacts several growing industries in a variety of ways. In the trade of ornamental plants for example, stunted, deformed plants are unmarketable contributing to revenue losses (Németh et al., 2010). During plant propagation, infection by PDV is associated with decreased grafting success and use of infected rootstocks or scions has been documented to cause a failure rate greater than 50% (Németh, 1986). In plum, PDV infection was associated with drastic reductions in vegetative growth of trees including shoot length and diameter reduction by 40% and 35%, respectively (Németh, 1986). The fresh fruit industry is also affected. PDV infection causes yield losses, with reports ranging from 37% to total losses (Topchiiska, 1982; Way and Gilmer, 1963). In addition to yield loss, the quality of fruit is also deteriorated in some hosts. One example of this is in cherry cv. Bing, where PDV infected trees often does not suffer severe yield losses, however fruit from these infected trees are more susceptible to rain splitting, resulting in unmarketable fruit (Proebsting et al., 1995).

1.3.3 Virion and genome structure

Virions of PDV are most commonly found as quasi-isometric shapes comprised of 180 CP units, ranging in diameter from 26-35 nm (Kozieł et al., 2017a). Each viral RNA fragment is separately encapsulated as a virion and the size and shape are influenced by

the amount of contained vRNA, as a result, PDV also produces bacilliform particles with a diameter of 18-26 nm and length of 30-85 nm (Kozieł et al., 2017a; Pallas et al., 2013). Like all other ilarviruses, PDV has a tripartite genome consisting of three separate ssRNA(+) molecules, all having a 5' 7-methyl-G (m^{7}G) capped untranslated region (UTR) and has a 3' UTR which lacks a polyadenylated (poly-A) tail (**Figure 2**; Pallas et al., 2012, 2013). The 3' ends of these genomic RNAs contain repeats which are predicted to form complex secondary structures involved in replication and translation (Bol, 2005; Reusken and Bol, 1996). Among the three genomic RNAs, RNA1 is the largest genomic RNA containing a single open reading frame (ORF), ORF1, which encodes the P1 or replicase protein. P1 has a methyltransferase (Met) domain near the N-terminus, a helicase (Hel) domain near the C-terminus and a putative transmembrane domain at the C-terminus. It has been suggested that P1 recruits and anchors vRNA to the assembly site to support viral replication (Bol, 2005; Kozieł et al., 2017a; Pallas et al., 2013). Visualization by electron microscopy (EM) shows that P1 is associated with the vacuolar membrane, supporting its functional role in membrane anchoring (Kozieł et al., 2017b). The second largest genomic RNA, RNA2, contains ORF2a which encodes the P2 protein or RdRp. P2 consists of several conserved domains typically found in RdRps, such as the RNA binding domain and the triple residue GDD motif (Kozieł et al., 2017a). The presence of the RdRp domain suggests that P2, similar to P1 is part of the viral replication complex (VRC) and is responsible for the synthesis of vRNA (Pallas et al., 2012). RNA1 is monocistronic, only encoding P1. In most ilarviruses, RNA2 encodes a single protein (P2), however some members encode a second protein known as 2b. In contrast, RNA3, is bi-cistronic, containing ORF3a and ORF3b. Like ORF1 and and ORF2a, ORF3a encodes the MP which is directly translated from RNA3. A putative sub-genomic (sg) promoter region downstream of ORF3a allows for the transcription of a sgRNA fragment, sgRNA4 encoding ORF3b from which the CP is translated (Pallas et al., 2013). The CP is a multifunctional protein and plays essential roles at different stages of the virus infection cycle. During replication, the CP has been found in close proximity to P1 and P2 at the VRC (Kozieł et al., 2017b). Furthermore, the CP is involved in the intercellular movement of PDV by either forming

mature virions or as part of a viral ribonucleoprotein complex (RNP) (Kozieł et al., 2017a,b).

1.4   The infection cycle of PDV

1.4.1   Entry into the host

The infection cycle of PDV has not been studied extensively. Based on currently available knowledge, this cycle can be divided into several stages (**Figure 3**). First, PDV enters the host cell via mechanical damage to the cell wall which can be caused by many factors such as a herbivorous insect (**Figure 3A**; Card et al., 2007; Dijkstra and de Jager, 1998; Pallas et al., 2012). Common horticultural practices may also facilitate PDV infection, for example, when using grafting for fruit tree propagation, the grafting of PDV infected rootstocks to uninfected scions will likely result in systemic infection as PDV can move with photosynthates through the phloem to new developing leaves and meristematic tissues (Kozieł et al., 2017a). Upon entry into host cells, the shell (or capsid) protecting viral RNA (vRNA) comprised of CP subunits is removed in the process of decoating (**Figure 3B**), which exposes the viral genome allowing for viral translation to occur (Wang, 2015).

Initially, it was suspected that *Brome mosaic virus* (BMV), of the *Bromovirus* genus in the *Bromoviridae* used a swelling mechanism to initiate decoating (Zulauf, 1977). It appeared that virions of BMV would swell when suspended in solutions with a pH greater than 7.0 (Zulauf, 1977). This swelling was initially concluded to be a prerequisite for uncoating, until Albert *et al* (1997) showed that swelling was not needed for disassembly. The same work showed during pH change, the virion structure of *Cowpea chlorotic mottle virus* (CCMV; another member of the *Bromovirus*) is altered and forms a channel like structure for vRNA to exit, gaining exposure to host factors (Albert et al., 1997). Recent work on BMV showed a basic pH resulted in a cleavage of BMV virions into a nearly intact virion which leads part of the vRNA being exposed while the majority of vRNA is protected by CP subunits before the initiation of translation (Bond et al., 2020). The exposed vRNA serves as template for viral protein translation (**Section 1.4.2**)

Figure 2 General ilarvirus genome structure

A diagram showing the typical genome structure of ilarviruses . In some members, a second protein is encoded by a second ORF in RNA2 (Pallas et al., 2013). Every genomic ssRNA(+) fragment is shown with approximate lengths in parentheses. Encoded proteins are shown as gray boxes. All RNA fragments have putative m^7G cap structures at the 5' UTR, and each 3' UTR is predicted to adopt complex secondary structures. RNA 1 encodes the P1 protein which has Met and Hel domains which are essential for viral replication. RNA 2 encodes the RdRp (P2). RNA 3 directly encodes the MP. The fourth RNA fragment, sgRNA4 is transcribed from a promoter region in RNA 3 downstream of ORF3a, this fragment encodes the viral CP.

m^7G: 5'-7-methyl-G cap; ᒥᒪᒪᒪ: 3' UTR secondary structure; aa: amino acids; bp: base pair; P1: replicase protein; P2: RNA dependent RNA polymerase (RdRp); MP: movement protein; CP : coat protein.

RNA 1 (~3.3 KB) 5' m⁷G — ORF 1 / P1 (Rep; ~1000aa) — 3'

RNA 2 (~2.5 KB) 5' m⁷G — ORF 2a / P2 (RdRp; ~800aa) — ORF 2b / 2b — 3'

RNA 3 (~2.2 KB) 5' m⁷G — ORF 3a / MP (~300aa) — 3'

sgRNA 4 (~1 KB) 5' m⁷G — ORF 3b / CP (~200 aa) — 3'
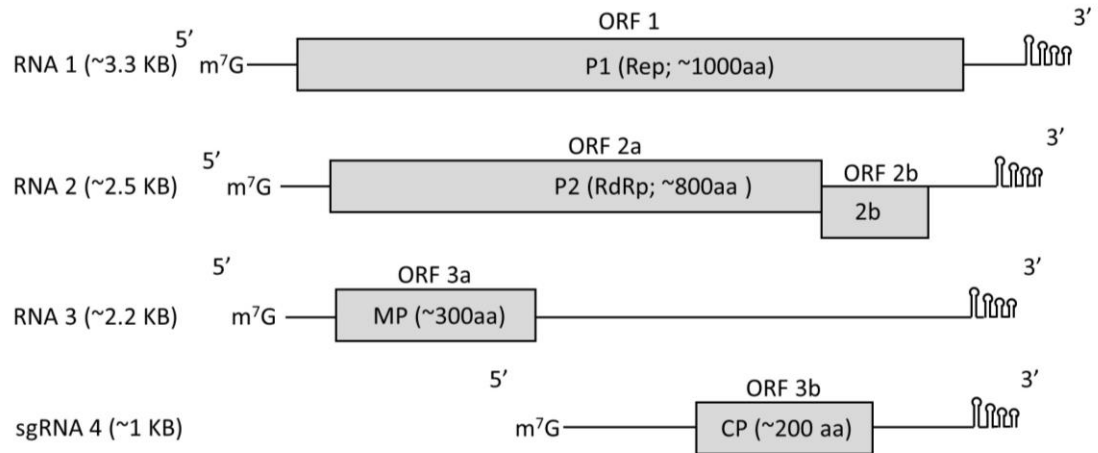
1.4.2   PDV replication and translation

Once the vRNA is exposed, host translational machinery is recruited for viral protein translation where proteins required for replication are translated first, like many other viruses, this occurs at the endoplasmic reticulum (ER) where small PDV induced invaginations have been visualized by EM (**Figure 3C, E, F**; Kozieł et al., 2017b; Sanfaçon, 2005). Upon viral protein translation, viral factors including viral RdRp and viral RNA (vRNA) together with recruited host proteins (host factors) form VRCs which are often anchored at organelle membranes and catalyze viral genome replication (Pallas and García, 2011; Sanfaçon, 2005).

EM studies suggest that viral proteins associated with PDV replication include P1, P2 and CP as they co-localize and induce small invaginations in membranes of the ER, chloroplasts and vacuole, forming small vesicular structures where VRCs are likely assembled (**Figure 3C , E, F**; Kozieł et al., 2017b; Pallas et al., 2013). Based on studies on AMV, the VRC catalyzes the synthesis of the minus (-) strand RNA using the viral genomic RNA as a template, and further replicates the (+) strand RNA using the newly synthesized (-) RNA as a template (Bol, 2005). However, biosynthesis of (+) and (-) RNA proceeds in an asymmetrical manner as (+) RNA accumulates to a higher degree than (-) RNA, often in a ratio of 100:1 (Bol, 2005; Tao and Ye, 2010). After transcription, progeny (+) RNAs are then bound by CP, this binding likely prevents the RdRp from using this (+) RNA strand as template for (-) RNA synthesis, explaining the asymmetrical replication as the RdRp binds to (-) RNA for further genome replication (Sztuba-Solińska and Bujarski, 2008).

Most members of the *Bromoviridae* possess transfer RNA-like structures (TLS) in the 3' UTR of their genomic RNAs (Bol, 2005). These TLS regions interact with the m^7G cap to circularize the vRNA and promote the translation process (**Figure 3C**; Choi et al., 2002; Dreher et al., 1984; Guogas et al., 2004). Interestingly, both alfamo- and ilarviruses lack TLS, and CP is required to establish infection possibly by interacting with host translation machinery and regulating transcription of new (+)/(-) vRNA. The requirement of CP and

Figure 3 Model of the PDV infection cycle

The PDV infection cycle has not been studied in detail, however it is likely similar to members of *Ilar-* and *Alfamovirus* genera (Bol, 2005; Kozieł et al., 2017a; Pallas et al., 2013).

A   PDV enters the host cell via mechanical damage or horticultural practices such as grafting.

B   The removal of the CP (decoating) results in the exposure of vRNA to host factors.

C   Viral proteins are translated on the rough endoplasmic reticulum by host factors.

D   After translation, viral proteins localize to organelle membranes such as the tonoplast (**E**) and chloroplast (**F**) (Kozieł et al., 2017b).

G   After replication vRNA, MP and CP of PDV likely assembles as a virion (**H**) or RNP (**I**).

J   PDV intercellular movement occurs through tubular structures which span modified host PD.

K   Some viruses with MPs of the 30K superfamily (such as TMV) can dilate host PD allowing for virus transport between adjacent cells (Melcher, 2000).

L   A representative PD which has not been altered by a viral MP (dilation, or tubule formation).

Infected Cell

Neighbouring Cell

A

B

Vacuole

E

C

D

Endoplasmic
reticulum

Nucleus

Chloroplast

F

Progeny
vRNA

G

Assembly

H

I

MP
Tubule

J

Dilated PD

K

PD

Desmotubule

L

virion   vRNA   CP   host factors   P1   P2   MP   VRC   RNP
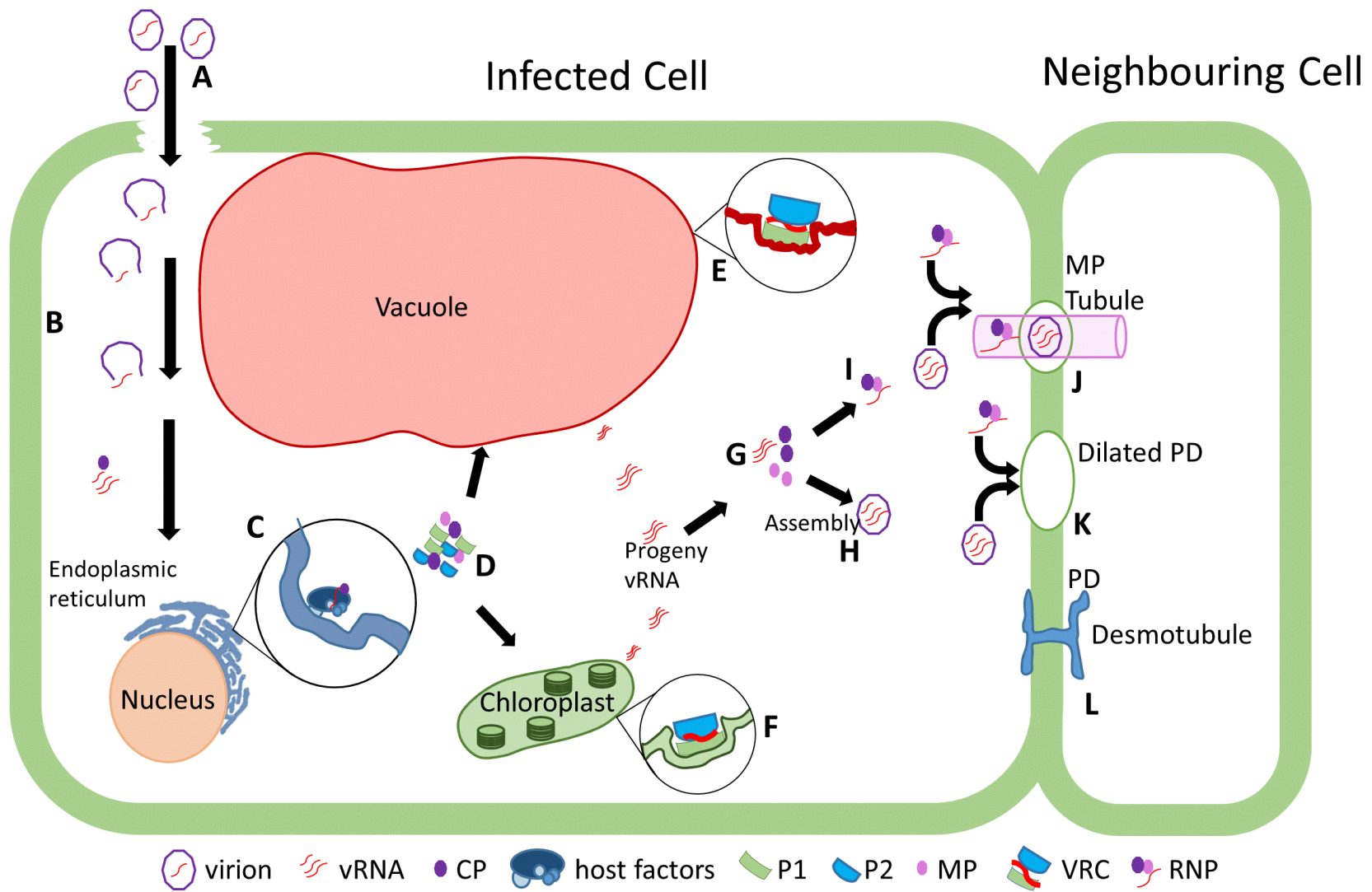
its ability to drive the establishment of infection is a phenomenon termed genome activation (Bol et al., 1971; Jaspars, 1999; van Vloten-Doting, 1975). In lieu of a TLS, the requirement of CP for virus replication is now a distinguishing feature of both *alfamo-* and *ilarvirus* genera (Van Der Heijden et al., 2001). The viral replication mechanism has been studied more extensively in AMV than ilarviruses. Due to the similarity between alfamo- and ilarviruses, including the dependence of CP for genome activation, the replication cycle of ilarviruses is likely similar to that of AMV (Kozieł et al., 2017a). The process of genome activation is based on interactions between the viral CP and secondary structures found within the 3'UTR of vRNAs (Gonsalves and Fulton, 1977; Jaspars, 1999; MacFarlane and McGavin, 2009; van Vloten-Doting, 1975). The presence of a highly conserved RNA binding domain (RBD), with the consensus sequence Q/K/R-P/N-T-X-**R**-S-R/Q-Q/N/S-W/F/Y-A containing a crucial arginine (shown in bold) in the N-terminal CP sequences of AMV and some ilarviruses, is likely necessary for genome activation where the binding of CP and vRNA is involved in protein translation (Ansel-McKinney et al., 1996). Additional sequence analyses have identified a second putative RNA binding consensus sequence V(T/S)(R/N)RQ(S/R)RNA(A/R)RAAX(Y/F)R which is also conserved in at least six other ilarviruses (Aparicio et al., 2003; Bol, 2005). Some ilarviruses such as *Prunus necrotic ringspot virus* (PNRSV) do not have either of these two consensus RNA-binding sequences. However, these viruses have CP domains rich in arginines such as the CP of PNRSV which contains a stretch of 20 aa residues with five arginines, giving PNRSV the capacity to bind to the 3'UTR of RNA3 (Aparicio et al., 2003; Pallas et al., 2013). Additionally, the N-terminal region of some ilarviral CPs, including that of PNRSV, possess a zinc finger motif believed to increase RNA binding affinity (Mathur et al., 2014; Pallas et al., 2013). The process of genome activation is not species-specific as *in vitro* studies have shown that genome activation still occurs in the presence of CPs from various ilarviruses (Pallas et al., 2013). This ability to reciprocally activate infectivity of the different viruses by their CPs can extend to the intergenus level as shown by the substitution of AMV CP with ilarviral CPs to induce genome activation (Clemente-Moreno et al., 2015). In the absence of CP, the presence of sgRNA4 is sufficient for genome activation as the CP is translated from

this sgRNA (Guogas et al., 2004). In the absence of sgRNA4 or CP, the transcription of vRNA is favoured, while the addition of CP or sgRNA4 causes a shift to translation which is likely caused by the binding of CP to RNA secondary structures found in the 3' UTRs of viRNAs (Chen and Olsthoorn, 2010; Swanson et al., 1998). Conserved single stranded (A/U)(U/A/G)GC motifs have been identified in the 3' UTRs of ilar- and alfamoviral vRNAs, these motifs flank regions which can form hairpin loop structures thereby acting as CP binding sites (Gallo-García et al., 2018; Pallás et al., 1999; Reusken and Bol, 1996). It has been suggested that the CP-RNA complex formed in ilarviruses is functionally analogous to the complex formed by the poly-A tract and the poly-A binding protein in eukaryotes, which is known to enhance protein translation (Neeleman et al., 2004). This has been further supported by the finding that the AMV CP does in fact interact with eukaryotic translation initiation factor (eIF) subunits 4G and its isoform eIF(iso)4G (Krab et al., 2005). To date, no host encoded proteins have been determined to interact with viral proteins encoded by PDV.

Two alternative models have been proposed to explain the role of CPs in the early stages of the alfamo- and ilarviral infection cycle. The first model, known as the conformational switching model, proposes the 3' UTR of AMV and ilarviruses can fold into two separate structures. The predominant structure of the 3' UTR of vRNAs is a pseudoknot (**Figure 4A**), functionally equivalent to a TLS, promoting the binding of viral RdRp and synthesis of (-) RNA (Olsthoorn et al., 1999). The binding of CP to the 3' UTR of genomic RNA fragments causes a conformational change (**Figure 4B**) the pseudoknot is unwound resulting in the second structure which is an expanded series of hairpin loops (**Figure 4C**). The expanded series of loops can no longer be bound by the RdRp, preventing further transcription of vRNA (Olsthoorn et al., 1999). This model proposes the CP-vRNA complex then leads to viral protein translation. Based on this model, the pseudoknot in the 3'UTR is essential for replication of AMV and ilarviruses and disruption of this structure inhibits viral replication. Oolsthoorn *et al* (1999) showed stabilization of the pseudoknot structures by addition of magnesium inhibits binding of the 3' UTR by CP, however the CP can bind to mutated 3' UTR sequences which are unable to form

Figure 4 Two potential structures of RNA: pseudoknots and hairpin loops

Both models of replication acknowledge the binding of CP to 3' UTR of AMV and ilarviruses likely induces structural changes (Bol, 2005; Guogas et al., 2005). This diagram utilizes a generic sequence which is artificially numbered beginning at 1 to illustrate the formation of the two structures likely formed by the 3' UTRs of PDV. Bases are coloured to allow their tracking as they change location during the formation of alternate structures. This diagram was drawn using RNAstructure (version 6.2) and visualized using RNAstructure structure editor (Version 1.0) (Reuter and Mathews, 2010)..

The conformational switching model of replication is shown on the left (A-C)

A A pseudoknot is the proposed predominant structure of the 3' UTR favours the binding of the viral RdRp and transcription of RNA.

B Introduction and binding of the CP to the 3' UTR induces a structural change as the pseudoknot disassembles and begins to form an alternate structure.

C After CP binding, the final structure resembles a series of expanded hairpin loops (a single hairpin loop is shown), this expanded structure cannot be bound to the RdRp and thus translation of viral proteins is favoured

The 3' organizational model of replication is shown on the right (D-F)

D A series of extended hairpin loops serve as binding sites for the viral CP.

E Binding of the CP initiates a structural change of the 3' UTR which cannot be bound by the viral RdRp thus inhibiting transcription.

F The structure favouring protein translation is a compacted structure, possibly a pseudoknot serving as a TLS.

Conformational Switching Model
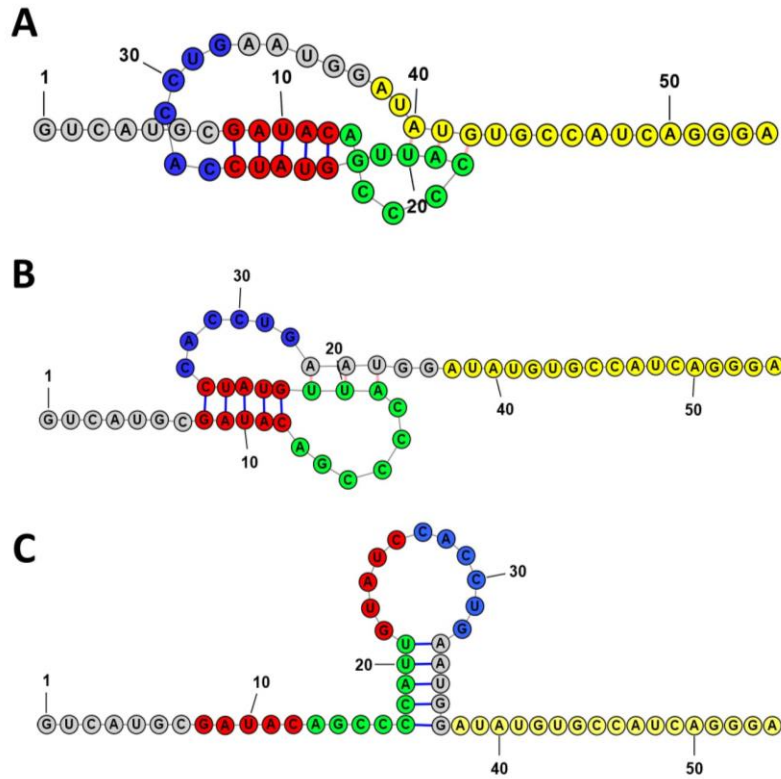
3' Organizational Model
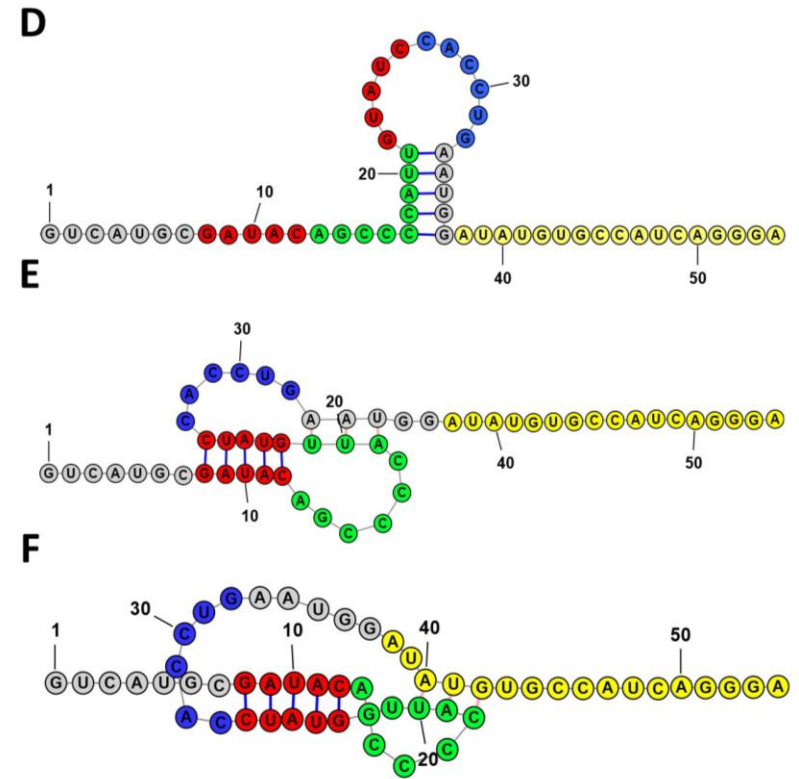
pseudoknots even after addition of magnesium. Evidence supporting this model has also been obtained from studies with some ilarviruses. For example, the CP of PNRSV is unable to bind to the 3' UTR of genomic RNAs whose secondary structure has been stabilized by the addition of magnesium (Aparicio et al., 2003). This model illustrates that the 3' UTR of alfamo- and ilarviruses does indeed adopt different structures associated with the presence and binding of CP, however an alternate model for replication has been proposed.

The second model, termed the 3' organization model, suggests that hairpin loops function as CP binding sites (**Figure 4D**). Upon binding, the 3'UTR forms a complex that is critical for viral replication and protein translation. In contrast to the first, this model predicts the structure of the 3' UTR undergoes a conformational change (**Figure 4E**) where CP binding to the 3'UTR creates a compacted structure instead of forming a TLS (**Figure 4F**). Structural analyses show that the unbound 3'UTR of AMV is flexible which supports this model (Baer et al., 1994). When a truncated protein identical in sequence to the AMV CP RNA binding domain is bound to AMV genomic RNA, the resulting CP-RNA complex is more rigid and compact due to base pairing between the AUGC repeats that flank hairpin loops (Petrillo et al., 2005). Modelling of the CP binding along the entire length of the AMV 3' UTR, shows that the predicted molecule has a compact, rod shaped structure with hairpins protruding from the centre (Guogas et al., 2004). *In vitro* studies have shown that in absence of CP, the binding of the RdRp protein to labelled RNA is weak, and addition of CP significantly enhances the binding ability of RdRp to the labelled RNA (Guogas et al., 2005). A peak CP : vRNA ratio of 5:1 was found as the maximum CP concentration allowing for transcription, when more CP was added replication was inhibited and translation was favoured (Guogas et al., 2005). In summary, the binding of CP to 3' UTR creates a more compact structure possessing the equivalent function to a TLS and is required for the initiation of RNA replication. Overall, the 3' organizational model suggests a structural change does occur based on CP binding to the 3' UTR of AMV and ilarviruses, however this model states that CP is required for both transcription and translation, but the regulation of these processes is based on CP concentration.

1.4.3 PDV movement

After replication, (+) vRNA is either encapsidated by CP subunits to form virions (**Figure 3H**), or the CP-RNA complex interacts with the MP to form a ribonucleoprotein complex (RNP; **Figure 3I**). Although the formation of virions is not required for virus movement, the presence of both CP and MP is required (Pallas et al., 2012, 2013). These virions or RNPs are then transported intracellularly to the PD (**Figure 3J**). Normally, the PD is responsible for regulating the local intercellular transport of molecules primarily based on size (Heinlein, 2015). The threshold allowing the transport of molecules of specific sizes to pass through the PD is referred to as the size exclusion limit (SEL) (Heinlein, 2015). The SEL varies depending on the cell type, however PD which connect mesophyll cells have an SEL of ~0.75-1.0 kDa (Hull, 2014). Mechanisms for passing through the PD vary among viruses, and includes dilating the PD to increasing the SEL (**Figure 3K**) allowing for the passage of viruses, another mechanism involves the formation of tubules that displace the native desmotubule of the PD, creating a passage for viral RNP or virions (**Figure 3L** ; Melcher, 2000;Park et al., 2017; Sánchez-Navarro et al., 2006; Wei et al., 2010). Once modified, the PD is the site for local movement as PDV moves from primarily infected cells to neighboring cells (Bol, 1999, 2005; Pallas et al., 2013). Based on size and the presence of conserved secondary structures, the MP of PDV is classified as a member of the 30K movement protein superfamily (Melcher, 2000).

The MP of tobacco mosaic virus (TMV) is the most studied member of this superfamily and viruses containing similar MPs possess a conserved core domain which consists of series of β-sheets flanked by at least one *a*-helix (Melcher, 2000). A common feature of 30K MPs is the binding of single stranded RNA or DNA, suspected to aid in the formation of RNPs (**Figure 3I**) for virion independent movement (Mushegian and Elena, 2015). Another common feature is the localization of the MP to the PD. Additionally, 30K MPs may modify the PD in different manners. Some 30K members are able to increase the SEL of PD, allowing for larger particles to pass through (**Figure 3K**), whereas others form hollow tubular structures composed of MP subunits (**Figure 3J**), which pass through the dilated PD into adjacent cells (Melcher, 2000; Mushegian and Elena, 2015). A common

structural feature of 30K MPs known to form tubules is the presence of a longer N-terminus which contains a predicted *a*-helix (Melcher, 2000). The MP of AMV produces tubular structures crucial for viral movement (Kasteel et al., 2015; Zheng et al., 1997). An early study showed that complementation using the MP of PNRSV allows for intercellular movement of AMV, suggesting that the mechanism of viral movement of ilarviruses is similar to that of AMV (Sánchez-Navarro et al., 2006). The MP of PDV shares 40% sequence identity to that of AMV. This similarity further supports the idea that PDV moves in a tubule dependent manner (Kozieł et al., 2015). Indeed, a very recent EM study that visualized the ultrastructure spanning adjacent cells of PDV infected cucumber has suggested that PDV uses tubules for intercellular movement (Kozieł et al., 2018). For long-distance movement from primary infection sites to distal plant tissues, PDV is likely transported in a manner like most plant viruses (Wang, 2015). PDV would likely move from the mesophyll via bundle sheath cells, phloem parenchyma, and companion cells into phloem sieve tube elements (Hipper et al., 2013). Once inside the phloem, PDV would be translocated with photosynthates from photosynthetic source leaves towards growing sink tissues such as meristems and newly developing leaves where it would be unloaded from the phloem (Kozieł et al., 2015,2018; Pallas et al., 2012, 2013).

1.4.4   Transmission of PDV between hosts

The natural host range of PDV is limited to woody fruit trees and shrubs (**Section 1.3.2**). Perhaps the most common mode of transmission in these hosts is by vegetative propagation, a common horticultural practice. For example, grafting of scions to rootstocks is used for clonal propagation of woody fruit trees. In grafting, the use of infected material as either a root stock or scion facilitates the spread of viruses (Dijkstra and de Jager, 1998). Although not as common as grafting, PDV is also spread through pollen and seeds (Caglayan et al., 2011). A previously proposed model for transmission by pollen has four main points, firstly proposing infectious virus particles are present in mature pollen. This is supported by work showing that PDV cannot be transmitted from infected trees to uninfected trees without flowers indicating that flowers must be present

for pollen based transmission (George and Davidson, 1963; Mink, 1992). Secondly, insects which cause mechanical wounds in plants such as *Thrips spp.* must be present within the flowers of infected trees and become covered with virus infected pollen grains. Thirdly, the transfer of pollen covered thrips to uninfected tree flowers is either by direct flight, or some other association with pollinating insects such as honeybees (*Apis spp.*). The second and third points are supported by findings that PDV is only transmitted in a plant to plant manner by arthropods when *Apis spp.* and *Thrips spp.* are present (George and Davidson, 1963). This work also showed that there was no transmission of PDV when other arthropod combinations were used such as *Apis spp.* and aphids (members of the *Aphididae*) which cause far less mechanical damage than thrips (George and Davidson, 1963). The ability of thrips to transmit PDV using pollen from infected *Prunus* species to seedlings of cucumber has also been shown that PDV transmission is much higher than that of PNRSV using the same methods (Greber et al., 1992). Finally the transmission of PDV is likely performed by mechanical damage as a result of wounds caused by thrips feeding on the uninfected plant (Mink, 1992).

1.5   Pathogenesis

Like other ilarviruses, PDV infection often causes a rapid onset of symptoms referred to as the initial shock phase. During the shock phase, the strongest foliar symptoms are visible for a short period of time. This phase is then followed by symptom attenuation and for some cases, an eventual recovery from symptoms on new leaves (Bristow and Martin, 2002; Cropley et al., 1964; Pallas et al., 2013). It is important to note that symptom attenuation in ilarviral infection is different than recovery phenomena during infection described for other viruses, in which the reduction of symptoms is associated with antiviral RNA silencing (a mechanism of post transcriptional gene silencing; PTGS) and decreased viral accumulation (viral clearance). Symptom recovery following infection by some ilarviruses may be caused by different mechanisms, allowing the virus to persist within the host (Ghoshal and Sanfaçon, 2015; Pallas et al., 2013).

The molecular determinant for the recovery phenomenon in the type member of the *Ilarvirus* genus, *Tobacco streak virus* (TSV), has been identified (Xin and Ding, 2003). A single nucleotide substitution (A→G) in the intergenic region of RNA3, upstream of the transcription start site of sgRNA4, prevents a specific isolate of TSV to initiate recovery in the host. Plants infected with this recovery deficient isolate develop disease symptoms which never subside (Xin and Ding, 2003). Interestingly, the TSV isolate that is unable to induce symptom recovery persists at lower titers in plants, compared to wild type TSV which does induce symptom recovery, contradicting conventional thought that lower viral titers are associated with reduced symptom severity. These data support the idea that symptom recovery in plants infected by at least some ilarviruses is not always due to reduced viral titer. It is possible that ilarvirus-induced RNA silencing downregulates host resistance genes, which may contribute to an infection with reduced symptoms while a higher viral titer is maintained (Boccara et al., 2014; Ghoshal and Sanfaçon, 2015; Jovel et al., 2007; Li et al., 2010; Shivaprasad et al., 2012). Determinants of pathogenicity have been identified in some ilaviruses such as *Asparagus virus 2* (AV-2) and PNRSV. For example, the 2b protein encoded by AV-2 ORF2b acts a RNA silencing suppressor (RSS) to indirectly function as a determinant by counteracting the host plants defense mechanism (Shimura et al., 2013). A more direct example of a disease determinant comes from a study of PNRSV, in which full-length infectious cDNA clones derived from pathogenically aggressive and mild isolates of PNRSV were used. Comparisons of nucleotide sequences between these two isolates lead to the finding a single lysine in the viral RdRp, together with the 3' terminal sequence of RNA1 is responsible for the virulent phenotype of this isolate (Cui et al., 2013).

1.6   Detection and diagnostics

Visual diagnosis of PDV infection is temporally sensitive, as the most obvious symptoms of PDV infection are observed during the initial shock phase. However over time, these symptoms are reduced and differentiating infected and uninfected plants becomes difficult (Gilmer et al., 1976). In the field, symptoms are easily seen at the

beginning of growing seasons before peak seasonal temperatures are reached as young, newly emergent leaves usually display the strongest symptoms. Common diagnostic techniques for other plant viruses can be used to detect PDV. A common practice of virus diagnostics is indexing of plant material. Indexing involves using sampled tissues to inoculate susceptible host plants known to present specific symptoms (often termed indicator plants) of the virus in question. The wide experimental host range of PDV allows for easy indexing on herbaceous (by mechanical inoculation) and woody indicators (by grafting) for detection (Cropley et al., 1964; Fulton, 1966). PDV is known to infect cucumber leading to initial symptoms of small chlorotic spots on the plants first true leaves, quickly followed by systemic mottling and leaf deformation (Caglayan et al., 2011; Fulton, 1966). Woody indicators can also be used to successfully detect PDV. *Prunus serrulata* cv. *Shirofugen* infected by PDV presents with tissue necrosis and dwarfing, infected *peach* cv. GF305 displays narrowed leaves in addition to a dwarfing phenotype. In some woody hosts such as sweet cherry cv. Bing, PDV infection also causes small outgrowths on the undersides of leaves which are referred to as enations (Gilmer et al., 1976). In plum, PDV often causes leaf deformation, mottling and dwarfing (Caglayan et al., 2011). When plant tissues are homogenized for indexing studies, endogenous RNA and protein degrading enzymes, reactive oxygen species (ROS), tannins and other compounds are released from macerated tissues and can degrade or inactivate virions of ilarviruses hindering their ability to be transmitted (Fulton, 1966; Hull, 2009). To minimize virion degradation and inactivation, chemical additives such as 2-mercaptoethanol, ethylenediaminetetraacetic acid, cysteine hydrochloride, sodiumdiethyldithiocarbamate and polyvinylpyrrolidone are added to inoculum preparations (Fulton, 1966; Hill, 1984; Németh, 1986). These additives serve as antioxidants, bind to tannins and inactivate enzymes allowing for intact virions to be transmitted to the indicator host. The generation of antibodies specific to the PDV CP has led to the commercial availability of serological diagnostic kits using an enzyme-linked immunosorbent assay (Boonham et al., 2014). Antibody based detection methods provide fast, accurate and highly specific means of detecting PDV compared to biological assays such as indexing. ELISA is widely used and is

often part of pathogen detection and certification of plant materials as being free of a specific virus before plant materials are imported or exported.

Nucleic acid-based detection techniques such as reverse transcription polymerase chain reaction (RT-PCR), are more sensitive and can detect viruses at lower titers compared to antibody-based methods. Multiplex PCR can be used to detect multiple viruses simultaneously with greater sensitivity and specificity compared to serological techniques which either detect a single virus or a group of viruses based on conserved viral proteins. The use of multiplex PCR has been used to identify mixed infections of PDV with PNRSV (Saade et al., 2000). One caveat of RT-PCR is due to its high specificity, primers designed for a virus isolate may not anneal to vRNA due to differences in nt sequence. Great care must be taken to design appropriate primers for detection, it is common practice to design degenerate primers, or design primers complementary to highly conserved virus genes (Pallás et al., 2018). Next generation sequencing (NGS) is another nucleic acid-based technique which has increased in popularity for virus detection (Pecman et al., 2017). NGS platforms allow for complete sequencing of isolated nucleic acids (often total RNA, or small interfering RNAs (siRNAs)) from an infected sample. The total viral population (virome) in a sample can be characterized using NGS allowing for detection of a broad spectrum of viruses or to examine the genetic diversity of virus populations in the sample (Kutnjak et al., 2017; Kutnjak et al., 2015). The isolation and sequencing of siRNAs is extremely useful for detection of viruses, as siRNAs are a by-product of the host defense process of RNA silencing. The isolation of siRNAs creates a sample likely to be enriched with fragments of viral genomes which can be sequenced and reassembled into longer transcripts using *in silico* methods (Baráth et al., 2018; Wu et al., 2010).

1.7   Control of plant viruses

Treatment of any infections by plant viruses including ilarviruses is difficult. Prevention of viral infections is a more successful strategy, therefore *ad hoc* methods to mitigate viral infections and related crop diseases are implemented. Furthermore,

ilarviruses are transmitted in different manners presenting additional challenges when trying to control virus transmission. Transmission by seed is problematic as most commercial rootstocks are grown from seed, therefore the use of certified, virus-free seeds is crucial for the control of PDV (Caglayan et al., 2011). The ability for PDV to be transmitted by infected pollen presents an additional challenge as this renders the host susceptible to transmission each growing season during flowering periods as *Prunus spp.* require cross pollination for fruit production (Card et al., 2007; Gilmer and Way, 1960).

Cross protection, also known as preimmunization, is a strategy where a mild isolate of a virus is used to protect the host from a closely related, more severe isolate of that same virus. A mild isolate is defined as an isolate that is either latent, or causes the mildest symptoms in susceptible indicator plants under growth conditions conducive to viral infection and disease progression (Lee and Keremane, 2013). The high specificity of cross protection means broad resistance to unrelated viruses is not conferred, and in fact, for some viruses, cross protection is only strain specific (Folimonova, 2013). Additionally, cross protection is not seen as an ideal, *ad hoc* method to prevent crop losses of resistance to viral infection and should only be considered as a means to extend the productive life of currently productive plants (Lee and Keremane, 2013). Cross protection has been successfully used to protect citrus trees from virulent isolates of *Citrus tristeza virus* (CTV) of the *Closterovirus* genus which has killed nearly 100 million citrus trees globally (Moreno et al., 2008). In Brazil, *Citrus aurantiifolia* L. (lime) trees protected with mild isolates of CTV produce five times greater yields compared to trees which had not been preimmunized (Lee and Keremane, 2013). In the United States, citrus growers in Florida have used mild isolates of CTV to protect orchards from a severe isolate known as CTV-D. In greenhouse trials, it was found that trees previously exposed to mild isolates of CTV did not suffer any adverse effects when later challenged with CTV-D. In contrast, of the trees which received no preimmunization 50% were killed by CTV-D infection (Yokomi et al., 1991).

Cross protection has also been used to offer protection from severe isolates of ilarviruses. Mild isolates of *Apple mosaic virus* (ApMV) another member of the *Ilarvirus*

genus have been used to protect trees from severe isolates (Chamberlain et al., 1964). After inoculation with a severe isolate of ApMV, trees previously grafted with scions containing mild isolates of ApMV produced 6 times more fruit compared to trees grafted with uninfected scions (no preinoculation; Chamberlain et al., 1964). Cherry rugose mosaic diseases, a serious disease of cherry, is caused by a virulent isolate of PNRSV (Howell and Mink, 1988). In the Wang laboratory, a mild isolate of PNRSV was identified and is being evaluated for the control of this severe isolate (Cui et al., 2012b). The underlying mechanism(s) leading to cross protection are not yet fully understood. Initial theories proposed that the first isolate prevents entry of a challenging isolate, however this theory does not explain how a mild isolate can systemically protect a plant from a more severe isolate (Folimonova, 2013). Recently, viral proteins have been found to mediate cross protection for some viruses. The multifunctional matrix protein of *Sonchus yellow net virus* (SYNV) has been implicated in cross protection. Researchers have found that nuclear localization of this protein and interaction with the SYNV nucleocapsid protein are necessary for cross protection by inhibiting transcription of a challenging isolate (Zhou et al., 2019). In the case of CTV, mutational and complementation studies show a viral protein, p33, is necessary for cross protection (Bergua et al., 2014). Recently, p33 of CTV was identified as an effector which negatively affects virus pathogenicity and this protein is likely recognized by the host, triggering host-immune responses to restrict CTV movement and disease development (Sun and Folimonova, 2019). Another proposed mechanism of cross protection is virus induced gene silencing (VIGS). According to this theory, infection by a first isolate induces host mediated RNA silencing. Subsequent Infection by a second virus isolate (with high sequence similarity to the first isolate) infects the same plant, VIGS which is already induced by the first isolate, is able to silence gene expression of this second isolate in rapid succession before the challenging isolate can become established (Ratcliff et al., 1999). VIGS explains why infection by an attenuated version of a virus can induce resistance to the virus isolates sharing similar sequences with the attenuated isolate (Nishiguchi and Kobayashi, 2011). VIGS can also be used to silence host genes by insertion of a short fragment of a target gene into the

attenuated virus. The silencing of the host gene of interest can sometimes provide resistance to a specific virus. Recently, a modified infectious clone of PNRSV has been used to silence *eIF(iso)4E* in peach, a host gene which is required for infection by plum pox virus (PPV) (Wang and Krishnaswamy, 2012). Resultantly, the *eIF(iso)4E*-silenced peach plants are resistant to PPV infection (Cui and Wang, 2016).

Despite technological innovations and increased knowledge of host factors involved in the virus life cycle, cultural practices such as removal of infected plants, crop rotation, and soil sterilization continue to be used most often for the control of virus diseases. Crop management to minimize risk of infection, and methods of early detection are the most effective strategy to prevent infections by ilarviruses (Barba et al., 2015; Pallas et al., 2013; Rubio et al., 2017). In response to the spread of viral diseases caused by transportation of infected plant materials, some countries have imposed legislative methods to fight plant disease by enforcing strict regulations to restrict the movement of plant material in and out of established quarantine zones and across international borders (Gougherty and Nutter, 2015; Wang et al., 2006). One legislative measure commonly adopted is the development of certification programs to determine plant material as being virus-free before they can be sold, transported or used for commercial plant propagation (Barba et al., 2015). These certification programs use methods such as visual inspection, DAS-ELISA, RT-PCR and NGS to test plant materials such as seed, rootstocks and scion cuttings for virus infection (Barba et al., 2015; Gougherty and Nutter, 2015). A shortcoming of these programs is that only previously identified viruses are detected but they fail to detect novel or undescribed viruses. A recent example of this problem was encountered when a disease of apples with unknown etiology was found in Ontario. Using a list of known plant viruses previously detected in Canada to analyze NGS data resulted in the detection of viruses known to latently infect apple (*Malus domestica* L.; Liping Wang and Aiming Wang, 2019, unpublished data). Just prior to this work being performed, a new virus, *Apple luteovirus* was identified in the Northern United States (Liu et al., 2018) . Repeating the NGS data analysis including the newly sequenced luteovirus revealed that an isolate of this virus was in fact present in the diseased apples in Ontario

and is currently being studied as a potential causal agent of the newly emerging disease termed "rapid apple decline" (Liping Wang and Aiming Wang, 2019, unpublished data). Hygienic practices including cleaning of pruning shears and other implements which contact plants should be routinely performed. When virus infections are found, common practices place emphasis on sanitation and eradication. These practices are referred to as cultural controls and includes the removal and destruction of infected plant material , the removal of nearby weeds or other plants which may act as alternative hosts (Barba et al., 2015). Other cultural practices to mitigate crop losses caused by viruses includes the control of vectors such as insects to minimize spread of viruses (Barba et al., 2015).

1.8   Identification of host factors involved in the virus infection

All viruses including PDV must recruit host factors to complete various steps in the virus infection cycle (**Sections 1.2, 1.4.2**; Sanfaçon, 2017; Wang, 2015). Using techniques such as NGS and proteomic analyses coupled with powerful bioinformatics analyses has lead to the identification of significant genomic and proteomic changes associated with viral infections (Wang, 2015). Further studies of these identified genes and proteins has led to the identification of many host factors crucial for virus infection. Some identified host factors involved in translation of viral proteins are subunits of the eukaryotic initiation factor4F (eIF4F) complex. During infections by potyviruses, eIF4E or its isoform interact with the viral genome linked protein (VPg). This interaction between viral protein and host protein is crucial for the initiation of viral protein translation (Wang, 2015; Wang and Krishnaswamy, 2012). The CP of AMV has also been shown to interact with subunit G of this complex (eIF4G; Krab et al., 2005). During infection by *Turnip mosaic virus* (TuMV), the α expansin protein of tobacco was found to interact with the RdRp of TuMV and was involved in both replication and intercellular movement (Park et al., 2017). The identification of host factors integral to the viral infection cycle is one of the most important goals of virus research. Not only does the identification of host factors allow for increased understanding of the infection process and viral life cycle, this research is also driven by potential practical applications including beneficial biotechnological uses

of viruses and development of new antiviral strategies (Wang, 2015). Antiviral strategies can be developed by altering expression of host factor genes to disrupt the viral processes: advances in precision guided genome editing techniques has simplified the process of genome editing (Carroll, 2014; Salsman and Dellaire, 2016). One strategy that has been used to successfully introduce virus resistance involves the coupling of modern technology and traditional techniques: after plant transformation to introduce precise genome editing, the transgene can be removed by traditional plant breeding(Wang, 2015). This strategy has been used successfully in cucumber generating resistance to *Cucumber vein yellowing virus* (CVYV; of the *Ipomovirus* genus) and two potyviruses: *Zucchini yellow mosaic virus* (ZYMV) and *Papaya ring spot mosaic virus-W* (PRSV-W) (Chandrasekaran et al., 2016). In this work, clustered regularly interspaced short palindromic repeats (CRISPR/Cas9) was used to mutate eIF4E in cucumber, a known host factor for many viruses (Sanfaçon, 2015; Wang and Krishnaswamy, 2012). After the mutation was introduced using the CRISPR/Cas9 system, mutated plants were crossed (a traditional breeding technique) to remove the transgene and *efi4e* homozygous plants were grown. Subsequent inoculation with CVYV, ZYMV or PRSV-W (separately) showed homozygous eif4e mutant plants were resistant to these viruses, whereas wild type plants, and heterozygous mutants were susceptible (Chandrasekaran et al., 2016). Although the identification of host factors has been a long-time goal of virus research, very few host factors have been identified in ilarviruses, and none have been found specifically for PDV.

1.9   The use of infectious clones

Several factors complicate the study of PDV. First, PDV and other members of the *Bromoviridae* persist at lower titers in host plants making isolation and purification of this virus difficult. Secondly, PDV is inherently unstable and virions degrade quickly outside of the host, complicating simple procedures such as virus isolation and mechanical inoculation of indicator plants (Fulton, 1966, 1982). A major tool which mitigates some obstacles associated with the study of ssRNA(+) viruses is the development of infectious complementary DNA (cDNA) viral clones. An infectious cDNA clone is the complete viral

genome reverse transcribed into cDNA so it can be amplified as double stranded (ds) DNA and ligated into a plasmid vector. The amplified DNA copy of the viral genome is then situated between a strong promoter element (often the *Cauliflower mosaic virus* (CaMV) 35S Promoter) and a terminator sequence to initiate and terminate *in vivo* transcription of the cloned virus (Mori et al., 1991; Nagyova and Subr, 2007). Once agroinfiltrated into the plant, the DNA copy of the viral genome is delivered to the nucleus and transcription of this DNA as template results in the viral genome being transcribed, resulting in viral infection. One of the greatest advantages of infectious clones is the stability of the cloned virus when stored as plasmid DNA. When transformed into bacteria, the clone can be cultured and isolated at high concentrations (Bedoya and Daròs, 2010). Reverse genetic studies have been used to uncover molecular functions of many viruses using such cDNA clones. For example, in the Wang laboratory, the first cDNA clones of an ilarvirus, PNRSV, was used to uncover the pathogenicity determinant of this virus in both herbaceous and natural hosts (**Section 1.5**; Cui et al., 2013). A modified infectious clone of PNRSV has been used to confer resistance in *Prunus spp.* to PPV by silencing *eIF(iso)4e*, a known host factor crucial for PPV replication (**section 1.7**; Cui and Wang, 2016). The use of a TuMV infectious clone has provided insights regarding virus movement by identifying crucial domains of the CP for this process (Dai, 2018; Dai et al., 2020). The same infectious clone of TuMV, coupled with quantitative proteomics led to the identification of the host factor EXPA1, an expansin protein encoded by tobacco that interacts with the viral RdRp during viral infection (Park et al., 2017). Overall, these examples illustrate potential uses of cloned viruses to identify viral genomic domains critical for processes such as movement and symptom development. Additionally, host factors are being identified using infectious clones which may be useful for downstream applications such as VIGS to combat viral crop diseases.

1.10 Koch's postulates for plant virology

Koch's postulates were a set of rules originally designed to evaluate candidate microbes as causal agents of disease (Rivers, 1937). To evaluate a virus of interest as the

causal agent of a disease, a modified version of these postulates must be used (Bos, 1981; Prescott et al., 2017; Rivers, 1937). Infectious clones of viruses have been used extensively to study virus disease development and are used in lieu of growing an organism in pure culture (Tatineni et al., 2001). In plant virology, infectious clones have been used to further understand molecular processes in the viral infection cycle in both herbaceous and woody hosts (Cui et al., 2013). The modified version of Koch's postulates which will be used in this work are as follows

1. Nucleic acids are isolated from symptomatic plant tissues containing the viral genome of interest.

2. An infectious clone of the virus obtained from the symptomatic plant tissue is constructed.

3. The infectious clone is used to inoculate healthy experimental and natural host plants.

4. The symptoms which were initially observed on orchard grown cherry must be observed on the inoculated host, and the cloned virus must be detected in the newly diseased host.

1.11   Research goals and objectives

Initially, foliar symptoms typical of viral infection were identified on cherry in a research farm in Jordan, Ontario. The primary goal was to identify the causal viral pathogen(s). Based on results obtained through NGS it was determined that PDV is present as a possible causal agent, and a plan to further study PDV was developed: to develop a PDV-derived infectious clone, and study PDV pathogenesis, molecular PDV-host interactions and the functions of the MP of PDV. The MP was chosen as this protein plays key roles in intercellular movement.

Therefore, the specific objectives of this study are:

1. To Identify causal agents of the disease symptoms found on cherry using NGS and subsequent data analysis.

2. To develop an infectious cDNA clone of PDV and further introduce the clone into herbaceous and woody hosts to determine if PDV is the causal agent of the severe foliar symptoms found on cherry.

3. To determine if the MP of PDV is responsible for PD localization and tubule formation.

4. To characterise the elements crucial for the function of the MP of PDV.

5. To understand PDV pathogenesis by identification of host proteins that are differentially accumulated in infected plants using label-free quantitative proteomics.

The long-term goal of this study is to develop a better understanding of the impact of PDV infection on susceptible hosts. This work may allow for identification of host factors that are involved in the viral infection cycle of PDV which will lead to the development of effective strategies to control viral diseases in cherry and potentially other members of the *Prunus* genus for sustainable fruit production in Canada.

2. Materials and methods

2.1 Media, solutions and additives

Note: to prepare solid media, 15 g of agar were added to 1 L of liquid media before autoclaving.

Lysogeny broth (LB)

For 1 L: 10 g tryptone 5 g yeast extract, 10g NaCl

RNA extraction buffer

For 1 L: 20g hexadecyltrimethylammonium bromide (CTAB; Sigma #1102974), 20 mM ethylene diamine tetracetic acid (EDTA) pH 8, 1.4 M NaCl, 100 mM Tris-HCl pH 8, 20 g polyvinylpyrrolidone (PVP-40; Sigma #PVP40-500G).

Liquid plant fertilizer

For 1L: 1 g water soluble fertilizer 20:20:20 (N:P:K; Plant-Prod # 10529)

Mechanical inoculation buffer

For 1L: 20 g PVP-40, 1 % 2-mercaptoethanol, 5 mM cysteine HCL, 1 mM Na-diethyldithiocarbamate, 2 mM EDTA, 750 mg activated charcoal, 750 mg carborundum powder.

Protein extraction buffer

For 10 ml: 290 mM sucrose, 250 mM Tris-HCL pH 7.6, 25 mM EDTA pH 8, 10 mM KCl, 25 mM NaF, 50 mM Na pyrophosphate, 1 mM ammonium molybdate, 1 mM phenylmethylsulfonyl fluoride (PMSF; Sigma # P7626-1G), 100 µl protease inhibitor cocktail (Sigma # P8340-1ML).

Protein lysis buffer

For 10 mL: 8M urea, 50 mM Tris-HCL pH 8, 30 mM NaCl, 1 mM $CaCl_2$, 20 mM Na butyrate (Sigma # B5887-250MG), 10 mM nicotinamide, 1 tablet PhosStop protease inhibitor (Sigma # 4906845001).

Protoplast enzyme solution

For 100 mL: 1.5g cellulase R-10 (Yakult Pharmaceuticals #216016), 400 mg macerozyme R-10 (Yakult Pharmaceutical #202051), 0.4 M mannitol, 20 M morpholinoe-thanesulfonicacid (MES; Sigma #M8250), 10 mM $CaCl_2$, 1% bovine serum albumin (BSA; Sigma # A6793).

Protoplast washing solution (W5)

For 1 L: 150 mM NaCl, 150 mM CaCl2, 5 mM KCl, 5 mM Glucose, 2 mM MES.

Protoplast MMG buffer

For 100 ml: 400 mM mannitol, 15 mM $MgCl_2$, 4 mM MES.

PEG Transfection Buffer

For 10 mL: 2 g polyethylene glycol 3350 (PEG-3350; Sigma # 1546547), 100 mM CaCl2, 200 mM mannitol.

Seed sterilization solution

For 500 mL: 500 mg Maestro 80DF (TerraLink # 1107220), 0.5 ml Tween-20 (Sigma # P9416)

Agroinfiltration buffer

For 50 ml : 100 mM MES pH 5.6, 100 mM $MgCl_2$, 100 mM acetosyringone, 15 µl Tween-20.

Acetosyringone

For 200 mM stock: 98.1 mg acetosyringone (Sigma #134406) dissolved in 2.5 ml dimethyl sulfoxide (DMSO).

Ribonuclease free solutions

To remove Ribonuclease (RNAse) from solutions, 0.01% of diethyl pyrocarbonate (DEPC; Sigma # D5758-5ML) was added to solutions, shaken vigorously and stored in a fume hood overnight. The following morning, the solution was sterilized by autoclaving at 121°C under 15 psi for 20 minutes.

Antibiotics

Stocks of carbenicillin (100 mg/ml), kanamycin (100mg/ml), streptomycin (50mg/ml) spectinomycin (50mg/ml) were prepared by dissolving in filter sterilized distilled water. Rifampicin (50 mg/ml) was dissolved in DMSO. Antibiotic stocks were added to previously autoclaved media to final concentrations of 50 µg/ml for all antibiotics other than rifampicin which was used at a concentration of 25 µg/ml.

2.2   Bacteria and plants

Escherichia coli DH5α (New England Biolabs #C2988J) was used for maintenance of infectious clone plasmid constructs. *E. coli* DH10B (New England Biolabs # C3019I) was used for maintenance of constructs generated using the Gateway system. *E. coli* DB3.1 (Invitrogen 11782-018) was used to maintain donor and destination vectors for use with the Gateway system. Liquid cultures of *E. coli* harboring desired constructs were grown in liquid LB media supplemented with appropriate antibiotics by shaking at 220 rpm at 28°C (infectious clone constructs) and 37°C (all other constructs) for 16-18 hours.

Agrobacterium tumefaciens EHA105 (a gift from the laboratory of Dr. Rima Menassa, Agriculture and Agri-food Canada) was used to deliver infectious clone constructs and fluorescent tagged proteins and transient gene expression studies in plants. *A. tumefaciens* liquid cultures were grown in LB media at 220 rpm at 28°C for 16-18 hours.

2.3 Plant materials and growth conditions

2.3.1 Plant growth conditions

All plants were grown in a greenhouse with a day/night cycle of 16 hours (22°C)/8 hours (18°C) with an average relative humidity of 70%. All plants used in this study were potted with Pro-Mix BX Mycorrhizae amended soil. Arabidopsis (*Arabidopsis thaliana*; Columbia-0; TAIR accession # CS907) were sown on the soil surface and cold stratified for 2 days in the dark at 4°C and were then transferred into a growth chamber. Cucumber cv. 'Wisconsin' (OSC seeds #1620-PKT), squash cv. 'Buttercup' (OSC seeds #2255-PKT), and tobacco were grown in 3" pots. Tobacco seeds were sown on soil and grown for 4-6 weeks for transient gene expression studies, however plants were maintained for longer periods (up to 8 weeks) to test for symptom development and when infectious clones were used.

Seeds of cherry were collected from ripened drupes and were cleaned by mechanically removing the mesocarp and exocarp. The cleaned seeds were dried at room temperature for at least 24 hours. The seeds were then forced into dormancy by storing at 4°C for a period of no less than 3 months. Dormancy was broken by removing the endocarp and seeds were soaked in seed sterilization solution for 48 hours. The soaked seeds were rinsed four times with water and the seed coat was carefully removed before planting in 3" pots at a depth of 2 cm after approximately 4 weeks, seedlings were transplanted to 8" pots. These plants were maintained for 6-8 weeks and were examined three times per week for symptom development.

2.3.2 Field sample collection

Foliar tissues of cherry cv. Vista were collected from the Vineland research farm in Jordan, Ontario, during the months of June and July of 2014-2018. In order to adequately sample an orchard tree , approximately 4 newly emerging leaves were collected from three branches (a total of 12 leaves) and were pooled together. The pooled leaf samples were flash frozen in liquid nitrogen and stored at -80°C until future use. To

determine the in-field incidence of virus infection (**Section 3.1.4**), half of the cherry trees (42 of 92) at very other tree in a plot were selected for sampling.

2.4   Cloning procedures and construct design

2.4.1   Primer design

Primers compatible with the Gateway system (**Appendix 2**) were designed to amplify full length and truncated PDV protein coding sequences based on sequences obtained by NGS and primer walking. Gateway compatible primers were designed to amplify coding sequences of cherry host proteins based on sequences obtained from the Genome database for Rosaceae (Jung et al., 2019). Forward and reverse primers were designed to include 5' and 3' *att* sites, respectively. To amplify the genomic fragments of PDV for infectious clone construction, primers were designed with sequences complementary to the 5' and 3' termini of each RNA fragment. These primers also included sequences complementary to the backbone vector PCB301-d35sRZT which allows for the use of the Gibson assembly system (**Section 2.4.4**; Gibson et al., 2009). To obtain the complete sequence of viruses detected via NGS, primers were designed from the assembled contigs.

2.4.2   Polymerase chain reaction conditions

Amplification was performed using two polymerase enzymes. Phusion high fidelity DNA polymerase (New England Biolabs #M0530S) was used for sequencing and amplification of viral genomes and was used according to the manufacturer's specifications. For virus detection and bacterial colony PCR, the 2X *Taq* FroggaMix (Froggabio #FBTAQM) was used following the manufacturer's specifications. A standard PCR protocol was used (30 seconds denaturation 95°C, 30 seconds annealing at 54°C, extension 30 seconds/KB at 72°C. 25 cycles).

2.4.3   Plasmid DNA isolation and sequencing

Plasmid DNA was isolated from *E. coli* using two kits: the high speed plasmid extraction mini kit (Froggabio # PD300) was used for small-scale plasmid extractions, when large amounts of plasmid DNA (500 µl or more at approximately 1 µg µl^{-1}) were required, the Maxi Spin DNA plasmid kit (Geneaid # PME25) was used. Both kits were used following the manufacturer's specifications. To confirm the accuracy of construct sequences, samples were sent to Eurofins Genomics sequencing facility (Louisville, KY). Sequence results were analyzed using Lasergene (DNAstar, Version 16).

2.4.4   Cloning strategies

Three cloning strategies were used in this project: Traditional restriction enzyme ligation cloning, Gateway®, and Gibson assembly. Traditional cloning strategies were used with restriction enzymes, and ligating enzymes purchased from New England Biolabs. When using the Gateway system (Hartley et al., 2000), amplicons generated by PCR were recombined into pDonor221 (Invitrogen # 1236017) using the BP Clonase recombination reaction (Invitrogen # 11789020). These constructed entry vectors were sequenced to confirm the successful insertion, and to ensure no mutations were introduced by PCR. Confirmed entry constructs were then recombined into various destination vectors using LR Clonase (Invitrogen # 11791020) to generate various expression vectors. To determine subcellular localization of proteins, expression vectors pEarleyGate_101 and pEarleyGate_102 were utilized to create C-terminal fusions of yellow and cyan fluorescent proteins (YFP and CFP), respectively (Earley et al., 2006). For BiFC studies, expression vectors pEarleyGate_201-YN and pEarleyGate_202-YC, which are designed to only contain the N- and C-terminal halves of YFP, were used (Earley et al., 2006; Lu et al., 2010).

2.5   Bacterial transformation

E. coli chemically competent cells were prepared as described (Sambrook and Russell, 2006) and were transformed using Hanahan's method (Hanahan, 1983; Sambrook and Russell, 2006). *A. tumefaciens* electrocompetent cells were prepared as described

(Weigel and Glazebrook, 2006). Immediately after transformation, *E. coli* and *A. tumefaciens* cells were incubated in LB broth without antibiotics for 1 hour, and two hours, respectively. After incubation, bacterial cells were plated on selective media plates supplemented with antibiotics for selection and were incubated for 24 hours.

2.6   Small RNA extraction and next generation sequencing

Small RNAs (sRNA)s were extracted from the collected frozen foliar tissue using the mirPremier microRNA isolation kit (Sigma #SNC-10) according to manufacturer's specifications. sRNA libraries were constructed with the TruSeq small RNA sample prep kit (Illumina #RS-200-0012) according to manufacturer's instructions. Sequencing of the constructed sRNA libraries was carried out with the MiSeq Desktop Sequencer utilizing the MiSeq v2 reagent 50 cycle PE kit (Illumina #MS-102-2001). The raw results were processed through an online platform (Virtool, http://www.virtool.ca) to remove the sequences of ligated adapters and to remove reads homologous to the host cherry genome (Shirasawa et al., 2017), and to map the remaining clear reads against the Virtool reference list of viral genomes (version 1.4.0). The mapped reads were then aligned with the reference genomes and consensus sequences were obtained using CLC Genomics Workbench 11.0 (https://www.qiagenbioinformatics.com). The consensus sequences were analyzed with the basic local alignment search tool (BLAST) (Altschul et al., 1990) against both NCBI (https://blast.ncbi.nlm.nih.gov) and NCBI Virus databases (https://www.ncbi.nlm.nih.gov/labs/virus/vssi/#/).

2.7   RNA extraction

RNA was extracted from both woody and herbaceous hosts using two protocols, depending on the plant sample. A modified CTAB based method was used to extract RNA from foliar and vascular tissues of woody plants (Li et al., 2008). Briefly, 100 mg of plant tissue was added to a 2.0 ml microcentrifuge tube which contained a single copper ball bearing (Crosman corp. #0767), the samples were then flash frozen in liquid nitrogen. The tissues were homogenized using a tissue lyser II machine (Qiagen #85300) at a frequency

of 30 Hz, for 1 minute. The homogenate was resuspended and incubated in RNA extraction buffer which had been supplemented with 1% 2-mercaptoethanol for 15 minutes at 65°C. The incubated homogenate was then centrifuged at 10 000 x g for 5 minutes at 4°C to pellet the tissue debris. The protocol was modified by the addition of an acid phenol/chloroform extraction to facilitate the removal of proteins and lipids (Chomczynski and Sacchi, 1987). After centrifugation and transferring the clarified supernatant to a new microcentrifuge tube, equal volumes of acidic phenol solution (Sigma # P4682) and chloroform were added and the sample was again homogenized by vortexing. After centrifuging again, the aqueous (top) phase of the supernatant was transferred to a new 2.0 ml tube and an equal volume of chloroform/isoamyl alcohol (24:1; Sigma # C0549) was added prior to centrifuging. After centrifugation, the supernatant was transferred to a new 1.5 ml centrifuge tube and an equal volume of isopropanol was used to precipitate total nucleic acids. After centrifugation at 10 000 x g for an additional 15 minutes, the supernatant was removed, and the pellet was dissolved in 300 µl of DEPC treated water. RNA was precipitated by the addition of an equal volume of 4 M LiCl and storing at 4°C overnight. The RNA pellet was collected by centrifugation at 10 000 x g for 10 minutes and the supernatant was removed, the pellet was then resuspended in 50 µl of DEPC treated water for immediate use, or stored in 1 ml of 70% ethanol at -80°C. For extracting RNA from herbaceous plants, a plant specific total RNA mini kit (Geneaid # RP100) was used following the manufacturer's specifications.

2.8   Complementary DNA synthesis

After the extraction of RNA, complementary DNA (cDNA) was synthesized with provided random hexamer or oligodT primers using the superscript III cDNA synthesis system (Invitrogen # 18080051) following the manufacturer's specifications. The concentration and quality of RNA was determined using a nanodrop 2000c spectrophotometer (ThermoFisher # ND-2000) and the nanodrop 2000c software version 1.5.

2.9 Virus detection by RT-PCR and DAS-ELISA

cDNA was used as template for PCR based detection which was performed using the 2x Froggamix PCR master mix (Froggabio # FBTAQM) using virus specific detection primers (**Appendix 2**) following the manufacturer's specifications. Double antibody sandwhich (DAS) ELISA was performed using the PDV ELISA kit to detect the viral CP of PDV (Agdia # SRA 98700) following the manufacturer's specifications. Results from DAS-ELISA were analyzed using a FisherScientific BioTek Epoch 2 microplate reader.

2.10 Genome sequencing of detected viruses

Based on the sequence of viral genomes identified by NGS, primers were designed to amply cDNAs of the near-full length of the viral genomes by RT-PCR (**Figure 5A**). The 5' and 3' genomic end sequences of the viruses were obtained by rapid amplification of cDNA ends (RACE) using 5' and 3' RACE kits (**Figure 5B, C**; ThermoFisher # 18374058 and 18373019) according to the manufacturer's specifications. All resulting PCR amplicons were ligated into the PCR zero blunt vector (ThermoFisher #K270020) and then transformed into *E. coli*. Plasmid DNA was extracted and the sequence was determined via Sanger sequencing (Eurofins Genomics, Louisville, KY). The sequence of large PCR-amplicons was determined by primer walking (**Appendix 2; Figure 5a**).

2.11 Extraction of the proteomes of cherry and cucumber

Total proteins were extracted from cherry and cucumber following a protocol described previously (Marx et al., 2016). First, 100 mg of plant tissue was frozen and homogenized (**Section 2.7**). The homogenate was resuspended and incubated in ice cold protein extraction buffer, after vortexing, the samples were subjected to probe sonication for a total of two minutes using repeated cycles of 10 seconds on and 15 seconds off while the tubes were kept on ice. After sonication, the samples were centrifuged at 1000 x g for 5 minutes at 4°C. After centrifugation, the supernatant was transferred to a new 2.0 ml tube prior to protein precipitation.

Proteins were precipitated by adding an equal volume of chloroform. Three

Figure 5 Strategy used to sequence viral genomes

To obtain the full genome sequences of the viruses detected by NGS, a PCR based strategy was used.

A   Using sequences obtained from NGS, primer pairs were designed (**Appendix 2**) to amplify viral genomes as multiple fragments to span the entire length of the viral genome. All primer pairs were designed to create sequence overlap between various fragments (coloured ends). After amplification, the same PCR primers were used for Sanger sequencing. Primer names in this diagram are generic, virus specific sequencing primers contain the virus abbreviation (ie. CVAsqF1).

B   To ensure the full genome sequences were determined the 5' end was sequenced using the 5' RACE system using a nested amplification approach. The first amplification used the supplied universal adapter primer (AUAP) in combination with the first gene specific primer (5prGSP1f). The PCR product from the first amplification (green dashed line) was used as template for the second amplification. For the second amplification, the second gene specific primer (5prGSP2) was used in combination with the AUAP primer, this amplicon (red dashed line) was sequenced using the same primers to obtain the sequence of the 5' end.

C   The sequence of the 3' UTR was obtained using the 3' RACE system using a nested amplification approach. Firstly, poly-A polymerase is used to polyadenylate the tail of isolated RNA fragments. The first amplification uses the supplied poly-T adapter primer (DTAP) in combination with the first gene specific primer (3prGSP1). The PCR product from the first amplification (green dashed line) was used as template for the second amplification. The second amplification involved use of the second gene specific primer (3prGSP2) was used in combination with the DTAP primer, this amplicon (red dashed line) was sequenced using the same primers to obtain the sequence of the 3' end.

A

VirsqF1 + R1

VirsqF2 + R2

VirsqF3 + R3

VirsqF4 + R4

VirsqF5 + R5

VirsqF6 + R6

VirsqF7 + R7

B

AUAP   5prGSP1

5prGSP2

C

3prGSP1   DTAP

3prGSP2
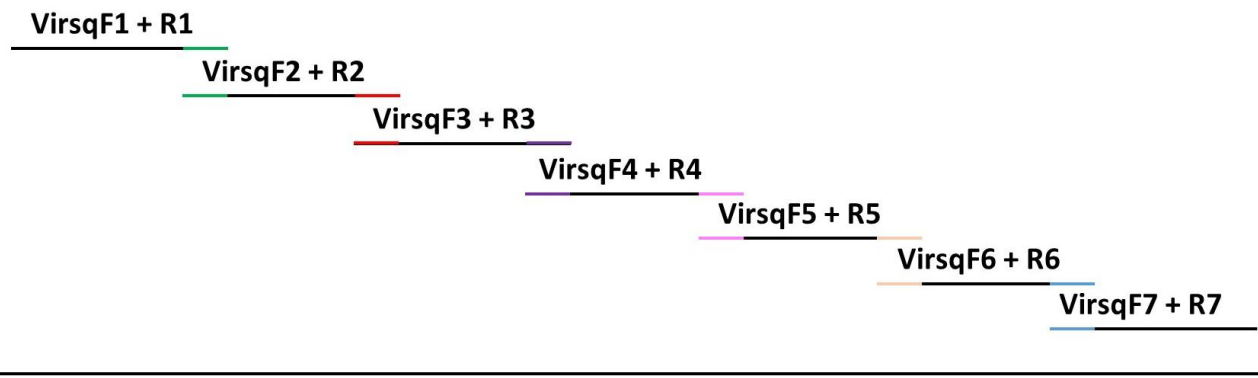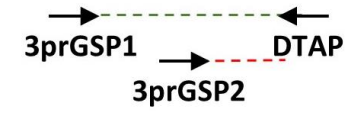
volumes of distilled water were added, this mixture was centrifuged for 5 minutes at 3000 x g at 4˚C. The top aqueous phase was removed and discarded, three volumes of methanol were added and the sample was centrifuged for 5 minutes. After centrifugation, the protein pellet was transferred to a new 2.0 ml microcentrifuge tube and the pellet was washed three times with pre-chilled 80% acetone. The pellets were dried at room temperature for 20 minutes and resuspended in 300 μl of lysis buffer and the pellets were resuspended by probe sonication as described above. Proteins were quantified by Bradford assay (Sigma # B6916-500ML) following the manufacturer's specifications.

2.12   Protein preparation, LC-MS/MS and data analysis

After quantification, 75 μg of protein were resuspended in 200 μl of lysis buffer and proteins were reduced by the addition of 5 mM dithiothreitol (DTT) and incubation of 58˚C for 40 minutes. Proteins were then alkylated with 15 mM iodoacetamide (Sigma # I1149) and incubated in the dark for 40 minutes at room temperature. Alkylation was quenched by addition of 5mM DTT and incubated at room temperature for an additional 40 minutes. To digest the proteins endoproteinase Lys-C (Sigma # 11420429001) was added at a ratio of 1:200 (enzyme:protein) and incubated for 2.5 hours at 37˚C. Prior to the second digestion, 50 mM Tris, pH 7.0 and 5 mM $CaCl_2$ was added to dilute the concentration of urea to 1.5 M. The samples were then digested by the addition of trypsin protease (sigma # T0303) at a ratio of 1:50 (enzyme:protein) and were incubated overnight at 37˚C.

The digestion was quenched by adjusting the pH to ~2 using 3 mL of 0.1% trifluoroacetic acid. To remove salts, the samples were then passed through Waters Oasis HLB (1 ml, 30 mg sorbent) vacuum cartridges (Sigma # WAT094225), which were activated with methanol and pre-conditioned with filter sterilized distilled water containing 0.1% formic acid. The cartridges were dried under vacuum for five minutes, the samples were then eluted into new 1.5 ml microcentrifuge tubes by addition of 800 μl of 40% acetonitrile. The samples were subsequently dried by vacuum centrifugation. The

samples were then reconstituted in 75 µl of 0.1% formic acid and transferred to an HPLC vial (Sigma # C4011-LV2W).

The digested peptides were separated on an Easy-nLC 1000 nano-flow HPLC system fitted with a 2 cm Acclaim C18 PepMap[TM] trap column and a 75 µm x 25 cm Acclaim C18 PepMap[TM] analytical column. The flow rate was held at 300 nL min^{-1} throughout the run and 10 µL of the digest was injected. The mobile phase A (97%) (LC/MS Optima water, 0.1% formic acid) was first decreased to 90% over four minutes. Peptides were then eluted with a linear gradient of 10 to 40% mobile phase B (LC/MS Optima acetonitrile, 0.1% formic acid) over 150 minutes, followed by 40–90% over 10 minutes, and maintained constant for an additional 10 minutes. Each sample was then analyzed using a top 10, data-dependent acquisition method in the mass range of *m/z* 300–2000 using a Thermo Q-Exactive Orbitrap mass spectrometer coupled to an Agilent 1290 HPLC system. The nanospray voltage was set at 2.4 kV, capillary temperature at 275°C, and the S-lens radio frequency (RF) level at 70. The full scan was acquired at 70,000 resolution with an automatic gain control (AGC) of 1×10^6 and a maximum injection time (IT) of 250 milliseconds. The MS/MS scans were acquired at 17500 resolution, AGC of 5×10^5, maximum IT of 110 milliseconds, intensity threshold of 1×10^5, normalized collision energy of 27 and an isolation window of 1.7 m/z. Unassigned, singly charged, and >4 charged peptides were not selected for MS/MS, and a 30 second dynamic exclusion was used.

For protein identification, proteomes of cherry and cucumber were downloaded from the Genome Database for *Rosaceae* (GDR) and Uniprot, respectively (Uniprot, 2018; Jung et al., 2019). The Thermo® raw files were searched against the respective proteomes using Maxquant v1.6.10.43 (Cox et al., 2014) using label-free quantification with default settings. LysC and trypsin were selected as enzymes with a maximum of three missed cleavages. Carbamidomethylation was selected as the fixed modification and oxidation of methionine residues were set as the variable modification. The false discovery rate (FDR) for peptide and protein identification was set to 1% and the minimum peptide length to 20 amino acids (aa). Proteins that were identified by MS/MS in a minimum of three biological samples were retained. The MaxLFQ algorithm for label-free quantification

(LFQ), and the "matching between runs" feature was enabled (Cox et al., 2014). Protein levels were estimated in Maxquant using intensity-based absolute quantification (iBAQ) (Schwanhäusser et al., 2011). The data were imported into Perseus software for LFQ comparisons and missing values were imputed with default settings (Tyanova et al., 2016). Only protein groups with measured LFQ values in 2 of the 3 sample replicates were retained. The post-hoc Benjamini-Hochberg (BH; Benjamini and Hochberg, 1995) FDR correction was used to calculate P values (unpaired t-test, $P > 0.05$).

The identified protein groups were then submitted to the Proteomics IDEntification Database (PRIDE; https://www.ebi.ac.uk/pride/).

2.13 Agroinfiltration of herbaceous and woody host plants

Agroinfiltration was performed following previously developed methods (Cui et al., 2013; Cui and Wang, 2016). Cultures of *A. tumefaciens* harboring constructs corresponding to the infectious clone of PDV were infiltrated into fully expanded true leaves of five week old tobacco plants, fully expanded cotyledons of cucumber, expanded cotyledons of squash, expanded rosette leaves of Arabidopsis or expanded true leaves of ten to twelve day old seedlings of cherry. Cultures of *A. tumefaciens* harboring the infectious clone constructs were grown in antibiotic supplemented LB at 28°C until an optical density (OD_{600}) of $0.8 - 1.0$. Liquid cultures were then centrifuged at 4000 rpm and washed twice with agroinfiltration buffer. The washed *A. tumefaciens* were resuspended in agroinfiltration buffer at a final OD_{600} of 0.5 and were incubated at room temperature for at least two hours. Immediately before infiltration, equal volumes of the cultures of *A. tumefaciens* were mixed and amended with 0.03% Tween-20. Herbaceous plants were infiltrated by injecting approximately 200 µl of culture using a needleless syringe into the abaxial side of leaves or cotyledons (Sigma # Z192090). After infiltration, the plants were covered with a transparent plastic cover to maintain a high level of humidity for 24 hours and were grown as described (**Section 2.3.1**).

To inoculate woody hosts, the 10-12 day old plants were removed from soil and the whole plant was washed with sterile distilled water to remove all soil particles. The

cotyledons, and stem were wounded several times using a sterile 26 gauge needle (Sigma # Z192392). The wounded seedlings were submerged in the mixture of *A. tumefaciens* cultures and subsequently subjected to vacuum infiltration for 5 minutes at -70 kPa. The pressure of the vacuum chamber was increased to ambient pressure over a period of one minute. The Infiltrated plants were then transplanted into new pots, covered with a transparent plastic cover to maintain high humidity for 48 hours and were maintained using standard lighting and temperature conditions (**Section 2.3.1**)

2.14   Isolation of cucumber protoplasts

To isolate protoplasts from cucumber previously published protocols were used with some modifications (Huang et al., 2013; Wu et al., 2009). Fully expanded cotyledons of cucumber were collected approximately 8 days after seeds were planted. The frozen protoplast enzyme solution was thawed in a 55°C water bath for 10 minutes and was stored at room temperature. Scotch® Magic™ Tape (3M # 7000137297) was used to separate the lower epidermis from the underside of cotyledons to expose the mesophyll cells. The cotyledons were then placed in a plastic weigh boat (Sigma # HS1425B) and were covered with the enzyme solution. The weigh boat containing cotyledons submerged in the enzyme solution was transferred to a benchtop vacuum desiccator (Sigma # Z119024) and full vacuum was applied for 1 minute, after closing the vacuum valve the cotyledons remained under vacuum for an additional 5 minutes. The desiccator valve was slowly opened to release the vacuum and cotyledons were kept in the enzyme solution in the dark for 3 hours. An equal volume of W5 solution was added to the weigh boat and a plastic pipette was used to gently wash away mesophyll protoplasts from the partially digested cotyledons. The diluted enzymolysate was gently mixed and filtered through a nylon membrane (200 mesh; Sigma # Z290807). The filtrate was centrifuged for 2 minutes at 80 x g. The supernatant was discarded, and the protoplasts were washed again with 10 ml of W5. After washing, the protoplasts were resuspended in fresh W5 at a concentration of $2x10^6$ protoplasts/ml.

2.15   Transfection of cucumber protoplasts

Isolated protoplasts were transfected using previously published protocols with some modifications (Huang et al., 2013; Wu et al., 2009). Isolated protoplasts were kept on ice for 30 minutes so they can settle to the bottom of the centrifuge tube. The supernatant was discarded, and protoplasts were resuspended in an equal volume of protoplast MMG buffer. 5 ug of plasmid DNA and 100 µl of resuspended protoplasts were combined and gently mixed. An equal volume of 20% PEG4000-Ca^{2+} (prepared immediately before use) was added and mixed very gently by rotating the centrifuge tube, not by inversion. The protoplasts were transfected for 30 minutes in the dark at room temperature. 600 µl of W5 solution was added to stop the transfection. Mixtures were centrifuged at 80 x g for 2 minutes and protoplasts were washed three times with 2 ml of W5. After the final wash, protoplasts were gently resuspended in 500 µl of W5 solution. The transfected protoplasts were incubated in the dark for 18-24 hours. After incubation the protoplasts were visualized with the laser scanning confocal microscope.

2.16   Mechanical inoculation of herbaceous hosts

Approximately 1 g of infected plant material was ground in the presence of 3 ml of mechanical inoculation buffer using a mortar and pestle, the homogenate was then decanted into a glass beaker or culture tube which was then placed on ice. The cotyledons of herbaceous hosts were inoculated when they were fully expanded (approximately 8 days after seeds were sown). The cotyledons were moistened by misting with water, and a small amount of carborundum powder was sprinkled on top of the cotyledons. The plants were inoculated by dipping a gloved finger into the homogenate and then gently rub the homogenate onto the cotyledon in a single direction several times with very light pressure. After all plants were inoculated, the cotyledons were gently misted with water to remove excess homogenate. The inoculated plants were then covered with a plastic bag to maintain an environment with high humidity and were kept in the dark overnight. After the overnight incubation, the inoculated plants were maintained using standard conditions (**Section 2.3.1)**

2.17   Confocal microscopy

Confocal microscopy was performed using an Olympus LSM FV 1200 microscope. Images were acquired with a 60x water objective lens. Fluorescent tagged proteins were visualized in tobacco epidermal leaf cells 2 days after agroinfiltration. Transfected protoplasts were visualized 18-24 hours post transfection. Z-stack images were used to visualize fluorescent tagged proteins in cucumber protoplasts. All images were captured digitally and processed using Olympus Fluoview Software (v4.2).

2.18   Software and web-servers

To perform *in silico* analyses on the MP of PDV several prediction servers were used. The Phyre2 server (http://www.sbg.bio.ic.ac.uk/~phyre2/html/page.cgi?id=index; Kelley et al., 2015) was used to predict the secondary structure of the MP. The I-TASSER server (https://zhanglab.ccmb.med.umich.edu/I-TASSER/; Zhang, 2008) was used as a second means of structure prediction, only structural elements predicted with high confidence by both servers were included in this work. Additionally, the PSIPRED server (http://bioinf.cs.ucl.ac.uk/psipred/; Buchan and Jones, 2019) was used to study the structural organization of the MP and to predict differentially localized domains of this protein (ie. Cytosolic, transmembrane and extracellular). To examine the sequenced viruses, the HHPRED server (https://toolkit.tuebingen.mpg.de/tools/hhpred; Söding et al., 2005) was used to search for functional domains of the sequenced viral proteins.

For sequence alignment and evaluation of Sanger sequencing results, the DNAstar Lasergene (Version 16) software was used (DNASTAR, 2020). Alignment of protein sequences was performed using MEGA (Version 7;Kumar et al., 2016). The BOXSHADE server (https://embnet.vital-it.ch/software/BOX_form.html; Hofmann and Baron, 1999) was used to create black and white figures of sequence alignments which were conducted using MEGA. The gProfiler server (https://biit.cs.ut.ee/gprofiler/gost; Raudvere *et al.* 2019) to perform gene ontology (GO) analysis.

3. Results

3.1 Next generation sequencing leads to identification of four viruses infecting cherry in Ontario

Long-term maintenance of fruit orchards often results in the accumulation of viral pathogens (**Section 1.1**). Indeed, symptoms were observed on leaves of sweet cherry which were typical of viral infection (**Figure 1D, E, F**), and in the past, PNRSV has been detected in the region of Jordan, Ontario (Cui et al., 2012a, b). NGS was performed to determine if other viral pathogens were infecting cherry as the isolates of PNRSV previously characterized are not associated with any disease symptoms, and latent in cherry (Cui et al., 2013). This study was initiated by construction and sequencing of sRNA libraries isolated from separate composite samples consisting of asymptomatic or symptomatic foliar tissues collected from four separate cherry trees. NGS yielded a total of 5,380,196 raw reads. After the removal of ligated adapter sequences, a total of 4,733,804 clear reads longer than 22 nucleotides (nt) in length were obtained. After host genome subtraction, 168,753 clear reads remained and were mapped against a set of plant virus reference genomes (Brister et al., 2014). The viruses with the greatest degree of genome coverage and depth were: PNRSV, PDV, *Cherry virus A* (CVA), and *Little cherry virus 1* (LChV1; **Table 2**). Since PNRSV has been well studied in this region (Cui et al., 2012a, b, 2013), it was not investigated further.

3.1.1 Cloning and sequencing the full-length genome of *CVA*

NGS and subsequent analyses detected CVA from cherry trees in Ontario. This was the first report of CVA in Ontario. CVA belongs to the genus *Capillovirus* in the *Betaflexivirideae* (Noorani et al., 2013). This virus was first described from cherry in Germany (Jelkmann, 1995). Since then, CVA has been reported all over the world. To better understand the genetic diversity of CVA, the full-length viral genome sequence was determined and *in silico* analyses were used to further characterize this virus.

The genome of CVA is comprised of a ssRNA (+) molecule of approximately 7.3 kb in length and encodes a polyprotein, an MP and a CP. In *Prunus*, CVA not associated with

Table 2 Viruses identified in cherry using NGS

Detected Virus	Reference Isolate[a]	Accession[b]	Length (nt)[c]	Coverage (%)[d]
CVA	Unnamed	NC_003689	7383	95.2
LChV1	Ponferrada	KX192367	16933	83.7
PDV RNA 1	ch 137	NC_008039	3374	73.8
PDV RNA 2	ch 137	NC_008038	2129	88.1
PDV RNA 3	ch 137	NC_008037	2593	84
PNRSV RNA 1	Unnamed	NC_004362	3332	44.6
PNRSV RNA 2	Unnamed	NC_004363	2591	95
PNRSV RNA 3	Unnamed	NC_004364	1957	67.5

[a] Name of reference isolate

[b] Virus genomes were obtained from the NCBI GenBank reference database

[c] Sequence length of reference isolate

[d] Percent similarity of sequenced sRNA to reference sequence

any disease complexes and is suspected to infect in a latent manner (Kesanakurti et al., 2017). First, the 5' and 3' termini were determined by RACE based PCR. For RACE-PCR, conventional RT-PCR and primer walking, virus specific primers were designed based on NGS results (**Appendix 2**). The full length CVA genome of two Niagara isolates was amplified and sequenced and the resulting sequences were deposited to GenBank (GenBank accession nos. MF062118 and MF062119). The genome of CVA sequenced in this study was determined to be 7,434 nt long (**Figure 6**), sharing 99% nt sequence identity with an isolate found previously in British Columbia, Canada (GenBank accession no. KY510911). The 5' and 3' UTRs are 106 and 298 nt in length, respectively. The first ORF encodes a polyprotein of 2342 aa in length. Analyses using the HHpred web server (Söding et al., 2005) shows that this polyprotein has several functional domains: from the N-terminus: methyltransferase, protease (Prot), helicase, and RdRp. Two sgRNAs are predicted to encode the MP and CP. The MP and CP encoded by the two sgRNA are 463 aa and 443 aa in length, respectively (**Table 3**).

3.1.2 Cloning and sequencing the full length-genome of Little Cherry Virus 1

Another virus identified by NGS was LChV1 is a member of the *Velarivirus* genus within the *Closteroviridae* (Fuchs et al., 2020). LChV1 is one of the causal agents of little cherry disease (LCD) which has caused decline of tree health and fruit yield in the Western United States of America and in Western Canada (Candresse et al., 2013; Galinato et al., 2019). This detection presents the first documented occurrence of this virus in the province of Ontario. The full genome sequence of LChV1 was sequenced and features of the genome were further characterized using *in silico* methods to better understand the sequence diversity of this virus and its genome. LChV1 has a ssRNA(+) genome of approximately 17 kb in length and is predicted to encode nine proteins (**Figure 7**). The full genome of LChV1 was amplified by RACE and RT-PCR using primers based on sequences obtained in the NGS study (**Appendix 2**). The amplicons were then sequenced via primer walking and the genomic sequence of the Niagara LChV1 isolate was deposited

Figure 6 Genomic structure of CVA

Schematic representation of the genome structure of CVA. CVA has a ssRNA(+) genome with an uncapped 5' end and a polyadenylated tail at the 3' end. A polyprotein containing methyltransferase, papain like protease, helicase and RNA-dependent RNA polymerase domains is encoded directly from the viral RNA. The MP and CP are encoded by sub-genomic RNA fragments.

Genomic RNA (7434 bp)

5' Met Pro Hel RdRp 3' AAAAAAA(n)

Polyprotein (2342 aa)

MP (463 aa) AAAAAAA(n)

CP (443 aa) AAAAAAA(n)
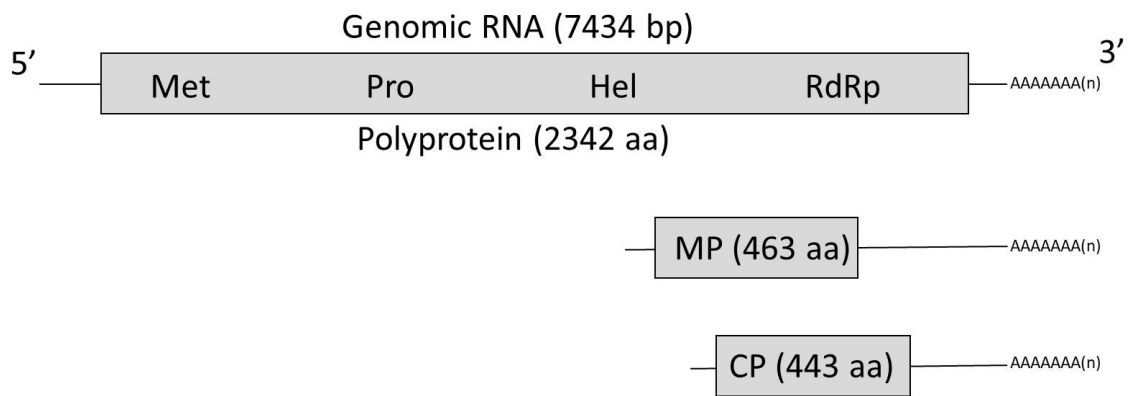
Table 3 Features of the sequenced genome of CVA

nt position	Description[a]	Protein ID[b]	HHpred Hit	% probability	E-value[c]
1-106	5'UTR	-	-	-	-
107-7135	ORF1	AWW17058.1	-	-	-
-	Met	-	PF01660.17	100	3.70E-34
-	Prot	-	5LW5	98.4	3.20E-06
-	Hel	-	3VKW_A	99.83	1.20E-22
-	RdRp	-	PF00978.21	99.93	8.90E-28
5452-6843	MP	AWW17059.1	PF01107.18	99.97	9.30E-30
5516-6843	CP	AWW17060.1	PF05892.11	100	3.70E-36
7136-7434	3'UTR	-	-	-	-

[a] UTR: untranslated region, ORF: open reading frame, Met: methyltransferase domain, Prot: protease domain, Hel: helicase domain, RdRp: RNA dependent RNA polymerase, MP: movement protein, CP: coat protein

[b] Genbank protein identifiers were used in this study

[c] E-value: expected number of false positives per database search which scores the same or better than the sequence match

Figure 7 Genomic structure of LChV1

The genome of LChV1 is a ssRNA(+) of about 17 kb which is predicted to have a methylated cap at the 5' end (Katsiani et al., 2015), the 3' UTR lacks a poly-A tail. A polyprotein is directly translated from the genomic RNA and has Prot, Met, and Hel protein domains as predicted by HHpred. The RdRp is translated by ribosomal frameshift, and remaining proteins are translated via sgRNAs (Katsiani et al., 2018).

Genomic RNA (16934 bp)
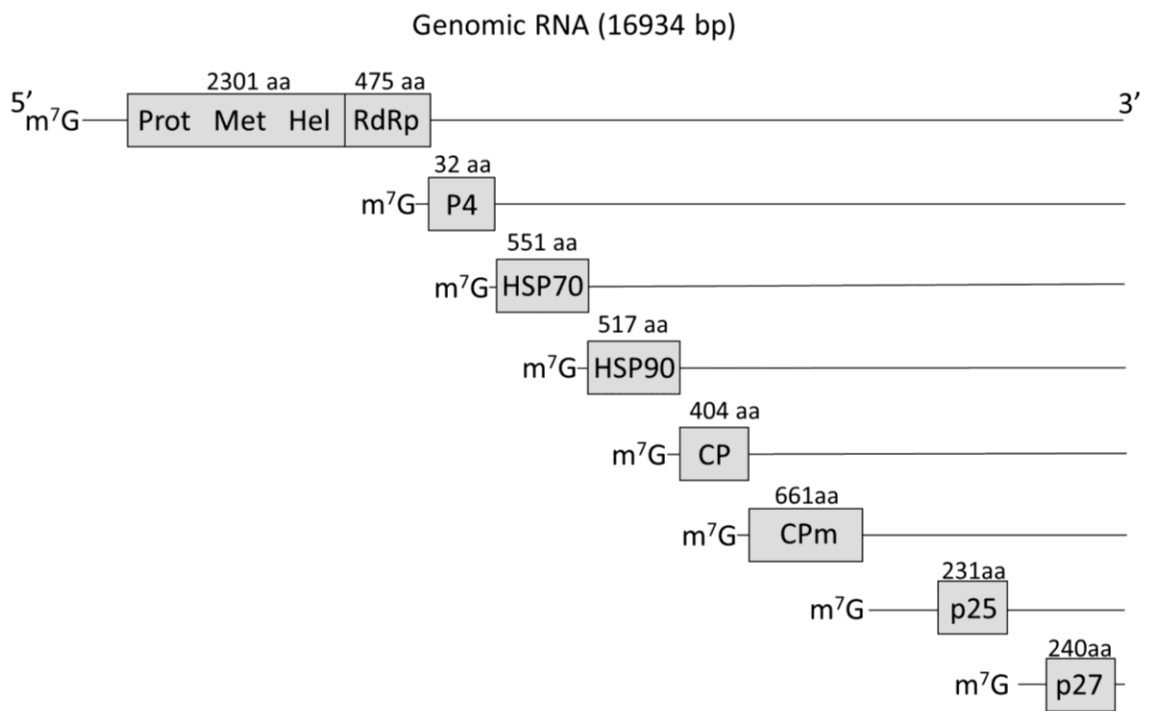
Table 4 Features of the sequenced genome of LChV1

nt position	Description[a]	Protein ID[b]	HHpred Hit	% probability	E-value[c]
1-77	5' UTR	-	-	-	-
78-6983	Polyprotein	QHU23861.1	-	-	-
-	Rep	-	3VKW_A	100	1.40E-34
-	Met	-	PF01660.17	99.95	3.60E-32
-	Hel	-	6JIM_B	99.73	1.50E-20
7072-8499	RdRp	QHU23862.1	PF00978.21	100	2.40E-57
8504-8599	ORF3 P4 (DUF)	QHU23863.1	PF06803.12	77.42	4.04E+02
8604-10259	HSP70	QHU23864.1	5TKY_B	100	4.60E-59
10431-11984	ORF5 P61 (HSP90)	QHU23865.1	PF03225.14	100	1.60E-83
12064-13278	ORF6 (CP)	QHU23866.1	PF01785.17	100	2.90E-33
13284-15269	ORF7 (CPm)	QHU23867.1	PF03225.14	96.9	4.60E-05
15274-15969	ORF8 P25	QHU23868.1	3NRK_A	51.13	5.70E+01
16006-16728	ORF9 P27	QHU23869.1	3M2P_C	37.4	1.80E+02
16729-16934	3'UTR	-	-	-	-

[a] UTR: untranslated region, Rep: replicase domain, Met: methyltransferase domain, Hel: helicase domain, RdRp: RNA dependent RNA polymerase, ORF: open reading frame, DUF: domain with unknown function, HSP: heat shock protein, P61: actin dependent transport protein,CP: coat protein, CPm: minor coat protein, P25,P27: uncharacterized proteins

[b] Genbank protein identifiers were used in this study

[c] E-value: expected number of false positives per database search which scores the same or better than the sequence identity %

into GenBank (accession no. MN508820). The Niagara isolate is 16934 nt in length and shares 98% sequence identity with a Spanish isolate (GenBank accession no. KX192367). The 5' and 3' UTRs of LChV1 are 77 and 206 nt in length, respectively. Protein structure prediction using the HHpred server (Söding et al., 2005) identified functional protein domains and several ORFs in the sequence of this isolate. The first two ORFs are predicted to be directly translated using the viral genomic RNA (Candresse et al., 2013). ORF1 appears to encode a polyprotein contains domains with significant matches to Met, Rep and Hel and the second ORF encodes a viral RdRp (**Figure 7; table 4**). Previous studies have shown members of the *Closteroviridae* adopt a sgRNA strategy for the remaining ORFs (Dolja and Koonin, 2013). ORF3 encodes a hypothetical protein p4 and the function of this protein is still unknown. ORF4 and ORF5 each encode a heat shock protein: 70 (HSP70) and HSP90, respectively. LChV1 encodes two CPs which form the virion, the major CP encoded by the ORF6 and the minor CP (CPm) encoded by ORF7. The last two ORFs proximal to the 3' end of LChV1, ORF8 and ORF9 encode p25 and p27, respectively two proteins with unknown functions (**Figure 7; Table 4**; Fuchs *et al.* 2020).

3.1.3 Cloning and sequencing the full-length genome of PDV

PDV is a member of the *Ilarvirus* genus and has a genome comprised of three separate ssRNA(+) components (**Section 1.3.1; Figure 8**). All three genomic components of PDV were amplified using primers designed from sequences obtained in the NGS study (**Appendix 2**). The full-length sequence of all three RNA fragments, and thus the complete viral genome, were obtained by RACE-PCR and primer walking and was deposited into GenBank with accession nos. MK522387, MK522388 and MK560342). The sequence of RNA1 is 3374 nt in length and shares 96% sequence identity with an isolate from Slovakia (GenBank accession no. MF078478). This genomic RNA has a 5' UTR of 38 nt in length and has a single ORF which is 3168 nt long encoding the P1 protein. Analysis using the HHpred server (Söding et al., 2005) indicates P1 contains a methyltransferase and a helicase domain **(Figure 8; Table 5)**. The 3' UTR of RNA1 is 169 nt in length and possesses four

Figure 8 Genome structure of PDV

Each genomic ssRNA(+) fragment is labelled with the nt length shown in parentheses to the left of the illustrated fragment. RNA fragments are shown as black lines with grey boxes showing encoded proteins. The aa lengths of each protein are shown in parentheses. RNA 1 encodes the replicase protein (P1). RNA 2 encodes the RdRp (P2). RNA 3 directly encodes the MP, a sub-genomic promoter leads to transcription of sgRNA 4 which encodes the CP. Each genomic segment has a 5' m^{7}G cap and a 3' UTR which can form complex secondary structures.

m^{7}G: 5'-7-methyl-G cap; ល្ងាច: 3' UTR secondary structure; aa: amino acids; bp: base pair; P1: replicase protein; P2: RNA dependent RNA polymerase (RdRp); MP: movement protein; CP : coat protein

ORF 1

RNA 1 (3374 bp) 5′ m⁷G — P1 (Rep 1055 aa) — 3′

ORF 2a

RNA 2 (2596 bp) 5′ m⁷G — P2 (RdRp 788 aa) — 3′

ORF 3a

RNA 3 (2296 bp) 5′ m⁷G — MP (293 aa) — 3′

ORF 3b

sgRNA 4 (986 bp) 5′ m⁷G — CP (218 aa) — 3′
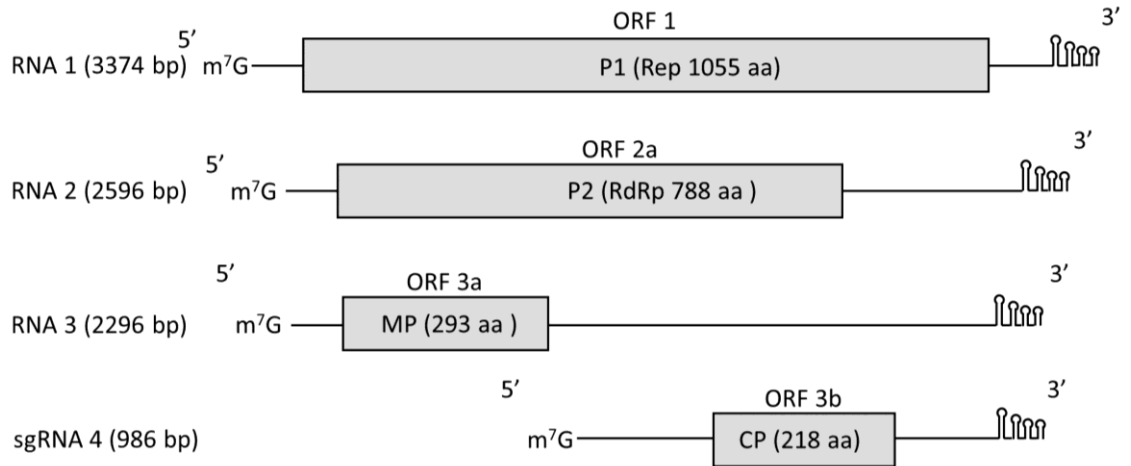
Table 5 Features of the sequenced genome of PDV

nt position	Description[a]	Protein ID[b]	HHpred Hit	% probability	E-value[c]
PDV RNA 1					
1-38	5'UTR	-	-	-	-
39-3206	P1	QGA70955.1	-	-	-
-	Rep	-	3VKW_A	100	3.20E-42
-	Met	-	PF01660.17	100	3.10E-35
-	Hel	-	6JIM_B	99.91	1.40E-25
-	DNA Binding	-	4B3F_X	99.89	3.10E-25
3207-3375	3'UTR	-	-	-	-
PDV RNA 2					
1-33	5'UTR	-	-	-	-
34-2400	P2	QGA70956.1	-	-	-
-	RdRp	-	PF00978.21	100	2.20E-52
2401-2593	3'UTR	-	-	-	-
PDV RNA 3					
1-428	5'UTR	-	-	-	-
429-1310	MP	QGA72060.1	PF01573.16	100	1.60E-75
1382-2038	CP	QGA72061.1	PF01787.16	100	5.00E-65
2039-2296	3'UTR	-	-	-	-

[a] UTR: untranslated region, Rep: replicase domain, Met: methyltransferase domain, Hel: helicase domain, RdRp: RNA dependent RNA polymerase, MP: movement protein, CP: coat protein

[b] Genbank protein identifiers were used in this study

[c] E-value: expected number of false positives per database search which scores the same or better than the sequence identity %

AUGC repeats which are predicted to form complex secondary structures involved in the viral infection cycle (**Section 1.4.2; Figure 9A**).

The RNA2 of PDV is 2596 nt in length with 95% sequence identity to an isolate of PDV identified in the United States (GenBank accession no. AF277662). This RNA has a 5' UTR of 33 nt in length, and the single ORF which is 2367 nt long and encodes the P2 protein (**Figure 8**). Using HHpred (Söding et al., 2005), a domain with characteristics of a viral RdRp was identified (**Figure 8; Table 5**). The 3' UTR of this gRNA is 192 nt in length with a series of AUGC repeats likely involved in the formation of alternate RNA structures (**Figure 9B**).

The RNA 3 of PDV is 2296 nt in length sharing 91% sequence similarity with an isolate sequenced in the United States (GenBank accession no. L28145). The 5' UTR of RNA3 is 428 nt in length. ORF3a, which encodes the viral MP has a length of 879 nt. The RNA3 also contains a region downstream of ORF3a with a high A/T composition (66%). This region resembles a sub-genomic promoter to allow for the transcription of a sgRNA molecule sgRNA4 (**Figure 8**) which is 986 nt long and codes for ORF3b. This 654nt ORF encodes the CP, in which the highly conserved RNA binding motif KPTARSQNFA was easily identified (**Section 1.4.2**). Some ilarviruses have a second RNA binding motif in their CPs (which was not found in the CP of PDV. The 3' UTR of sgRNA4 is 257 nt in length and contains 4 AUGC repeats likely permitting the formation of alternate RNA structures (**Figure 9C**).

3.1.4   The incidence of viral infections in the field

Knowledge of the prevalence of viral pathogens, or the incidence of viral infection may help growers to select and implement management of strategies (**Section 1.7**). To estimate the incidence of infection of these viruses, foliar tissue samples were collected from every other tree (46 of 92) of a cherry plot on the research farm. These samples were subjected to RNA purification. Primers specific to CVA, PDV and LChV1 were used for virus detection (**Appendix 2**). RT-PCR of the purified RNA samples was performed for virus detection. None of the primer pairs generated non-specific or off-target amplicons

Figure 9 The 3' termini of PDV RNAs potentially form secondary structures

(A-C) The 3' terminal 94 nt sequences of all the three PDV RNAs contain AUGC repeats flanking the stems of four hairpin loops (L1-L4). Such secondary structures of the 3' terminus are predicted to be involved in viral replication, mediated by the binding of CP, its exact role is a subject of debate. The portion of 3' UTRs containing the AUGC repeats are nearly identical between all 3 RNA fragments, two nucleotides differ in the UTR of RNA1 (shown in green). Bases shown in red are suspected to be base-paired while the 3' UTR is in the pseudoknot formation. The numbers show the nucleotide initiation of these regions in the genome of PDV.
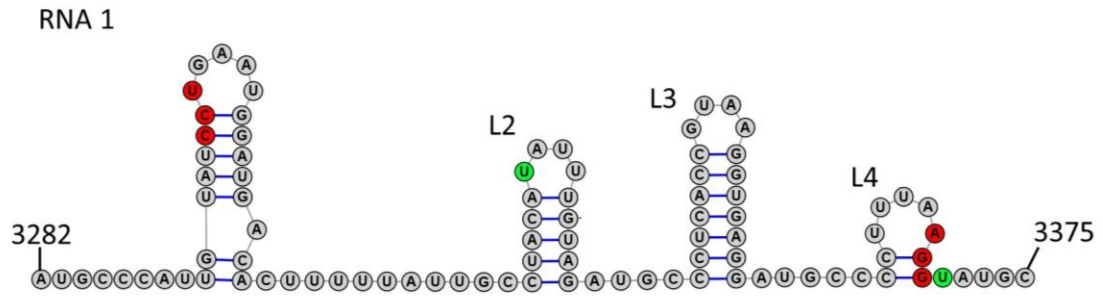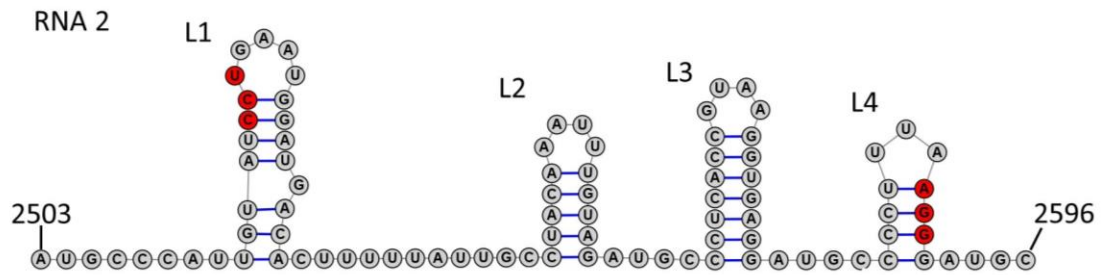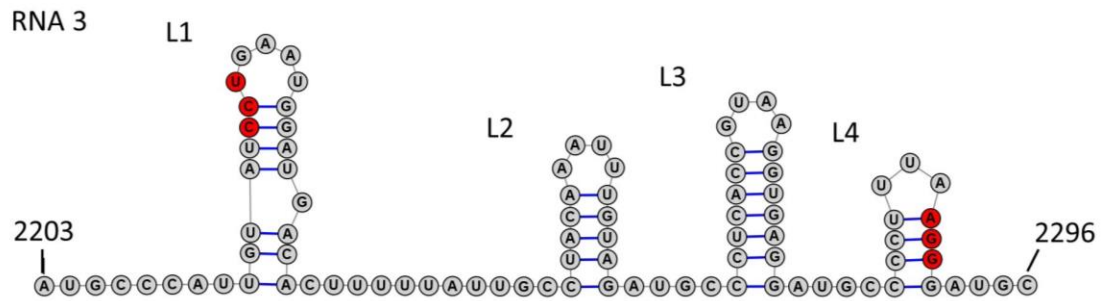
(**Figure 10A**). Of the sampled trees, 30 (65%) were found to be infected by CVA, 23 (50%) by PDV, and two (4%) by LChV1. Previously, 45% of trees in the same farm were shown PNRSV-positive (Cui et al., 2012a). The entire plot of 92 trees was sampled and tested with a commercial ELISA kit specific for the PDV CP (**Figure 10B**). Unfortunately, no ELISA kits for the detection of CVA, and LChV1 were available. The ELISA result showed that 39 (42%) of the trees were infected with PDV. As two other viruses (CVA and PNRSV) also had high incidence of infection, cherry trees infected by more than one virus were very common in this orchard (**Figure 11**). Despite the various combinations of infecting viruses, No relationship could be determined between the observed foliar symptoms, and the detected virus in those samples (**Figure 11 A-D**) Of the surveyed trees which were determined to be infected by PDV, only 4 were singly infected by this virus. Of these trees, 3 displayed no foliar symptoms, or mild chlorosis on some branches (**Figure 11D**). Interestingly, one tree which was singly infected by PDV displayed strong foliar symptoms, including chlorosis, deep vein suturing and leaf deformation (**Figure 12B-D**).

3.2   Assembly of an infectious full-length cDNA clone of PDV

The finding that PDV is the only virus present in the severe symptomatic cherry leaves (**Figure 11 B-D**) and the incidence of PDV infection of nearly 50% suggests that PDV is the causal agent of these severe foliar symptoms observed on infected cherry**.** To determine if PDV is the causal agent of the observed symptoms, a full-length infectious cDNA clone of PDV is needed to test this idea. Using a modified version of Koch's postulates (**Section 1.10**), an infectious clone of PDV was developed to infect cherry to determine if PDV causes symptoms like those observed in the orchard (**Figure 12 B-D**). To develop an infectious clone of PDV, the plasmid vector pCB301 was selected as this vector is relatively small in size (approximately 3 KB in length) and produces a low copy number in bacterial cells (Xiang et al., 1999). A smaller vector can be amplified by PCR, and a low copy number means less foreign DNA will accumulate in bacteria, reducing the likelihood of cytotoxic effects (Pasin et al., 2019). pCB301 was modified by inserting a duplicated enhancer 35s promoter (d35s), a hammerhead ribozyme (RZ) from a satellite RNA of

Figure 10 Detection methods of CVA, LChV1 and PDV

A   To demonstrate that virus specific detection primers work well, plant tissues known to be separately infected with CVA, PDV and LChV1 were subjected to RT-PCR based detection using virus specific primers, amplicons were separated electrophoretically on an agarose gel.

B   A typical DAS-ELISA test plate used for detection of PDV, yellow coloured wells indicate a positive result. A foliar sample of cherry which was shown to be uninfected by PDV using RT-PCR served as the negative control. The PDV DAS-ELISA positive control, provided with the PDV DAS-ELISA kit was used as a positive control when performing DAS-ELISA based detection.

A

1000bp →
800bp →
500bp →

PDV   CVA   LChV1   PDV -   CVA -   LChV1-

B

Infected Samples

-ve control →

Unused wells

+ve control ←
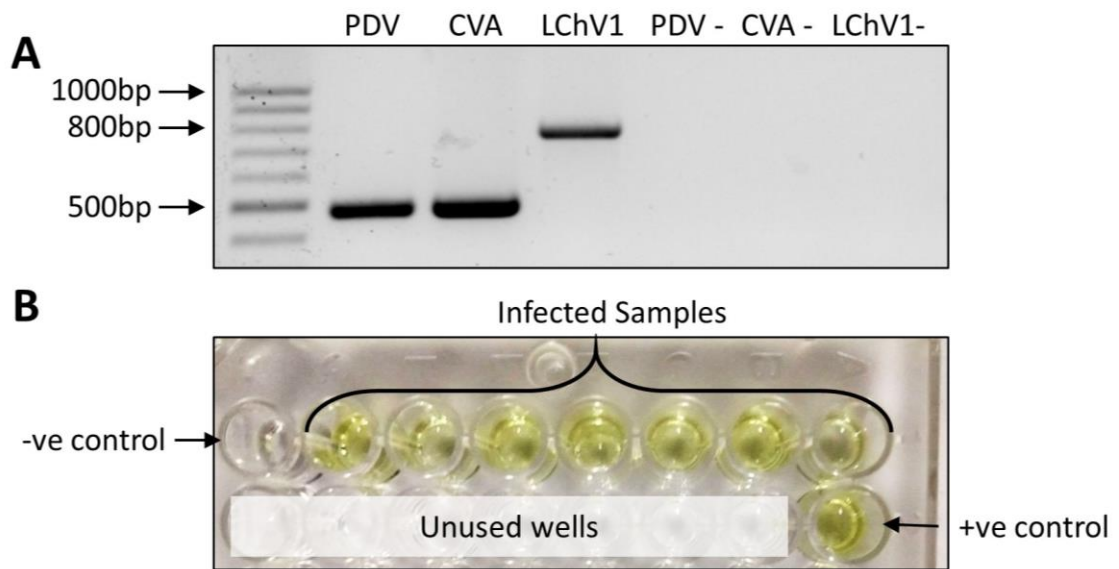
Figure 11 Virus presence is not related to symptom presentation

Photos of cherry leaves which were subjected to detection methods to determine the presence or absence of viral pathogens. The abbreviation of the virus detected in these samples are shown above. Each photo represents a separate cherry tree.

A   LChV1 was only detected in 2 cherry trees and only mild symptoms were identified in these trees.

B   CVA was the virus with the highest in-field incidence and presence of CVA alone was sometimes associated with mild vein suturing, this was inconsistent as many asymptomatic trees were identified as being infected by this virus.

C   As the virus with the highest in-field incidence, CVA was often found to be infected in combination with PDV. Despite the presence of both viruses, observed symptoms ranged from mild ringspotting and chlorosis (top) to no observable symptoms (bottom).

D   The virus with the second greatest incidence of infection was PDV. Only 4 trees were found to be singly infected by PDV, and 3 of these trees either did not present any foliar symptoms, or only mild chlorosis was visible on PDV infected leaves.

LChV1	CVA	PDV + CVA	PDV
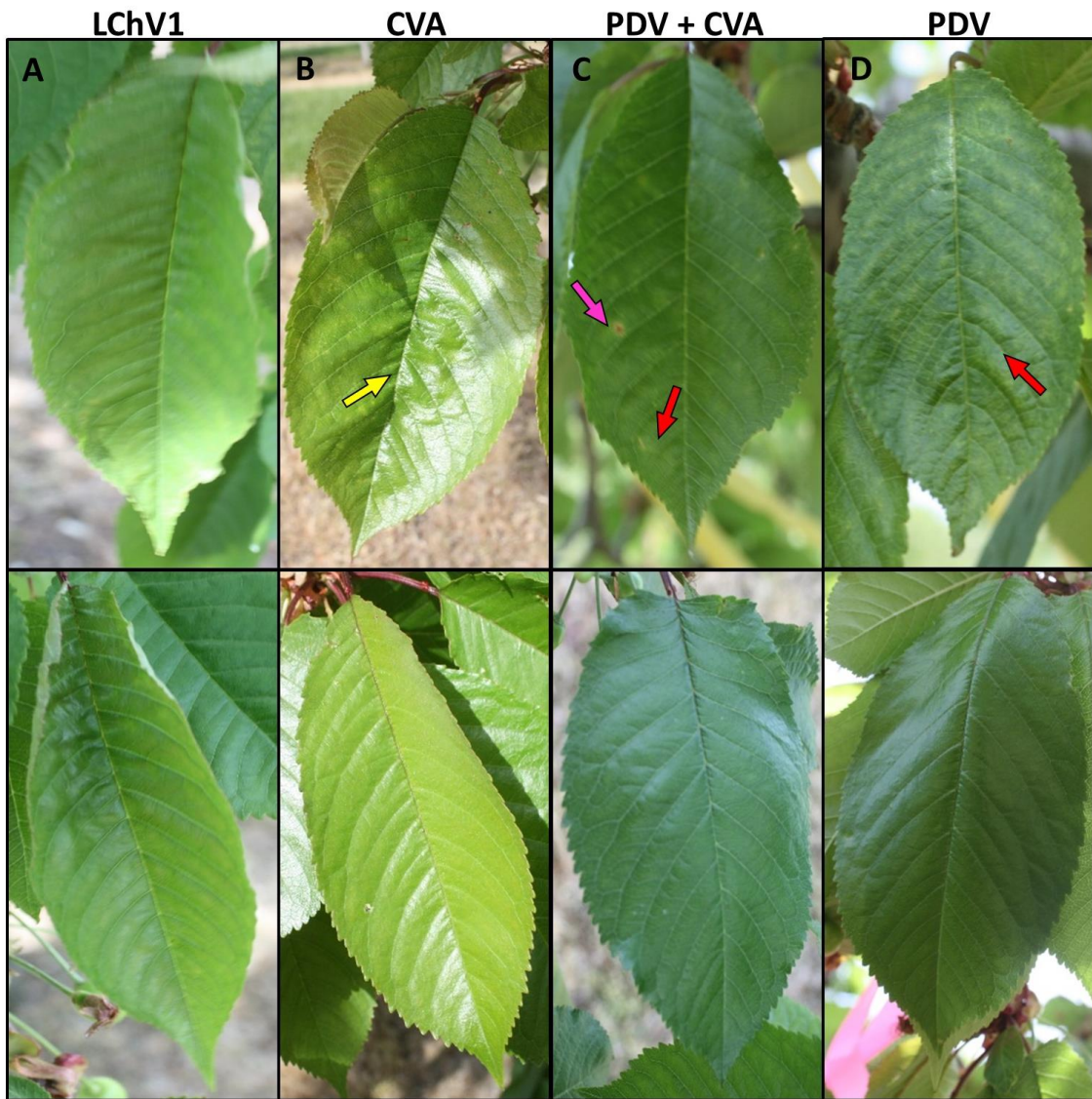
→ Chlorosis   → Vein suturing   → Ringspot

Figure 12 Severe symptoms observed on a PDV infected cherry tree

Photos of cherry leaves displaying severe foliar symptoms from a tree which was only infected by PDV.

A   An asymptomatic leaf from cherry which was determined to be free of LChV1, CVA and PDV.

B-D   Foliar samples from three separate main branches of a cherry tree which displayed severe foliar symptoms. Symptoms observed included chlorosis between leaf veins, deep suturing of the leaf veins, and in some cases, leaf deformation (cupping of the leaf edges).
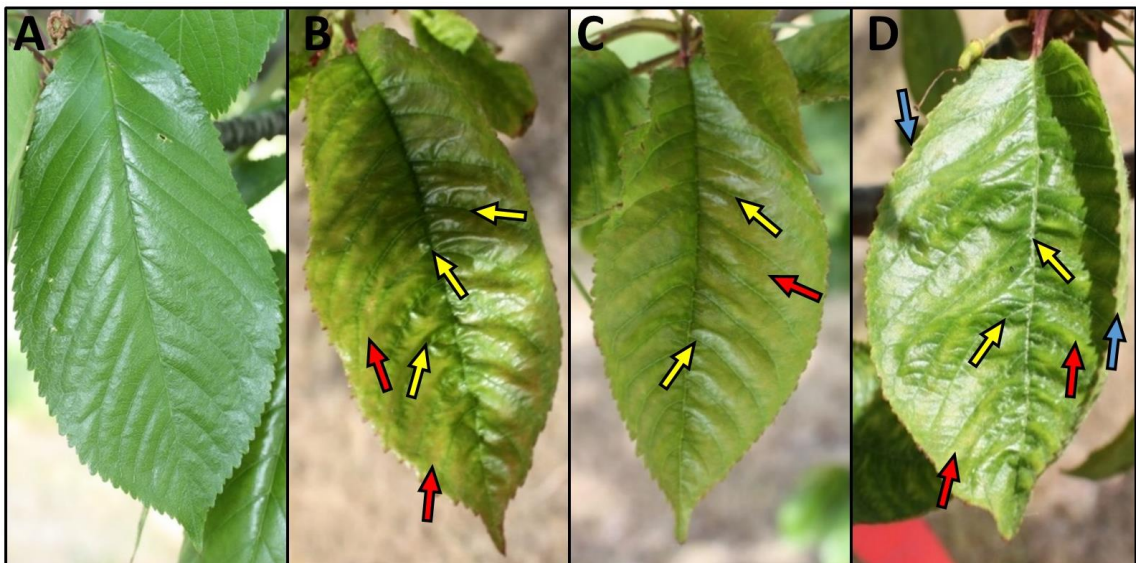
Chlorosis ➡ Vein suturing ➡ Leaf cupping ➡

Tobacco ringspot virus (TRSV) was fused to the nopaline synthase terminator (Nos-T; **Figure 13**). To perform these modifications, the cassette containing d35s,RZ and Nos-T was amplified from the vector pCASS4rz (**Figure 13A**; Annamalai and Rao, 2005). Next, primers were designed to amplify the backbone of pCB301 to prepare for the ligation of the regulatory cassette into the vector (**Figure 13B**). The d35s, RZ and Nos-T cassette was amplified with primers designed to have sequences homologous to the pCB301 vector (**Figure 13C**), which had been linearized by PCR (**Figure 13D**) to allow for ligation using a Gibson assembly style reaction using the NEBuilder HiFi DNA assembly kit (NEB # E5520S; Gibson et al., 2009). Once this vector was assembled it was named pCB301-d35sRZT (**Figure 13E**). Next, the full length cDNAs of RNA1, RNA2 and RNA3 of the PDV isolate detected and sequenced in Ontario from cherry displaying strong foliar symptoms (**Figure 12B-D**) were successfully amplified and ligated into pCB301-d35sRZT and the resulting plasmids were named pPDV1_301, pPDV2_301, and pPDV3_301, respectively (**Figure 14A-C**). Each cDNA was placed between d35s and the tobacco ring spot virus (TRSV) satellite ribozyme (RZ) cassette fused to a NOST. A Gibson style reaction was used to insert the three cDNAs between the d35s and the RZ which was integrated to catalyze the cleavage of these genomic fragments at a conserved AUGC cleavage site which resulted in the additional transcription of 29 nucleotides downstream of the native 3' TGC sequence of all three RNAs (**Figure 14A-C**).

3.2.1 The full-length cDNA clone of PDV does not infect arabidopsis

To study the viral infection cycle, disease development and virus-host interactions, model plants are commonly used as they have a short growing cycle and are amenable to laboratory techniques such as genetic transformation (Goodin et al., 2008). The most commonly used model plants in plant virology are arabidopsis and tobacco (Goodin et al., 2008; Goodman et al., 1995). To test the infectivity of the PDV clone, rosette leaves of arabidopsis were agroinfiltrated with an equal mixture of three cultures of *A. tumefaciens* strain EHA105 each harboring PDV1_301, PDV2_301, and PDV3_301. Plants were closely

Figure 13 Modification of the vector pCB301 for construction of an infectious clone

To construct an infectious clone of PDV, the plasmid vector pCB301 (Xiang et al., 1999) was modified by adding regulatory elements amplified from the vector pCass4RZ (Annamalai and Rao, 2005)

A   The regulatory elements were amplified by PCR using primers pCassF + pCassR (Appendix 2).

B   The entire pCB301 backbone was linearized by PCR amplification using primers pCB301F + pCB301R (Appendix 2).

C   PCR products (regulatory elements from pCass4rz, and the linearized pCB301 vector) were combined and ligated using a modified Gibson style assembly reaction.

E   The ligated construct was named pCB301-d35sRZT and was confirmed via Sanger sequencing.
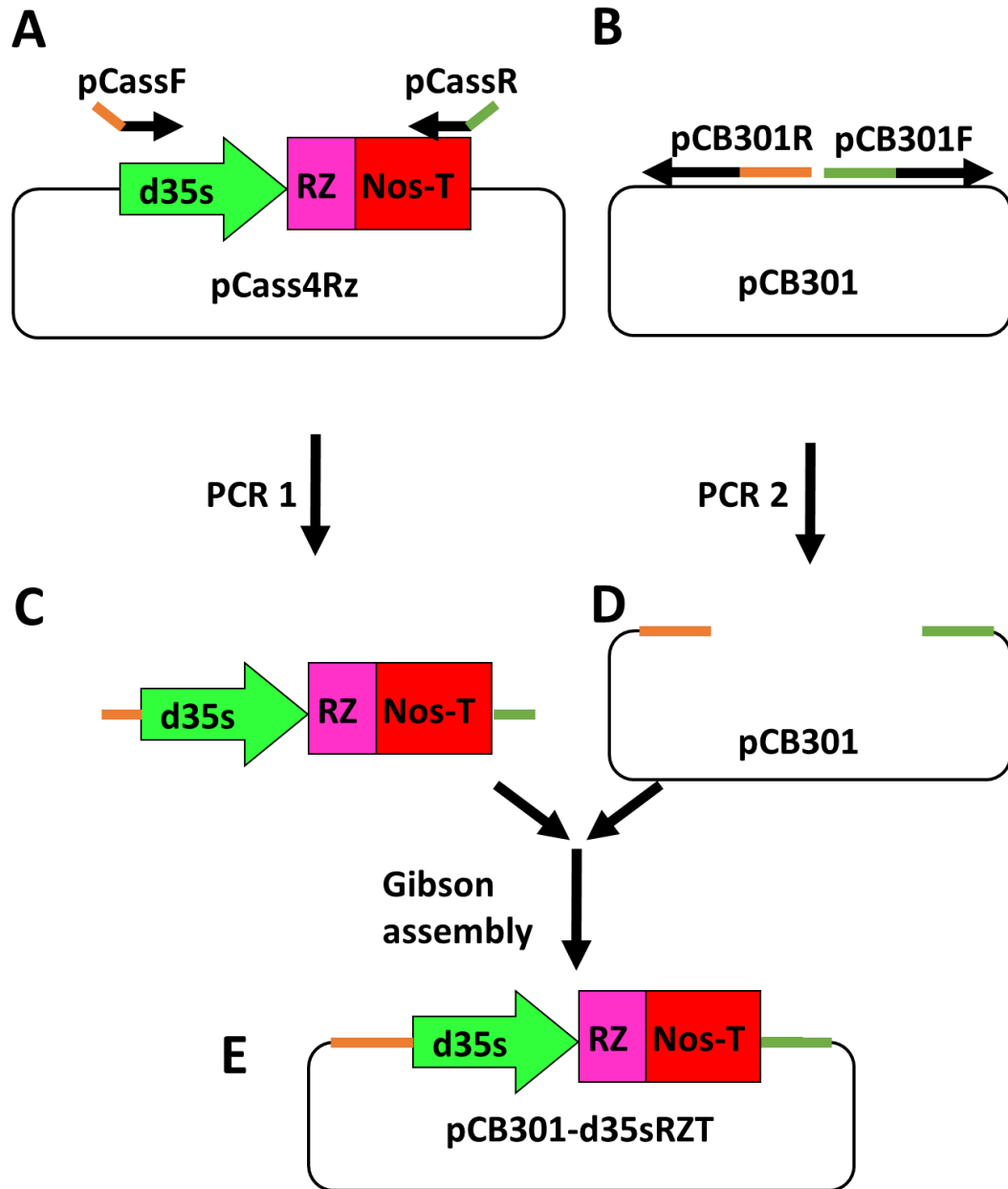
Figure 14 Schematic diagram of the tripartite infectious clone of PDV for studies *in planta*

To determine if PDV was the causal agent of the severe foliar symptoms observed on cherry, a full-length cDNA clone of PDV was constructed.

A   The full-length cDNA of PDV genomic RNA1 was cloned into the vector PCB301-35sRZT.

B   The full-length cDNA of PDV genomic RNA2 was cloned into the vector PCB301-35sRZT.

C   The full-length cDNA of PDV genomic RNA3 was cloned into the vector PCB301-35sRZT.

Single black lines and coloured boxes represent noncoding and coding regions of each RNA fragment (respectively). The protein encoded by each coding region is labelled: P1 (replicase), P2 (RdRp), MP, CP. Transcription start sites are shown at the 5' end of each construct by a bent arrow following the promoter (green arrow) sequence. At the 3' sequence the uppercase and lowercase letters represent the 3' sequence of viral RNA and the non viral sequence of the hammerhead ribozyme (purple box containing "RZ"), respectively. The bent arrow at the 3' end indicates the self cleavage site of the ribozyme. The nucleotide length of RNA1, RNA2 and RNA3 is shown to the right with the number of additional nucleotides after ribozyme self cleavage provided in parentheses.

A

catttggagaggGG....

...GTATGCggtacctctagaggatccgataccctgtcaccgg

pPDV1_301 | d35s | **P1** | RZ | Nos-T | 3375 nt (+29)

B

Transcription

catttggagaggGG....

...GGATGCggtacctctagaggatccgataccctgtcaccgg

pPDV2_301 | d35s | **P2** | RZ | Nos-T | 2596 nt (+29)

C

Transcription

catttggagaggGT....

...GGATGCggtacctctagaggatccgataccctgtcaccgg

pPDV3_301 | d35s | **MP** | **CP** | RZ | Nos-T | 2296 nt (+29)
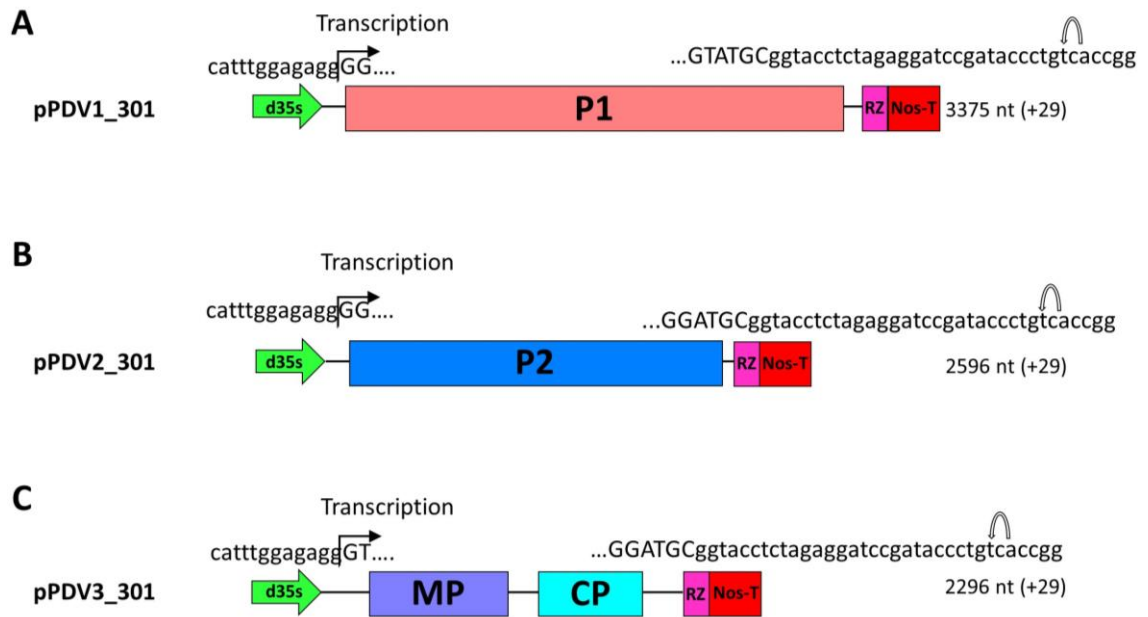
monitored for the development of symptoms. At seven days post agroinfiltration (dpa), samples of the infiltrated leaves of arabidopsis were frozen for later use. At 21 dpa no disease symptoms were observed. Plants agroinfiltrated with the infectious clone could not be distinguished from plants agroinfiltrated with the empty plasmid vector (mock treatment; **Figure 15A**). At 21 dpa, distal new leaves of the plants agroinfiltrated with the full-length cDNA clone or empty vector were collected. All tissue samples were analyzed by RT-PCR and DAS-ELISA to determine if they plants were infected by PDV. RT-PCR to detect the CP of PDV resulted in small amounts of amplicons of correct size in infiltrated arabidopsis leaves but not in distal leaves of the same plant, nor in the mock treated plants (**Figure 15B**). DAS-ELISA failed to detect PDV in all plant tissues tested including locally infiltrated and distal tissues of PDV infiltrated, and mock inoculated plants (**Figure 15C**). These results suggest that the full-length cDNA clone of PDV is not infectious on arabidopsis.

3.2.2 The full-length cDNA clone of PDV can infect tobacco

To determine if another model plant could be infected by the cDNA clone of PDV, fully expanded leaves of tobacco plants were infiltrated with an equal mixture of three cultures of *A. tumefaciens* each harboring the t-DNA construct pPDV1_301, pPDV2_301 and pPDV3_301. At 21 dpa, all plants appeared healthy showing no disease symptoms as PDV and mock infiltrated plants could not be visually differentiated (**Figure 16A**). When RT-PCR and DAS-ELISA were performed to detect PDV, positive results for both tests were found in the distal leaf tissues of tobacco agroinfiltrated with the full-length cDNA clone. RT-PCR did not detect PDV in mock infiltrated plants, and the absorbance reading was insignificant when DAS-ELISA was performed (**Figure 16B, C**). These data suggest that the full-length cDNA of PDV is infectious on tobacco where PDV infection is latent.

3.2.3 The full-length clone of PDV infects cucumber

Previous reports have shown that an infectious clone of PNRSV readily infects cucumber (Cui *et al,* 2013. Additionally, cucumber has been used as a host indicator for

Figure 15 The full-length cDNA clone of PDV does not infect arabidopsis

        To test the suitability of arabidopsis as an experimental host of PDV, the cDNA clone of PDV was used to infiltrate young arabidopsis plants. Plants were maintained for a total of 5 weeks after infiltration. This study was performed in 3 separate experiments consisting of 12 arabidopsis seedlings receiving each treatment during each experiment. For all studies, mock inoculated plants did not generate PDV specific amplicons nor positive results by DAS-ELISA.

A   Arabidopsis seedlings agroinfiltrated with the full-length cDNA clone of PDV (left) did not develop any visible symptoms and could not be differentiated from mock inoculated plants (right) at 21 dpa.

B   Detection of PDV using RT-PCR. RT-PCR was used to detect PDV in locally infiltrated leaves at 7 dpa and distal, non infiltrated leaf tissues at 21 dpa. RT-PCR for PDV detection resulted in a weak amplicon of correct size being generated in the infiltrated rosette leaf sample, but not in the distal samples. No amplicons were generated when samples from mock treated plants were analyzed. A sample of foliar tissue known to be infected with PDV served as a positive control.

C   Detection of PDV with DAS-ELISA. Relative levels of PDV accumulation in locally infiltrated leaves at 7 dpa and distal leaf tissues at 21 dpa were determined by DAS-ELISA. Error bars represent the standard deviation of the mean.

A

PDV   Mock

B

+ve control   Local   Mock Local   Mock Distal

1000bp →
800bp →
500bp →

C

Absorbance at 405nm

PDV-local   PDV-distal   m-local   m-distal   +ve control
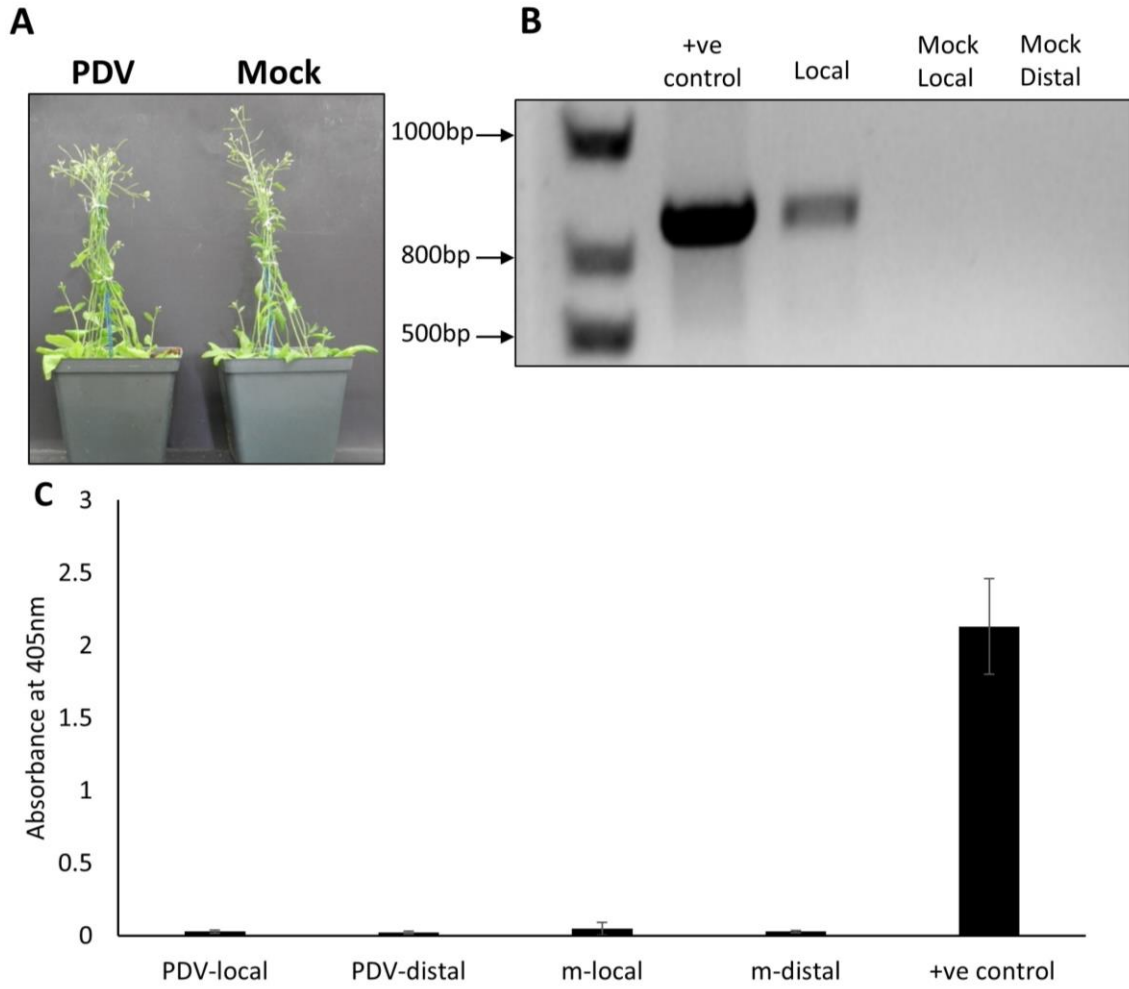
Figure 16 The full-length cDNA clone of PDV is infectious on tobacco

To test the suitability of tobacco as an experimental host of PDV, the cDNA clone of PDV was used to infiltrate young tobacco plants. Plants were maintained for a total of 5 weeks after infiltration. This study was performed in 3 separate experiments consisting of 12 tobacco seedlings receiving each treatment during each experiment. For all studies, mock inoculated plants did not generate PDV specific amplicons nor positive results by DAS-ELISA.

A   Tobacco plants at 21 dpa. The plants agroinfiltrated with the full-length   cDNA clone of PDV did not develop any visible symptoms and could not be differentiated from mock treated plants at 21 dpa.

B   Detection of PDV RNA by RT-PR. The presence of PDV RNA in upper non inoculated leaves of PDV infiltrated tobacco plants was detected by RT-PCR.

C   Detection of PDV with DAS-ELISA. Relative levels of PDV accumulation were determined by DAS-ELISA to confirm PDV accumulation in distal tissues of tobacco. Error bars represent the standard deviation of the mean.
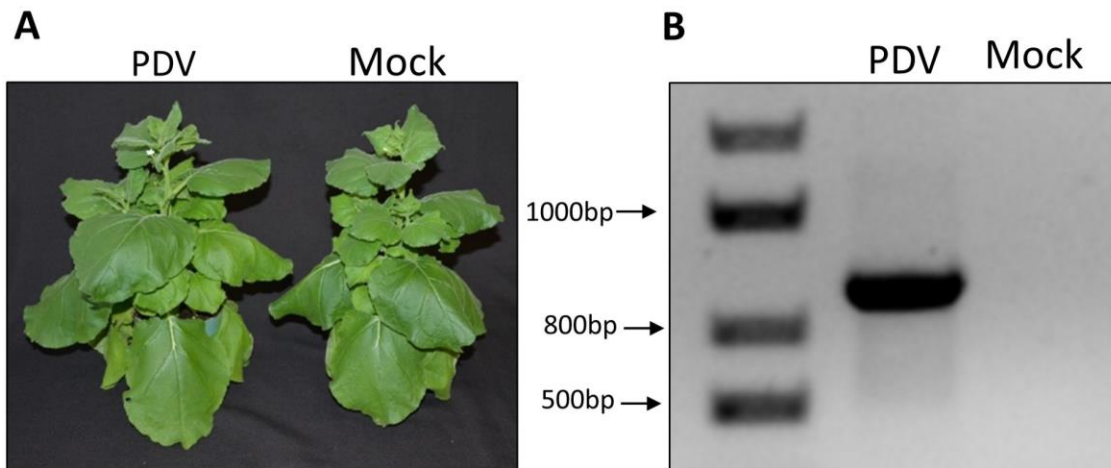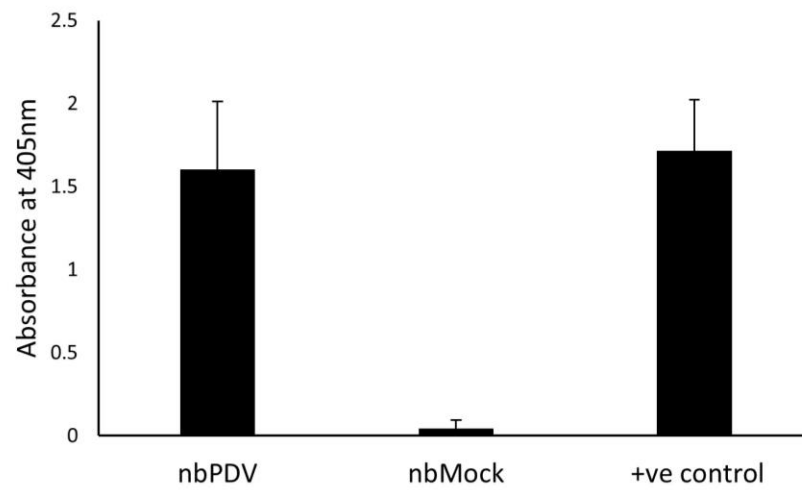
PDV (Fulton, 1966). To test if cucumber would serve as a more appropriate host to study processes such as disease symptom development, fully expanded cotyledons of cucumber cv. 'Wisconsin' were agroinfiltrated with the PDV cDNA clone. When plants were closely examined, PDV agroinfiltrated plants showed disease symptoms and these plants were easily differentiated from mock infiltrated plants (**Figure 17A-C**). The symptoms on cucumber progressed over time and increased in severity. At 7 dpa, newly emerged first true leaves showed vein clearing and mild chlorosis (**Figure 17A**). At 10 dpa, symptom severity increased on the first true leaves including chlorotic spots (**Figure 17B**). At approximately 12 dpa, the second true leaves exhibited stronger symptoms including severe leaf deformation, mottling, vein clearing and mosaic symptoms (**Figure 17C**). Plants which were mock inoculated with *A. tumefaciens* harboring the empty vector PCB301-d35sRZT did not display any symptoms at any time points (**Figure 17A-C**). To confirm that these symptoms were caused by PDV infection, RT-PCR and DAS-ELISA were used and symptomatic plants were indeed positive for PDV using both tests (**Figure 17D, E**). Initial studies showed the infectious clone had a low average infectivity rate of 30% (3 out of 10 infiltrated plants) in cucumber. Cui *et al.* (2016) have shown that the integration of RNA1 and RNA2 of a PNRSV infectious clone into a single construct greatly increased infection efficiency. Like work on PNRSV, the infectious clone of PDV was modified to increase the probability of infection, two expression cassettes for RNA1 and RNA2 were combined into a single construct (pPDV1&2-301; **Figure 18**). Co-infiltration with the mixed *A. tumefaciens* cultures separately harboring the constructs pPDV1&2_301 and pPDV3_301 (**Figure 14C**) achieved a higher average rate of infection of 80% (8 out of 10 infiltrated plants, data not shown).

3.2.4 PDV derived from the infectious clone can be mechanically transmitted to uninfected plants.

A classical method of inoculation for studying of viruses is mechanical inoculation, which predates *Agrobacterium*-mediated inoculation but is still widely used today (Fulton, 1966). As PDV is readily transmitted mechanically (**Section 1.4.4**), I tested if

Figure 17 The full-length cDNA clone of PDV is infectious on cucumber

To evaluate the use of cucumber as an experimental host for PDV infection, cotyledons of cucumber cv. 'Wisconsin' were agroinfiltrated with the full-length cDNA clone of PDV. Left, mock-inoculated; middle, agroinfiltrated with the PDV infectious clone; right, enlarged true leaf of the middle plant.

This study was performed in 3 independent experiments consisting of 9 cucumber seedlings receiving each treatment during each experiment. For all studies, mock inoculated plants did not generate PDV specific amplicons nor positive results by DAS-ELISA.

A   At 7 dpa, PDV symptoms are visible on the newly emerging first true leaves as small chlorotic spots and some vein clearing (red arrows)

B   At 10 dpa chlorotic leaf spotting is present on the fully expanded first true leaf (red arrows)

C   At 12 dpa the second true leaf of PDV infected cucumber exhibits stronger symptoms including chlorosis and leaf deformation (red arrows)

D   The presence of PDV in upper non-inoculated leaves of symptomatic cucumber plants was detected by RT-PCR.

E   Relative levels of PDV accumulation in upper, non infiltrated leaves were determined by DAS-ELISA. Error bars represent the standard deviation of the mean of 9 seedlings for each treatment.
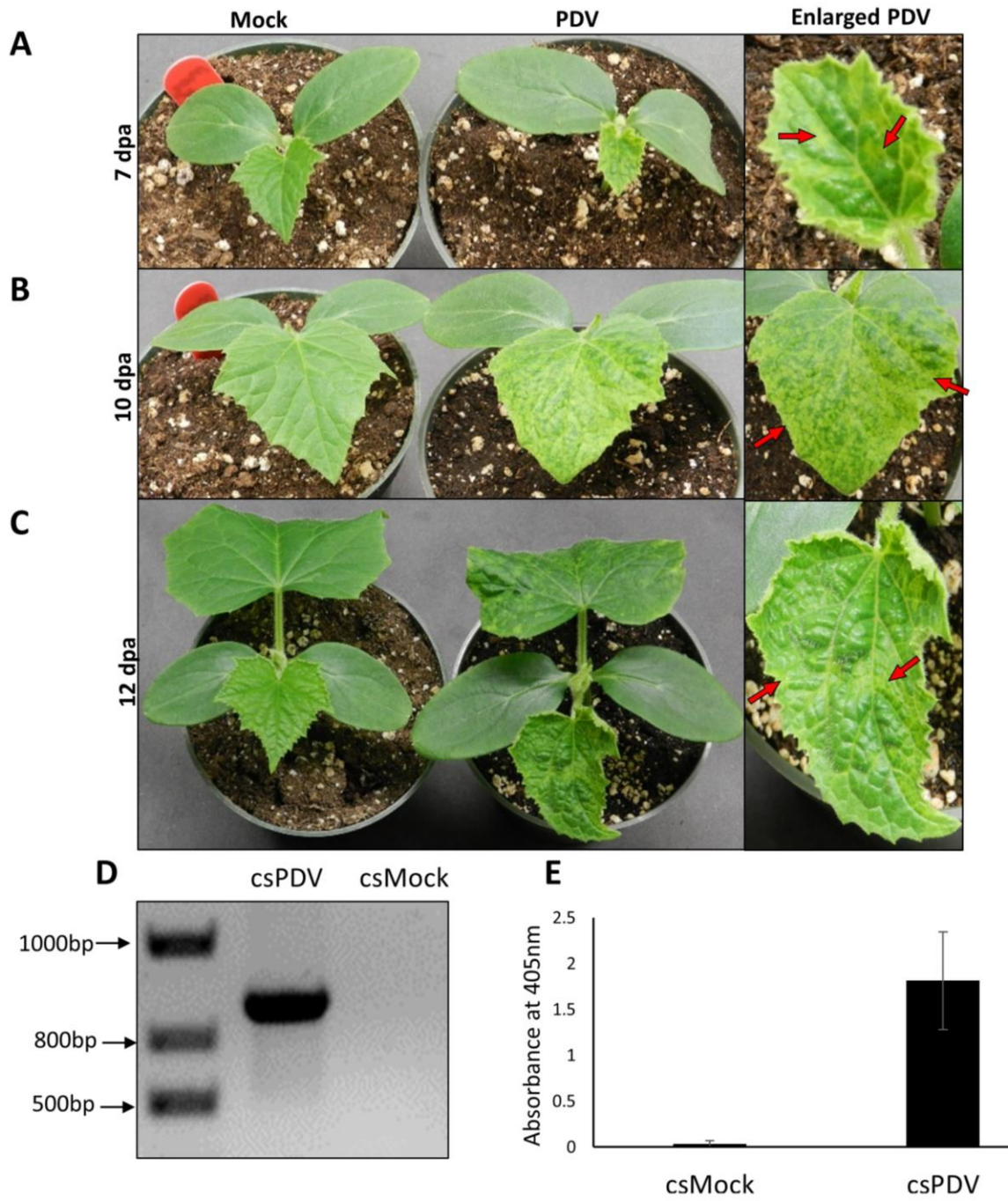
Figure 18 Construction of the improved cDNA infectious clone

To increase the likelihood of successful infection, expression cassettes for PDV RNAs 1 and 2 were combined into a single construct. All PCR primers are listed in Appendix 2

A   pPDV1_301 was digested with the restriction enzyme NarI.

B   The RNA2 fragment of PDV including regulatory elements from pPDV2_301 was amplified using primers R2NarF + R2NarR which also introduced flanking NarI enzyme sites.

C   Digestion of pPDV1_301 with NarI linearizes this construct

D   Sanger sequencing was used to confirm the introduction of flanking NarI sites by PCR and to ensure no errors were introduced by PCR. Subsequent digestion of this construct with NarI prepared it for ligation into the linearized pPDV1_301.

E   After ligation, Sanger sequencing was used to confirm the RNA2 fragment was ligated into pPDV1_301 in the correct orientation, this plasmid was named pPDV1&2_301.
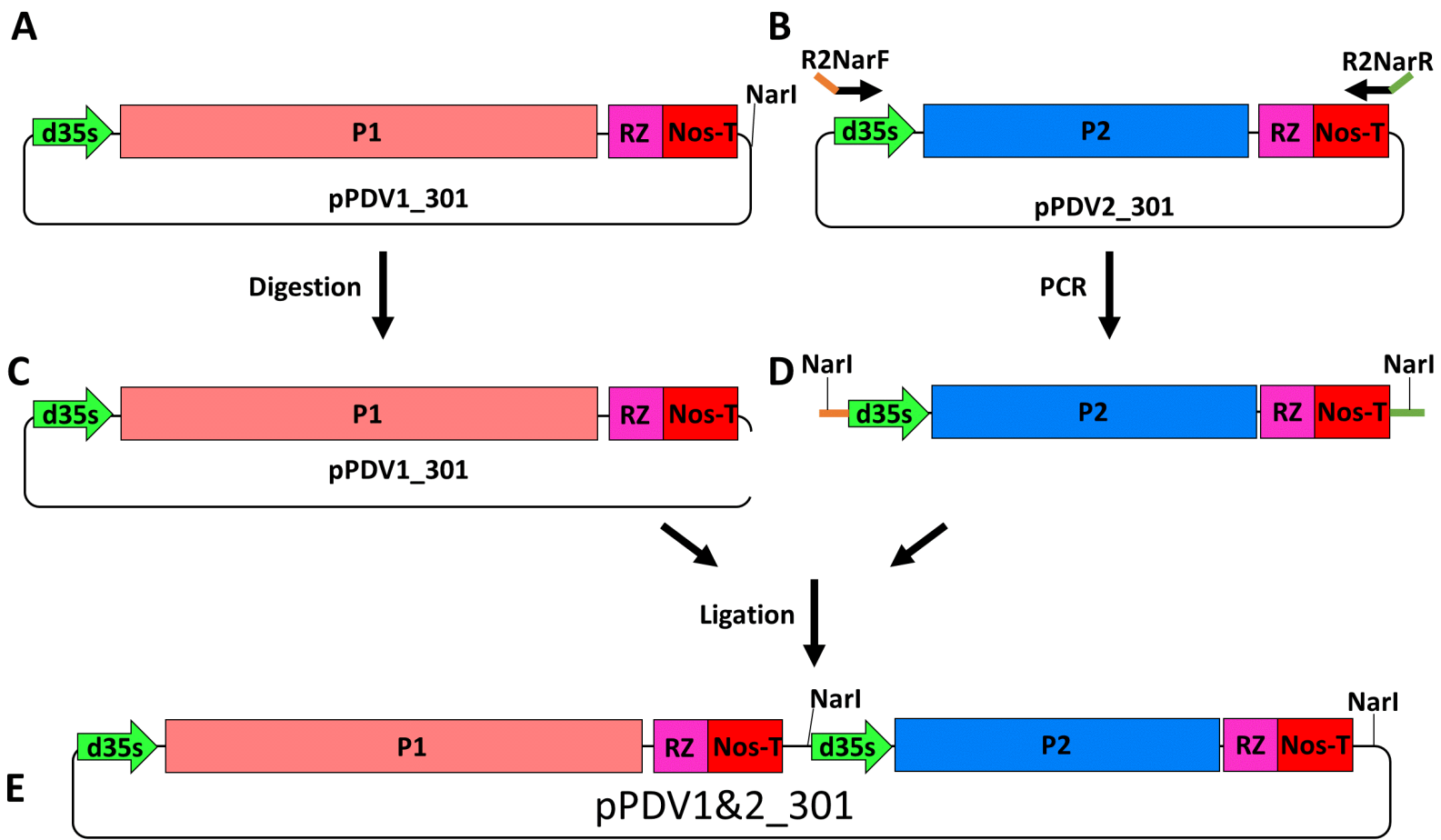
If the PDV infectious clone is mechanically transmissible. Therefore, symptomatic tissues of PDV infected cucumber plants (previously agroinfiltrated with the PDV infectious clone) were used as inoculum to rub-inoculate healthy cucumber and squash plants. At 9 days post inoculation (dpi) symptoms like those observed in agroinfiltrated cucumber plants were observed in mechanically inoculated cucumber (**Figure 19A**). Additionally, symptoms developed on the first true leaves of mechanically inoculated squash seen as chlorotic spots on the leaf margins (**Figure 19B**). For both cucumber and squash, mock inoculated plants did not display any symptoms. DAS-ELISA was used to confirm PDV was present in symptomatic plants, and absence of PDV in mock inoculated plants (**Figure 19C**).

In summary, these results suggest that arabidopsis is not susceptible to the PDV infectious clone, whereas tobacco may serve as an asymptomatic host and lastly, cucumber, and squash are symptomatic hosts of PDV to study processes involved in PDV infection such as disease development and virus movement. Moreover, the PDV infectious clone behaves in a manner like natural PDV in terms of the ability for mechanical transmission to different herbaceous species.

3.2.5 The full-length cDNA clone of PDV is infectious on natural hosts.

The primary reason for constructing the PDV infectious clone was to determine if PDV is the causal agent of the severe foliar symptoms observed on cherry (**Figure 12B-D**) by fulfilling a modified version of Koch's postulates. To test the infectivity of the PDV infectious clone on natural hosts, the PDV infectious clone (pPDV1&2_301 and pPDV3_301; **Figures 14C and 18E**) was agroinfiltrated into seedlings of sweet cherry cv. 'Vista'. Prior to agroinfiltration, RT-PCR analysis confirmed that that these seedlings were free from PDV. Approximately 8 weeks post agroinfiltration, no foliar symptoms were observed on PDV infiltrated seedlings (**Figure 20A, B**). However, the seedlings agroinfiltrated with the infectious clone are stunted in height and had less vegetative growth (shorter leaf stems and fewer leaves) compared to mock-infiltrated plants (**Figure 20A, B**). RT-PCR and DAS-ELISA were performed on distal, non-infiltrated leaves of these

Figure 19 PDV derived from the infectious clone is mechanically transmissible

To determine if PDV derived from the cDNA clone could be transmitted mechanically, the cotyledons of the seedlings were mechanically inoculated with leaf tissues from healthy control plants (left) or with the symptomatic leaves from cucumber plants agroinfiltrated with the PDV infectious clone (right). Three independent experiments were performed with 5 seedlings of each species for each treatment during each experiment.

A Foliar tissue from PDV infected cucumber seedlings was used to mechanically inoculate the cotyledons of healthy cucumber seedlings. PDV symptoms are clearly seen as chlorotic leaf spots at 9 dpi (red arrows).

B Cotyledons of squash were mechanically inoculated in a similar manner as in cucumber. Similarly, at 9 dpi chlorotic spots were seen at the margins of the first true leaves (red arrows)

C DAS-ELISA was used to confirm PDV infection and was used to compare relative abundance of PDV at nine dpi. Error bars represent the standard deviation of the mean (n=5).

Mock
PDV

A
cucumber
9 dpi

B
squash
9 dpi

C
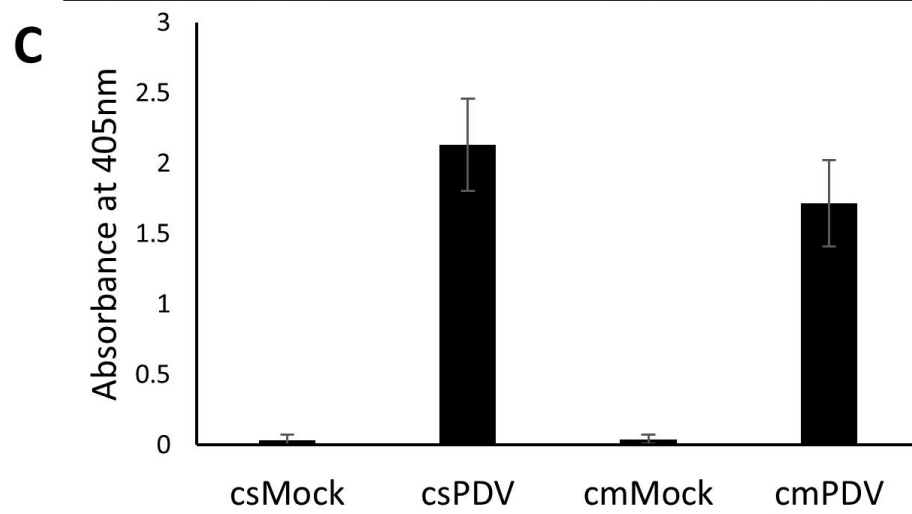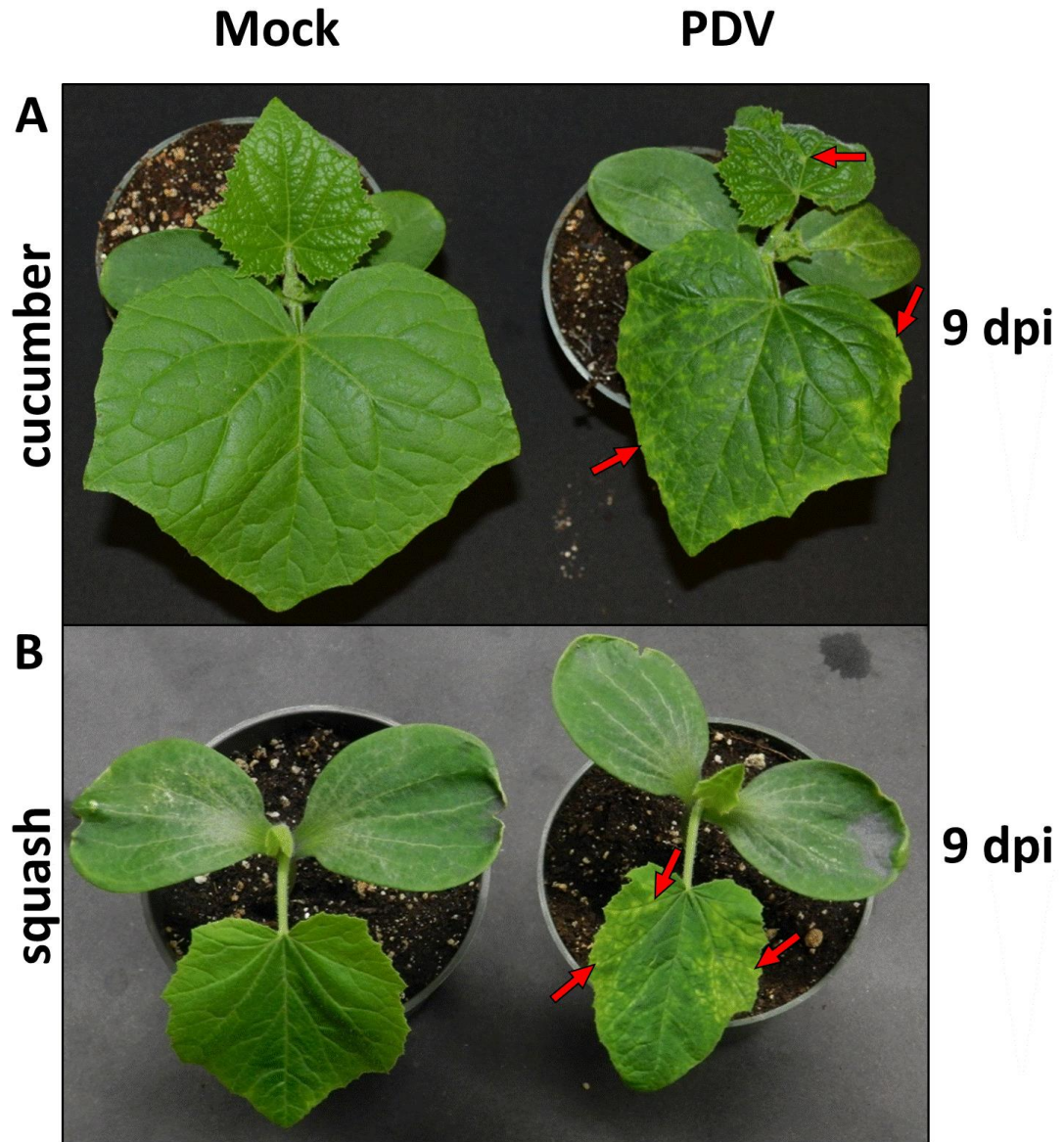
seedlings to confirm the presence and long-distance movement of PDV in symptomatic trees, and absence of PDV in mock-infiltrated seedlings (**Figure 20C, D**).

3.3   Molecular characterization of the PDV MP

3.3.1   *In silico* analysis of the PDV MP

Little research has been performed directly on PDV and current knowledge of the PDV infection cycle is mainly drawn from studies on closely related viruses such as AMV (**Section 1.4.1**). An essential step required for viruses to establish systemic infection is intercellular movement. The PDV RNA3-encoded MP was chosen for molecular characterization to further understand spread of this virus. The MP of PDV is a member of the diverse 30K superfamily of MPs (**Section 3.1.2**). *In silico* analyses were performed to compare the aa sequence of the PDV MP with other ilarviral MPs. A search using the HHpred webserver on aligned MP sequences identified a match to the *Bromoviridae* 30K movement protein (**Table 5**). Further *in silico* analysis using the Phyre2 server predicted the secondary structure of the PDV MP (Kelley et al., 2015). It was found that the MP has a central (core) domain similar to the consensus core domain of the 30K superfamily members (Melcher, 2000) and this core domain between residues S_{75} and I_{226} consists of 8 β-sheets which are flanked by 2 α-helices (**Figure 21**). This core domain also contains a $LXNX_{50-70}G$ motif common to ilar- and alfamo- viruses, (**Figure 21**; Koonin et al., 1991; Melcher, 2000). A proline and several aromatic residues (boxed in red) between β3 and β4 are present, consistent with other 30K members (**Figure 21**; Margaria et al., 2016; Melcher, 2000). The secondary structure prediction also revealed that there is an α-helix in the N-terminal region of the MP outside of the predicted core domain (**Figure 21**). In the C-terminal region, the MP lacks the SIS motif which is conserved in many other 30K members (Melcher, 2000). The PSIPRED server was also employed to study protein structural organization (Buchan and Jones, 2019). It was found that both N and C termini are disordered regions (M_1-A_{17} and N_{266}-G_{293}) with potential protein binding abilities

Figure 20 The infectious clone of PDV is infectious on cherry

To determine if PDV was the causal agent of foliar symptoms found on orchard grown cherry, seedlings of cherry were agroinfiltrated with the PDV infectious clone. This experiment was performed twice, and each experiment consisted of 5 seedlings receiving each treatment.

A   Side view of seedlings infiltrated with the PDV infectious clone and empty vector (mock). Seedlings infected by PDV (left) have shorter internodal lengths resulting in a dwarfed or stunted phenotype compared to mock treated plants (right).

B   Aerial view of seedlings infiltrated with the PDV infectious clone or empty vector (mock). PDV infected seedlings (left) produce fewer leaves compared to mock treated plants (right).

C   The presence of PDV in upper non-infiltrated leaves of dwarfed cherry plants (left) was detected by RT-PCR. No amplicons were generated when distal tissues of mock treated plants were subjected to RT-PCR (right).

D   DAS-ELISA confirmed the presence of PDV in the distal, non-infiltrated leaf samples of the seedlings agroinfiltrated with the PDV infectious clone. The absence of PDV was confirmed in mock treated plants. The error bars represent the standard deviation of the means (n=5).
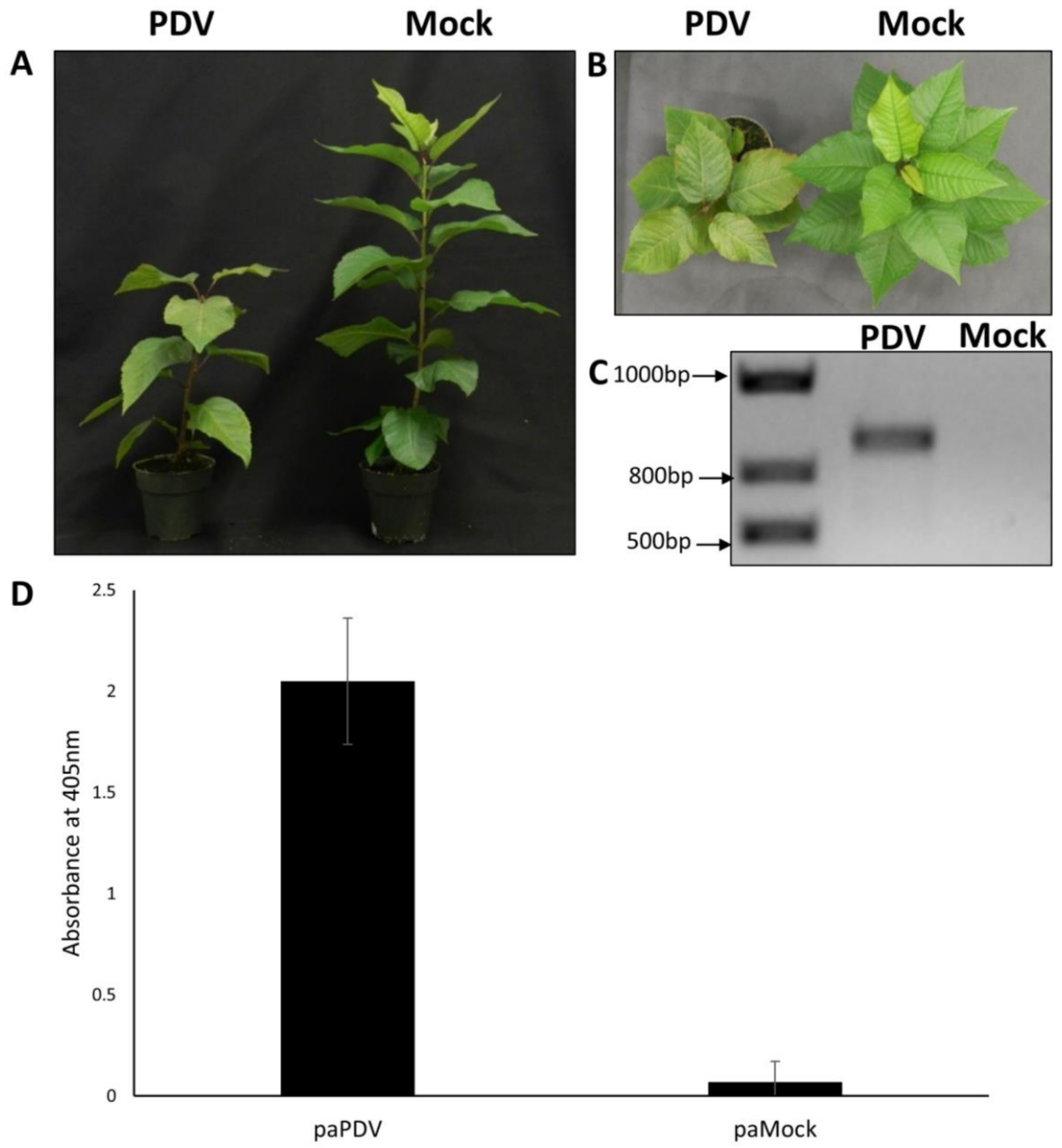
Figure 21 Predicted secondary structures of the PDV MP

The Phyre2 and LOMETS prediction servers were used to predict the secondary structure of the PDV MP and similarities to other members of the 30K MP superfamily were found. The N-terminus of the MP is like other tubule forming MPs with a predicted *a*-helix anterior to the 30K core domain (highlighted in yellow). The core (boxed by single black lines) consists of 8 β-strands (shown as blue arrows labelled β1-β8) which are flanked by 2 *a*-helices (shown as green coils labelled *a*A and *a*B). A LXNX$_{50-70}$G motif common to both ilar- and alfamo- viruses is presented as LFNV$_{52}$G (boxed in purple). Coloured bars underneath predicted secondary structures indicates the confidence of the prediction using the Phyre2 prediction server. Numbers overlapping the coloured bars indicate the confidence of the same structure predicted using the LOMETS prediction server.
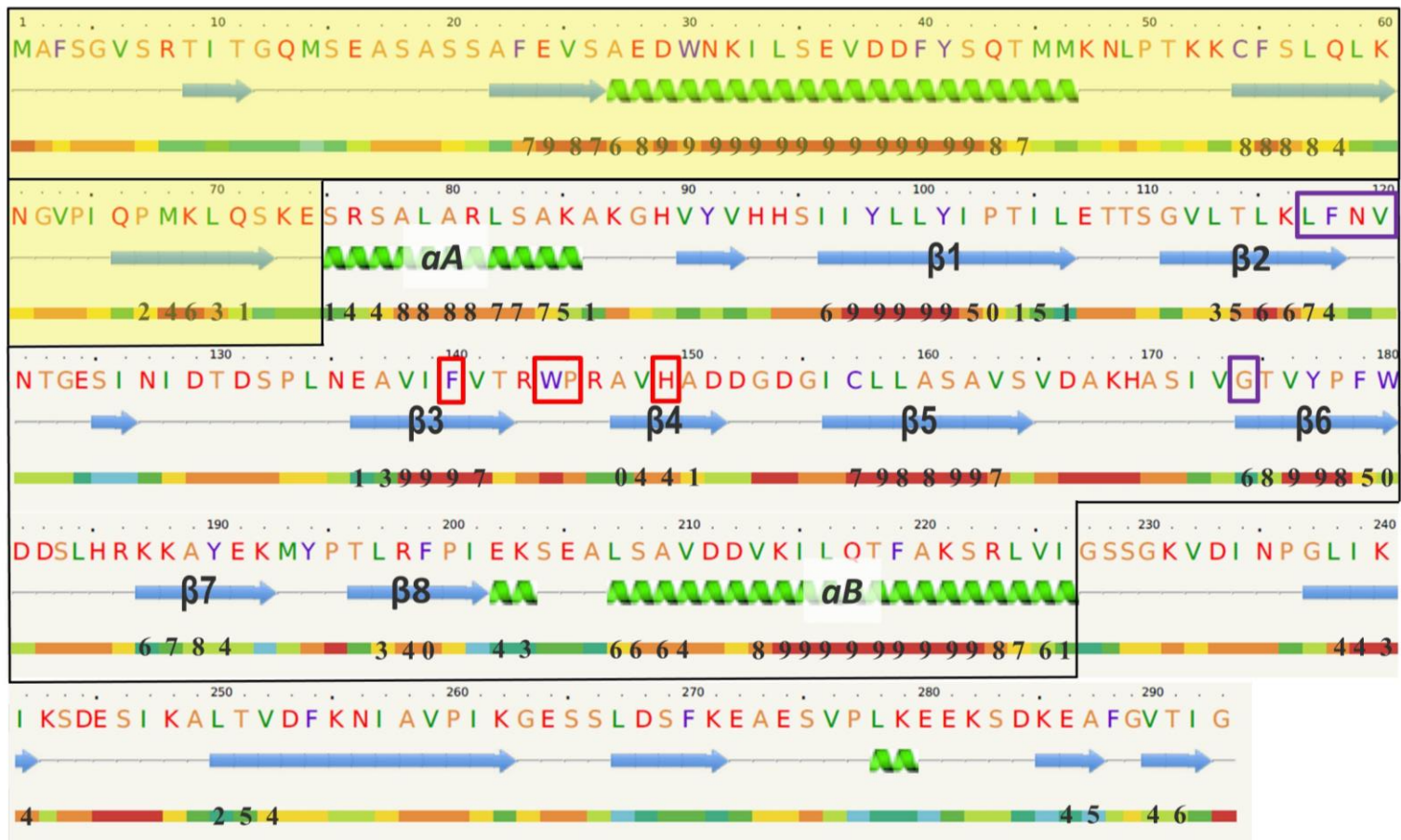
Legend

Prediction confidence

High   Low

10   1

95

Figure 22 Predicted characteristics of MP domains

The PSIPRED prediction server was used to characterize domains of the PDV MP regarding putative protein binding capacity and subcellular localization.

A   Plot showing disordered probability of the MP sequence shows both N- and C-termini have a high probability of being disordered with potential protein binding properties (residues are shown as green circles).

B   MP sequence shows residues predicted to be disordered with potential protein binding properties (outlined in green). Residues are highlighted based on predicted localization of domains: cytosolic (white), transmembrane (blue) and extracellular (orange).

A

B
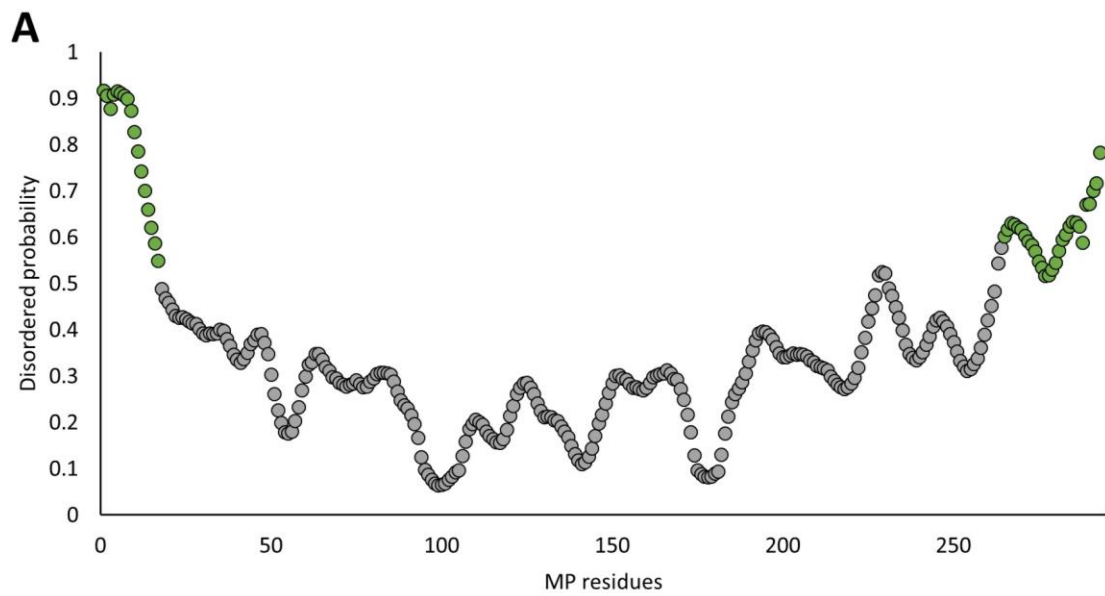
MAFSGVSRTITGQMSEAS ASSAFEVSAEDWNKILSEVDDFYSQTMMKNLPTKKCFSLQLKNGVP
IQPMKLQSKESRSALARLSAKAKGHVYVHHSI IYLLYIPTILETTSGV LTLKLFNVNTGESINIDTDSPL
NEAVIFVTRWPRAVHADDGDGICLLASAVSVDAKHASIVGTVYPFWDDSLHRKKAYEKMYPTLR
FPIEKSEALSAVDDVKILQTFAKSRLVIGSSGKVDINPGLIKIKSDESIKALTVDFKNIAVPIKGES SLDS
FKEAESVPLKEEKSDKEAFGVTIG

(**Figure 22A, B**). Other predicted features include cytosolic, transmembrane, and extracellular domains (**Figure 22B**).

3.3.2 The PDV MP localizes to the PD

For intercellular movement, viruses move through the PD (utilizing different mechanisms; **Section 1.4.3**). Therefore, it is not surprising that a nearly universal feature shared by viral MPs is their ability to target and localize to the PD (Heinlein, 2015). To determine if the PDV MP targets PD, the MP-coding sequence was amplified and ligated into a plant expression vector that allows for the transient expression of a PDV MP fusion protein in which the C-terminus of the MP was fused to the N-terminus of yellow fluorescent protein (YFP; MP-YFP). This construct was co-agroinfiltrated into tobacco leaf cells with the established PD marker Plasmodesmata Localization Protein V (PDLPV). This marker was amplified from arabidopsis and ligated into an expression vector to create a C-terminal fusion with cyan fluorescent protein (CFP; PDLPV-CFP). When visualized by confocal microscopy, PDLPV-CFP forms punctate patterns at the periphery of leaf cells, indicating localization to the PD (Saatian et al., 2018). Transient expression of the two proteins was visualized by laser scanning confocal microscopy. MP-YFP formed punctate structures along the periphery of tobacco leaf cells, and many of them co-localized with the punctate structures highlighted by PDLPV-CFP (**Figure 23A**). As a negative control, the coding sequence of YFP was amplified and ligated into an expression vector (pEarleyGate-100; Earley et al., 2006) this construct was named pYFP-100. This construct was then transformed into *A. tumefaciens* and was co-infiltrated into leaf cells with PDLPV-CFP. Using pYFP-100, free YFP was seen to localize within the cytosol in a diffuse pattern and did not form punctate patterns (**Figure 23B**) Taken together, these results suggest that the PDV MP does in fact target and localize at the PD of tobacco epidermal leaf cells.

3.3.3 Characterization of domains required for PD localization

Since the PDV MP does localize to PD, identification of domains and aa residues in the MP crucial for targeting and localization to PD will allow for a better understanding

Figure 23 The PDV MP localizes to the PD

To determine the subcellular localization of the PDV MP constructs were transiently expressed in tobacco leaves and the subcellular localization of the MP-YFP fusion was visualized at 48 hpa. As a negative control, the YFP-100 construct was used to observe the sub-cellular distribution of free YFP. In both experiments, YFP constructs were co-infiltrated with PDLPV-CFP, an established PD marker. A schematic representation of each MP truncation is shown to the left of the confocal images: The grey box represents the viral MP. Green arrow: d35s promoter, yellow rectangle: coding region of YFP, red box; NOS terminator.

YFP and CFP fluorescence are shown separately in the left and middle columns. The merged image combines both fluorescent images and the brightfield image and is shown in the right column. The observed YFP fluorescence pattern is described to the right of the merged image (P: punctate; D: diffuse)

A   The MP-YFP fusion protein formed yellow punctate patterns which localized to the cell periphery and was found to co-localize with the PD marker (shown by white arrows).

B   Free YFP was found to localize within the cytosol at the periphery of leaf cells in a diffuse pattern.

| | YFP | PDLPV-CFP | Merged/Bright | Enlarged |
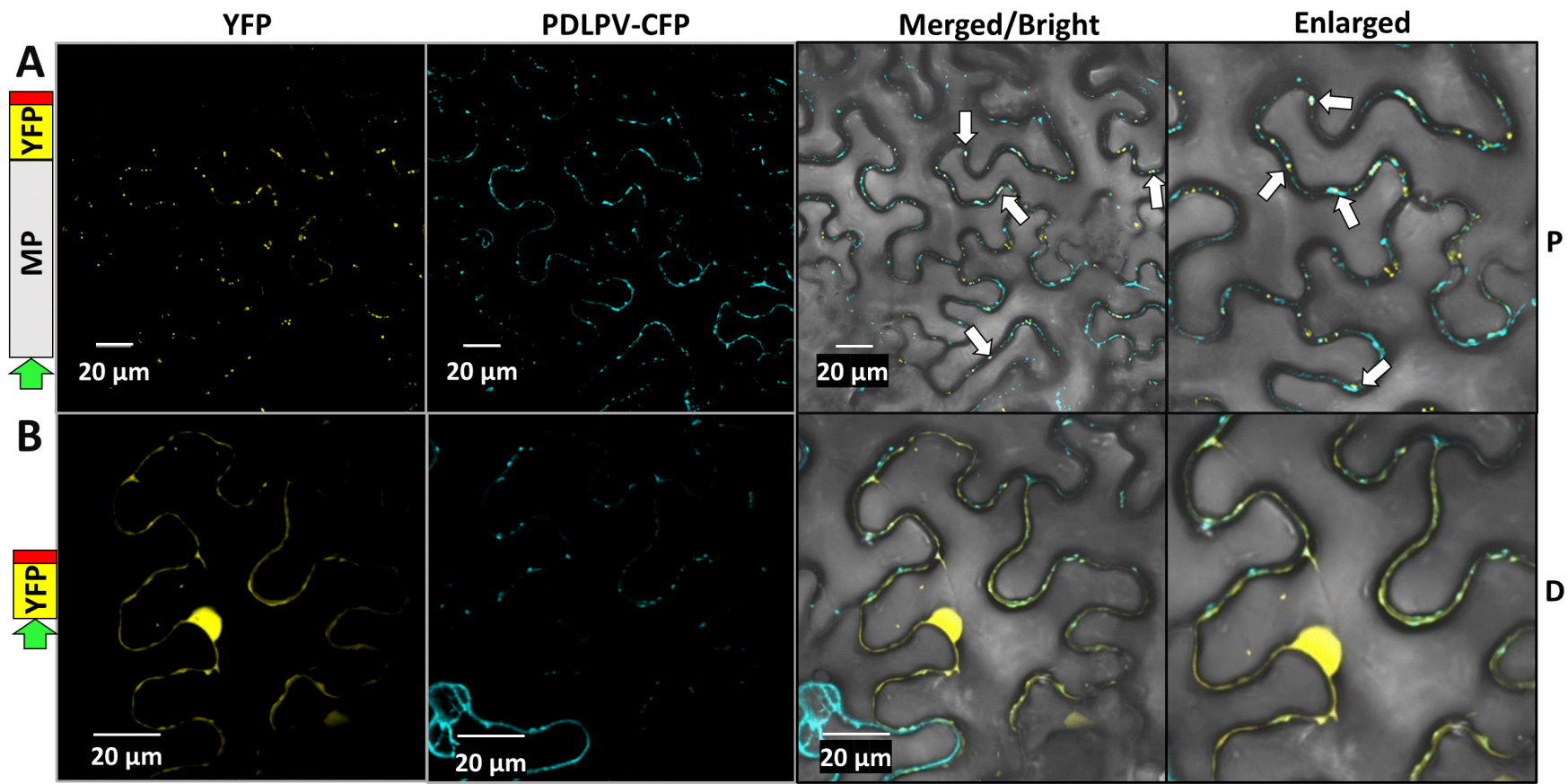
of MP-mediated PDV intercellular movement. Other viral MPs have been characterized including the MP of TMV, also a member of the 30K superfamily (Melcher, 2000). This protein is one of the best characterized viral MPs and has at least three N-terminally located PD localization signals (PLS)s (Liu et al., 2020; Yuan et al., 2016). The MP of AMV is also well studied and the aa sequence of this MP shares 40% sequence identity with the sequence of the PDV MP. The predicted secondary structure of AMV is very similar to that of PDV and was not included in this study (Kozieł et al., 2017a). Additionally, at least one domain crucial for PD localization has been identified in the MP of AMV (Huang et al., 2001). To determine if the MP of PDV contains the same PD localization domain as AMV, protein sequences of the group IV ilarviruses (PDV and Fragaria chiloensis latent virus; FCilV) and AMV were compared (**Figure 24**). Alignment of the MP sequences showed a higher degree of sequence conservation within the N-terminal half (43 residues are identical) compared to the C-terminal half (26 identical residues; **Figure 24**). Additionally, several residues were conserved in these viruses within the previously described AMV PD localization domain (**Figure 24**, outlined in green; Erny et al., 1992). Since the TMV MP has three N-terminally located PLSs, and conserved residues were found in the N-terminus of AMV, FCLiV, and PDV the N-terminus was further studied to determine if it could localize to PD.

To determine if the N-terminus of the PDV MP is enough for PD localization, the coding sequence of the PDV MP was divided into two halves (**Figure 24**; solid blue line), each fused to YFP for *in planta* visualization. The N-terminal MP fusion was constructed by deletion of the C-terminal coding region of the MP (MPΔ146-293-YFP). The C-terminal MP fusion was constructed by deletion of the N-terminal coding region (MPΔ1-146-YFP). To determine if these partial sequences could direct YFP expression to the PD, the expression vectors were separately co-agroinfiltrated with the PD marker PDLPV-CFP into tobacco leaves and expression was observed using confocal microscopy (**Figure 25**). This showed that the N-terminal half of the PDV MP was able to localize to the PD, as YFP formed punctate patterns, co-localizing with the CFP tagged PD marker (**Figure 25A**). However, when the N-terminal half was deleted YFP signal was diffuse at the periphery

Figure 24 MP sequence conservation among group IV ilarviruses and AMV

The MPs of group IV ilarviruses and AMV were compared to identify domains rich in conserved aa residues which may be important elements for proper MP functions. Sequence alignment of the of MP sequences of FCiLV (accession YP_164804.1), PDV (accession QGA72060) and AMV (accession P03595) shows there is higher sequence conservation among the three MP sequences in the N-terminal region. A domain previously determined to be crucial for AMV MP localization to the cell periphery is boxed in green (Huang et al., 2001). Additionally, the core domain (Flanked by residues S75 and I226 which are labelled with green arrows) also contains many conserved residues, however the C-terminal domain shows the least amount of sequence conservation.

Three N-terminal truncations were constructed including the deletion of the first 14 (MPΔ1-14-YFP; purple dashed arrow), 44 (MPΔ1-44-YFP; orange dashed arrow) and 69 (MPΔ1-69-YFP; brown dashed arrow) residues. Three C-terminal truncations were constructed including the deletion of the last 14 (MPΔ279-293-YFP; red dashed arrows), 24 (MPΔ269-293-YFP; green dashed arrows) and 41 (MPΔ252-293-YFP; blue dashed arrows) residues.

Site directed mutagenesis was used to identify residues crucial for MP localization to the PD within the N-terminal region and the core domain of the MP (shown by red arrows, with residues labelled above). A vertical blue line with boxed ends shows the centre of the MP aa sequence.

Shading in black: conserved sequence, shading in grey: conserved type of side chain, *: identical sequence, **.** : >50% residue identity, -: gaps between sequences.
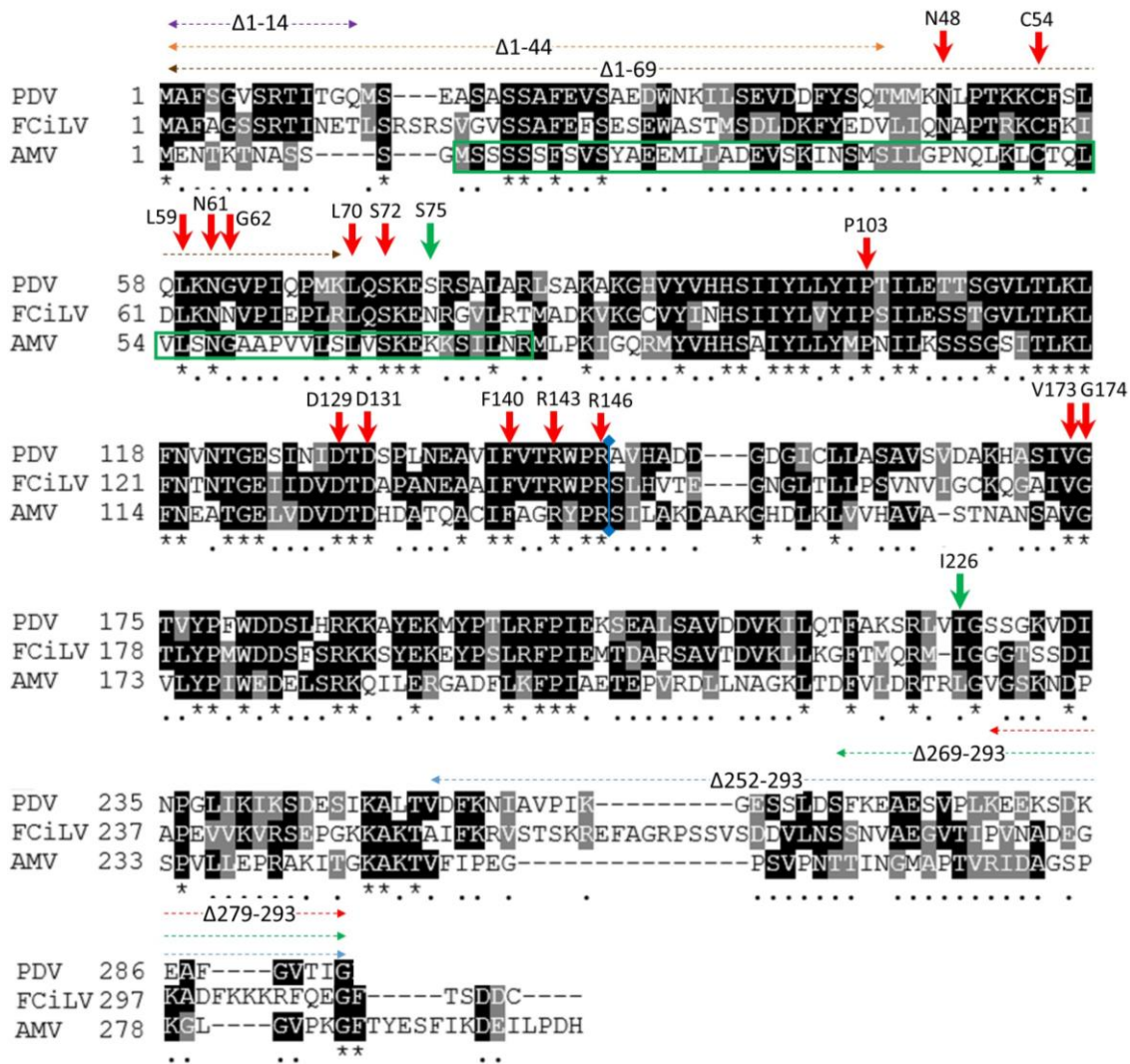
Figure 25 The N-terminal half of the PDV MP is enough for PD localization

To determine if the N-terminal half of the PDV MP could localize to the PD, MP deletion constructs were transiently expressed in tobacco leaves and the subcellular localization of the YFP fusion was visualized at 48 hpa. In both experiments, YFP constructs were co-infiltrated with PDLPV-CFP, an established PD marker. A schematic representation of each MP truncation is shown to the left of the confocal images: The grey box represents the viral MP, angled lines represent deleted portions of the MP sequence. Green arrow: d35s promoter, yellow rectangle: coding region of YFP, red box: NOS terminator.

YFP and CFP fluorescence are shown separately in the left and middle columns. The merged image combines both fluorescent images and the brightfield image and is shown in the right column. A portion of the merged image has been enlarged and is shown on the far right. The construct names are shown on the left. The observed YFP fluorescence pattern is described to the right of the merged image (P: punctate; D: diffuse)

A The N-terminal half of the PDV MP YFP fusion was visualized forming punctate patterns at the cell periphery and was also found to co-localize with PDLPV-CFP (shown by white arrows).

B The C-terminal half of the PDV MP YFP fusion has a diffuse pattern at the cell periphery, nor did it co-localize with PDLPV-CFP

	YFP	CFP	Merged/Bright	Enlarged
A Δ146-293	20 μm	20 μm	20 μm	P
B Δ1-146	20 μm	20 μm	20 μm	D
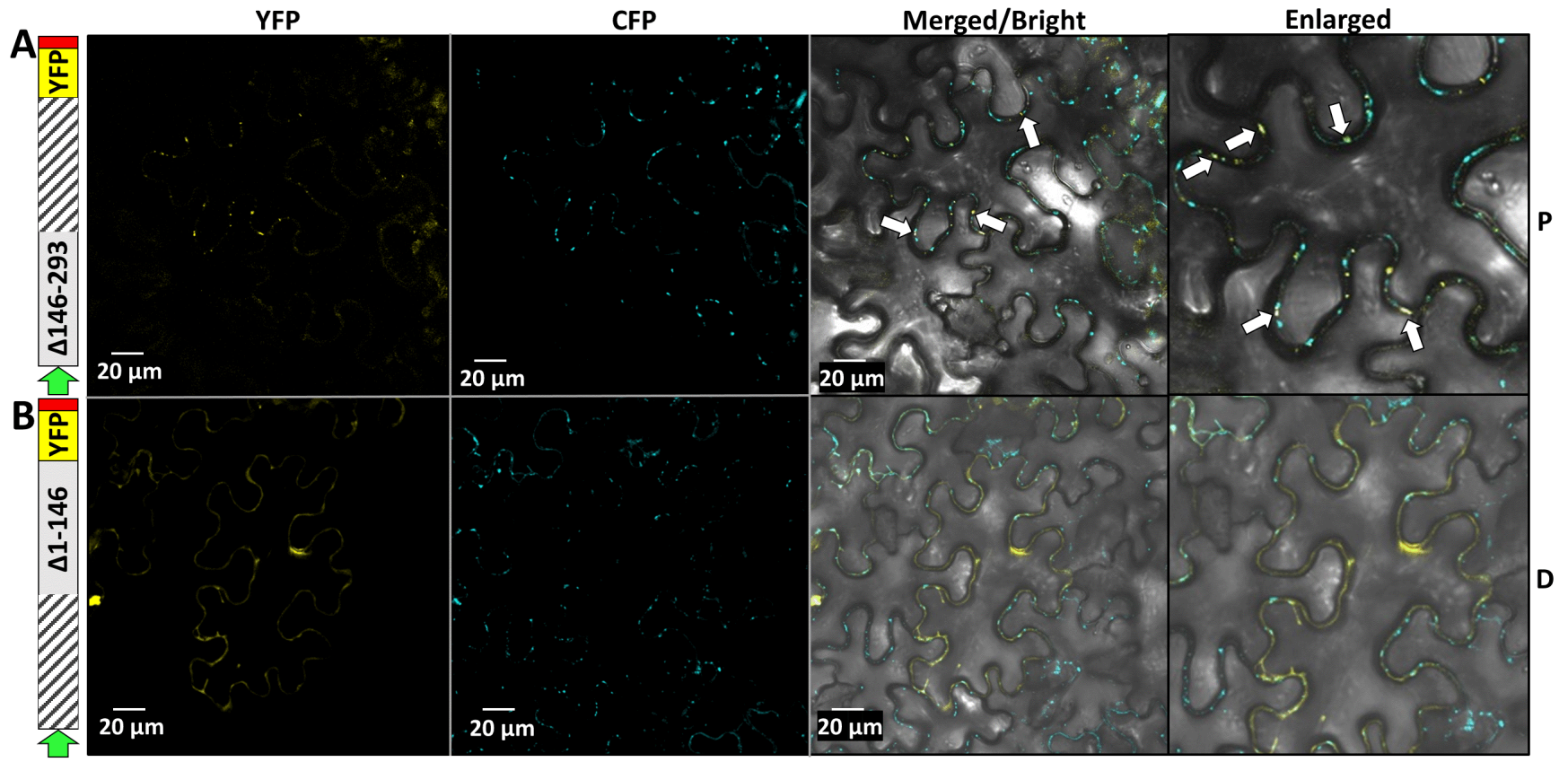
of the cell and did not colocalize with the PD marker (**Figure 25B**). These results suggest that deletion of the C-terminal half of the PDV MP does not impact PD localization.

The N-terminal half was further studied based on its ability to localize to the PD. Elements including a predicted N-terminal *a*-helix (**Figure 21**) and conserved aa residues (**Figure 24**) were targeted to evaluate their importance in PD localization, this was performed by creating N-terminally truncated MP sequences which were fused to YFP. The first truncation mutant involved the deletion of the N-terminal 14 residues (MPΔ1-14-YFP; **Figure 24,** indicated by a purple dashed arrow). A larger truncation mutant was designed which disrupted the predicted *a*-helix upstream of the 30K core domain (MPΔ1-44-YFP; **Figure 24,** indicated by an orange dashed arrow). The last N-terminal truncation involved the deletion of the *a*-helix and a β-strand (MPΔ1-69-YFP; **Figure 24,** indicated by a brown dashed arrow). Deletions of the first 14 or 44 residues (MPΔ1-14-YFP and MPΔ1-44-YFP) did not impact PD localization as punctate patterns of the YFP fused MP overlapped with the PD marker (**Figure 26A, B**). In contrast, when the first 69 residues were deleted, the mutant (MPΔ1-69-YFP) failed to form punctate patterns at the periphery of the infiltrated cells, displayed a diffuse distribution and lost the ability to target to the PD (**Figure 26C**). These data suggest that there is an element crucial for PD localization residing within the N-terminal 69 residues where a short stretch (residues 45-69) may be essential.

Although the deletion of the C-terminal half of the PDV MP coding region did not impact PD localization (**Section 3.3.3; Figure 25A**), other studies showed that the C-terminus of the 30K MPs is required for movement despite the apparent lack of PD localization function (Aparicio et al., 2010). Based on *in silico* analyses, the C-terminal region was predicted to be disordered that likely has protein binding abilities (**Section 3.3.1**; **Figure 22B**). The presence of some conserved residues prompted further investigation of the importance of the C-terminus in PD, or other aspects of sub-cellular localization. In a manner like the N-terminal mutants, several C-terminal truncation mutants were constructed by deletion of the C-terminal 14 (MPΔ279-293-YFP; **Figure 24**; red dashed arrow), 24 (MPΔ269-293-YFP; **Figure 24;** green dashed arrow) and

Figure 26 An element crucial for MP localization to the PD lies within the N-terminus

To determine if MP localization was impacted by truncations of the MP aa sequence, N-terminal deletion mutants fused to YFP were transiently expressed in tobacco leaves and the subcellular localization of the YFP fusion was visualized at 48 hpa. In all experiments, YFP constructs were co-infiltrated with PDLPV-CFP, an established PD marker. A schematic representation of each MP truncation is shown to the left of the confocal images: The grey box represents the viral MP, angled lines represent deleted portions of the MP sequence. Green arrow: d35s promoter, yellow rectangle: coding region of YFP, red box; NOS terminator.

YFP and CFP fluorescence are shown separately in the left and middle columns. The merged image combines both fluorescent images and the brightfield image and is shown in the right column. The construct names are shown on the left. The observed YFP fluorescence pattern is described to the right of the merged image (P: punctate; D: diffuse)

A, B   Deletion of the first 14 or 44 residues of the MP does not obviously affect PD localization (shown by white arrows).

C   Deletion of the N-terminal 69 residues abolishes PD localization.
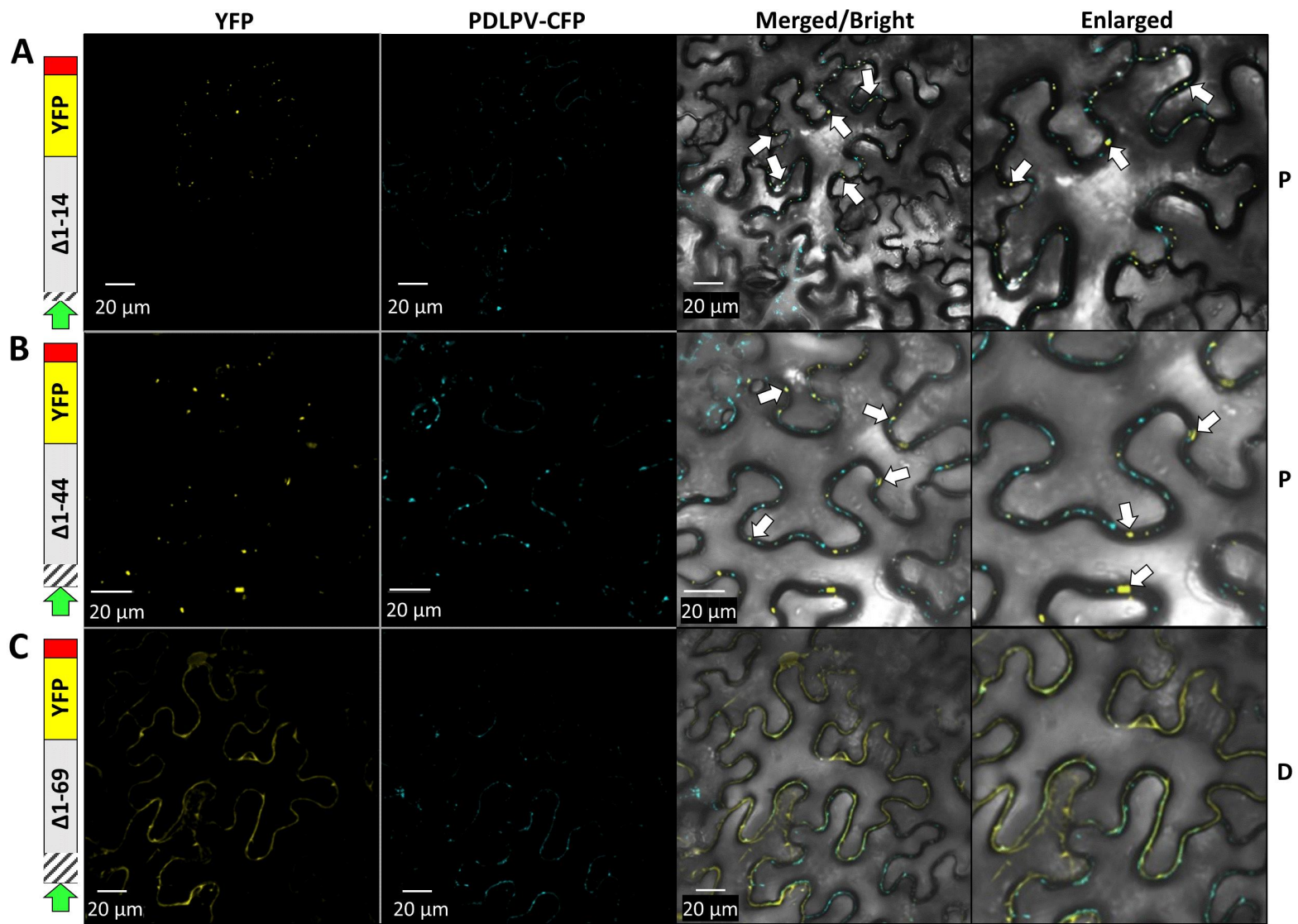
41 residues (MPΔ252-293-YFP; **Figure 24**; blue dashed arrow) based on the presence of conserved residues. Like the N-terminal truncation mutants, these C- terminal mutants were co-agroinfiltrated with the PD marker into tobacco leaves. Confocal microscopy analysis revealed that these C-terminal deletions all localized as punctate patterns that colocalized well with the PD marker (**Figure 27A-C**) suggesting the C-terminal domain of the PDV MP is not crucial for localizing to the PD.

There are several conserved residues within the region of residues 45-69 among the subgroup IV ilarviruses and AMV **(Figure 24;** shown by red arrows). To evaluate their importance in PD localization, these residues were selected for site directed mutagenesis and were replaced by an alanine. The resultant mutant sequences were fused to the N-terminus of YFP. After being agroinfiltrated into epidermal leaf cells of tobacco which were subsequently analyzed by confocal microscopy, it was found that constructs with an altered N48 or G62 formed punctate patterns at the cell periphery and co-localized with the PD marker (**Figure 28A, B**). In contrast either a single substitution at residue C54 or a double-substitution of L59 and N61 abolished PD localization as these YFP tagged mutant sequences formed diffuse patterns at the cell periphery and could not co localize with the PD marker (**Figure 29A, B**).

The importance of these residues which are proximal to the core domain suggests this domain may be important for PD localization as well. When the 30K core domain sequences of subgroup IV ilarviral and AMV MPs were aligned, many identical residues were totally conserved (**Figure 24**). To select conserved residues for point mutagenesis analysis, the 30K core sequences of MPs of subgroup III ilarviruses were included for sequence alignments (data not shown). Residues were selected for site directed mutagenesis at the beginning and middle of the core domain as these regions had an abundance of conserved residues (**Figure 24**). The constructs used included 4 double substitution mutants: L70S72, D129D131, F140R143, V173G174 and 2 single mutants: P103 and R146 (**Figure 24**; red arrows). When residues at the beginning of the core domain were mutated, PD localization was disrupted as no punctate patterns of fluorescence were visible (**Figure 30A-C**). Similarly, mutation of residues in the middle of

Figure 27 The C-terminal disordered region of the PDV MP is not required for PD localization

To determine if MP localization was impacted by truncations of the MP aa sequence, C-terminal deletion mutants fused to YFP were transiently expressed in tobacco leaves and the subcellular localization of the YFP fusion was visualized at 48 hpa. In all experiments, YFP constructs were co-infiltrated with PDLPV-CFP, an established PD marker. A schematic representation of each MP truncation is shown to the left of the confocal images: The grey box represents the viral MP, angled lines represent deleted portions of the MP sequence. Green arrow: d35s promoter, yellow rectangle: coding region of YFP, red box; NOS terminator.

YFP and CFP fluorescence are shown separately in the left and middle columns. The merged image combines both fluorescent images and the brightfield image and is shown in the right column. The construct names are shown on the left. The observed YFP fluorescence pattern is described to the right of the merged image (P: punctate)

(**A**, **B**, **C**)   C-terminal deletions of the PDV MP did not impact PD localization. The YFP tagged MP deletion mutants were observed forming punctate yellow patterns at the cell periphery (white arrows) and were also found to co-localize with PDLPV-CFP

	YFP	PDLPV-CFP	Merged/Bright	Enlarged

A — YFP Δ279-293

B — YFP Δ269-293

C — YFP Δ252-293

20 μm

P
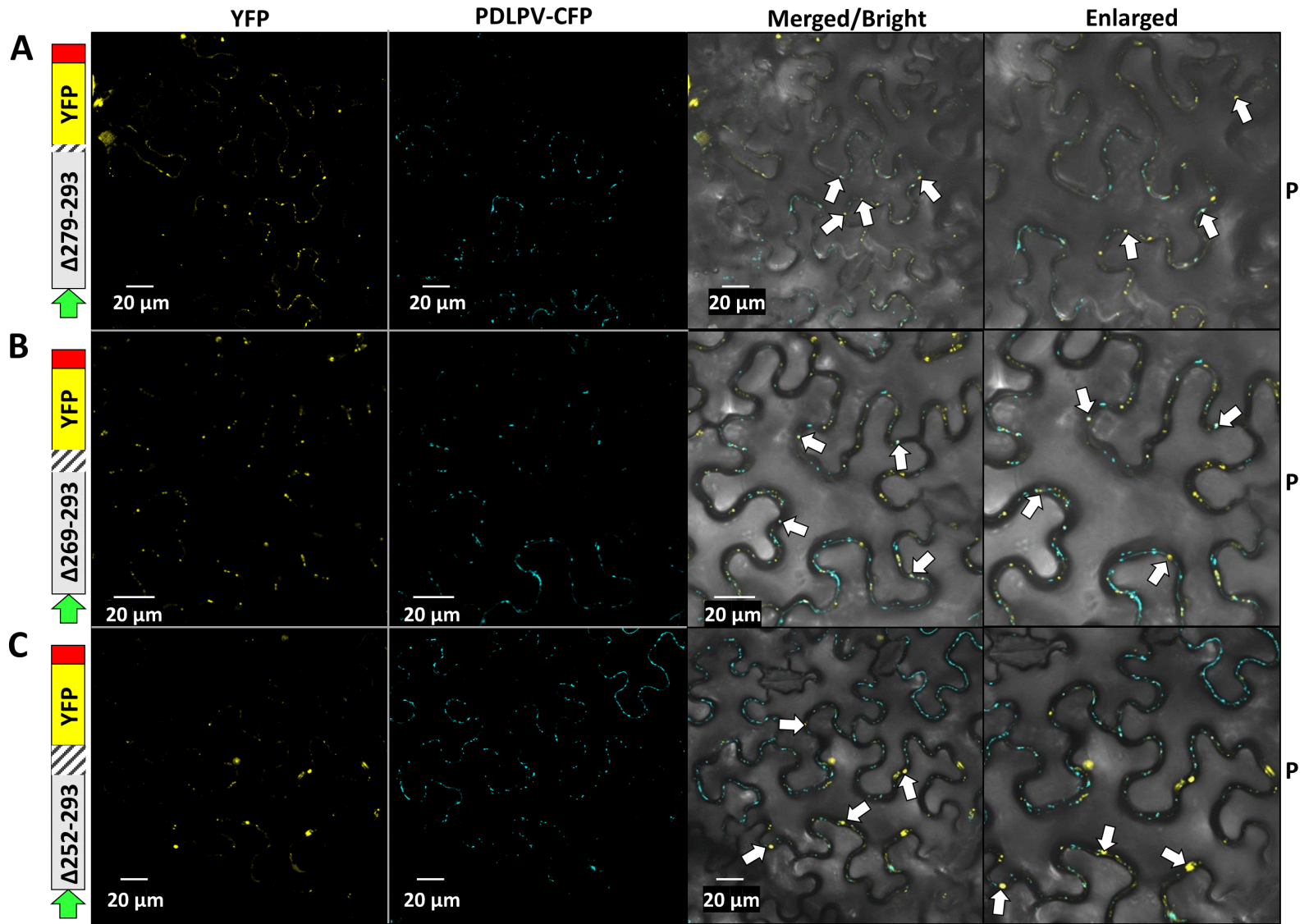
Figure 28 PD localization is affected by mutation of some residues within the MP N-terminus

To identify residues crucial for MP localization to the PD mutant MP sequences fused to YFP were transiently expressed in tobacco leaves and the subcellular localization of the YFP fusion was visualized at 48 hpa. The known PD marker, PDLPV is fused to CFP. A schematic representation of each MP truncation is shown to the left of the confocal images: The grey box represents the viral MP and the residue(s) substituted with alanine are labelled, green arrow: d35s promoter, yellow rectangle: coding region of YFP, red box: NOS terminator.

YFP and CFP fluorescence are shown separately in the left and middle columns. The merged image combines both fluorescent images and the brightfield image and is shown in the right column. The construct names are shown on the left. The observed YFP fluorescence pattern is described to the right of the merged image (P: punctate; D: diffuse)

A   When N48 was mutated to alanine, the mutated MP was able to form punctate patterns and co-localize with the PD marker at the periphery of the cell (white arrows).

B   When G62 was mutated to alanine, the mutated MP was able to form punctate patterns and co-localize with the PD marker at the periphery of the cell (white arrows).

YFP PDLPV-CFP Merged/Bright Enlarged

A

YFP

N48a

20 μm 20 μm 20 μm P

B

YFP

G62a

20 μm 20 μm 20 μm P
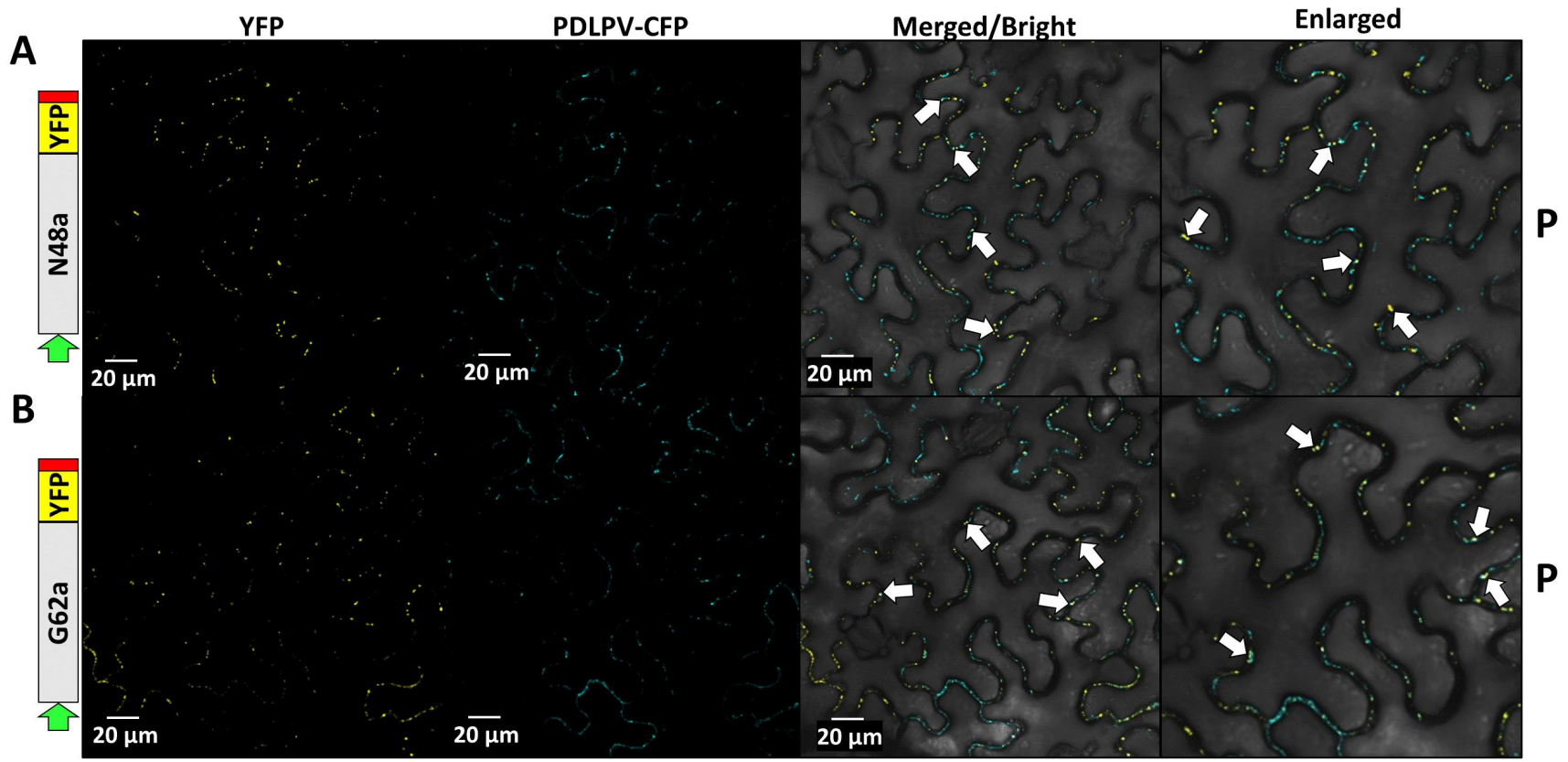
Figure 29 PD localization is affected by mutation of some residues within the MP N-terminus

To identify residues crucial for MP localization to the PD mutant MP sequences fused to YFP were transiently expressed in tobacco leaves and the subcellular localization of the YFP fusion was visualized at 48 hpa. The known PD marker, PDLPV is fused to CFP. A schematic representation of each MP truncation is shown to the left of the confocal images: The grey box represents the viral MP and the residue(s) substituted with alanine are labelled, green arrow: d35s promoter, yellow rectangle: coding region of YFP, red box: NOS terminator.

YFP and CFP fluorescence are shown separately in the left and middle columns. The merged image combines both fluorescent images and the brightfield image and is shown in the right column. The construct names are shown on the left. The observed YFP fluorescence pattern is described to the right of the merged image (P: punctate; D: diffuse)

A   When C54 was mutated to alanine, the mutated MP formed diffuse patterns at the cell periphery.

B   When two residues (L59 and N61) were both mutated to alanine, the mutated MP formed diffuse patterns at the cell periphery.

| | YFP | PDLPV-CFP | Merged/Bright | Enlarged |
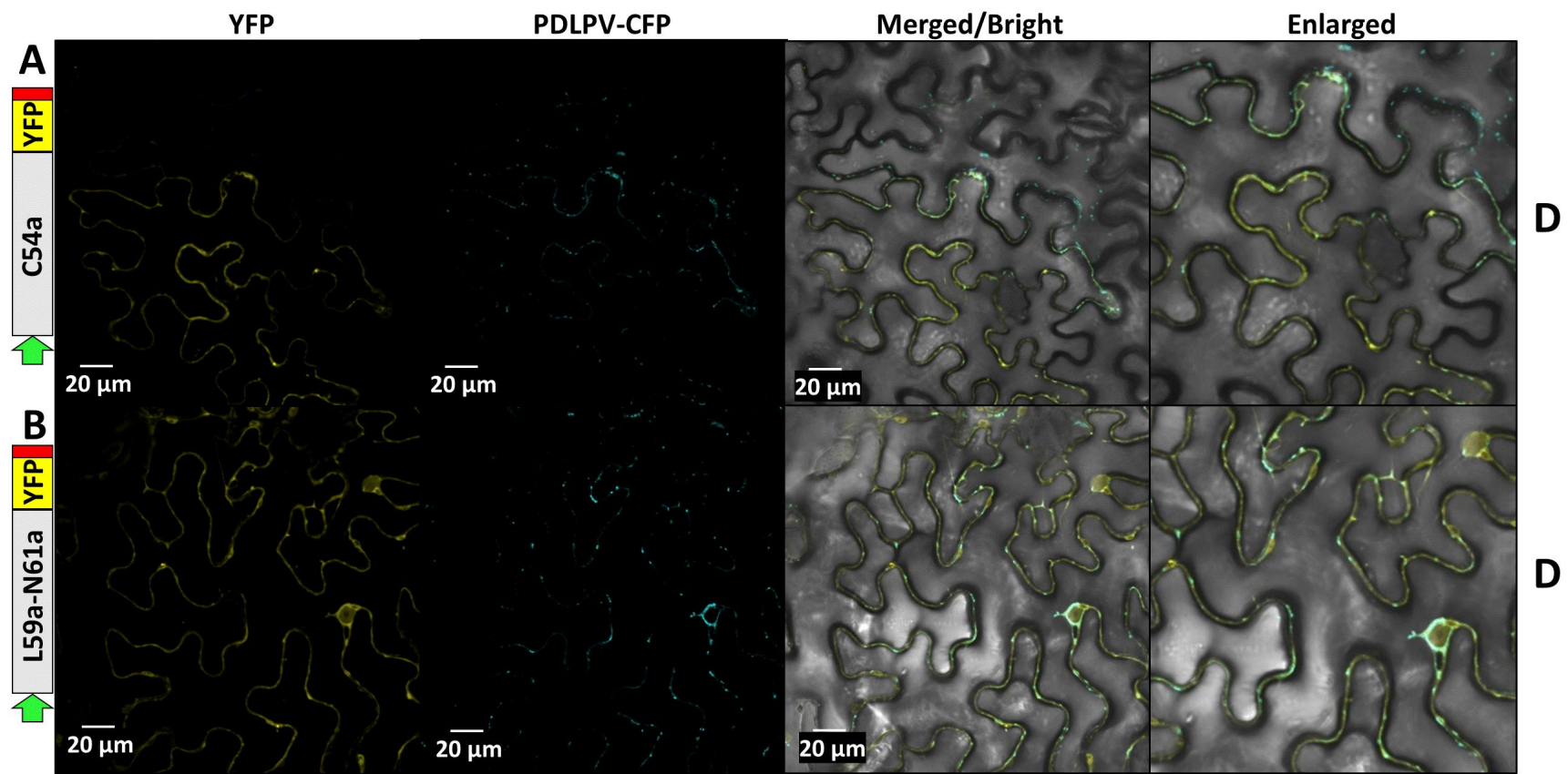
Figure 30 Identification of residues within the 30K core domain crucial for PD localization

A. tumefaciens cells harboring constructs of MP point mutants within the 30K core domain were fused to YFP were transiently expressed in tobacco leaves and the subcellular localization of the YFP fusion was visualized at 48 hpa. The known PD marker, PDLPV is fused to CFP. A schematic representation of each MP truncation is shown to the left of the confocal images: The grey box represents the viral MP and the residue(s) substituted with alanine are labelled, green arrow: d35s promoter, yellow rectangle: coding region of YFP, red box: NOS terminator.

YFP and CFP fluorescence are shown separately in the left and middle columns. The merged image combines both fluorescent images and the brightfield image and is shown in the right column. The construct names are shown on the left. The observed YFP fluorescence pattern is described to the right of the merged image (D: diffuse).

A   When two highly conserved residues (L70 and S72) proximal to the 30K core domain were mutated to alanine, the mutated MP was unable to form punctate structures, nor was it able to co-localize with the PD marker at the cell periphery.

B   When P103 was mutated to alanine, the mutant MP was unable to form punctate structures, nor was it able to colocalize with the PD marker at the cell periphery.

C   When two residues (D129 and D131) were both mutated to alanine, the mutated MP was unable to form punctate structures, nor was it able to co-localize with the PD marker at the cell periphery.

| | YFP | PDLPV-CFP | Merged/Bright | Enlarged |

A L70a-S72a

B P103a

C D129a-D131a

20 μm

D

117
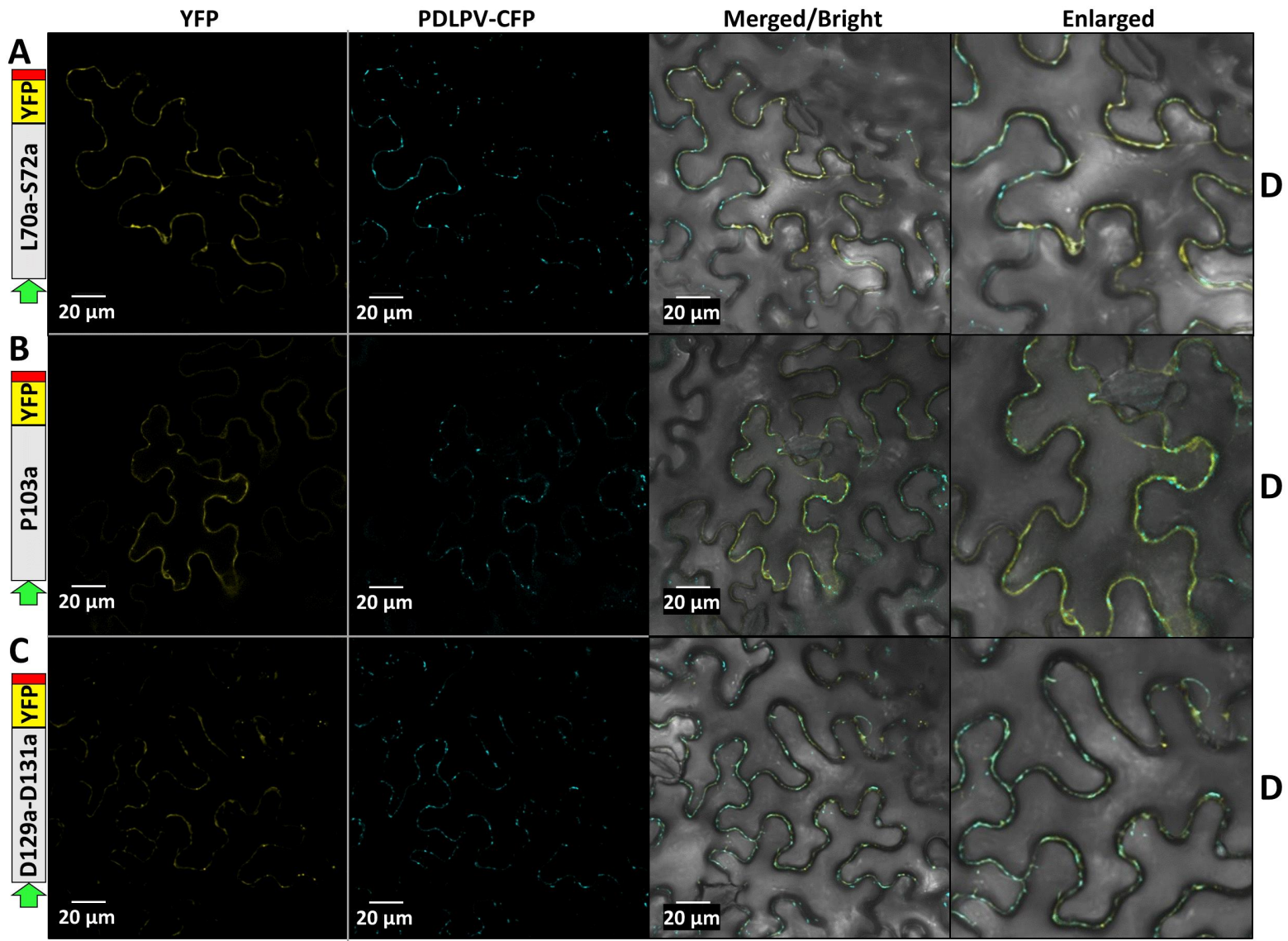
the core domain disrupted PD localization (**Figure 31A-C**). MP sequence alignment of all members within the *Ilarvirus* genus (AMV was included) showed several of the residues which were found to be important for MP localization to the PD were completely conserved (P103, R146 and G174).

3.3.4 The PDV MP alone can form tubular structures in plant cells

Recent electron microscopy work has provided evidence that PDV infection in cucumber induces the formation of tubular structures spanning adjacent cells (Kozieł et al., 2018). Based on previous studies for some MPs within the 30K superfamily the PDV MP likely forms tubules and is a strong candidate for further studies (Kasteel et al., 2015; Melcher, 2000; Zheng et al., 1997). To determine if the PDV MP alone can form tubules, the same MP-YFP construct was transfected into protoplasts isolated from cucumber. After 18-24 hours post transfection (hpt), laser scanning confocal microscopy was carried out and it was determined that yellow tubules were clearly visible protruding from transfected protoplasts (**Figure 32A**). As a negative control, YFP-100 was transfected into protoplasts and free YFP was clearly localized in the cytoplasm and did not produce any tubular structures (**Figure 32B**). These results show that the PDV MP alone can form the tubules in plant cells.

To determine what MP sequences are essential for tubule formation, the N-terminal MP truncation mutants (**Section 3.3.4**) were transfected into protoplasts isolated from cucumber. Deletion of the first 14 residues (MPΔ1-14-YFP) had no or little impact on the formation of tubules (**Figure 33A**). However, the deletion of the first 44 (MPΔ1-44-YFP) and 69 residues (MPΔ1-69-YFP) affected the formation of tubules (**Figure 33B, C**). MPΔ1-44-YFP still formed some punctate patterns which had localized to the periphery of the protoplast (**Figure 33B**), whereas the mutant MPΔ1-69-YFP is unable to form as many distinct punctate patterns (**Figure 33C**). These data are consistent with the earlier observation that the smaller N-terminal truncations (MPΔ1-14 and MPΔ1-44) did not impact the ability to form punctate patterns, presumably at the PD (**Figure 26A, B**).

Figure 31 Identification of residues within the 30K core domain crucial for PD localization

    A. tumefaciens cells harboring constructs of MP point mutants within the 30K core domain were fused to YFP were transiently expressed in tobacco leaves and the subcellular localization of the YFP fusion was visualized at 48 hpa. The known PD marker, PDLPV is fused to CFP. A schematic representation of each MP truncation is shown to the left of the confocal images: The grey box represents the viral MP and the residue(s) substituted with alanine are labelled, green arrow: d35s promoter, yellow rectangle: coding region of YFP, red box: NOS terminator.

    YFP and CFP fluorescence are shown separately in the left and middle columns. The merged image combines both fluorescent images and the brightfield image and is shown in the right column. The construct names are shown on the left. The observed YFP fluorescence pattern is described to the right of the merged image (D: diffuse).

A   When two residues (F140 and R143) were both mutated to alanine, the mutated MP was unable to form punctate structures, nor was it able to co-localize with the PD marker at the cell periphery.

B   When R146 was mutated to alanine, the mutant MP was unable to form punctate structures, nor was it able to colocalize with the PD marker at the cell periphery.

C   When two residues (V173 and G174) were both mutated to alanine, the mutated MP was unable to form punctate structures, nor was it able to co-localize with the PD marker at the cell periphery.
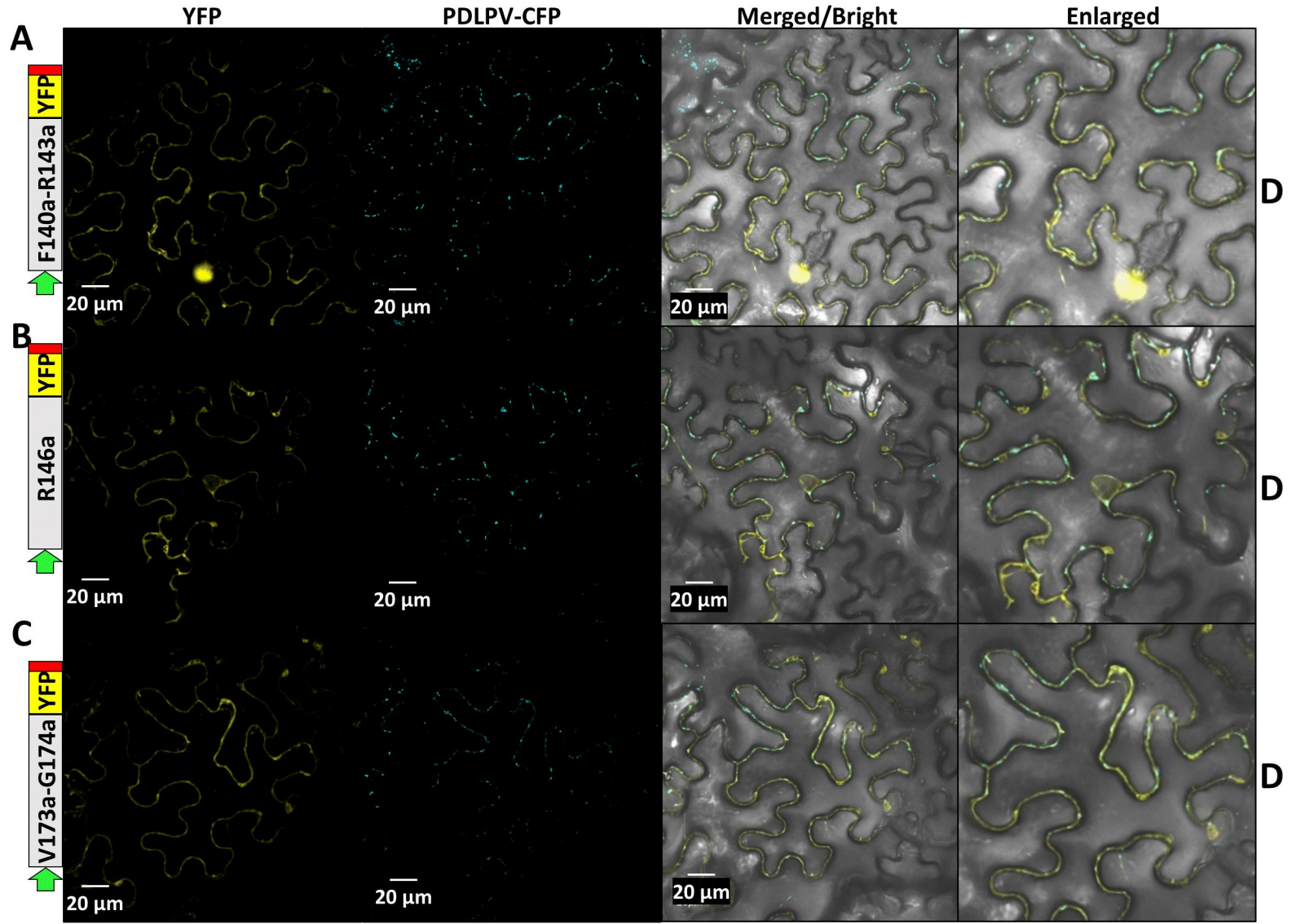
Figure 32 The MP of PDV forms tubular structures

 To determine if the MP of PDV forms tubular structures to facilitate intercellular movement, protoplasts isolated from cucumber were transfected with the MP-YFP fusion construct. As a negative control, YFP-100 used. A schematic representation of each construct use for transfection is shown to the left of the confocal images: The grey box represents the viral MP, green arrow: d35s promoter, yellow rectangle: coding region of YFP, red box: NOS terminator.

 Z-stack images of protoplasts transfected with YFP-tagged constructs are shown. YFP fluorescence is shown separately in the left column. The merged image combines both fluorescent and brightfield images and is shown in the right column. Construct names are shown on the left. Images were taken at 24 hpt.

A The full-length MP can form tubular structures which protrude from the transfected protoplasts.

B Free YFP is distributed in the cytoplasm of transfected protoplasts.
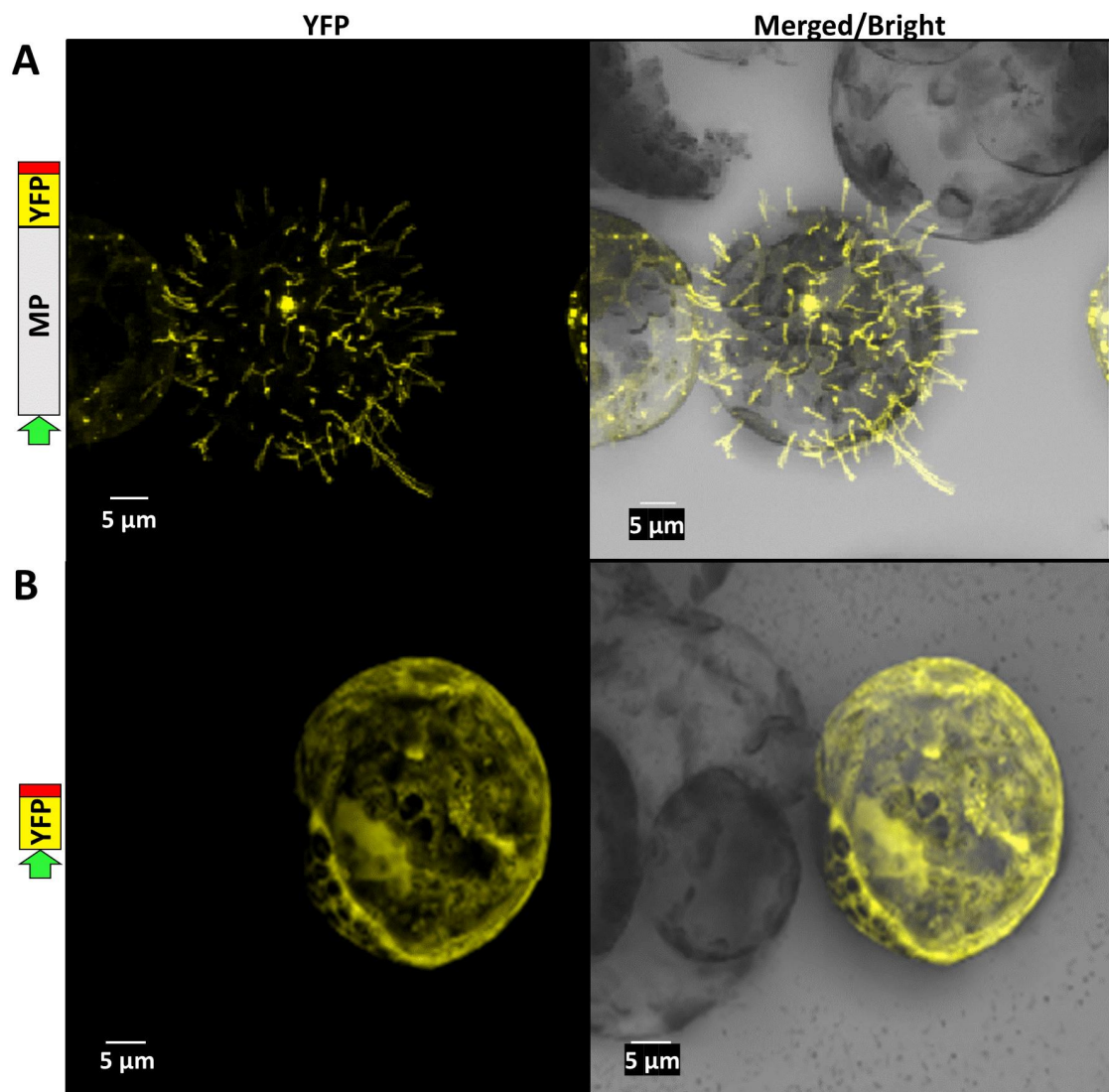
Figure 33 Sequences crucial for tubule formation are in the N-terminus of the PDV MP

To identify elements crucial to tubule formation protoplasts isolated from cucumber were transfected with the MP-YFP fusion construct, as well as the same N- and C-terminal truncated sequences which were used for MP PD localization studies. A schematic representation of each MP truncation is shown to the left of the confocal images: The grey box represents the viral MP, angled lines represent deleted portions of the MP sequence. Green arrow: d35s promoter, yellow rectangle: coding region of YFP, red box; NOS terminator.

Z-stack images of protoplasts transfected with YFP-tagged constructs are shown. The merged image combines both fluorescent and brightfield images and is exclusively shown to allow for comparison between images. Construct names are shown on the left of each image. The top image shows the full-length MP fused to YFP. Images were taken at 24 hpt.

A   Deletion of the first 14 residues had little or no impact on the formation of tubules.

B   Deletion of the first 44 residues disrupted the formation of tubules, however this truncated sequence was still able to form punctate patterns at the periphery of transfected protoplasts.

C   Deletion of the first 69 residues disrupted tubule formation and impacted the formation of punctate patterns at the periphery of protoplasts.

D-F   C-terminal deletions had little or no impact on tubule formation, regardless of the size of sequence deletions.

Full length MP

N-terminal truncations

C-terminal truncations
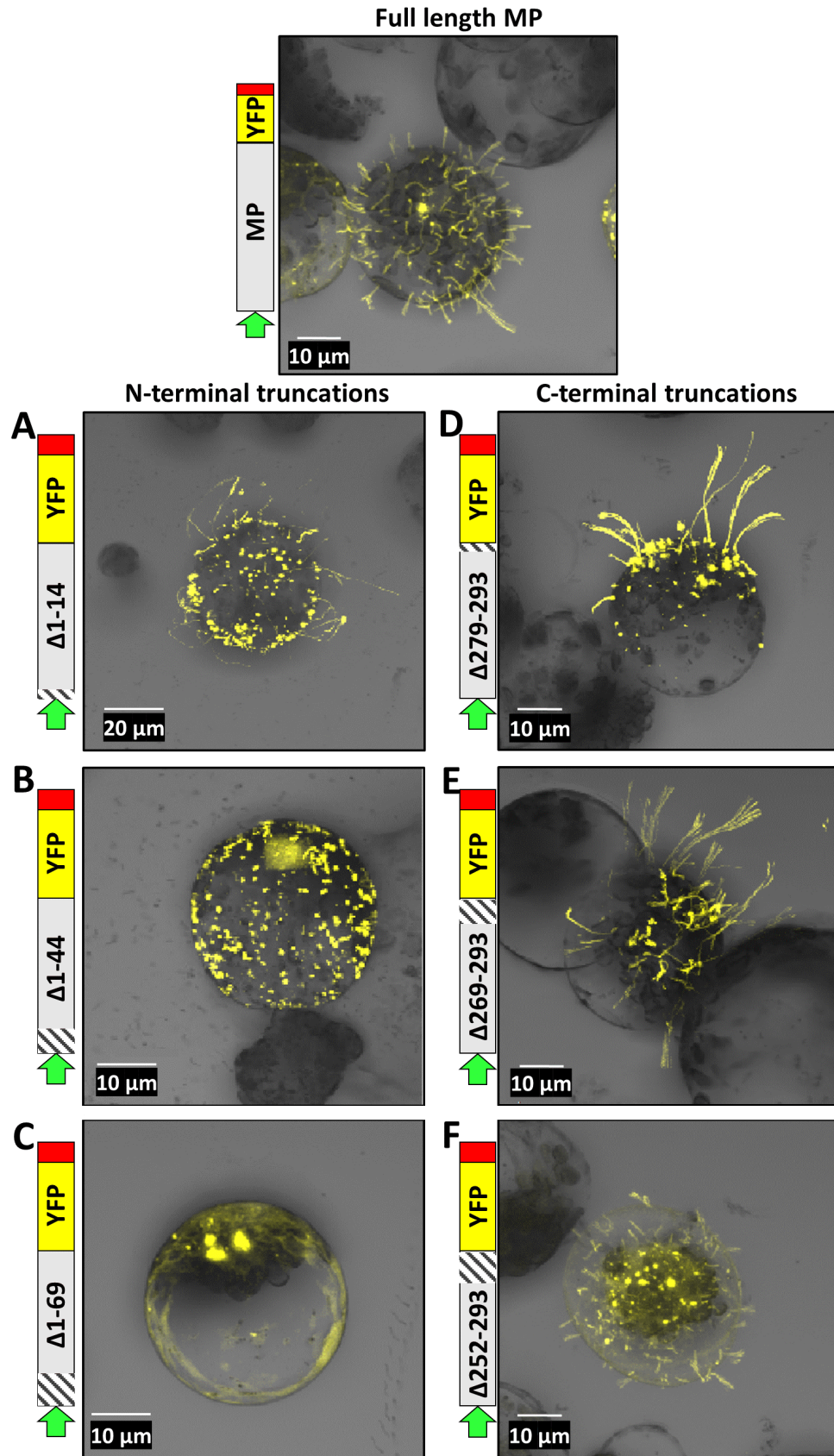
truncation mutants (**Figure 24,** shown as red, green and blue dashed arrows) were transfected into cucumber protoplasts to see if they can form tubules. The C-terminal truncation mutants were still able to form tubular structures in cucumber protoplasts (**Figure 33D-F**). These findings suggest the N-terminus contains an element crucial for tubule formation.

3.4   Proteomic analysis of PDV infection

3.4.1   Identification of protein distribution changes in cherry in response to PDV infection

To understand which biological processes are impacted by PDV infection, the changes in accumulation of host proteins were examined in orchard grown cherry. Proteins were extracted from both uninfected, asymptomatic leaves of cherry (**Figure 12A**) and symptomatic, PDV infected leaves (**Figure 12B-D**). The presence or absence of PDV in asymptomatic and symptomatic leaves was confirmed by RT-PCR using primers specific for the RNA sequence of the viral CP. Leaves were also tested for the presence of the viruses identified in NGS studies (**Section 3.1**, **Table 2**). When primers specific to the sequences of CVA, PNRSV and LChV1 were used for RT-PCR based detection in the cherry foliar samples, no amplicons were generated, suggesting these symptomatic samples were only infected with PDV, and asymptomatic samples were free of these viruses. Additionally, the presence of PDV in the symptomatic samples was confirmed by DAS-ELISA using an antibody against the viral CP (data not shown).

Proteins were quantified by label-free quantitation against the predicted protein database from a draft proteome of cherry (Jung et al., 2019). A total of 791 proteins were identified in both infected and uninfected samples. Protein abundance was estimated using intensity based absolute quantification, the most abundant protein in both infected and uninfected cherry extracted with this method was the ribulose bisphosphate carboxylase small chain (RuBisCO_SC) accounting for 8.29% and 12.05% respectively. The sole viral protein detected was the CP of PDV accounting for 0.15% of proteins identified

in infected cherry samples. In agreement with RT-PCR and DAS-ELISA detection methods, the CP was not identified in uninfected samples used in this study.

Principal component analysis (PCA) was used to compare the proteomes of each sample by reducing the large number of variables (identified host proteins), into protein groups for easier comparison (Ivosev *et al.* 2008). Based on the comparison of identified protein groups the PDV infected cherry samples formed a single cluster which was distinct from the cluster formed by the un-infected samples suggesting samples have similar proteomic profiles with respect to being infected or uninfected (**Figure 34**). Upon closer analysis in appears some replicates of PDV infected tissues cluster together within the larger cluster of PDV infected samples (**Figure 34**). The fact that PDV infected cherry samples did not cluster with uninfected samples suggests there is a proteomic change in cherry associated with PDV infection.

3.4.2 Proteomic analysis of cherry reveals significant protein accumulation changes during PDV infection.

Among the proteins identified in cherry, the accumulation levels of 135 proteins were significantly (P<0.05) altered when infected and uninfected samples were compared (**Figure 35**). Of these proteins, 75 increased in accumulation and 60 decreased significantly (P<0.05; **Appendix 4**). Further analysis showed that 101 proteins had at least a twofold change in accumulation (|log2fc|≥1; P<0.05), 59 were upregulated and 42 were downregulated (**Appendix 4**). Gene ontology (GO) was used to categorize biological processes impacted during infection based on these significantly altered proteins (Raudvere et al., 2019). GO analysis indicated multiple responses to external stimuli, immune responses, and protein degradation are upregulated in PDV infected samples. Conversely, biological processes related to photosynthesis, respiration, and transmembrane processes were downregulated in the infected samples (**Table 7**).

Upon closer inspection, it was found that decreased proteins were those related to translation, such as elongation factor 1B (eEF1B) and elongation factor G2 (eEFG2) and photosynthesis exemplified by decreased accumulations of photosystem II reaction

Figure 34 Principal component analysis of isolated cherry proteomes

Each point in the PCA graph represents the whole protein profile of one biological replicate. Photos of cherry leaves indicate the tissues the proteomes were isolated from. Samples with similar protein profiles are grouped together based on LFQ data showing clear separation between PDV infected, symptomatic cherry samples (red, yellow and pink) and uninfected samples (blue). The grouping of samples within the formed clusters indicates these samples do not contain a significantly different proteomic profile from other samples within the same group.

Component 1
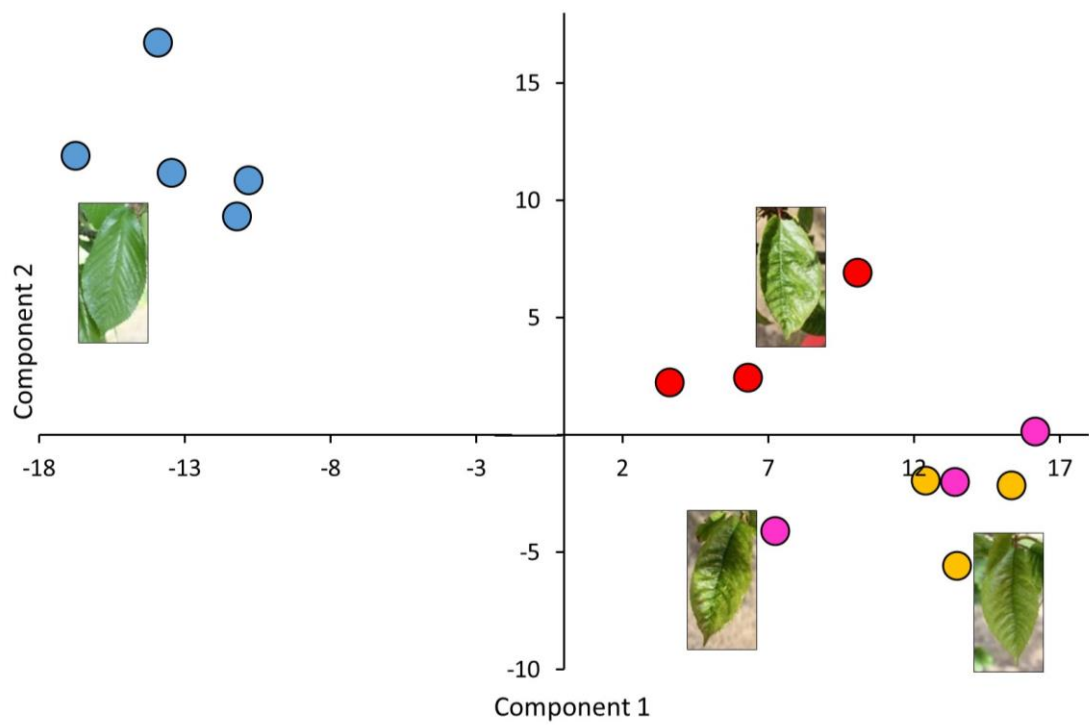
Figure 35 Differentially accumulated protein groups between healthy and asymptomatic cherry

To understand the biological processes being altered in association with PDV infection, proteins were extracted from infected and uninfected cherry foliar tissue samples. The changes in accumulation of proteins were measured by mass spectrometry.

A scatterplot representing protein accumulation changes in the identified cherry proteome when asymptomatic, uninfected foliar samples were compared to symptomatic, PDV infected samples (**Figure 12; Appendix 3**). Green circles represent protein groups which have significantly higher levels in PDV infected, symptomatic samples. Red circles represent protein groups which have significantly lower levels in PDV infected, symptomatic samples. White circles represent identified proteins, with insignificant accumulation changes. The purple circle denotes the viral CP of PDV which was only identified in symptomatic samples. Labels are assigned to proteins with the top 10 increases and decreases in accumulation when the samples were compared (**Table 6**). Additionally, labels which are underlined were identified to have significant accumulation changes in both plant hosts (**Section 3.4.5; Table 10**)
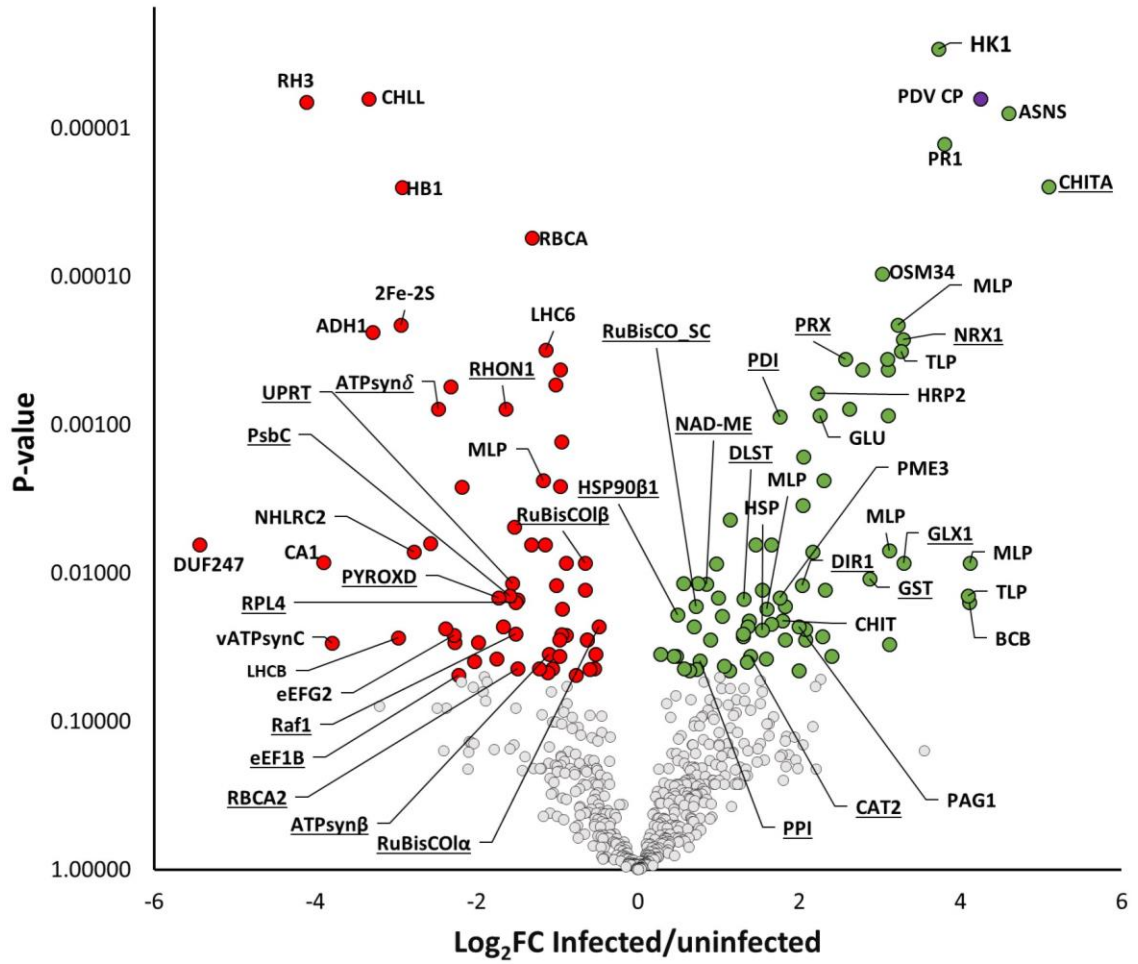
Table 6 The top 20 proteins with the greatest increases and decreases in accumulation identified in cherry associated with PDV infection

Accession	Protein	Log$_2$ ratio (PDV+/PDV-)	P-value
Pav_sc0001405.1_g1990.1.mk	Chitinase A (CHITA)	5.10	2.48E-05
Pav_sc0000638.1_g680.1.mk	Asparagine synthetase (ASNS)	4.60	7.95E-06
Pav_sc0000174.1_g1420.1.mk	MLP-like protein 423 (MLP)	4.12	8.53E-03
Pav_sc0000311.1_g1290.1.mk	Blue-copper-binding protein (BCB)	4.11	1.57E-02
Pav_sc0001488.1_g010.1.br	Pathogenesis-related thaumatin superfamily protein (TLP)	4.10	1.42E-02
Pav_sc0000568.1_g820.1.br	Basic pathogenesis-related protein 1 (PR1)	3.80	1.28E-05
Pav_sc0000044.1_g310.1.mk	Histidine kinase 1 (HK1)	3.73	2.91E-06
Pav_sc0000648.1_g160.1.mk	Lactoylglutathione lyase / glyoxalase I (GLX1)	3.30	8.53E-03
Pav_sc0000354.1_g620.1.mk	DC1 domain-containing protein (Nucleoredoxin 1; NRX1)	3.29	2.66E-04
Pav_sc0000058.1_g230.1.mk	glucan endo-1,3-beta-glucosidase	3.27	3.18E-04
Pav_sc0003747.1_g040.1.mk	Plant protein of unknown function (DUF247)	-5.44	6.41E-03
Pav_sc0001938.1_g620.1.mk	DEAD box RNA helicase (RH3)	-4.11	6.70E-06
Pav_sc0000009.1_g390.1.mk	Carbonic anhydrase 1 (CA1)	-3.90	8.45E-03
Pav_sc0001080.1_g400.1.mk	Vacuolar ATP synthase subunit C (vATPsynC)	-3.79	2.95E-02
Pav_sc0000037.1_g050.1.mk	magnesium-chelatase subunit ChlI (CHLL)	-3.34	6.35E-06
Pav_sc0002842.1_g230.1.mk	Alcohol dehydrogenase 1 (ADH1)	-3.29	2.37E-04
Pav_sc0001289.1_g560.1.mk	Chlorophyll A/B binding protein 1 (LHCB)	-2.97	2.73E-02
Pav_sc0000174.1_g1650.1.mk	Rieske domain-containing protein (2Fe-2S)	-2.94	2.12E-04
Pav_sc0000544.1_g100.1.mk	Hemoglobin 1 (HB1)	-2.92	2.51E-05
Pav_sc0000907.1_g230.1.mk	NHL repeat-containing protein 2 isoform X1 (NHLRC2)	-2.78	7.18E-03

Table 7 GO analysis of the 30 proteins with the greatest increases and decreases in accumulation identified in cherry associated with PDV infection

GO term ID	Description	p-value
Increased in association with PDV infection		
GO:0010038	response to metal ion	1.67E-13
GO:0046686	response to cadmium ion	1.94E-12
GO:0050896	response to stimulus	9.03E-11
GO:0010035	response to inorganic substance	2.20E-10
GO:0042221	response to chemical	7.81E-09
GO:0010498	proteasomal protein catabolic process	6.11E-07
GO:0043161	proteasome-mediated ubiquitin-dependent protein catabolic process	3.82E-06
GO:0010499	proteasomal ubiquitin-independent protein catabolic process	1.58E-05
GO:0051230	spindle disassembly	2.93E-05
GO:0051228	mitotic spindle disassembly	2.93E-05
GO:0097352	autophagosome maturation	1.17E-04
GO:0010043	response to zinc ion	2.14E-04
GO:0045087	innate immune response	4.41E-04
GO:0030163	protein catabolic process	4.72E-04
GO:1901565	organonitrogen compound catabolic process	5.01E-04
Decreased in association with PDV infection		
GO:0015979	photosynthesis	3.80E-25
GO:0019253	reductive pentose-phosphate cycle	5.14E-15
GO:0019685	photosynthesis, dark reaction	5.14E-15
GO:0015977	carbon fixation	5.40E-14
GO:0009765	photosynthesis, light harvesting	3.06E-08
GO:0019684	photosynthesis, light reaction	3.19E-08
GO:0050896	response to stimulus	3.74E-08
GO:0009853	photorespiration	9.23E-07
GO:0065002	intracellular protein transmembrane transport	9.25E-07
GO:0043094	cellular metabolic compound salvage	1.00E-06
GO:0006091	generation of precursor metabolites and energy	1.84E-06
GO:0071806	protein transmembrane transport	5.48E-06
GO:0018298	protein-chromophore linkage	7.07E-06
GO:0009735	response to cytokinin	7.61E-06
GO:0006952	defense response	8.89E-06

centre subunit C (PsbC) and RuBisCO accumulation factor 1 (Raf1). Some proteins which had increased in accumulation in PDV infected leaves were associated with stress and pathogen defense including the basic pathogenesis related protein 1 (PR1). Accumulations of proteins related to oxidative stress responses were significantly increased, including enzymes involved in the production and degradation of ROS such as Catalase 2 (CAT2) and Peroxidases (PRX). Responses to abiotic factors such as chemical and osmotic stress (drought and salt stress) were also upregulated. Several proteins implicated in defense of other pathogens such as fungi were significantly increased including two chitin binding and degrading chitinases (CHIT), two members of the thaumatin superfamily (TLP), a blue copper binding protein (BCB), osmotin 34 (OSM34) and beta-1,3-glucanase 3 (βGluc). Taken together, the presence of proteins related to antimicrobial defense responses suggest the altered proteomes in cherry may have been influenced by the presence of additional stressors including other pathogens and cannot be attributed to PDV alone.

3.4.3 Identification and distribution of proteins in cucumber in response to PDV infection

The identified proteins in cherry with significantly differential accumulation provided insights as to which biological processes were affected in PDV-infected cherry. However, as a perennial crop, cherry may be exposed to extensive abiotic stress and multi-pathogen attack. To mitigate biotic and abiotic confounding variables that can occur in field conditions, the PDV infectious clone was used to infect cucumber under controlled conditions (temperature, lighting, humidity) to study protein accumulation changes in response to PDV infection. The use of cucumber as an experimental host has a few advantages compared to seedlings of cherry. Firstly, the proteome of cucumber is a curated proteome which has been updated several times since available publication, compared to the proteome of cherry which is only based on *in silico* predicted protein sequences and have not been validated *in vivo.* Secondly, cucumber is much more

amenable to being raised in laboratory conditions (ie. smaller stature, higher seed germination rate, and higher infectivity rate with the infectious clone).

To study proteomic alterations caused by PDV, total proteins were extracted from upper, non-inoculated mildly symptomatic leaves of PDV- and mock- agroinfiltrated plants at 10 dpa (**Figure 36 A, B**). As in work done in cherry, the presence or absence of PDV was confirmed in all plants using DAS-ELISA and RT-PCR (data not shown). The proteomes of cucumber were analyzed in a similar manner as in cherry. PCA was used to evaluate the general sample to sample variation derived from their individual proteomic profiles. Based on the first and second component the uninfected samples formed a unique cluster signifying they share similar proteome profiles (**Figure 37**). Conversely, samples from infected cucumber plants formed two distinct clusters that were separated by first and second components. Neither of the infected cucumber groups clustered with the mock treated samples suggesting there was a proteomic change following PDV infection. However, the presence of two separate clusters suggest the response of at least 2 samples to PDV infection were different than response to the other 3 samples in the experiment.

Proteins were quantified by LFQ proteomics against the predicted protein database from a proteome of cucumber (Uniprot, 2018). A total of 1596 proteins were identified in both PDV infected and mock treated samples. In contrast with cherry, the most abundant protein in cucumber differed between infected and uninfected samples. The RuBisCO_SC was the most abundant protein in PDV infected samples accounting for 6.59% of identified proteins (3.95% in uninfected). The most abundant protein in uninfected cucumber was the beta form of RuBisCO activase (RBCA) accounting for 4.89% of proteins (3.31% in infected). Like results from cherry, the sole viral protein detected was the CP of PDV; in agreement with RT-PCR and DAS-ELISA detection methods, the CP was not identified in mock inoculated samples.

Figure 36 Differentially accumulated protein groups between PDV infected and mock inoculated cucumber

To understand the biological processes being altered following PDV infection, proteins were extracted from infected and uninfected cucumber foliar tissue samples. The changes in accumulation of proteins were measured by mass spectrometry.

A, B   Seedlings of cucumber were inoculated with the PDV infectious clone. At 10 dpa, foliar samples of uninoculated first true leaves were taken from mock (**A**) inoculated plants and PDV infected (**B**) plants showing chlorotic lesions and used for protein extraction and further analyses.

C   A volcano plot representing protein accumulation changes in the identified cucumber proteome when mock and PDV infected samples were compared (**Appendix 4**). Green circles represent protein groups which have significantly higher levels in PDV infected, symptomatic samples. Red circles represent protein groups which have significantly lower levels in PDV infected, symptomatic samples. White circles represent identified proteins, with insignificant accumulation changes. The purple circle denotes the viral CP of PDV which was only identified in symptomatic samples. Labels are assigned to proteins with the top 10 increases and decreases in accumulation when the samples were compared (**Table 8**). Additionally, labels which are underlined were identified to have significant accumulation changes in both plant hosts (**Section 3.4.5; Table 10**).

Mock   **Infected**
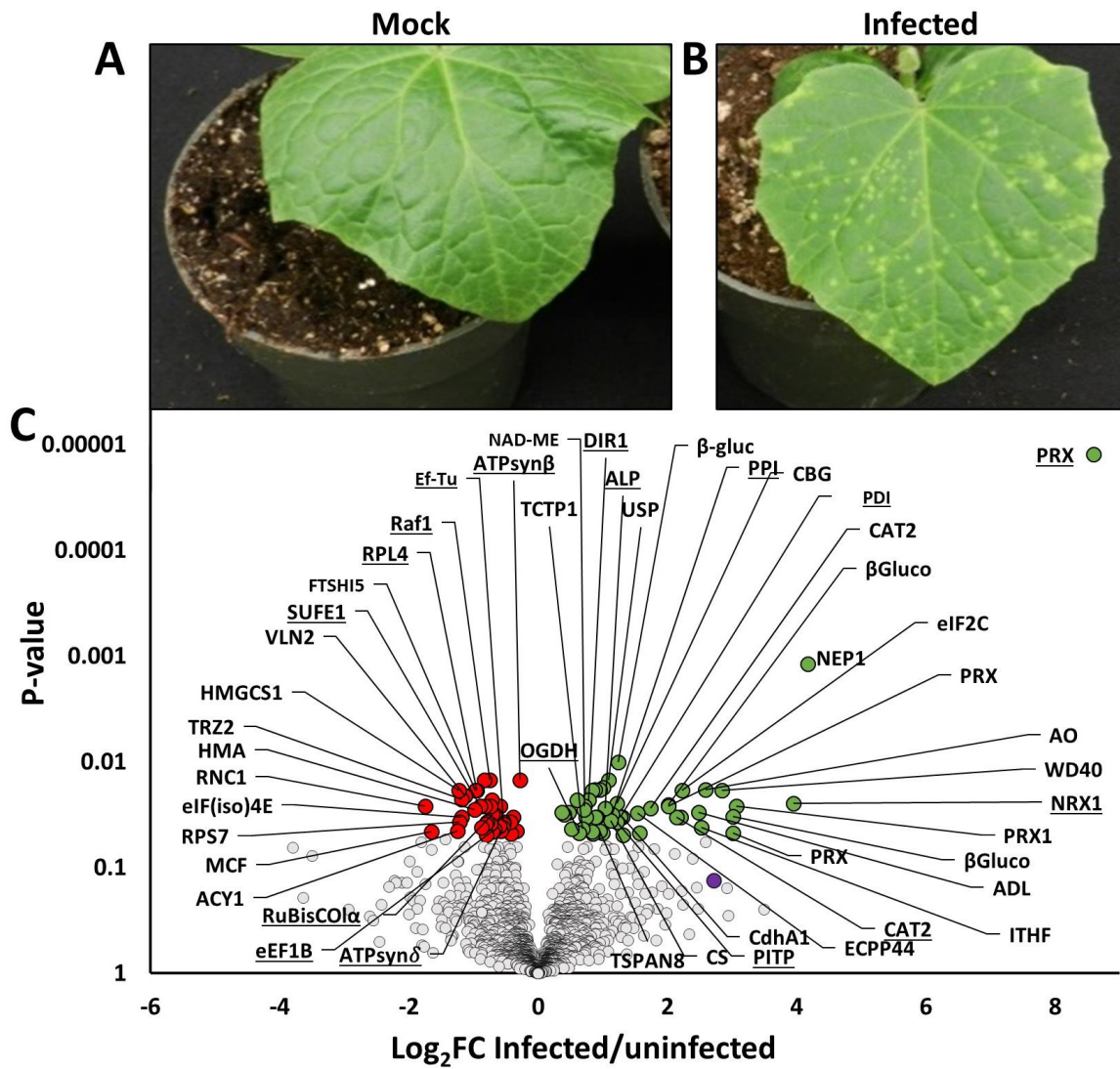
Figure 37 Principal component analysis of cucumber

Each point in the PCA graph represents the whole protein profile of one sample. The grouping of samples within the two clusters illustrates samples within the same group do not contain a significantly different proteomic profile from each other. Photos of cucumber plants illustrate the treatment of the samples: PDV infected (pink circles), and mock treated plants (blue circles) are shown. The clustering of mock treated samples indicates these samples do not contain a significantly different proteomic profile from each other. The two separate clusters of symptomatic samples suggests there is some difference in proteomic profile between samples, however overall there is still a significant difference in proteomes between PDV infected, and mock treated plants.
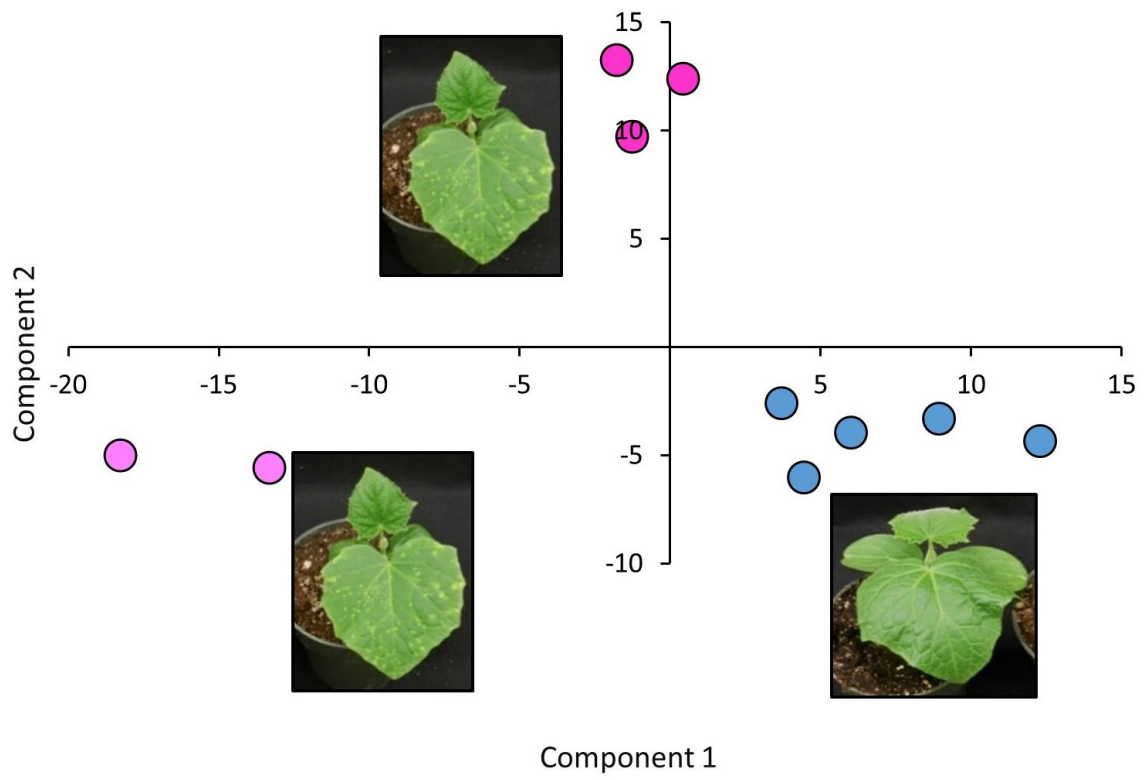
3.4.4 Label - free quantitative proteomic analysis of cucumber

Of the 1596 proteins identified in cucumber the accumulations of 87 proteins were significantly (P<0.05) altered following PDV infection. Of these proteins, 50 were increased and 37 were decreased (**Figure 36C; Table 8**; **Appendix 4**). GO analysis indicated processes related to oxidative stress, abiotic stimulus responses and chemical stressors were upregulated following PDV infection. Conversely, biological processes related to protein translation, peptide biosynthesis, and various metabolic processes were downregulated because of PDV infection (**Table 9**).

Closer inspection of the differentially accumulated proteins showed that in PDV infected cucumber, proteins with greatest accumulation decreases were associated with translation such as eIF(iso)4E and Ef-Tu. Proteins related to photosynthesis such as Raf1 and FTSHI5 are decreased as well. Proteins with the greatest accumulation increases are those involved in oxidative stress such as PRX and CAT2, and antiviral defense such as eukaryotic translation initiation factor 2C (eIF2C), a component of RNA silencing machinery.

3.4.5 Orthologous proteins are identified in both species

Orthologous proteins with significant accumulation (unpaired t-test p<0.05) changes following PDV infection in both hosts were identified using the BLAST algorithm (Altschul et al., 1990). Overall, the levels of 31 similar proteins which were identified in both hosts species had similar, significant accumulation changes when PDV infected, and uninfected sample proteomes were compared. Of these proteins nearly half are involved in photosynthesis, and 5 are involved in oxidative stress (**Table 10**).

3.5 Characterization of two differentially accumulated proteins associated with PDV infection in cucumber

To explore the possible functional roles of the differentially accumulated proteins identified in PDV-infected cucumber, two proteins were selected for further study: the translationally controlled tumor protein 1 (TCTP1), which was insignificantly changed in

cherry and tetraspanin 8 (TSPAN8), which was only identified in cucumber, had both increased significantly in response to PDV infection (**Appendix 4**). TCTP1 has been recently identified as a required host factor for potyviral infection in tomato (*Solanum lycopersicum L.*) and tobacco (Bruckner et al., 2017). TSPAN8 has been implicated in responses to multicellular pathogens and the formation of exosomes, which may participate in movement of potyviruses (Cai et al., 2018; Movahed et al., 2019). To study potential roles of these proteins in PDV infection, primers were designed to amplify the coding regions of the cherry encoded orthologs of TCTP1 and TSPAN8 (henceforth denoted as TCTP1 and TSPAN8, respectively) based on the available genome sequence retrieved from the cherry genome database (Jung et al., 2019). The amplified coding regions were then cloned into pEarleyGate expression vectors to create fusion constructs consisting of C-terminal CFP fusions for localization studies, and fusion constructs containing N- and C- terminal halves of YFP for BiFC assays (**Section 2.4.4**).

3.5.1   TSPAN8 localizes to the PD and interacts with the viral CP

To study potential roles of TSPAN8 in PDV infection, the subcellular localization of this protein was determined *in planta* as a fusion with CFP (TSPAN8-CFP). TSPAN8-CFP was transiently expressed with the PD marker PDLPV (which had been fused to YFP; PDLPV-YFP) in tobacco epidermal leaf cells. Using confocal microscopy, TSPAN8-CFP and PDLPV-YFP were observed co-localizing as punctate patterns along the cell periphery (**Figure 38A;** white arrows), suggesting TSPAN8 is a PD-located protein with a possible role involved in viral cell-to-cell movement. As both the MP and CP of PDV are known to be involved in intercellular movement, it is possible that the PDV MP and CP interact with TSPAN8. To determine if TSPAN8 co-localizes with the viral MP or CP, TSPAN8-CFP was co-expressed with YFP tagged viral CP (CP-YFP) and MP (MP-YFP) in tobacco leaves and visualized by confocal microscopy. Transient expression showed that TSPAN8-CFP co-localizes with CP-YFP however, it appears that TSPAN8-CFP and MP-YFP do not co-localize (**Figure 38B, C;** white arrows). Based on a previous study showing that TSPAN8 interacts with pathogens in vivo (Wang et al., 2015), a potential interaction between TSPAN8 and

Table 8 The top 20 proteins with the greatest increases and decreases in accumulation identified in cucumber following PDV infection

Accession	Protein	Log$_2$ ratio (PDV+/PDV-)	P- Value
A0A0A0L0I0	Peroxidase superfamily protein (PRX)	8.60	1.24E-05
A0A0A0LPJ3	Aspartic proteinase nepenthesin-1 (NEP1)	4.17	1.18E-03
A0A0A0KSQ4	Nucleoredoxin 1 (NRX1)	3.94	2.47E-02
A0A0A0K3Z5	Peroxidase (PRX)	3.06	2.61E-02
A0A0A0L1T4	Peroxidase (PRX)	3.02	4.69E-02
A0A0A0LTR4	β-glucosidase 44-like (βGluco)	3.01	3.30E-02
A0A0A0KTH7	WD40 TOPLESS (WD40)	2.85	1.87E-02
A0A0A0LXB9	L-ascorbate oxidase (AO)	2.59	1.84E-02
A0A0A0LFD4	Inhibitor of trypsin and hageman factor-like (ITHF)	2.52	4.19E-02
A0A0A0KT33	AMP dependent ligase (ADL)	2.48	3.01E-02
A0A0A0KGG7	Ribonuclease III domain-containing protein (RNC1)	-1.75	2.61E-02
A0A0A0KTN2	Mitochondrial substrate carrier family protein C (MCF)	-1.65	4.54E-02
A0A0A0KAV8	Aminoacylase-1 (ACY1)	-1.24	4.51E-02
A0A0A0L5T1	3-hydroxy-3-methylglutaryl coenzyme A synthase (HMGCS1)	-1.23	1.87E-02
A0A0A0K5K0	Ribosomal_S7 domain-containing protein (RPS7)	-1.22	3.69E-02
B0F832	Eukaryotic initiation factor iso4E (eIF(iso)4E)	-1.18	3.35E-02
A0A0A0KHX0	tRNAse Z (TRZ2)	-1.18	2.25E-02
A0A0A0KYB6	Villin-2 (VLN2)	-1.13	2.09E-02
A0A0A0LC88	Heavy metal associated domain-containing protein (HMA)	-0.98	2.84E-02
A0A0A0M3D4	Inactive ATP-dependent zinc metalloprotease FTSHI5 (FTSHI5)	-0.97	1.87E-02

Table 9 GO analysis of the 30 proteins with the greatest accumulation changes identified in cucumber following PDV infection

Increased in response to PDV infection		
GO term ID	Description	p-value
GO:0042744	hydrogen peroxide catabolic process	3.66E-10
GO:0055114	oxidation-reduction process	1.82E-09
GO:0042743	hydrogen peroxide metabolic process	3.19E-09
GO:0098869	cellular oxidant detoxification	6.63E-09
GO:1990748	cellular detoxification	1.35E-08
GO:0097237	cellular response to toxic substance	1.43E-08
GO:0010035	response to inorganic substance	1.56E-07
GO:0098754	detoxification	1.98E-07
GO:0072593	reactive oxygen species metabolic process	3.60E-07
GO:0042221	response to chemical	8.01E-07
GO:0009636	response to toxic substance	8.50E-07
GO:0006869	lipid transport	2.37E-06
GO:0010876	lipid localization	9.41E-06
GO:0006979	response to oxidative stress	2.43E-05
GO:0009628	response to abiotic stimulus	2.65E-04
Decreased in response to PDV infection		
GO term ID	Description	p-value
GO:0006412	translation	1.66E-10
GO:0043043	peptide biosynthetic process	1.79E-10
GO:0043603	cellular amide metabolic process	7.02E-10
GO:0006518	peptide metabolic process	7.47E-10
GO:0043604	amide biosynthetic process	7.87E-10
GO:1901566	organonitrogen compound biosynthetic process	6.37E-08
GO:0071786	endoplasmic reticulum tubular network organization	3.91E-07
GO:0007029	endoplasmic reticulum organization	6.31E-04
GO:0046854	phosphatidylinositol phosphorylation	7.88E-04
GO:0046834	lipid phosphorylation	1.08E-03
GO:0000103	sulfate assimilation	5.65E-03
GO:0009987	cellular process	1.94E-02
GO:0006996	organelle organization	2.23E-02
GO:0019637	organophosphate metabolic process	2.90E-02
GO:0006414	translational elongation	3.26E-02

Table 10 Orthologous proteins identified in both cherry and cucumber with significant accumulation changes following PDV infection

Protein identified in cherry	Log$_2$ ratio (PDV+/PDV-)	P-value	Log$_2$ ratio (PDV+/PDV-) cucumber ortholog	p-value	% ID[a]	Biological process	Reference
Chitinase A (CHITA)	5.10	2.48E-05	2.92	2.14E-02	65	Antifungal/PAMP	Sharma *et al.* 2011
Lactoylglutathione lyase/glyoxalase I (GLX1)	3.30	8.53E-03	0.79	9.11E-03	82	Detoxification	Souza *et al.* 2019
DC1 domain-containing protein (Nucleoredoxin 1; NRX1)	3.29	2.66E-04	3.94	3.72E-04	61	Protects ROS scavengers	Kneeshaw *et al.* 2017
Glutathione S-transferase (GST)	2.87	1.10E-02	2.14	3.33E-02	Name	Antioxidant	Gullner *et al.* 2018
Peroxidase superfamily protein (PRX)	2.58	3.62E-04	8.60	7.78E-09	Name	Antioxidant	Almagro *et al.* 2008
Bifunctional inhibitor/lipid-transfer /seed-storage 2S albumin (DIR1)	2.04	1.20E-02	0.78	3.18E-04	Name	Systemic resistance	Sarowar *et al.* 2009
Protein disulfide isomerase-like 1-2 (PDI)	1.76	8.79E-04	1.27	1.11E-03	50	Protein folding	Kromina *et al.* 2008
Catalase 2 (CAT2)	1.39	3.63E-02	2.23	1.77E-04	59	ROS scavenging	Roshan *et al.* 2018
Dihydrolipoamide succinyltransferase (DLST)	1.31	1.50E-02	1.16	7.32E-03	78	Lipoxidation	de Dios Alché 2019
NADP-dependent malic enzyme (NADP-ME)	0.85	1.18E-02	1.14	1.15E-02	78	Defense	Souza *et al.* 2019
Peptidyl-prolyl cis-trans isomerase 1 (PPI)	0.77	3.90E-02	1.15	8.72E-04	91	Protein folding	Kromina *et al.* 2008
ruBisCO small chain isoform X1 (RuBisCO_SC)	0.72	1.67E-02	0.62	1.40E-02	73	Photosynthesis	Li *et al* 2016
Endoplasmin homolog (HSP90β1)	0.49	1.91E-02	0.89	6.76E-03	84	Chaperone	Klein *et al.* 2006
ATP synthase delta-subunit (ATPsynδ)	-2.48	7.83E-04	-0.58	2.10E-03	81	ATP synthesis	Bhat *et al.* 2013
Translation elongation factor 1B (eEF1B)	-2.22	4.86E-02	-0.67	8.84E-04	61	Translation	Beligni *et al* 2004
Pyridine nucleotide-disulphide oxidoreductase (PYROXD)	-1.73	1.46E-02	-0.33	3.86E-03	88	Chlorophyl biosynthesis	Souza *et al.* 2019

Protein identified in cherry	Log$_2$ ratio (PDV+/PDV-)	P-value	Log$_2$ ratio (PDV+/PDV-) cucumber ortholog	p-value	% ID[a]	Biological process	Reference
rho-N domain-containing protein 1 (RHON1)	-1.64	7.83E-04	-0.48	4.44E-02	72	Chloroplast RNA processing	Souza *et al.* 2019
Photosystem II reaction center protein C (PsbC)	-1.59	1.42E-02	-2.11	1.57E-02	81	Photosynthesis	Li *et al* 2016
Uracil phosphoribosyltransferase (UPRT)	-1.56	1.17E-02	-0.62	6.78E-03	93	Development	Mainguet *et al.* 2009
Rubisco accumulation factor 1 (Raf1)	-1.52	2.57E-02	-0.75	5.08E-05	63	Chaperone	Souza *et al.* 2019
50S Ribosomal protein L4 (RPL4)	-1.50	1.51E-02	-0.95	1.91E-04	75	Translation	Li 2019
RuBisCO activase isoform X2 (RBCA2)	-1.49	4.40E-02	-0.51	1.62E-02	81	Photosynthesis	Souza *et al.* 2019
Rubisco activase (RBCA)	-1.31	5.47E-05	-0.51	1.62E-02	79	Photosynthesis	Souza *et al.* 2019
ATP synthase subunit β ' (ATPsynβ)	-1.11	3.52E-02	-0.28	4.40E-05	72	ATP synthesis	Souza *et al.* 2019
RuBisCO large subunit-binding protein subunit β (RuBisCOlβ)	-0.65	8.53E-03	-0.55	5.99E-03	76	Photosynthesis	Feki 2005
ruBisCO large subunit-binding protein subunit α (RuBisCOlα)	-0.48	2.29E-02	-0.71	8.50E-04	88	Photosynthesis	Feki 2005

Protein identified in cucumber	Log$_2$ ratio (PDV+/PDV-)	P-value	Log$_2$ ratio (PDV+/PDV-) cherry ortholog	p-value	% ID[a]	Biological process	Reference
Phosphatidylglycerol/inositol transfer protein DDB (PITP)	1.21	3.69E-02	1.52	1.99E-02	53	Development	Routt and Bankaitis 2004
Aleurain-like protease (ALP)	1.04	2.74E-02	0.87	2.31E-02	77	Defense	Havé *et al. 2018*
2-oxoglutarate dehydrogenase (OGDH)	0.63	4.67E-02	0.47	1.67E-02	88	Respiration	Condori-Apfata *et al.* 2019
SufE domain-containing protein (SUFE1)	-0.90	2.61E-02	-0.63	4.64E-03	67	Sulfur metabolism	Hoewyk *et al.* 2008
Elongation factor Tu (EF-Tu)	-0.54	3.86E-02	-0.45	3.77E-02	85	Translation	Sasikumar *et al.* 2012

[a] Minimum sequence identity of 30% was used to classify host proteins as being orthologs. Proteins with similar database descriptions which did not share at least 30% sequence identity were labelled "Name"

Figure 38 Cherry encoded TSPAN8 localizes at the cell periphery along with PDV proteins

To determine the subcellular localization of the cherry encoded TSPAN8, the CFP fusion construct TSPAN8-CFP was transiently expressed with the PD marker PDLPV which was fused to YFP (PDLPV-YFP). Additionally, TSPAN8-CFP was co-expressed with MP-YFP and CP-YFP to determine if TSPAN8 co-localized with either of these two viral proteins. Constructs were transiently expressed in tobacco leaves and the subcellular localization of the TSPAN8-CFP was visualized at 48 hpa. A schematic representation of each protein fusion construct is shown to the left of the confocal images: The grey box represents the fluorescent tagged protein. Green arrow: d35s promoter, yellow rectangle: coding region of YFP, red box; NOS terminator.

YFP and CFP fluorescence are shown separately in the left and middle columns. The merged image combines both fluorescent images and the brightfield image and is shown in the right column. The construct names are shown on the left.

A   TSPAN8-CFP formed punctate fluorescent patterns at the cell periphery, these patterns were also observed co-localizing with the yellow fluorescence of the PD marker (white arrows).

B   TSPAN8-CFP formed punctate fluorescent patterns at the cell periphery, these patterns were also observed co-localizing with the yellow fluorescence of the PDV CP YFP fusion construct (white arrows).

C   TSPAN8-CFP formed punctate fluorescent patterns at the cell periphery. However, the patterns formed by TSPAN8-CFP did not co-localize with the yellow fluorescence of the PDV MP YFP fusion construct.
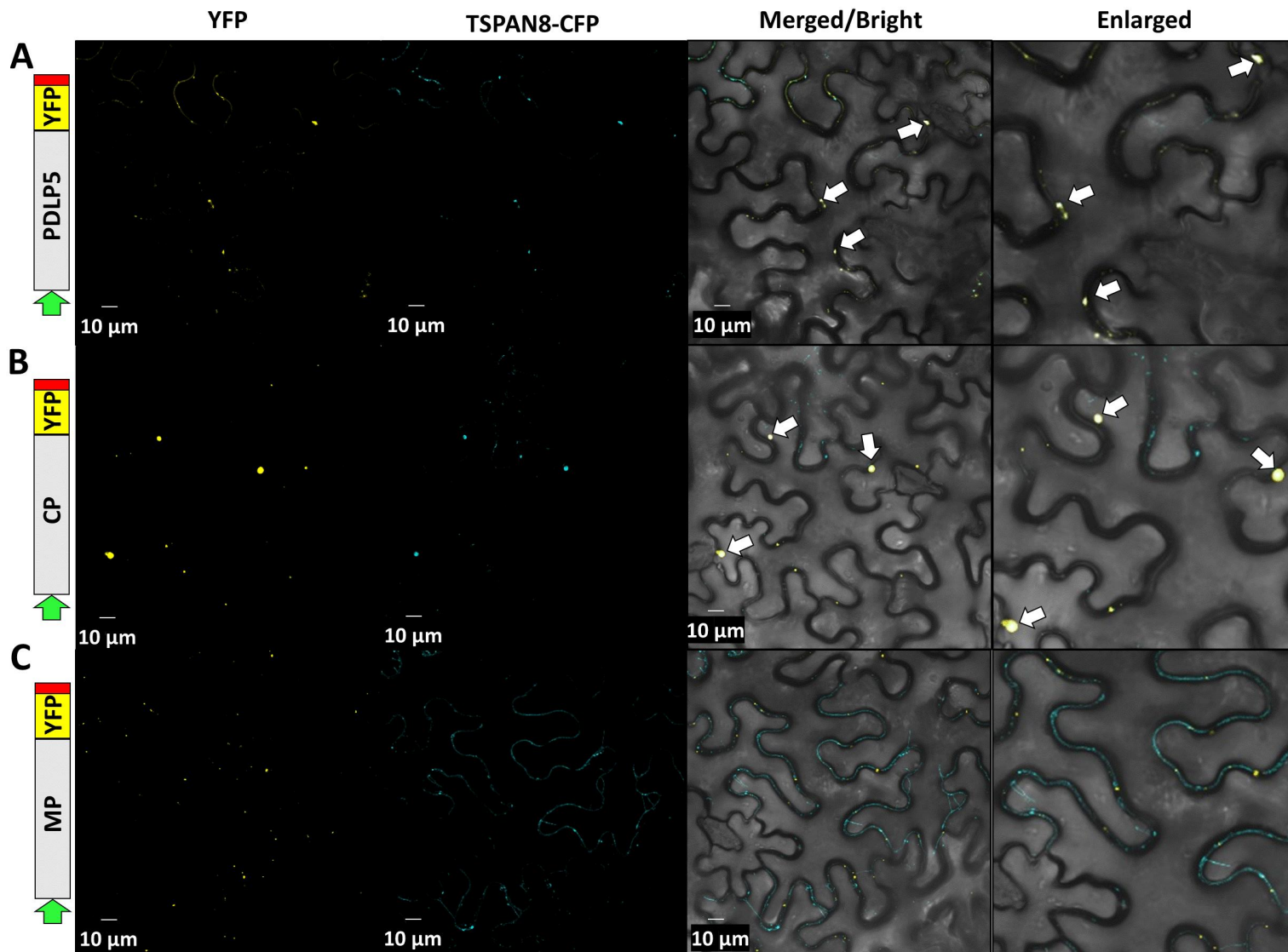
the CP of PDV was investigated *in planta*. BiFc was performed: TSPAN8 was fused to the C-terminal half of YFP (TSPAN8-YC) and the viral CP was fused to the N-terminal half (CP-YN). Previous studies on BMV show that the viral RdRp primarily interacts with itself and P1 while forming VRCs (O'Reilly et al., 1998) thus the viral RdRp of PDV was used as a negative control and was fused to the N-terminal half of YFP (RdRp-YN). These constructs were co-expressed in tobacco leaves and positive fluorescent signals were observed when CP-YN and TSPAN8-YC were co-expressed (**Figure 39A**), suggesting these two proteins interact with each other. When the RdRp-YN construct was co-expressed with TSPAN8-YC, no fluorescence was observed (**Figure 39B**), suggesting these two proteins do not interact with each other, in agreement with previously published studies (O'Reilly et al., 1998; Zhang et al., 2020).

3.5.2 Cherry encoded TCTP1 localization is altered in the presence of, and interacts with the CP of PDV

To study a potential involvement in PDV infection, TCTP1 was chosen as this protein is a known host factor of potyviruses (Bruckner et al., 2017). TCTP1 was fused with CFP (TCTP1-CFP). Sub-cellular localization of TCTP1 was performed as before (**Section 3.5.1**). When agroinfiltrated into tobacco and visualized by confocal microscopy, TCTP1-CFP was most visible as a large aggregate suggesting nuclear localization, however, CFP signal was also visualized at the periphery of the cell (**Figure 40A**). To further test this finding, TCTP1-CFP was co-expressed with the potyviral genome linked protein (VPg), known to localize to the nucleus, which had been fused to YFP (vPG-YFP; Cheng and Wang, 2017). Confocal microscopy revealed that paTCPTP1-CFP and vPG-YFP did colocalize together, suggesting TCTP1 primarily localizes at the nucleus (**Figure 40A**). TCTP1-CFP was also co-expressed with CP-YFP and MP-YFP to test the possibility of co-localization. Confocal microscopy of the transiently expressed proteins showed that TCTP1-CFP localizes mostly to the nucleus but also to the cell periphery while MP-YFP was visualized as punctate yellow patterns at the cell periphery, suggesting PD localization, but also suggesting these two proteins do not co-localize (**Figure 40B**). Interestingly, when TCTP1-CFP was co-expressed with

Figure 39 TSPAN8 interacts with the CP of PDV

To test for a potential interaction between TSPAN8 and the CP of PDV, BiFC was performed. Constructs of CP-YN and TSPAN8-YC were transiently expressed in tobacco leaves. As a negative control, TSPAN8-YC was co-expressed with RdRp-YN. BiFC was visualized at 48 hpa. A schematic representation of each protein fusion construct is shown to the left of the confocal images: The grey box represents the fluorescent tagged protein. Green arrow: d35s promoter, yellow rectangle: half of the coding sequence of YFP, red box; NOS terminator.

YFP fluorescence is shown separately in the left column. The merged image combines both fluorescent and brightfield images and is shown in the right column. The combinations of constructs are shown on the left.

A When TSPAN8-YC and CP-YN are co-expressed, YFP fluorescence reconstituted in tobacco leaf cells and is visible at the periphery (within the focal plane) and other parts (outside of the focal plane) of the visualized cell.

B When TSPAN8-YC and RdRp-YN are co-expressed, no fluorescence was observed.

YFP

Merged/Bright

A

CP TSPAN8

YFP

20 µm

20 µm

B

RdRp TSPAN8

YFP

20 µm

20 µm
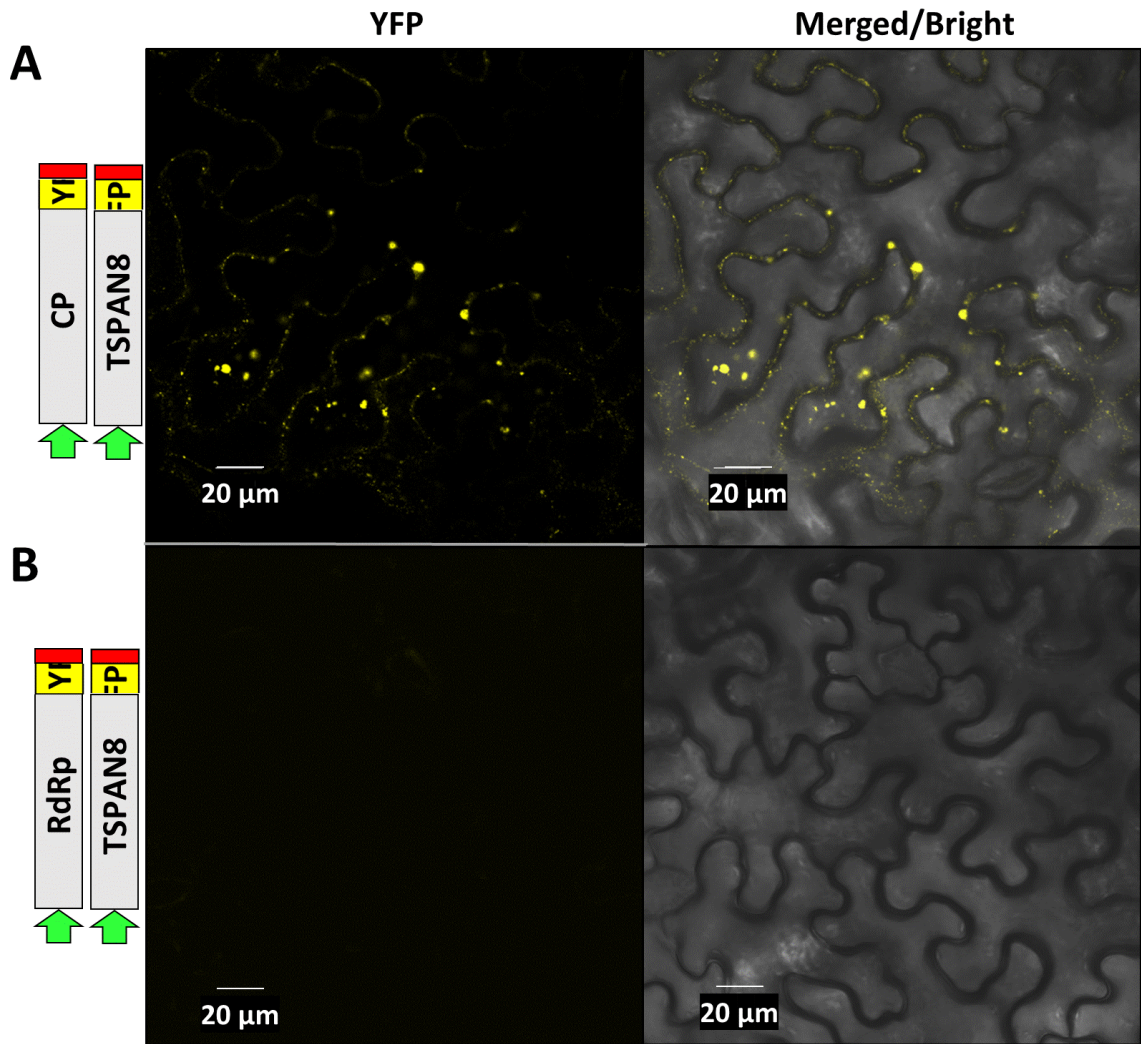
Figure 40 Subcellular localization of TCTP1 is dynamic and co-localizes with the viral CP

To determine the subcellular localization of TCTP1, the fusion construct TCTP1-CFP was transiently expressed with the nuclear marker VPg which was fused to TFP (VPg-YFP). Additionally, TCTP1-CFP was co-expressed with PDV MP-YFP or CP-YFP to determine if TCTP1 co-localized with either of these two viral proteins. Constructs were transiently expressed in tobacco leaves, and the subcellular localization of these proteins were visualized at 48 hpa. A schematic representation of each protein fusion construct is shown to the left of the confocal images: The grey box represents the fluorescent tagged protein. Green arrow: d35s promoter, yellow rectangle: coding region of YFP, red box; NOS terminator.

YFP and CFP fluorescence are shown separately in the left and middle columns. The merged image combines both fluorescent images and the brightfield image and is shown in the right column. The construct names are shown on the left.

A   TCTP1-CFP formed a large round pattern near the centre of tobacco leaf   cells and co-localizes with VPg-YFP, a marker of the nucleus (white arrow).

B   TCTP1-CFP forms smaller punctate patterns which co-localize with punctate yellow patterns formed by the CP-YFP fusion construct at the periphery of tobacco leaf cells (white arrows).

C   TCTP1-CFP forms a large round pattern near the centre of tobacco leaf cells (white arrow), and does not co-localize with MP-YFP, which is seen forming punctate patterns at the periphery of tobacco leaf cells.

	YFP	TCTP1-CFP	Merge/Bright	Enlarged
A (YFP-VPg)	20 μm	20 μm	20 μm	
B (YFP-CP)	20 μm	20 μm	20 μm	
C (YFP-MP)	20 μm	20 μm	20 μm	
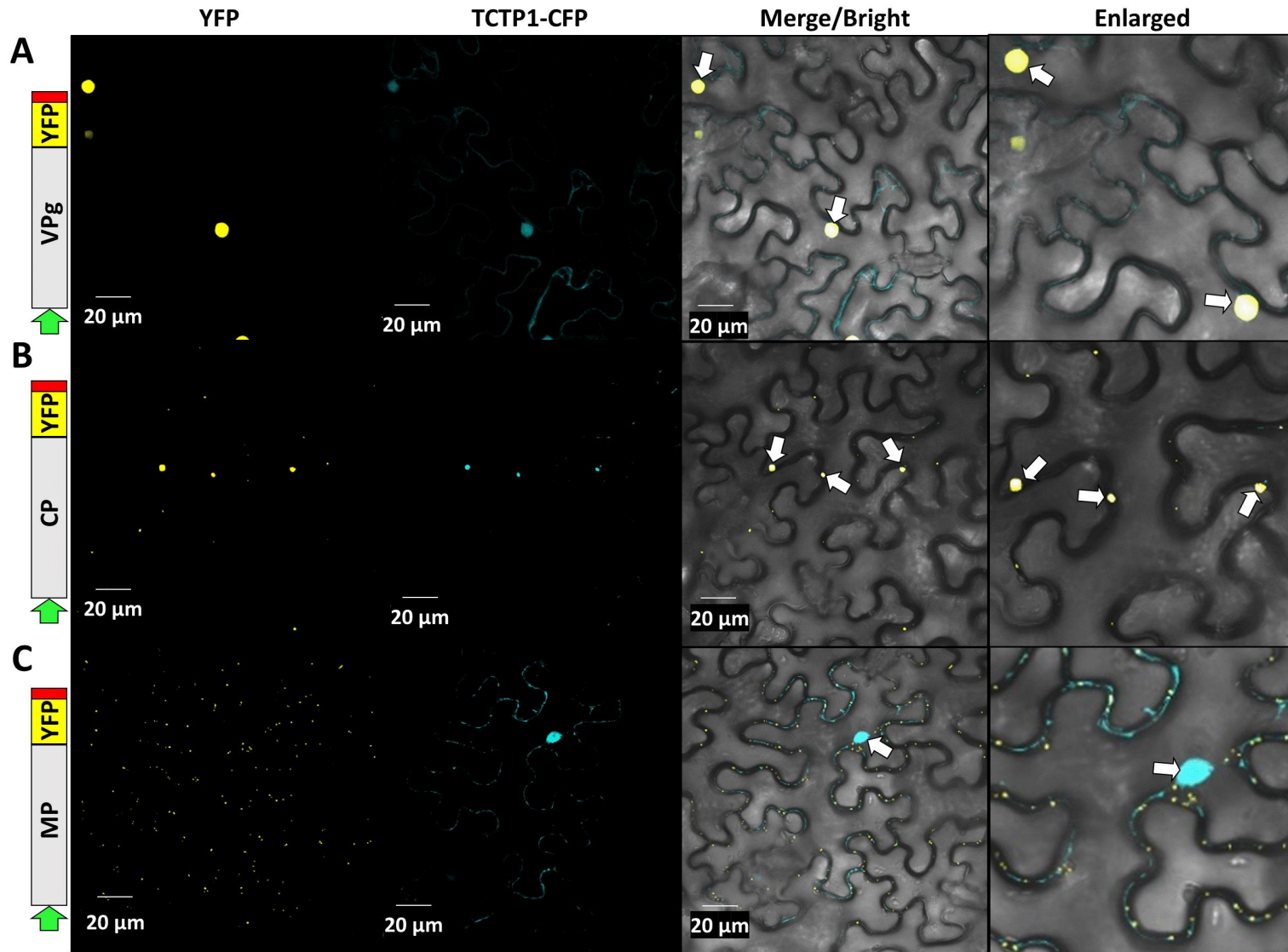
CP-YFP, CFP fluorescence was observed as punctate patterns, only at the periphery of leaf cells, co-localizing with the yellow punctate patterns of CP-YFP (**Figure 40C**), and did not resemble the patterns observed when this protein was co-expressed with vPG- or MP-YFP (**Figure 40A, B**). These findings suggest that TCTP1 primarily localizes to the nucleus, however the presence of the CP of PDV causes a change in the sub-cellular localization of the TCTP1-CFP fusion construct.

TCTP1 has previously been identified as an important host factor in potyviral infection (Bruckner et al., 2017). Based on the finding that TCTP1 increases upon PDV infection, BiFC was used to test for a potential interaction between TCTP1 and viral CP. Combinations of TCTP1 fused to the with the C-terminal half of YFP were transiently co-expressed with CP the N-terminal half of YFP in tobacco leaf cells and positive signals were observed, suggesting TCTP1 interacts with the viral CP (**Figure 41A**). When the RdRp-YN construct was co-expressed with TCTP1-YC, no fluorescence was observed (**Figure 41B**), suggesting these two proteins do not interact with each other. These results indicate that the normal subcellular localization of TCTP1 is altered upon the presence of the viral CP. Additionally, the positive results obtained by BiFC analysis suggests that these two proteins interact, making TCTP1 and the viral CP important targets for future studies.

4.   Discussion

This thesis initially focused on the detection and identification of viral pathogens in the Niagara region of Ontario (**Section 3.1**). The research farm where detection and surveying was performed is maintained following standard industry practices (Mr. Brad Arbon, Agriculture and Agri-Food Canada, personal communications), and thus serves as a suitable representation of the Niagara fruit belt growing region. The high in-field incidence of PDV (42%; **Section 3.1.4**) illustrates that PDV is likely endemic to the Niagara region. Observations that PDV was the only virus detected in cherry with severe foliar symptoms (**Section 3.1.4**) prompted further study of this virus. A newly constructed infectious clone of PDV (**Section 3.2**) was used to fulfill a modified version of Koch's

Figure 41 TCTP1 interacts with the CP of PDV

To test for a potential interaction between TCTP1 and the CP of PDV, BiFC was performed. *A. tumefaciens* cells harboring constructs of CP-YN + TCTP1-YC were transiently expressed in tobacco leaves. BiFC was visualized at 48 hpa.

A schematic representation of each protein fusion construct is shown to the left of the confocal images: The grey box represents the fluorescent tagged protein. Green arrow: d35s promoter, yellow rectangle: half of the coding sequence of YFP, red box; NOS terminator.

YFP fluorescence is shown separately in the left column. The merged image combines both fluorescent and brightfield images and is shown in the right column. The construct names are shown on the left.

A   When TCTP1-YC and CP-YN are co-expressed, YFP fluorescence is seen forming punctate patterns in tobacco leaf cells.

B   When TCTP1-YC and RdRp-YN are co-expressed, no fluorescence was observed.

YFP   **Merged/Bright**

A

YI | FP
CP | TCTP1

20 µm   20 µm

B

YI | FP
RdRp | TCTP1

80 µm
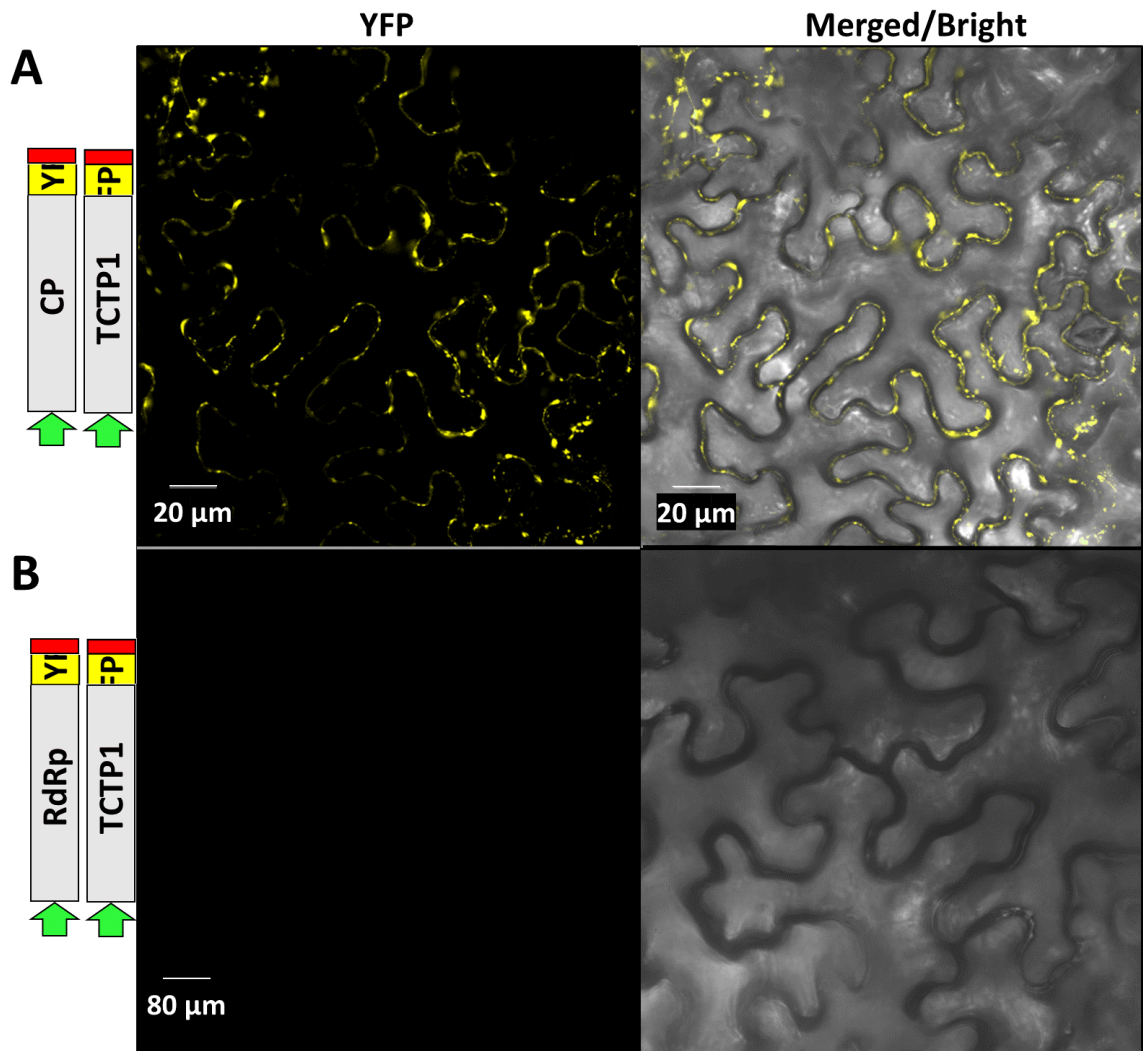
postulates and it was determined that PDV does not cause the same foliar symptoms in young cherry seedlings (**Section 3.2**). However, it was not determined that PDV is not the causal agent of the field-observed symptom. A greater understanding of how PDV moves within the host was obtained by identifying elements critical for MP localization to the PD (**Sections 3.3.2 and 3.3.3**). Determining that the MP of PDV is responsible for tubule formation, and identification of a crucial domain for this process furthers the understanding of PDV movement (**Section 3.3.4**). Results from proteomic analyses indicated that in addition to PDV, proteins associated with responses to other micropathogens such as fungi and bacteria, as well as environmental stressors were identified. If other pathogens and stressors are altering the proteomes of the sampled cherry, these would in fact serve as confounding variables when trying to understand the impact of PDV infection (**Section 3.4.2**). The identification of orthologous proteins with significant accumulation changes in both hosts gives insights as to which biological processes are altered following PDV infection (**Section 3.4.5**). Lastly, to test the suitability of cucumber as a model host to study PDV infection, two proteins significantly increased in this host following PDV infection were studied. The subcellular localization of these host proteins in relation to viral proteins was determined, and putative host-virus protein-protein interactions were identified (**Section 3.5**). Overall, an improved model of the PDV infection cycle is proposed, providing more insight regarding processes involved in the viral infection cycle, and the impact of host biological processes.

4.1   Identification of viral pathogens in cherry using NGS

Some cherry trees in the Jordan station research farm presented foliar symptoms that are typically associated with viral infection. To determine if viral pathogens were infecting cherry in the research farm located in Jordan, Ontario, NGS was performed. This technique was chosen as it is a powerful, sensitive and rapid tool for the identification of multiple pathogens from infected plants (Villamor et al., 2017). Additionally, the use of NGS escapes the constraints of other virus detection methods including the need for virus specific primers (for RT-PCR) or antibodies against specific viral proteins (for ELISA based

methods). Further, NGS does not require specific antibodies or genomic sequence of pathogens, such as viruses (Duan et al., 2009; Prabha et al., 2013). NGS has been used to identify new viruses in several disease complexes of perennial crops, such as fruit trees (Liu et al., 2018). In this work, sRNAs extracted from foliar tissues of cherry were sequenced using the Illumina MiSeq platform. This semi-targeted approach for the identification of plant viruses is based on the principle that host encoded RNA silencing recognizes and cleaves dsRNA (an intermediate product of ssRNA(+) virus replication) producing a pool of viral siRNAs to be sequenced (Bol, 2005; Niu et al., 2017; Sanfaçon, 2005). Despite the identification of several viral proteins with RSS functions, no RSS is known to completely inhibit RNA silencing, In fact, the mechanisms by which RSSs function varies, as some permit the formation of sRNA, yet these RNAs are sequestered by the viral RSS, permitting integration into the host RNA induced silencing complex (Cheng and Wang, 2017). Lastly, not all viruses encode an RSS, therefore the use of isolated sRNA for virus detection is a very useful method to detect viruses, even those which do encode a protein with strong RSS function.

Four different viruses were identified in the sequenced samples (CVA, PNRSV, PDV and LChV1). The detection of PNRSV is not surprising as this virus has been previously reported and thoroughly studied in the same orchard (Cui et al., 2012a, b, 2013). Historically, both ilarviruses PNRSV and PDV were thought to exist in this region based on anecdotal evidence including observed symptoms on natural hosts and indexing studies on herbaceous indicators (Gilmer et al., 1976; Thomas and Hildebrand, 1936). Nevertheless, this thesis presents the first direct evidence of PDV using molecular detection methods (NGS, RT-PCR and Sanger sequencing) and serological methods (DAS-ELISA). The other viruses, CVA and LChV1, were detected in Ontario for the first time. CVA is regarded as a latent virus, it is present in all regions where Prunus spp. are cultivated. The etiology of this virus is likely understudied for two reasons: firstly, CVA itself was discovered in the 1990s (Jelkmann, 1995), much later than other viruses such as PDV or PNRSV, which have been described since the 1930s (Thomas and Hildebrand, 1936).

The somewhat recent identification and description of this virus means there was less time for individual CVA related research to be performed. A second reason for the lack of studies on this virus is likely linked to the latency of CVA infections (Noorani et al., 2010). Most viruses are discovered and studied based on observed field symptoms (Lacroix et al., 2016). Crop growers and researchers are concerned with observable disease phenotypes and it is primarily these samples which are processed and screened for viruses, however much less concern is placed on seemingly healthy plants. Since CVA is not believed to cause any disease symptoms, it often escapes detection by visual inspection.

The detection of LChV1 presents a significant finding as this virus is one of three known causal agents of little cherry disease (LCD), which has devastated cherry crops in British Columbia and the United States of America (Candresse et al., 2013; Galinato et al., 2019). Although LChV1 was detected in cherry, this virus infects a variety of *Prunus spp.* such as peach and plum (Lim et al., 2015; Marais et al., 2016). Since PNRSV and PDV also infect a variety of *Prunus spp.*, their presence in this important fruit growing region could pose great challenges to the fruit growing industry if appropriate management strategies are not developed and implemented.

4.2   Incidence of the identified viruses in the research farm

The incidence of the identified viruses in the research farm was estimated (**Section 3.1.4**). The most abundant virus was CVA infecting 60% of the surveyed trees. Since CVA is known as a latent virus in *Prunus*, and is only transmitted by grafting (Kesanakurti et al., 2017), it is likely that asymptomatic rootstock and scion wood acted as the source of CVA during tree propagation and planting. The fact that CVA was first detected in Ontario in trees older than ten years suggests that Ontario lacks an effective pathogen monitoring program for fruit trees. Indeed, there is no detection regimen for this virus and many other viruses (with the exception of PPV; Gougherty and Nutter, 2015) during plant material selection, propagation and planting, which easily allows for infected plants to be used for initial orchard planting.

The incidence of PDV was initially estimated to be half of the sampled trees when RT-PCR was used for virus detection. However, when DAS-ELISA was used to sample all trees in the orchard plot, incidence of PDV was lower than this initial estimate (42%). This discrepancy could be a consequence of DAS-ELISA having a lower sensitivity than RT-PCR potentially leading to false negative detection results. Because of the higher sensitivity of RT-PCR, it is also possible that the viral titer of PDV was low in some trees, and not enough of the viral CP had been produced, for detection by DAS-ELISA. Another reason for the discrepancy between the two detection methods is that viruses are often unevenly distributed among different branches of the infected trees (Gilmer and Brase, 1963). Of course, it is also possible that when the entire orchard plot was sampled using DAS-ELISA, more trees which were not infected by PDV were included in this survey, which would result in a lower incidence of infection compared to the previous survey which only studied half of the trees.

The low incidence of LChV1 (4% of sampled trees) suggests this virus has not spread throughout the orchard, which may be a result of LChV1 being recently introduced. However, since no insect vector has been identified for LChV1 and this virus is suspected to only be transmitted by grafting (Fuchs et al., 2020; Galinato et al., 2019), a recent introduction is not likely as the trees found to be infected with LChV1 were planted in 1985 and grafting was done before planting (Mr. Brad Arbon, Agriculture and Agri-Food Canada, personal communication). Therefore, it is possible that LChV1 has persisted in these trees since they were propagated and planted, additionally, the limited means of transmission could explain the low incidence of this virus. LCD is one of a few major devastating diseases of cherry and is caused by three agents: LChV1, Little Cherry Virus 2 (LChV2) and Western X phytoplasma (Cieślińska and Morgaś, 2010). LCD causes dramatic reductions of fruit size and quality (colour and flavour) resulting in an unmarketable crop (Galinato et al., 2019). In most cases, LChV2 is associated with severe symptoms whereas LChV1-infected cherry develops comparably milder symptoms or may be asymptomatic (Galinato et al., 2019; Katsiani et al., 2018). Based on this information, LChV1 alone is not likely a great threat to cherry production in this region. A large-scale

survey is needed to further evaluate the incidence and economic importance of LChV1 in Ontario. The low incidence and limited transmission modes of LChV1 suggest that this virus may be controlled though a certification program similar to programs implemented by many countries to ensure that growing materials such as rootstocks and scion cuttings are free from devastating pathogens (Gougherty and Nutter, 2015; Karuppuchamy and Venugopal, 2016).

4.3   Construction of the PDV infectious clone

PDV was studied further because it was the only virus detected in the symptomatic cherry samples (**Figure 12B-D**) and it had a high in-field incidence of infection. To determine if PDV was the causal agent of the observed symptoms, a full-length cDNA clone of PDV was constructed (**Section 3.2**; **Figures 13 and 17**). The inability of PDV to infect arabidopsis indicates that this plant not a suitable host to study this virus. PDV is no exception as other ilarviruses such as PNRSV do not infect this model plant either (Martínez-Pérez et al., 2017).

PDV, however, was able to infect tobacco and spread systemically through the plant without causing any disease symptoms (**Figure 15**). This confirmed that the full-length cDNA clone of PDV is in fact infectious. tobacco is susceptible to a variety of viral pathogens and is the most widely used model host in plant virology (Goodin et al., 2008). In a previous study from the Wang lab, it has been shown that, similar to PDV, an infectious clone of PNRSV also infects this plant latently (Cui and Wang, 2016). The latency of PDV in tobacco may be a result of the host not recognizing pathogen associated molecular patterns presented by PDV, allowing PDV to evade host defenses which have not been induced.

Inoculation of cucumber with PDV resulted in the development of strong foliar symptoms (**Figure 17A-C**) and PDV from infected leaf tissues was mechanically transmissible to other herbaceous hosts (**Figure 19A, B**). Clearly, the hypersensitive response (HR) is induced following PDV infection, as seen by chlorotic and necrotic lesions

(**Figures 17B, C**, **19A**, **and 36B**) and increased oxidative stress responses in this experimental host.

4.4 PDV infection impacts growth of cherry without inducing severe foliar symptoms

Cherry seedlings infected by PDV presented a dwarfed phenotype, but no severe foliar symptoms were observed (**Figure 20A, B**). This was somewhat unexpected as PDV was the only virus found in the field grown cherry showing severe foliar symptoms (**Figure 12B-D**). Previous studies have suggested that disease symptoms caused by PDV are not only dependent on the infected host, but also on the viral isolate (Kozieł et al., 2017a; Németh, 1986). Although this is not likely the case here, the possibility that there was an undetected isolate of PDV responsible for the observed symptoms in this work cannot be excluded. Several conditions could explain the difference in symptom development, including the difference in plant age: the seedlings used in infiltration experiments were only a few weeks old whereas cherry in the field are at least 35 years old (planted in 1985). Additionally, although cherry seedlings used for experiments came from the field grown trees, these seedlings were not grafted and are likely to exhibit different growth patterns compared to trees that have been grafted onto rootstocks to promote certain growth traits (Martínez-Gómez et al., 2003). The genotype of the seedlings is also different to those of field grown trees. cherry requires cross pollination for seed production and resultantly seedlings will not break true to type, meaning the seedlings will not be genetically identical to the prior generation, presenting another factor which may explain the different symptom presentation in PDV infected seedlings (Bourguiba *et al.* 2012). The duration of PDV infection is quite different between the PDV infected seedlings and orchard trees, over time, PDV has replicated in the field grown trees and may have a higher titer compared to the infected seedlings, which may influence symptom development. Environmental conditions maintained during laboratory experiments are different than those in the field including temperature, lighting and humidity. Other factors that are controlled for in the laboratory environment and may influence cherry

growth in the field include chemical and osmotic stressors, and other biological agents such as bacteria and fungi. As outdoor environmental conditions vary over time, many external stressors could impact the development and growth of the plants. The synergistic effects of PDV with other biotic and abiotic stressors may also induce the severe symptoms observed in cherry at the research farm which could explain why only one tree which appeared to only be infected by PDV displayed these severe foliar symptoms. Based on the infection assay on cherry seedlings (**Figure 20A, B**), under given conditions, PDV alone does inhibit vegetative growth causing dwarfing and reduced plant stature but does not induce severe foliar symptoms on cherry seedlings. A study of PDV infected, clonally propagated cherry seeds maintained under field-like conditions may provide more definitive results, although this would be a long process, measured in years and decades, not in days or weeks.

4.5   The PDV MP is a PD-located protein

To better understand the intercellular movement of PDV, the viral MP was further studied and characterized. The PDV MP subcellularly localized to the PD (**Figure 23A**), which is consistent with the default function of viral MPs (Melcher, 2000). The PDV MP belongs to the 30K MP superfamily which can be divided into two groups based on the mechanism by which MPs facilitate viral intercellular movement. One group of MPs form tubules demonstrated in PDV (**Figure 31A**) that pass-through PD. Other MPs dilate PD, to allow passage to adjacent cells (exemplified by TMV; Melcher, 2000). Like the MPs of TMV and AMV, the PDV MP contains elements required for PD localization in the N-terminus (**Figure 25A**). Further, only the largest N-terminal truncation of the MP (MPΔ1-69-YFP; **Figure 24**) resulted in disrupted PD localization (**Figure 26C**). The residues essential for PD localization within this region are proximal to the 30K core domain (**Figure 24**). When conserved residues within the core domain were changed to alanine, PD localization was disrupted (**Figures 30**, **31**), demonstrating the importance of the core domain for PD localization. Together, both the N-terminal and core domains are involved in PD targeting.

The absence of a *bona-fide* PLS in the N-terminal domain of the PDV MP is consistent with findings in the AMV MP, which also lacks a dedicated sequence for PD localization. In fact, a previous study on the MP of AMV showed MP localization to the PD was disrupted when a large N-terminal deletion (residues 13-77) was performed, which included a portion of the 30K core domain (**Figure 24,** boxed in green) (Erny et al., 1992). Considering the sequence diversity of PDV and AMV MPs compared to their TMV counterpart, PDV and AMV MPs may localize to PD through functional domains different from the TMV MP, which has three PLSs in the N-terminus (Liu et al., 2020; Yuan et al., 2016).

The N-terminus of the PDV MP was predicted to contain an N-terminal *α-helix* upstream of the 30K core domain (**Figure 21**). Deletion of the N-terminal 44 residues disrupted tubule formation, suggesting the predicted N-terminal *α-helix* (**Figure 21**) is required for tubule formation. The ability of the same truncated MP to form punctate structures at the PD of the leaf cell and the protoplast periphery (**Figures 28B** and **33B**) suggests the *α-helix* is not required for PD localization. The conservation of this *α-helix* in tubule forming MPs (such as PDV and AMV), but not in PD dilating MPs (such as TMV) suggests this structure is important for the tubule guided movement strategy used by some 30K MPs (Melcher, 2000). Regardless of the mechanism used for intercellular movement (tubule forming or PD dilating), the N-terminus of MPs within the 30K superfamily is important for PD localization, but the functional domains are different. In the case of the tubule forming 30K MPs, the involvement of the N-terminal *α-helix* in PD targeting and localization should be further studied.

The C-terminus was determined to be dispensable for both PD localization and tubule formation (**Figures 25B**, **27** and **33**). *In silico* analyses of the PDV MP sequence predict both the N- and C-termini can bind proteins (**Figure 22B**). Since ilarvirus movement requires the presence of the CP and is transported either as a virion, or as an RNP, the C-terminus of the PDV MP may be involved in virion or RNP formation (Bol, 1999; Fajardo et al., 2013; Sánchez-Navarro and Bol, 2001). Results from previous studies of other tubule forming 30K MPs have shown the importance of the MP C-terminus. In both

AMV and PNRSV the C-terminus is necessary for an interaction between the viral MP and CP, an interaction which was determined to be necessary for intercellular movement (Aparicio et al., 2010; Sánchez-Navarro et al., 2006). Additionally, the C-terminus of the tubule forming MP from *Cowpea mosaic virus* (CPMV), of the *Comovirus* genus within the *Secoviridae* has been shown to function as a domain crucial for the binding of virions and CP units (Carvalho et al., 2003). Although the C-terminus of the PDV MP is dispensable for PD localization and tubule formation, based on accumulated evidence of other 30K MPs, and results of *in silico* analyses, by elimination it is possible this domain is involved in an interaction between viral proteins and formation of a complex necessary for PDV movement.

4.6   Additional stressors on cherry

The use of the PDV infectious clone showed that this virus does not induce the severe foliar symptoms in young cherry seedlings under experimental conditions. To understand what biological processes are being altered in symptomatic cherry, proteomics was used. Quantitative proteomics has the potential to provide a comprehensive analysis including compositional changes of host proteomes in response to stress conditions such as viral infection (Di Carli et al., 2012; Xu and Nagy, 2010). Although transcriptomics have been used to study changes in host gene expression during pathogen attack, this method does not account for post translational modifications, protein degradation or altered localization within the cell (Di Carli et al., 2012).

When protein accumulation changes were studied in orchard grown cherry trees, it was found that proteins related to pathogen resistance and stress-related pathways in PDV infected samples had increased in accumulation (**Section 3.4.2**; **Figure 35; Appendix 3**). It is well known that abiotic and biotic stressors induce conserved pathways involved in pathogen and stress responses (Cohen and Leach, 2019). It is possible that in addition to PDV, the cherry with severe foliar symptoms was challenged by other pathogens, such as fungi or bacteria which are known causal agents of several diseases in *Prunus spp.* (APS, 1995). The increase of chitinases (CHIT), enzymes which degrade chitin, a major

component of fungal cell walls suggests a possibility that fungal pathogens also infect symptomatic cherry. Increases in other antifungal proteins such as thaumatin and copper binding proteins further supports this idea (**Figure 35**; **Appendix 3**; Casado-Vela et al., 2006; Rajam et al., 2007; Sharma et al., 2011). It would not be surprising if fungal or bacterial pathogens were detected in cherry displaying foliar symptoms as perennial crops such as fruit trees often become infected by multiple pathogens during their extended life cycle (Sanfaçon, 2017).

The GO analysis suggests proteins with putative responses to temperature, chemical and drought stressors are also upregulated in symptomatic cherry samples (**Figure 35**). In addition to the pathogens described, a variety of factors including osmotic and chemical stressors could have influenced symptom development, given that the use of some agricultural chemicals have been found to cause foliar symptoms as an unintended side-effect (Baumann, 2008). Environmental stressors may also be involved in abnormal growth, as proteins related to heat stress responses such as pectin methylesterase 3 (PME3) and a HSP are significantly altered in PDV infected samples (**Appendix 3**; Wu et al., 2018). The significant accumulation changes of proteins associated with responses to external stressors offers a possible explanation for why symptoms observed in the field were not replicated in studies on cherry using the PDV infectious clone.

4.7   Impact of PDV infection on cucumber

Protein accumulation changes in cucumber during PDV infection are similar to changes caused by other viruses: defense related proteins are increased in accumulation and proteins related to photosynthesis are decreased (**Table 8; Appendix 4**; Li et al., 2016). Proteins related to antiviral responses were increased in PDV infected cucumber such as eIF2C, a protein involved in host mediated RNA silencing, and nepenthesin-1 (NEP1), a proteinase that mediates virus triggered HR (**Figure 36C**; **Appendix 4**; Hatsugai et al., 2004; Thomas and van der Hoorn, 2018; Voinnet, 2001). Increases of several peroxidases indicates that PDV infection triggers oxidative stress responses (Hernández

et al., 2016). The induction of oxidative stress responses represents a host antiviral response to PDV infection, as ROS promote localized cell death as part of the HR, to control the spread of pathogens. This response explains the mild leaf spot symptoms seen on PDV infected cucumber leaves which were sampled for proteomic analyses (**Figure 36B**). Eventually, ROS also distribute to distal tissues to promote systemic acquired resistance (SAR) against invading pathogens (Li et al., 2016). In the context of PDV infection, the concept that ROS induction serves as a defense response is supported by results from a recent study, which attributes the inability of PDV to systemically spread in *Chenopodium quinoa* to increased ROS signaling and containment of PDV (Kozieł et al., 2020). Interestingly, PDV infection is also associated with increases of ROS scavenging CATs and Nucleoredoxin 1 (NRX1), an enzyme known to protect catalazes from ROS induced oxidation. As NRX1 protects catalazes, the efficiency of catalaze-mediated ROS degradation is increased, and extensive damage to host cells by ROS is reduced (Almagro et al., 2008; Kneeshaw et al., 2017).

The induction of HR, rapid local accumulation of ROS (sometimes called an oxidative burst) and subsequent upregulation of ROS degrading enzymes may serve another role during PDV infection. During the infection cycle of some viruses, an oxidative burst creates favourable conditions for viral replication as shown for BMV. Recently, it has been shown that BMV requires the presence of superoxide anion, and hydrogen peroxide for viral replication, which are formed during oxidative bursts catalyzed by the plant NADPH-oxidase (Hyodo et al., 2017). The increases of NAD- and NADP dependent malic enzymes, two proteins involved in NADPH and ROS production, during PDV infection suggests the importance of an oxidative burst during PDV infection (**Table 5**, **Appendix 5**; Chen et al., 2019). Since BMV and PDV are both members of the *Bromoviridae*, and PDV infection leads to an upregulation of enzymes related to oxidative bursts, it is possible that an oxidative burst may create conditions thar are favourable for virus replication in a similar manner to BMV.

Of the 37 proteins which were decreased upon PDV infection, nearly half of these are chloroplast-related proteins (**Figures 36C; Table 6**; **Appendix 4**). The chloroplast is

often affected during plant virus infection and is implicated in replication of some viruses, and damage to this organelle is associated with decreased host defense capabilities (Zhao et al., 2016). Many plant viruses undergo replication in association with the chloroplast as this organelle does not possess RNA silencing mechanism and therefore it is a safe site for virus replication (Bhattacharyya and Chakraborty, 2018; Li et al., 2016). Since PDV is not known to encode an RSS, PDV replication would favour a site which is absent in RNA silencing machinery. Studies using EM add support for chloroplast associated replication, in addition to tonoplast and ER, PDV replication proteins such as P1 and CP have been visualized at chloroplast membranes as well inside small invaginations of this membrane, further suggesting this organelle is also used for PDV replication (**Figure 3**; Kozieł et al., 2017b). Studies on AMV have included the visualization of VRCs at chloroplast membranes suggests similar replication strategies are used by both viruses and supports the hypothesis that the chloroplast acts as a site for PDV replication (De Graaff et al., 1993; Kozieł et al., 2017b). Alternatively, the localization of replication associated proteins at other organelles (such as the tonoplast and endoplasmic reticulum) suggests the chloroplast is not the sole site of PDV replication (Kozieł et al., 2017b). Again, more recent work on AMV supports this theory as P1 and P2 of AMV were visualized at the tonoplast of infected arabidopsis (Budziszewska and Obrępalska-Stęplowska, 2018). The visualization of replication associated proteins at organelles other than the chloroplast in both PDV and AMV may suggest that PDV alters chloroplast proteins for reasons other than replication (Budziszewska and Obrępalska-Stęplowska, 2018; Li et al., 2016).

When considering two of the major roles of the chloroplast, it is easy to understand why this organelle is a major target during viral infection. As the major site of energy production in the plant cell, chloroplasts are necessary for energetically costly pathogen defense responses to operate properly (Cipollini et al., 2017). Additionally, chloroplasts are responsible for the production of defense signal molecules such as salicylic acid, and they are a major source of ROS (Li et al., 2016; Zhao et al., 2016). Based on these features alone, intact, fully functional chloroplasts are necessary for plant defense responses to pathogens and stressors, which must be evaded by an infecting

virus (de Torres Zabala et al., 2015). It is not surprising that during viral infection, chloroplasts are often damaged, leading to impairment of photosynthesis. The decreased capability of host defense responses results in a host plant with increased susceptibility to viral infection (Li et al., 2016). By altering light conditions, research on TMV has shown that virus movement from inoculated epidermal cells to mesophyll cells is more effective in plants maintained in a long period of darkness compared to inoculated plants maintained under normal daylight conditions (Wieringa-Brants, 1981). Others have suggested that increased viral accumulations during dark treatments is a result of diminished defense pathways, suggesting that photosynthesis and other chloroplast functions must remain intact for effective antiviral defense (Zhao et al., 2016). Proteomic analysis showed that proteins associated with the light reactions of photosynthesis such as ATP synthase (ATPsyn) and the RuBisCO large subunit binding protein α (RuBisCOlα) are downregulated in PDV infected plants (**Appendix 4**). The decreased levels of these proteins suggests that photosynthesis is inhibited during PDV infection. Both proteins have been implicated in host defense responses to infections by other viruses. During TMV infection, ATPsyn is downregulated and the suppression of this protein is associated with increased virus accumulation (Bhat et al., 2013). During infection of tobacco, the interaction between the RuBisCOlα and the CP of *Potato virus Y* (PVY; a *Potyvirus*) was identified as a determinant for the development of mosaic symptoms (Feki et al., 2005). The fact that this protein is involved in host defense to PVY suggests PDV downregulates this protein to evade another host defense mechanism.

Downregulation of proteins essential for normal chloroplast function weakens plant defenses which is favourable for PDV infection. Downregulation of the inactive ATP-dependent zinc metalloprotease FTSHI 5 (FTSHI5) is an example of a crucial photosynthetic protein which is decreased following infection by PDV. Since FTSHI5 is involved in thylakoid biogenesis and the repair of photosystem II, this protein is upregulated during light stress conditions (Zaltsman et al., 2005). The reduced levels of FTSHI5 following PDV infection likely results in decreased thylakoid production and dysregulation of the photosystem II reaction centre, resulting in decreased

photosynthetic capabilities. Studies showing that downregulation of FTSHI5 creates a variegated phenotype in arabidopsis support the theory that decreased photosynthetic capabilities are associated with FTSHI5 downregulation (Kato et al., 2009).

When cucumber is infected by PDV, typical antiviral responses are upregulated; including RNA silencing machinery and components of oxidative stress immune responses (**Appendix 4**). As mentioned above, the chloroplast may not be a primary site of PDV replication, and therefore decreased levels of chloroplast proteins likely benefits PDV infection in some other way, such as the downregulation of host defenses.

4.8   Common biological processes affected by PDV in cherry and cucumber

The identification of proteins which are affected similarly in both cherry and cucumber (**Table 10**) identifies biological pathways that are important for PDV infection. Identification of these important pathways allows for speculation of how PDV triggers host defense responses, evades these defenses and even uses host proteins for replication and translation (**Figure 42**). Following PDV infection, levels of proteins involved in pathogen defense responses are increased in both hosts (**Figure 42**; **Table 10**). The increased levels of NADP-ME, CATs, PRXs and NRX1 in both infected hosts suggests oxidative stress plays an important role during PDV infection. However, the role of oxidative stress during PDV infection is unclear (**Section 4.7**) The role of oxidative stress should be further studied to determine if this response is involved merely as a host defense response to PDV, or if this pathway is involved in PDV replication as well.

Although the increase of chitinases in cherry initially led to the suspicion that fungal pathogens were present, the increase of a single CHIT in both hosts (**Table 10**) suggests that this protein is increased following PDV infection. CHITs are a diverse group of enzymes involved in stages of plant development such as embryogenesis and stress tolerance, which can be triggered by a variety of stressors, not only fungi (Collinge et al., 1993). Findings that infection by another virus, TMV, also results in increases of CHITs supports the theory that increased levels of CHIT is a host response to PDV infection (Punja and Zhang, 1993; Sharma et al., 2011). The significant increase of peptidyl-prolyl

Figure 42 An updated model of the PDV infection cycle

      This thesis presents novel findings improving the current knowledge of the PDV infection cycle regarding viral movement, replication, and impact. Impacts of PDV infection are shown in a diagram (not drawn to scale). Abbreviations are found in table 10

A   ER localized host chaperones increase in accumulation.

B   TCTP1 normally localizes to the nucleus. Co-expression studies show TCTP1 co-localizes and interacts with the viral CP of PDV at the periphery of the cell, the function of this interaction remains unknown.

C   Cytosolic and mitochondria localized proteins related to stress responses and respiration accumulate to higher levels, whereas proteins related to sulfur metabolism are decreased.

D   Cytosolic proteins related to oxidative stress are increased to scavenge and degrade ROS, other chaperone proteins are also increased.

E   Photosynthesis related proteins have decreased in accumulation. Proteins with defense roles against other viruses are increased (NAD-ME), whereas other defensive proteins are decreased (ATPβ/δ, PsbC).

F   Peroxisomal proteins involved in ROS response have increased in accumulation.

G   The N-terminal and core domains were shown to be crucial for PD localization. It is still unknown if PDV moves through PD as an RNP (**H**) or a virion (**I**).

J   The MP of PDV localizes to the PD and is responsible for forming tubular structures for PDV intercellular movement.

K   Other proteins associated with host defenses including proteases, chitin degrading enzymes are increased, additionally, proteins known to induce SAR are localized in the extracellular space and are transported systemically.

L   The accumulation of TSPAN8 is significantly increased. This protein co-localizes and interacts with the viral CP. The role of this protein during viral infection is currently unknown and may be related to the formation of exosomes for long distance movement or may serve as a host response to block viral movement.
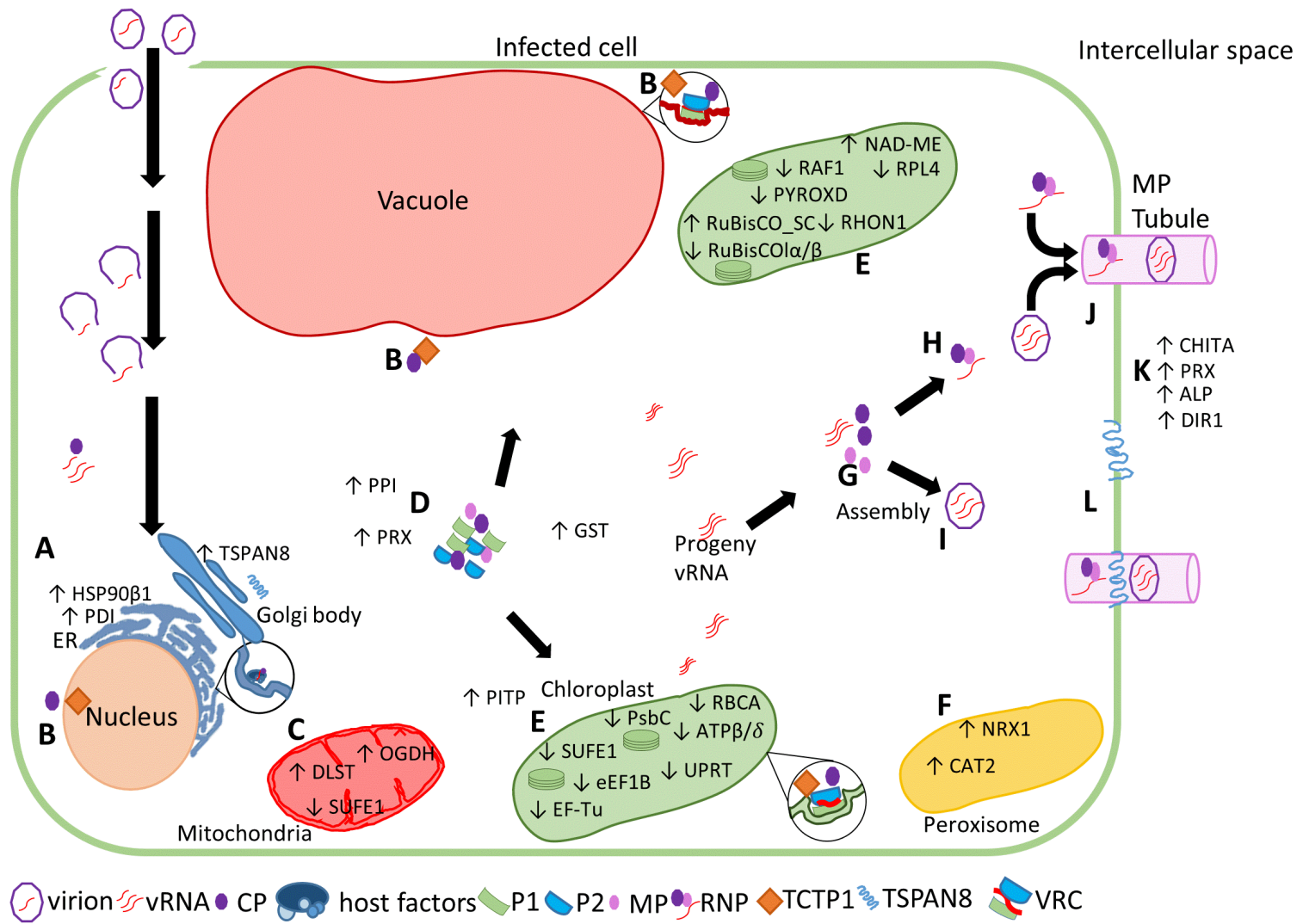
cis-trans isomerase (PPI; a cyclophilin) is another antiviral response present in both hosts as this protein interferes with virus replication of the *Tomato bushy stunt virus* (TBSV), a *Tombusvirus* (Mendu et al., 2010). PPI, an ER localized protein, has been found to bind to viral replication proteins of TBSV, thereby reducing their RNA binding abilities, which eventually leads to decreased viral accumulation (Nagy et al., 2011). If PDV replication occurs solely at the ER, the increase of PPI could inhibit viral replication. However, if alternative replication sites exist, the PDV VRC exposure to PPI would be minimized, preventing replication inhibition by this protein. The visualization of PDV replication proteins (such as P1 and CP) at other organelle membranes (chloroplast and tonoplast) supports the idea that PDV undergoes replication at alternative locations within the cell, not only at the ER (Kozieł et al., 2017b). By replicating at alternate sites within the infected cells, it appears PDV evades the PPI host defense mechanism by spatial separation (**Figure 42**).

Proteomic analyses showed that proteins involved in photosynthesis are altered in both hosts (**Table 6**). It has been suggested that the impairment of photosynthesis associated with virus infection creates an environment which is favourable for virus replication and spread (Souza et al., 2019). By impairing photosynthesis, energy for normal function is deprived allowing viruses to evade host defenses (Bolton, 2009; Souza et al., 2019). As the severity of foliar symptoms increase in younger, newly emerging leaves, it is likely that the impairment of photosynthesis is required for PDV infection and persistence (**Figures 12B-D**, **17A-C**). Infection by PDV may directly impair chloroplast protein translation as the level of Ef-Tu is decreased in both hosts (**Table 10**). Additionally, CO_2 fixation appears to be disrupted as a consequence of PDV infection as the levels of two RBCAs identified in both hosts are decreased (Souza et al., 2019). The decreased levels of two ATPsyn subunits (β and δ) further impacts CO_2 fixation as these enzymes are critical for RBCA function (**Table 6**; Crafts-Brandner and Salvucci, 2000). Interestingly, both RBCA and ATPsyn subunits are upregulated during TMV infection, suggesting that these proteins are involved in defense pathways which respond to TMV infection. The same researchers determined that RBCA and ATPsyn subunits were also found to block

movement of TMV, these host proteins have a non-canonical role in antiviral defense (Bhat et al., 2013). It is possible that the decreases in these proteins represent another example of decreased host defense mechanisms during PDV infection (**Figure 42**). The decreased accumulation of PsbC presents another example of how PDV may evade host defenses. PsbC is one of two major antenna proteins of the oxygen evolving complex (OEC; Souza et al., 2019). PDV and AMV share many similarities (**Sections 1.3.1** and **1.4.2**); in studies on AMV, another subunit of photosystem II (PsbP) was found to directly interact with the viral CP (Balasubramaniam et al., 2014). In addition to being a core component of the OEC (like PsbC), PsbP also interferes with AMV replication as overexpression of this protein was associated with a 40% reduction of AMV in arabidopsis (Balasubramaniam et al., 2014). Based on the similarities between AMV and PDV, and the observation of CPs from both viruses at the chloroplasts, decreased levels of OEC components may in fact provide another example of another host defense mechanism being impaired during PDV infection.

Following PDV infection, two elongation factors, which are essential for replication of other viruses are significantly altered in both hosts. Although EF-Tu is primarily associated with host protein translation, this protein has been implicated as a host factor for replication of the *Escherichia virus Qbeta*, of the *Allolevivirus* genus within the *Leviviridae* (Takeshita and Tomita, 2010). It is possible that PDV recruits EF-Tu to VRCs for an interaction with the viral replicase. The involvement of EF-Tu in PDV replication is supported by the finding that the plant homolog of elongation factor Ts (Translation elongation factor 1B; eEF1B), also required for maintaining the active conformation of the Qbeta replicase, is significantly altered in PDV infected hosts (Table 6; Takeshita and Tomita, 2010). In plant viruses such as TMV, eEF1B is known to interact with the viral RdRp, the silencing of eEF1B in tobacco was found to hinder TMV replication, identifying it as an important host factor for infection (Hwang et al., 2013). During infection by *Potato Virus X* (PVX), of the *Potexvirus* genus, a member of the *Alphaflexiviridae*, the triple gene block protein 1 (TGBp1) interacts with eEF1B. When PVX was inoculated onto eEF1B silenced tobacco plants, PVX replication appeared to be inhibited (Hwang et al., 2015).

These results showing that eEF1B is an important host factor for other viruses, supports the theory that eEF1B is likely a host factor involved in PDV infection.

Through comparison of the proteomic changes in both hosts, it can be presumed that during PDV infection, photosynthesis is impaired (**Figure 42D**). Some chloroplast host proteins which are increased in response to other viruses as defense responses are decreased during PDV infection (**Figure 42D**), suggesting PDV infection results in decreases of these specific host defenses allowing for a compatible interaction and systemic infection. The use of multiple sites for viral replication may also permit PDV to evade host defense proteins such as PPI based on spatial separation as well. Additionally, proteins which serve as host factors for other viruses are significantly altered during PDV infection, suggesting PDV uses similar strategies for replication.

4.9   Cucumber serves as a model host for identification of host factors required for PDV infection

Two proteins (TSPAN8 and TCTP) which increase in accumulation following PDV infection were identified in cucumber. To test if these proteins had important roles in PDV infection, these proteins were further investigated. TSPANS are primarily membrane spanning proteins forming extensive complex networks (Wang et al., 2015). Some TSPANS are known to form exosomes, small vesicular structures which are released from larger multi vesicular bodies into the extracellular space. Recent work suggests exosomes are a means for long distance movement of TuMV (Movahed et al., 2019). The localization of TSPAN8 at the PD of tobacco (**Figure 38A**) is similar to results obtained when TSPAN8 from *Capsicum chinense* was studied during infection by *Pepper mild mottle virus*, a *Tobamovirus* (PMMoV; Ibáñez, 2015). The observed co-localization of TSPAN8 and the viral CP could implicate a role for TSPAN8 in viral movement, although the exact role is unclear (**Figure 38B**). This theory is supported by findings that that TSPAN8 is able to impair movement of at least two tobamoviruses, however the movement of other viruses such as PPV and members of the *Tobra-* and *Potexvirus* genera were unaffected by overexpression of TSPAN8 (Ibáñez, 2015). The potential interaction between TSPAN8 and

the viral CP (**Figure 39**) suggests TSPAN8 serves as a receptor for CP and an interaction could trigger a defense response by TSPAN8 if this protein is involved in the impairment of PDV movement. As blocking of virus movement by TSPAN8 is virus specific, another possibility is that TSPAN8 may serve as a receptor for CP, and perhaps TSPAN8 is involved in exosome formation and long-distance movement of PDV in a manner similar with TuMV.

During infection by *Pepper yellow mosaic virus* (PYMV), a member of the *Potyvirus* genus, the increased expression of TCTP1 in tomato led to increased susceptibility of the host, whereas the silencing of TCTP1 in tomato and tobacco led to reductions of viral accumulation and symptoms in PYMV inoculated plants (Bruckner et al., 2017). It appears TCTP1 serves as a host factor for potyviruses although specific interactions between TCTP1 and specific viral proteins have not been identified *in planta*. When expressed alone, with the nuclear marker (VPg) or the MP of PDV, TCTP1 is primarily localized to the nucleus, with some cytosolic localization (**Figure 40A, B**). However, in the presence of the PDV CP, the sub-cellular localization of TCTP1 shifts from the nucleus to co-localize with the CP at the cell periphery (**Figure 39C**). During PYMV infection, the same localization change of TCTP1 occurs, TCTP1 leaves the nucleus and relocates to the cell periphery and cytoplasm (Bruckner et al., 2017). The observation that TCTP1 and the PDV CP potentially interact (**Figure 41**) may indicate that TCTP1 is a host factor for PDV infection.

4.10   Concluding remarks and future directions

Plant viruses infect all agricultural crops and are conservatively estimated to cause 50% of plant diseases (Wang et al., 2020). This thesis provides further insights regarding the presence of viral pathogens in the Niagara fruit belt of Ontario, a significant fruit growing region. Additionally, the results presented can be incorporated to form a stronger understanding of processes involved in the viral infection cycle of PDV (**Figure 42**), a relatively understudied yet important virus (Kozieł et al., 2017a).

Initial studies using NGS resulted in the detection of 4 viruses, 2 reported for the first time in Ontario (CVA and LChV1). A pathogen monitoring system could be initiated

using the presented detection data as a starting point, subsequent routine NGS-based orchard surveys could be used to track the emergence and incidence of viral pathogens. Additionally, data from this work such as the detection and genome sequence of LChV1 could be used immediately to develop sensitive, sequence-specific assays for the further detection of this virus. Since LChV1 was determined to have a low incidence of infection, a LChV1 specific management program based on these results could lead to the local eradication of this virus.

The successful construction of the first infectious clone of PDV made it possible to determine that although the severe foliar symptoms found on mature cherry trees were not seen on infected seedlings, this virus did inhibit growth and development of cherry, demonstrating the importance of this virus on cherry health, even at early stages of infection. Further proteomic analyses comparing PDV infected, asymptomatic cherry trees and the tree with severe symptoms should be performed, as differences in protein accumulations may indicate the mechanism by which PDV causes the observed symptoms. Additionally, a simple comparison of the viral titer of PDV in symptomatic and asymptomatic cherry trees will show if the severe symptoms are related to PDV accumulating to higher titers. This infectious clone provides a powerful tool which can be used in combination with other cloned viruses such as PNRSV to further study the impact of infection by multiple viruses on natural and experimental hosts. Additionally, the ability of the PDV infectious clone to cause a drastic phenotypic difference between cucumber and tobacco offers an excellent system to study the molecular mechanism by which PDV evades host immune response in tobacco, and triggers host defense responses in cucumber. Advancing knowledge in this topic will not only help better understand the viral infection cycle, but also identify molecular targets for the development of new strategies to control PDV or mitigate the impact of PDV infection.

This work reveals that PDV utilizes a tubule guided movement mechanism (**Figure 42I**) and the MP alone has at least two roles: targeting to the PD and generation tubular structures that line the PD. The identification of domains crucial for both roles of the MP furthers our knowledge of virus intercellular movement. The identification of the N-

terminal *a*-helix, which is absent in PD dilating 30K MPs suggests this secondary structure plays an important role in tubule formation. Additionally, results indicate the C-terminus of the PDV MP is dispensable for both PD localization and tubule formation. Based on studies of AMV, PNRSV and CPMV, this domain is likely involved in a MP-CP interaction for the formation of a virion or RNP (Aparicio et al., 2010; Carvalho et al., 2003; Sánchez-Navarro et al., 2006). The *in-silico* results from this thesis indicate the C-terminus has protein binding capabilities and can be used to develop a framework for the investigation of this domain's ability to bind to the viral CP and formation of virions or RNPs. The requirement of MP associated processes (PD localization, tubule formation, and or the requirement of the C-terminus) for PDV movement could be further studied by incorporating the mutant MP sequences described here into the PDV infectious clone and studied *in planta.*

Orthologous proteins identified in both host species which undergo similar, significant accumulation changes during PDV infection highlights important biological processes specifically involved in PDV infection (**Figure 42**). The decreased levels of host proteins which moonlight against viral infection may indicate a mechanism for PDV to evade host defenses. Additionally, potential host factors are identified which may be necessary for PDV replication. The differentially accumulated proteins identified in this work serve as strong candidates for future studies to further understand the PDV infection cycle. Molecular identification of host factors from these proteins may offer ideal targets to generate transgene-free *Prunus* crops using advanced technologies such as RNA guided nucleases or other "transgene-free" methods to control PDV and related viruses.

Using data obtained from cucumber, two orthologs encoded by cherry were studied to test the utility of cucumber as an experimental host for elucidation of molecular PDV-plant interactions. It is concluded that both TSPAN8 and TCTP1 co-localize with the viral CP, and both proteins likely (separately) interact with the CP. Although positive controls of known interactors were not included, the reconstitution of fluorescence during co-expression of viral and host proteins suggests the two interact.

However, a downfall of BiFC analysis is that false positives may contribute to misleading results. For example, when two proteins tagged with split halves of a fluorescent protein localize in close proximity, the two fluorescent moieties have a propensity to self assembly independent of a protein-protein interaction leading to fluorescence and a false positive result (Horstman et al., 2014). Future studies on interactions between the CP and TPAN8 or CP and TCTP1 should include an alternate method of interaction detection. Further experiments are required to determine if there is a true interaction. Given that both the CP-TCTP1 and CP-TSPAN8 interactions are at the cell periphery, the split-ubiquitin based yeast hybrid system, used to detect interactions outside of the nucleus would be an appropriate method to use (Snider et al., 2010). These data warrant further analyses of the proteins that are significantly altered in cucumber in response to PDV infection.

Literature Cited

Albert, F.G., Fox, J.M., Young, M.J. 1997. Virion swelling is not required for cotranslational disassembly of Cowpea chlorotic mottle virus *in vitro*. J Virol 71, 4296-4299.

Almagro, L., Gómez Ros, L.V., Belchi-Navarro, S., Bru, R., Ros Barceló, A., Pedreño, M.A. 2008. Class III peroxidases in plant defence reactions. J Exp Bot 60, 377-390.

Altschul, S.F., Gish, W., Miller, W., Myers, E.W., Lipman, D.J. 1990. Basic local alignment search tool. J Mol Biol 215, 403-410.

Annamalai, P., Rao, A.L.N. 2005. Replication-independent expression of genome components and capsid protein of Brome mosaic virus *in planta*: A functional role for viral replicase in RNA packaging. Virology 338, 96-111.

Ansel-Mckinney, P., Scott, S.W., Swanson, M., Ge, X., Gehrke, L. 1996. A plant viral coat protein RNA binding consensus sequence contains a crucial arginine. EMBO J 15, 5077-5084.

Aparicio, F., Pallás, V., Sánchez-Navarro, J. 2010. Implication of the c terminus of the Prunus necrotic ringspot virus movement protein in cell-to-cell transport and in its interaction with the coat protein. J Gen Virol 91, 1865-1870.

Aparicio, F., Vilar, M., Perez-Payá, E., Pallás, V. 2003. The coat protein of Prunus necrotic ringspot virus specifically binds to and regulates the conformation of its genomic RNA. Virology 313, 213-223.

American Phytopathological Society. 1995. Compendium of stone fruit diseases., St. Paul, MN.

Baer, M.L., Houser, F., Loesch-Fries, L.S., Gehrke, L. 1994. Specific RNA binding by amino-terminal peptides of Alfalfa mosaic virus coat protein. EMBO J 13, 727-735.

Balasubramaniam, M., Kim, B.S., Hutchens-Williams, H.M., Loesch-Fries, L.S. 2014. The photosystem II oxygen-evolving complex protein PsbP interacts with the coat protein of Alfalfa mosaic virus and inhibits virus replication. Mol Plant Microbe Interact 27, 1107-1118.

Baráth, D., Jaksa-Czotter, N., Molnár, J., Varga, T., Balássy, J., Szabó, L.K., Kirilla, Z., Tusnády, G., Preininger, É., Várallyay, É. 2018. Small RNA NGS revealed the presence of Cherry virus A and Little cherry virus 1 on apricots in Hungary. Viruses 10, 318-318.

Barba, M., Ilardi, V., Pasquini, G. 2015. Control of pome and stone fruit virus diseases. Adv Virus Res 91, 47-83.

Baumann, P.A. 2008. Herbicides: how they work and the symptoms they cause, Texas farmer collection. Texas A&M University, College Station, Texas.

Bedoya, L.C., Daròs, J.-A. 2010. Stability of Tobacco etch virus infectious clones in plasmid vectors. Virus Res 149, 234-240.

Beligni, M. V., Yamaguchi, K., & Mayfield, S. P. 2004. Chloroplast elongation factor ts pro-protein is an evolutionarily conserved fusion with the s1 domain-containing plastid-specific ribosomal protein-7. Plant cell, 16, 3357-3369.

Benjamini, Y., Hochberg, Y. 1995. Controlling the false discovery rate: A practical and powerful approach to multiple testing. J R Stat Soc B 57, 289-300.

Bergua, M., Zwart, M.P., El-Mohtar, C., Shilts, T., Elena, S.F., Folimonova, S.Y. 2014. A viral protein mediates superinfection exclusion at the whole-organism level but is not required for exclusion at the cellular level. J Virol 88, 11327-11338.

Bhat, S., Folimonova, S.Y., Cole, A.B., Ballard, K.D., Lei, Z., Watson, B.S., Sumner, L.W., Nelson, R.S. 2013. Influence of host chloroplast proteins on Tobacco mosaic virus accumulation and intercellular movement. Plant Phys 161, 134-147.

Bhattacharyya, D., Chakraborty, S. 2018. Chloroplast: The trojan horse in plant–virus interaction. Mol Plant Pathol 19, 504-518.

Boccara, M., Sarazin, A., Thiébeauld, O., Jay, F., Voinnet, O., Navarro, L., Colot, V. 2014. The *Arabidopsis* miR472-Rdr6 silencing pathway modulates PAMP- and effector-triggered immunity through the post-transcriptional control of disease resistance genes. PLoS Pathog 10, 1-16.

Bol, J.F. 1999. Alfalfa mosaic virus and Ilarviruses: Involvement of coat protein in multiple steps of the replication cycle. J Gen Virol 80, 1089-1102.

Bol, J.F. 2005. Replication of Alfamo- and Ilarviruses: role of the coat protein. Annu Rev Phytopathol 43, 39-62.

Bol, J.F., Van Vloten-Doting, L., Jaspars, E.M.J. 1971. A functional equivalence of top component a RNA and coat protein in the initiation of infection by Alfalfa mosaic virus. Virology 46, 73-85.

Bolton, M.D. 2009. Primary metabolism and plant defense-fuel for the fire. Mol Plant Microbe Interact 22, 487-497.

Bond, K.M., Lyktey, N.A., Tsvetkova, I.B., Dragnea, B., Jarrold, M.F. 2020. Disassembly intermediates of the Brome mosaic virus identified by charge detection mass spectrometry. J Phys Chem B 124, 2124-2131.

Boonham, N., Kreuze, J., Winter, S., Van Der Vlugt, R., Bergervoet, J., Tomlinson, J., Mumford, R. 2014. Methods in virus diagnostics: From ELISA to next generation sequencing. Virus Res 186, 20-31.

Bos, L. 1981. Hundred years of Koch's postulates and the history of etiology in plant virus research. Neth J Plant Pathol 87, 91-110.

Bourguiba, H., Audergon, J.M., Krichen, L., Trifi-Farah, N., Mamouni, A., Trabelsi, S., Khadari,B. 2012. Genetic diversity and differentiation of grafted and seed propagated apricot (*Prunus armeniaca* L.) in the Maghreb region. Sci Hort 142, 7-13.

Brister, J.R., Ako-Adjei, D., Bao, Y., Blinkova, O. 2014. NCBI viral genomes resource. Nucleic Acids Res 43, 571-577.

Bristow, P.R., Martin, R.R. 2002. Recovery of plants infected with Blueberry shock ilarvirus (BlShV). Acta Hortic, 85-89.

Bruckner, F.P., Xavier, A.D.S., Cascardo, R.D.S., Otoni, W.C., Zerbini, F.M., Alfenas-Zerbini, P. 2017. Translationally controlled tumour protein (TCTP) from tomato and Nicotiana benthamiana is necessary for successful infection by a Potyvirus. Mol Plant Pathol 18, 672-683.

Buchan, D.W.A., Jones, D.T. 2019. The PSIPRED protein analysis workbench: 20 years on. Nucleic Acids Res 47, 402-407.

Budziszewska, M., Obrępalska-Stęplowska, A. 2018. The role of the chloroplast in the replication of positive-sense single-stranded plant RNA viruses. Front Plant Sci 9, 1776-1776.

Bujarski, J., Gallitelli D., García-Arenal F., Pallás V., Palukaitis P. M., Krishna Reddy M. K., Wang, A. 2019. ICTV virus taxonomy profile: Bromoviridae. J Gen Virol, 965-976.

Caglayan, K., Ulubas Serce, C., Gazel, M., Varveri, C. 2011. Prune dwarf virus, in: Viruses of pomme and stone fruits. Hadidi, A., Barba, M., Candresse, T., Jelkmann, W. (Eds.). The American Phytopathological Society, St. Paul, MN, 199-205.

Cai, Q., Qiao, L., Wang, M., He, B., Lin, F. M., Palmquist, J., Huang, S.-D., Jin, H. 2018. Plants send small RNAs in extracellular vesicles to fungal pathogen to silence virulence genes. Science 360, 1126-1129.

Candresse, T., Marais, A., Faure, C., Gentit, P. 2013. Association of Little cherry virus 1 (LChV1) with the shirofugen stunt disease and characterization of the genome of a divergent lchv1 isolate. Phytopathology 103, 293-298.

Card, S.D., Pearson, M.N., Clover, G.R.G. 2007. Plant pathogens transmitted by pollen. Australas Plant Path 36, 455-461.

Carrington, J.C., Kasschau, K.D., Mahajan, S.K., Schaad, M.C. 1996. Cell-to-cell and long-distance transport of viruses in plants. Plant Cell 8, 1669-1681.

Carroll, D. 2014. Genome engineering with targetable nucleases. Annu Rev Biochem 83, 409-439.

Carvalho, C., Wellink, J., Ribeiro, S., Goldbach, R., Van Lent, J. 2003. The c-terminal region of the movement protein of Cowpea mosaic virus is involved in binding to the large but not to the small coat protein. J Gen Virol 84, 2271-2277.

Casado-Vela, J., Sellés, S., Martínez, R.B. 2006. Proteomic analysis of Tobacco mosaic virus-infected tomato (*Lycopersicon esculentum* m.) fruits and detection of viral coat protein. Proteomics 6, 196-206.

Chamberlain, E.E., Atkinson, J.D., Hunter, J.A. 1964. Cross-protection between strains of Apple mosaic virus. New Zeal J Agr Res 7, 480-490.

Chandrasekaran, J., Brumin, M., Wolf, D., Leibman, D., Klap, C., Pearlsman, M., Sherman, A., Arazi, T., Gal-On, A. 2016. Development of broad virus resistance in non-transgenic cucumber using CRISPR/Cas9 technology. Mol Plant Pathol 17, 1140-1153.

Chen, Q., Wang, B., Ding, H., Zhang, J., Li, S. 2019. Review: The role of NADP-malic enzyme in plants under stress. Plant Sci 281, 206-212.

Chen, S.-C., Olsthoorn, R.C.L. 2010. *In vitro* and *in vivo* studies of the RNA conformational switch in Alfalfa mosaic virus. J Virol 84, 1423-1429.

Cheng, X., Wang, A. 2017. The Potyvirus silencing suppressor protein VPg mediates degradation of sgs3 via ubiquitination and autophagy pathways. J Virol 91, 1-16.

Choi, Y.G., Dreher, T.W., Rao, A.L.N. 2002. tRNA elements mediate the assembly of an icosahedral RNA virus. Proc Natl Acad Sci U.S.A. 99, 655-660.

Chomczynski, P., Sacchi, N. 1987. Single-step method of RNA isolation by acid guanidinium thiocyanate-phenol-chloroform extraction. Annal Biochem 162, 156-159.

Cieślińska, M., Morgaś, H. 2010. Occurrence and detection of lesser known viruses and phytoplasmas in stone fruit orchards in Poland. Folia Hortic 22, 51-57.

Cipollini, D., Walters, D., Voelckel, C. 2017. Costs of resistance in plants: From theory to evidence, in: J.A., R. (Ed.), Annual plant reviews online, pp. 263-307.

Clemente-Moreno, M.J., Hernández, J.A., Diaz-Vivancos, P. 2015. Sharka: How do plants respond to Plum pox virus infection? J Exp Bot 66, 25-35.

Cohen, S.P., Leach, J.E. 2019. Abiotic and biotic stresses induce a core transcriptome response in rice. Sci Rep 9, 1-11.

Collinge, D.B., Kragh, K.M., Mikkelsen, J.D., Nielsen, K.K., Rasmussen, U., Vad, K. 1993. Plant chitinases. Plant J 3, 31-40.

Condori-Apfata, J. A., Batista-Silva, W., Medeiros, D. B., Vargas, J. R., Valente, L. M. L., Heyneke, E., Nunes-Nesi, A. 2019. The *Arabidopsis* E 1 subunit of the 2-oxoglutarate dehydrogenase complex modulates plant growth and seed production. Plant Molec Biol, 101, 183-202.

Cox, J., Hein, M.Y., Luber, C.A., Paron, I., Nagaraj, N., Mann, M. 2014. Accurate proteome-wide label-free quantification by delayed normalization and maximal peptide ratio extraction, termed Maxlfq. Mol Cell Proteomics 13, 2513-2526.

Crafts-Brandner, S.J., Salvucci, M.E. 2000. RuBisCO activase constrains the photosynthetic potential of leaves at high temperature and CO_2. Proc Natl Acad Sci U.S.A 97, 13430-13435.

Cropley, R., Gilmer, R.M., Posnette, A.F. 1964. Necrotic ring spot andPrune dwarf viruses in Prunus and in herbaceous indicators. Ann Appl Biol 53, 325-332.

Cui, H., Hong, N., Wang, G., Wang, A. 2012a. Detection and genetic diversity of Prunus necrotic ringspot virus in the Niagara fruit belt, Canada. Can J Plant Pathol 34, 104-113.

Cui, H., Hong, N., Wang, G., Wang, A. 2012b. Molecular characterization of two Prunus necrotic ringspot virus isolates from Canada. Arch Virol 157, 999-1001.

Cui, H., Hong, N., Wang, G., Wang, A., 2013. Genomic segments RNA1 and RNA2 of Prunus necrotic ringspot virus codetermine viral pathogenicity to adapt to alternating natural Prunus hosts. Mol Plant Microbe Interact 26, 515-527.

Cui, H., Wang, A. 2016. An efficient viral vector for functional genomic studies of Prunus fruit trees and its induced resistance to Plum pox virus via silencing of a host factor gene. Plant Biotechnol J 15, 344-356.

Dai, Z., 2018. Characterization of the coat protein of Turnip mosaic virus and its *Arabidopsis* interactors in the virus infection process, Department of Biology. The University of Western Ontario, Electronic Thesis and Dissertation Repository. 5800; https://ir.lib.uwo.ca/etd/5800, p. 125.

Dai, Z., He, R., Bernards, M.A., Wang, A. 2020. The cis-expression of the coat protein of Turnip mosaic virus is essential for viral intercellular movement in plants. Mol Plant Pathol 21, 1-18.

De Dios Alché, J. 2019. A concise appraisal of lipid oxidation and lipoxidation in higher plants. Redox Biol, 23, 1-11.

De Graaff, M., Coscoy, L., Jaspars, E.M. 1993. Localization and biochemical characterization of Alfalfa mosaic virus replication complexes. Virology 194, 878-881.

De Torres Zabala, M., Littlejohn, G., Jayaraman, S., Studholme, D., Bailey, T., Lawson, T., Tillich, M., Licht, D., Bölter, B., Delfino, L., Truman, W., Mansfield, J., Smirnoff, N., Grant, M. 2015. Chloroplasts play a central role in plant defence and are targeted by pathogen effectors. Nat Plants 1, 1-10.

Di Carli, M., Benvenuto, E., Donini, M. 2012. Recent insights into plant–virus interactions through proteomic analysis. J Prot Res 11, 4765-4780.

Dijkstra, J., De Jager, C.P. 1998. Virus transmission by grafting, practical plant virology: protocols and exercises. Springer, Berlin.

Dnastar, 2020. Lasergene®, 16.0 ed, Madison, WI.

Dolja, V., Koonin, E. 2013. The Closterovirus-derived gene expression and rna interference vectors as tools for research and plant biotechnology. Front Microbiol 4, 1-10.

Dreher, T.W., Bujarski, J.J., Hall, T.C. 1984. Mutant viral RNAs synthesized *in vitro* show altered aminoacylation and replicase template activities. Nature 311, 171-175.

Duan, Y., Zhou, L., Hall, D.G., Li, W., Doddapaneni, H., Lin, H., Liu, L., Vahling, C.M., Gabriel, D.W., Williams, K.P., Dickerman, A., Sun, Y., Gottwald, T. 2009. Complete genome sequence of Citrus huanglongbing bacterium, 'candidatus liberibacter asiaticus' obtained through metagenomics. Mol Plant Microbe Interact 22, 1011-1020.

Earley, K.W., Haag, J.R., Pontes, O., Opper, K., Juehne, T., Song, K., Pikaard, C.S. 2006. Gateway-compatible vectors for plant functional genomics and proteomics. Plant J 45, 616-629.

Erny, C., Schoumacher, F., Jung, C., Gagey, M.J., Godefroy-Colburn, T., Stussi-Garaud, C., Berna, A. 1992. An n-proximal sequence of the Alfalfa mosaic virus movement protein is necessary for association with cell walls in transgenic plants. J Gen Virol 73, 2115-2119.

Fajardo, T.V.M., Peiró, A., Pallás, V., Sánchez-Navarro, J. 2013. Systemic transport of Alfalfa mosaic virus can be mediated by the movement proteins of several viruses assigned to five genera of the 30k family. J Gen Virol 94, 677-681.

Feki, S., Loukili, M.J., Triki-Marrakchi, R., Karimova, G., Old, I., Ounouna, H., Nato, A., Nato, F., Guesdon, J.L., Lafaye, P., Elgaaied, A.B.A. 2005. Interaction between Tobacco Ribulose-l,5-Biphosphate Carboxylase/Oxygenase large subunit (RuBisCO-lsu) and the PVY coat protein (PVY-cp). Eur J Plant Pathol 112, 221-234.

Folimonova, S.Y. 2013. Developing an understanding of cross-protection by Citrus tristeza virus. Front Microbiol 4, 1-9.

Fridlund, P.R. 1963. Prevalence of the green ring mottle virus in Washington sweet cherry orchard trees and in foreign cherries introduced prior to 1953. Plant Dis Rep 47, 345-347.

Fuchs, M., Bar-Joseph, M., Candresse, T., Maree, H.J., Martelli, G.P., Melzer, M.J., Menzel, W., Minafra, A., Sabanadzovic, S., Consortium, I.R. 2020. ICTV virus taxonomy profile: Closteroviridae. J Gen Virol 101, 364-365.

Fulton, R.W. 1959. Purification of Sour cherry necrotic ringspot and Prune dwarf viruses. Virology 9, 522-535.

Fulton, R.W. 1966. Mechanical transmission of viruses of woody plants. Annu Rev Phytopathol 4, 79-98.

Fulton, R.W. 1982. Ilar-like characteristics of American plum line pattern virus and its serological detection in Prunus. Phytopathology 72, 1345-1348.

Galinato, S.P., Gallardo, R.K., Beers, E.H., Bixby-Brosi, A.J. 2019. Developing a management strategy for Little cherry disease: The case of Washington state. Plant Dis 103, 2184-2190.

Gallo-García, Y.M., Jaramillo-Mesa, H., Toro-Fernández, L.F., Marín-Montoya, M., Gutiérrez, P.A. 2018. Characterization of the genome of a novel Ilarvirus naturally infecting Cape gooseberry (Physalis peruviana). Arch Virol 163, 1713-1716.

George, J.A., Davidson, T.R. 1963. Pollen transmission of Necrotic ring spot and Sour cherry yellows viruses from tree to tree. Can J Plant Sci 43, 276-288.

Ghoshal, B., Sanfaçon, H. 2015. Symptom recovery in virus-infected plants: Revisiting the role of RNA silencing mechanisms. Virology 479-480, 167-179.

Gibson, D.G., Young, L., Chuang, R.Y., Venter, J.C., Hutchison, C.A., 3rd, Smith, H.O. 2009. Enzymatic assembly of DNA molecules up to several hundred kilobases. Nat methods 6, 343-345.

Gilmer, R., Brase, K. 1963. Nonuniform distribution of Prune dwarf virus in sweet and sour cherry trees. Phytopathology 53, 819-821.

Gilmer, R., Nyland, G., Moore, J.D. 1976. Prune dwarf, in: Gilmer, R., Moore, J.D., Nyland, G., Welsh, M.F., Pine, T.S. (Eds.), Virus diseases and noninfectious disorders of stone fruits in North America. U.S. Government Printing Office, Washington, D.C, 179-190.

Gilmer, R., Way, R. 1960. Pollen transmission of Necrotic ringspot and Prune dwarf viruses in sour cherry. Phytopathology 50, 624-625.

Gonsalves, D., Fulton, R.W. 1977. Activation of Prunus necrotic ringspot virus and Rose mosaic virus by RNA4 components of some Ilarviruses. Virology 81, 398-407.

Goodin, M.M., Zaitlin, D., Naidu, R.A., Lommel, S.A. 2008. Nicotiana benthamiana: Its history and future as a model for plant-pathogen interactions. Mol Plant Microbe Interact 21, 28-39.

Goodman, H.M., Ecker, J.R., Dean, C. 1995. The genome of *Arabidopsis thaliana*. Proc Natl Acad Sci U.S.A. 92, 10831-10835.

Gougherty, A.V., Nutter, F.W. 2015. Impact of eradication programs on the temporal and spatial dynamics of Plum pox virus on *Prunus spp*. In Pennsylvania and Ontario, Canada. Plant Dis 99, 593-603.

Greber, R., Teakle, D., Mink, G. 1992. Thrips-facilitated transmission of Prune dwarf and prunus necrotic ringspot viruses from cherry pollen to cucumber. J Plant disease 76, 1039-1041.

Guogas, L.M., Filman, D.J., Hogle, J.M., Gehrke, L. 2004. Cofolding organizes Alfalfa mosaic virus RNA and coat protein for replication. Science 306, 2108-2111.

Guogas, L.M., Laforest, S.M., Gehrke, L. 2005. Coat protein activation of Alfalfa mosaic virus replication is concentration dependent. J Virol 79, 5752-5761.

Gullner, G., Komives, T., Király, L., & Schröder, P. 2018. Glutathione S-transferase enzymes in plant-pathogen interactions. Front Plant Sci *9*, 1-19.

Hadidi, A., Barba, M., Candresse, T., Jelkmann, W. 2011. Virus and virus-like diseases of pome and stone fruits. The American Phytopathological Society.

Hanahan, D. 1983. Studies on transformation of *Escherichia coli* with plasmids. J Mol Biol 166, 557-580.

Hartley, J.L., Temple, G.F., Brasch, M.A. 2000. DNA cloning using *in vitro* site-specific recombination. Genome res 10, 1788-1795.

Hatsugai, N., Kuroyanagi, M., Yamada, K., Meshi, T., Tsuda, S., Kondo, M., Nishimura, M., Hara-Nishimura, I. 2004. A plant vacuolar protease, VPe, mediates virus-induced hypersensitive cell death. Science 305, 855-858.

Havé, M., Balliau, T., Cottyn-Boitte, B., Dérond, E., Cueff, G., Soulay, F., Gallois, P. 2018. Increases in activity of proteasome and papain-like cysteine protease in *Arabidopsis* autophagy mutants: back-up compensatory effect or cell-death promoting effect? J Exp Bot, 69, 1369-1385.

Heinlein, M. 2015. Plant virus replication and movement. Virology 479-480, 657-671.

Hernández, J.A., Gullner, G., Clemente-Moreno, M.J., Künstler, A., Juhász, C., Díaz-Vivancos, P., Király, L. 2016. Oxidative stress and antioxidative responses in plant–virus interactions. Physiol Mol Plant P 94, 134-148.

Hill, S.A. 1984. Methods in plant virology. Blackwell Scientific Publications, Boston.

Hipper, C., Brault, V., Ziegler-Graff, V., Revers, F. 2013. Viral and cellular factors involved in phloem transport of plant viruses. Front Plant Sci 4, 154-154.

Hofmann, K., Baron, M. 1999. Boxshade: Pretty printing and shading of multiple-alignment files. http://www.ch.embnet.org/software.

Horstman, A., Tonaco, I.a.N., Boutilier, K., Immink, R.G.H. 2014. A cautionary note on the use of split-YFP/BiFC in plant protein-protein interaction studies. Int J Mol Sci 15, 9628-9643.

Howell, W.E., Mink, G.I. 1988. Natural spread of Cherry rugose mosaic disease and two Prunus necrotic ringspot virus biotypes in a central Washington sweet cherry orchard. Plant Dis 72, 636-640.

Huang, H., Wang, Z., Cheng, J., Zhao, W., Li, X., Wang, H., Zhang, Z., Sui, X. 2013. An efficient cucumber (*Cucumis sativus* l.) protoplast isolation and transient expression system. Sci Hortic 150, 206-212.

Huang, M., Jongejan, L., Zheng, H., Zhang, L., Bol, J.F. 2001. Intracellular localization and movement phenotypes of Alfalfa mosaic virus movement protein mutants. Mol Plant Microbe Interact 14, 1063-1074.

Hull, R. 2009. Mechanical inoculation of plant viruses. Curr Protoc Microbiol 16, 1-4.

Hull, R. 2014. Movement of viruses within plants, in: Plant virology, fifthe edition. Hull, R. (Ed.). Academic Press Walltham, MA, 531-603.

Hwang, J., Lee, S., Lee, J.-H., Kang, W.-H., Kang, J.-H., Kang, M.-Y., Oh, C.-S., Kang, B.-C. 2015. Plant translation elongation factor 1bβ facilitates Potato virus x (PVX) infection and interacts with PVX triple gene block protein 1. PLoS One 10, 1-19.

Hwang, J., Oh, C.-S., Kang, B.-C. 2013. Translation elongation factor 1B (eEf1B) is an essential host factor for Tobacco mosaic virus infection in plants. Virology 439, 105-114.

Hyodo, K., Hashimoto, K., Kuchitsu, K., Suzuki, N., Okuno, T. 2017. Harnessing host ROS-generating machinery for the robust genome replication of a plant RNA virus. Proc Natl Acad Sci U.S.A. 114, 1282-1290.

Ibáñez, P.D. 2015. La tetraspanina TET8 de *Capsicum chinense*: Caracterización y análisis funcional en el contexto de la defensa vegetal, Cellular Biology. Complutense university of Madrid, Madrid, 1-180.

Ivosev, G., Burton, L., Bonner, R. 2008. Dimensionality reduction and visualization pin principal component analysis. Anal Chem. 80, 4933-4944

Jaspars, E.M.J. 1999. Genome activation in Alfamo- and Ilarviruses. Arch Virol 144, 843-863.

Jelkmann, W. 1995. Cherry virus A: cDNA cloning of dsRNA, nucleotide sequence analysis and serology reveal a new plant Capillovirus in sweet cherry. J Gen Virol 76, 2015-2024.

Jovel, J., Walker, M., Sanfacon, H. 2007. Recovery of *Nicotiana benthamiana* plants from a necrotic response induced by a Nepovirus is associated with RNA silencing but not with reduced virus titer. J Virol 81, 12285-12297.

Jung, S., Lee, T., Cheng, C.-H., Buble, K., Zheng, P., Yu, J., Humann, J., Ficklin, S.P., Gasic, K., Scott, K., Frank, M., Ru, S., Hough, H., Evans, K., Peace, C., Olmstead, M., Devetter, L.W., Mcferson, J., Coe, M., Wegrzyn, J.L., Staton, M.E., Abbott, A.G., Main, D. 2019. 15 years of GDR: New data and functionality in the genome database for *Rosaceae*. Nucleic Acids Res 47, 1137-1145.

Kaiser, W.J., Wyatt, S.D., Pesho, G.R. 1982. Natural hosts and vectors of Tobacco streak virus in eastern Washington. Phytopathology 72, 1508-1512.

Kamenova, I., Borisova, A., Popov, A. 2019. Incidence and genetic diversity of Prune dwarf virus in sweet and sour cherry in Bulgaria. Biotechnol Biotechno. Equip 33, 980-987.

Karuppuchamy, P., Venugopal, S. 2016. Integrated pest management. Tamil Nadu, India, 653-684

Kasteel, D.T., Van Der Wel, N.N., Jansen, K.A., Goldbach, R.W., Van Lent, J.W. 2015. Tubule-forming capacity of the movement proteins of Alfalfa mosaic virus and Brome mosaic virus. J Gen Virol 78, 2089-2093.

Kato, Y., Miura, E., Ido, K., Ifuku, K., Sakamoto, W. 2009. The variegated mutants lacking chloroplastic FTSHs are defective in d1 degradation and accumulate reactive oxygen species. Plant Phys 151, 1790-1801.

Katsiani, A., Maliogka, V., Katis, N., Svanella-Dumas, L., Olmos, A., Ruiz-García, A., Marais, A., Faure, C., Theil, S., Lotos, L., Candresse, T. 2018. High-throughput sequencing reveals further diversity of Little cherry virus 1 with implications for diagnostics. Viruses 10, 385-385.

Katsiani, A.T., Maliogka, V.I., Amoutzias, G.D., Efthimiou, K.E., Katis, N.I. 2015. Insights into the genetic diversity and evolution of Little cherry virus 1. Plant Pathol 64, 817-824.

Kelley, L.A., Mezulis, S., Yates, C.M., Wass, M.N., Sternberg, M.J.E. 2015. The Phyre2 web portal for protein modeling, prediction and analysis. Nat Protoc 10, 845-858.

Kesanakurti, P., Belton, M., Saeed, H., Rast, H., Boyes, I., Rott, M. 2017. Comparative analysis of Cherry virus A genome sequences assembled from deep sequencing data. Arch Virol 162, 2821-2828.

Klein, E. M., Mascheroni, L., Pompa, A., Ragni, L., Weimar, T., Lilley, K. S., Vitale, A. 2006. Plant endoplasmin supports the protein secretory pathway and has a role in proliferating tissues. Plant J, 48, 657-673.

Kneeshaw, S., Keyani, R., Delorme-Hinoux, V., Imrie, L., Loake, G.J., Le Bihan, T., Reichheld, J.-P., Spoel, S.H. 2017. Nucleoredoxin guards against oxidative stress by protecting antioxidant enzymes. Proc Natl Acad Sci U.S.A. 114, 8414-8419.

Koonin, E.V., Mushegian, A.R., Ryabov, E.V., Dolja, V.V. 1991. Diverse groups of plant RNA and DNA viruses share related movement proteins that may possess chaperone-like activity. J Gen Virol 72, 2895-2903.

Kozieł, E., Bujarski, J.J., Otulak, K. 2017a. Molecular biology of Prune dwarf virus-a lesser known member of the *Bromoviridae* but a vital component in the dynamic virus-host cell interaction network. Int J Mol Sci 18, 1-23.

Kozieł, E., Otulak-Kozieł, K., Bujarski, J.J. 2018. Ultrastructural analysis of Prune dwarf virus intercellular transport and pathogenesis. Int J Mol Sci 19, 1-22.

Kozieł, E., Otulak-Kozieł, K., Bujarski, J.J. 2020. Modifications in tissue and cell ultrastructure as elements of immunity-like reaction in *Chenopodium quinoa* against Prune dwarf virus (PDV). Cells 9, 1-22

Kozieł, E., Otulak, K., Garbaczewska, G. 2015. Phylogenetic analysis of PDV movement protein compared to Bromoviridae members as justification of possible intercellular movement. Acta Biol Cracov Bot 57, 106-114.

Kozieł, E., Otulak, K., Lockhart, B.E.L., Garbaczewska, G. 2017b. Subcelullar localization of proteins associated with Prune dwarf virus replication. Eur J Plant Pathol 149, 653-668.

Krab, I.M., Caldwell, C., Gallie, D.R., Bol, J.F. 2005. Coat protein enhances translational efficiency of Alfalfa mosaic virus RNAs and interacts with the elf4G component of initiation factor elf4F. J Gen Virol 86, 1841-1849.

Kromina, K. A., Ignatov, A. N., & Abdeeva, I. A. 2008. Role of peptidyl-prolyl-cis/trans-isomerases in pathologic processes. Memb Cell Biol, 2, 195-202.

Kumar, S., Stecher, G., Tamura, K. 2016. MEGA7: Molecular evolutionary genetics analysis version 7.0 for bigger datasets. Mol Biol Evol 33, 1870-1874.

Kutnjak, D., Elena, S.F., Ravnikar, M. 2017. Time-sampled population sequencing reveals the interplay of selection and genetic drift in experimental evolution of Potato virus Y. J Virol 91, 1-17.

Kutnjak, D., Rupar, M., Gutierrez-Aguirre, I., Curk, T., Kreuze, J.F., Ravnikar, M. 2015. Deep sequencing of virus-derived small interfering RNAs and RNA from viral particles shows highly similar mutational landscapes of a plant virus population. J Virol 89, 4760-4770.

Lacroix, C., Renner, K., Cole, E., Seabloom, E.W., Borer, E.T., Malmstrom, C.M. 2016. Methodological guidelines for accurate detection of viruses in wild plant species. Appl Environ Microbio 82, 1966-1976.

Lee, R., Keremane, M. 2013. Mild strain cross protection of Tristeza: a review of research to protect against decline on sour orange in Florida. Front Microbiol 4, 1-11.

Li, R., Mock, R., Huang, Q., Abad, J., Hartung, J., Kinard, G. 2008. A reliable and inexpensive method of nucleic acid extraction for the PCR-based detection of diverse plant pathogens. J Virol Methods 154, 48-55.

Li, S. 2019. Regulation of ribosomal proteins on viral infection. Cells, 8, 508.

Li, Y., Cui, H., Cui, X., Wang, A. 2016. The altered photosynthetic machinery during compatible virus infection. Curr Opin Virol 17, 19-24.

Li, Y., Zhang, Q., Zhang, J., Wu, L., Qi, Y., Zhou, J.M. 2010. Identification of microRNAs involved in pathogen-associated molecular pattern-triggered plant innate immunity. Plant Phys 152, 2222-2231.

Lim, S., Davaajargal, I., Yoo, R.H., Zhao, F., Cho, I.-S., Choi, G.-S., Lim, H.-S., Lee, S.-H., Moon, J.S. 2015. Genomic detection and characterization of a Korean isolate of Little cherry virus 1 sampled from a peach tree. Virus Genes 51, 260-266.

Liu, H., Wu, L., Nikolaeva, E., Peter, K., Liu, Z., Mollov, D., Cao, M., Li, R. 2018. Characterization of a new Apple luteovirus identified by high-throughput sequencing. Virol J 15, 1-9.

Liu, Y., Huang, C., Zeng, J., Yu, H., Li, Y., Yuan, C. 2020. Identification of two additional plasmodesmata localization domains in the Tobacco mosaic virus cell-to-cell-movement protein. Biochem Biophys Res Commun 521, 145-151.

Lu, Q., Tang, X., Tian, G., Wang, F., Liu, K., Nguyen, V., Kohalmi, S.E., Keller, W.A., Tsang, E.W., Harada, J.J., Rothstein, S.J., Cui, Y. 2010. *Arabidopsis* homolog of the yeast trex-2 mRNA export complex: Components and anchoring nucleoporin. Plant J 61, 259-270.

Macfarlane, S.A., Mcgavin, W.J. 2009. Genome activation by Raspberry bushy dwarf virus coat protein. J Gen Virol 90, 747-753.

Mainguet, S. E., Gakière, B., Majira, A., Pelletier, S., Bringel, F., Guérard, F., Renou, J. P. 2009. Uracil salvage is necessary for early *Arabidopsis* development. Plant J, 60, 280-291.

Marais, A., Faure, C., Theil, S., Svanella-Dumas, L., Brans, Y., Maurice, I., Blin, V., Candresse, T. 2016. First report of Little cherry virus 1 on plum in France. Plant Dis 100, 2544-2544.

Margaria, P., Anderson, C.T., Turina, M., Rosa, C. 2016. Identification of Ourmiavirus 30k movement protein amino acid residues involved in symptomatology, viral movement, subcellular localization and tubule formation. Mol Plant Pathol 17, 1063-1079.

Martelli, G.P., Savino V., 2008. Infectious diseases of Almond with special reference to the Mediterranean area 1. EPPO Bulletin 27, 525-534.

Martínez-Gómez, P., Sozzi, G.O., Sánchez-Pérez, R., Rubio, M., Gradziel, T.M. 2003. New approaches to *Prunus* tree crop breeding. J Food Agric Environ 1, 52-63.

Martínez-Pérez, M., Aparicio, F., López-Gresa, M.P., Bellés, J.M., Sánchez-Navarro, J.A., Pallás, V. 2017. *Arabidopsis* m6a demethylase activity modulates viral infection of a plant virus and the m6a abundance in its genomic RNAs. Proc Natl Acad Sci U.S.A. 114, 10755-10760.

Marx, H., Minogue, C.E., Jayaraman, D., Richards, A.L., Kwiecien, N.W., Siahpirani, A.F., Rajasekar, S., Maeda, J., Garcia, K., Del Valle-Echevarria, A.R., Volkening, J.D.,

Westphall, M.S., Roy, S., Sussman, M.R., Ane, J.M., Coon, J.J. 2016. A proteomic atlas of the legume *Medicago truncatula* and its nitrogen-fixing endosymbiont *Sinorhizobium meliloti*. Nat Biotechnol 34, 1198-1205.

Mathur, C., Mohan, K., Usha Rani, T.R., Krishna Reddy, M., Savithri, H.S. 2014. The n-terminal region containing the zinc finger domain of Tobacco streak virus coat protein is essential for the formation of virus-like particles. Arch Virol 159, 413-423.

Melcher, U. 2000. The '30k' superfamily of viral movement proteins. J Gen Virol 81, 257-266.

Mendu, V., Chiu, M., Barajas, D., Li, Z., Nagy, P.D. 2010. Cpr1 cyclophilin and Ess1 parvulin prolyl isomerases interact with the Tombusvirus replication protein and inhibit viral replication in yeast model host. Virology 406, 342-351.

Millikan, D. 1955. The influence of infection by Ring spot virus upon the growth of one-year-old Montmorency nursery trees. Phytopathology 45, 565-566.

Mink, G.I. 1992. Ilarvirus vectors, in: Harris, K.F. (Ed.), Advances in disease vector research. Springer New York, New York, NY, 261-281.

Moreno, P., Ambrós, S., Albiach-Martí, M.R., Guerri, J., Peña, L. 2008. Citrus tristeza virus: A pathogen that changed the course of the citrus industry. Mol Plant Pathol 9, 251-268.

Mori, M., Mise, K., Kobayashi, K., Okuno, T., Furusawa, I. 1991. Infectivity of plasmids containing Brome mosaic virus cDNA linked to the Cauliflower mosaic virus 35s RNA promoter. J Gen Virol 72, 243-246.

Movahed, N., Cabanillas, D.G., Wan, J., Vali, H., Laliberté, J.-F., Zheng, H. 2019. Turnip mosaic virus components are released into the extracellular space by vesicles in infected leaves. Plant Phys 180, 1375-1388.

Mushegian, A.R., Elena, S.F. 2015. Evolution of plant virus movement proteins from the 30k superfamily and of their homologs integrated in plant genomes. Virology 476, 304-315.

Nagy, P.D., Wang, R.Y., Pogany, J., Hafren, A., Makinen, K. 2011. Emerging picture of host chaperone and cyclophilin roles in RNA virus replication. Virology 411, 374-382.

Nagyova, A., Subr, Z. 2007. Infectious full-length clones of plant viruses and their use for construction of viral vectors. Acta Virol 51, 223-237.

Neeleman, L., Linthorst, H.J.M., Bol, J.F. 2004. Efficient translation of Alfamovirus RNAs requires the binding of coat protein dimers to the 3' termini of the viral RNAs. J Gen Virol 85, 231-240.

Németh, M. 1986. Viruses, mycoplasma and rickettsia diseases of fruit trees. Springer Netherlands, Heidelberg.

Németh, M., Nyerges, K., Hangyál, R., Kósa, G. 2010. Surveying viruses on ornamental trees and shrubs in two Hungarian botanical gardens and an arboretum. Julius-Kühn-Archiv 427, 293-299.

Nishiguchi, M., Kobayashi, K. 2011. Attenuated plant viruses: preventing virus diseases and understanding the molecular mechanism. J Gen Plant Pathol 77, 221-229.

Niu, X., Sun, Y., Chen, Z., Li, R., Padmanabhan, C., Ruan, J., Kreuze, J.F., Ling, K., Fei, Z., Gao, S. 2017. Using small RNA-seq data to detect siRNA duplexes induced by plant viruses. Genes 8, 1-8.

Noorani, M.S., Awasthi, P., Singh, R.M., Ram, R., Sharma, M.P., Singh, S.R., Ahmed, N., Hallan, V., Zaidi, A.A. 2010. Complete nucleotide sequence of Cherry virus A (CVA) infecting sweet cherry in India. Arch Virol 155, 2079-2082.

Noorani, M.S., Awasthi, P., Sukapaka, M., Singh, L., Ram, R., Sharma, M.P., Zaidi, A.A., Hallan, V. 2013. Immunodiagnostics for Cherry virus A and Cherry necrotic rusty mottle virus. J Plant Biochem Biot 24, 93-104.

O'reilly, E.K., Wang, Z., French, R., Kao, C.C. 1998. Interactions between the structural domains of the RNA replication proteins of plant-infecting RNA viruses. J Virol 72, 7160-7169.

Olsthoorn, R.C., Mertens, S., Brederode, F.T., Bol, J.F. 1999. A conformational switch at the 3' end of a plant virus RNA regulates viral replication. EMBO J 18, 4856-4864.

Ozturk, Y., Cevik, B. 2015. Genetic diversity in the coat protein genes of Prune dwarf virus isolates from sweet cherry growing in Turkey. Plant Pathol J 31, 41-49.

Pallas, V., Aparicio, F., Herranz, M.C., Amari, K., Sanchez-Pina, M.A., Myrta, A., Sanchez-Navarro, J.A. 2012. Ilarviruses of *Prunus spp*.: a continued concern for fruit trees. Phytopathology 102, 1108-1120.

Pallas, V., Aparicio, F., Herranz, M.C., Sanchez-Navarro, J.A., Scott, S.W. 2013. The molecular biology of Ilarviruses. Adv Virus Res 87, 139-181.

Pallas, V., García, J.A. 2011. How do plant viruses induce disease? Interactions and interference with host components. J Gen Virol 92, 2691-2705.

Pallás, V., Sánchez-Navarro, J.A., Díez, J. 1999. *In vitro* evidence for RNA binding properties of the coat protein of Prunus necrotic ringspot Ilarvirus and their comparison to related and unrelated viruses. Arch Virol 144, 797-803.

Pallás, V., Sánchez-Navarro, J.A., James, D. 2018. Recent advances on the multiplex molecular detection of plant viruses and viroids. Front Microbiol 9, 1-11.

Park, S.H., Li, F., Renaud, J., Shen, W., Li, Y., Guo, L., Cui, H., Sumarah, M., Wang, A. 2017. Nbexpa1, an α-expansin, is plasmodesmata-specific and a novel host factor for potyviral infection. Plant J 92, 846-861.

Pasin, F., Menzel, W., Daròs, J. A. 2019. Harnessed viruses in the age of metagenomics and synthetic biology: An update on infectious clone assembly and biotechnologies of plant viruses. Plant Biotechnol J 17, 1010-1026.

Pecman, A., Kutnjak, D., Gutiérrez-Aguirre, I., Adams, I., Fox, A., Boonham, N., Ravnikar, M. 2017. Next generation sequencing for detection and discovery of plant viruses and viroids: Comparison of two approaches. Front Microbiol 8, 1-10.

Petrillo, J.E., Rocheleau, G., Kelley-Clarke, B., Gehrke, L. 2005. Evaluation of the conformational switch model for Alfalfa mosaic virus RNA replication. J Virol 79, 5743-5751.

Prabha, K., Baranwal, V.K., Jain, R.K. 2013. Applications of next generation high throughput sequencing technologies in characterization, discovery and molecular interaction of plant viruses. Indian J Virol 24, 157-165.

Prescott, J., Feldmann, H., Safronetz, D. 2017. Amending Koch's postulates for viral disease: when "growth in pure culture" leads to a loss of virulence. Antiviral Res 137, 1-5.

Proebsting, E.L., Ophardt, D., Howell, W.E., Mink, G.I., Patten, K.D. 1995. Variation in horticultural traits of 'Bing' sweet cherry associated with Ilarvirus infection. Hort Science 30, 333-335.

Punja, Z.K., Zhang, Y.Y. 1993. Plant chitinases and their roles in resistance to fungal diseases. J Nematol 25, 526-540.

Rajam, M., Chandola, N., Goud, P.S., Singh, D., Kashyap, V., Choudhary, M., Sihachakr, D. 2007. Thaumatin gene confers resistance to fungal pathogens as well as tolerance to abiotic stresses in transgenic tobacco plants. Biol Plantarum 51, 135-141.

Ratcliff, F.G., Macfarlane, S.A., Baulcombe, D.C. 1999. Gene silencing without DNA. RNA-mediated cross-protection between viruses. Plant Cell 11, 1207-1216.

Raudvere, U., Kolberg, L., Kuzmin, I., Arak, T., Adler, P., Peterson, H., Vilo, J. 2019. G:Profiler: A web server for functional enrichment analysis and conversions of gene lists (2019 update). Nucleic Acids Res 47, 191-198.

Reusken, C.B., Bol, J.F. 1996. Structural elements of the 3'-terminal coat protein binding site in Alfalfa mosaic virus RNAs. Nucleic Acids Res 24, 2660-2665.

Reuter, J.S., Mathews, D.H. 2010. RNAstructure: Software for RNA secondary structure prediction and analysis. BMC Bioinformatics 11.

Rivers, T.M. 1937. Viruses and Koch's postulates. J Bacteriol 33, 1-12.

Roshan, P., Kulshreshtha, A., Kumar, S., Purohit, R., & Hallan, V. 2018. AV2 protein of Tomato leaf curl Palampur virus promotes systemic necrosis in *Nicotiana benthamiana* and interacts with host Catalase2. Sci rep, 8, 1-15.

Routt, S. M., & Bankaitis, V. A. 2004. Biological functions of phosphatidylinositol transfer proteins. Biochem cell biol, 82, 254-262.

Rubio, M., Martínez-Gómez, P., Marais, A., Sánchez-Navarro, J.A., Pallás, V., Candresse, T. 2017. Recent advances and prospects in *Prunus* virology. Ann Appl Biol 171, 125-138.

Saade, M., Aparicio, F., Sánchez-Navarro, J.A., Herranz, M.C., Myrta, A., Di Terlizzi, B., Pallás, V. 2000. Simultaneous detection of the three Ilarviruses affecting stone fruit trees by nonisotopic molecular hybridization and multiplex reverse-transcription polymerase chain reaction. Phytopathology 90, 1330-1336.

Saatian, B., Austin, R.S., Tian, G., Chen, C., Nguyen, V., Kohalmi, S.E., Geelen, D., Cui, Y. 2018. Analysis of a novel mutant allele of gsl8 reveals its key roles in cytokinesis and symplastic trafficking in *Arabidopsis*. BMC Plant Biol 18, 295-295.

Salsman, J., Dellaire, G. 2016. Precision genome editing in the crispr era. Biochem Cell Biol 95, 187-201.

Sambrook, J., Russell, D.W. 2006. Preparation and transformation of competent *E. coli* using calcium chloride. CSH Protoc 2006, pdb.prot3932.

Sánchez-Navarro, J.A., Bol, J.F. 2001. Role of the Alfalfa mosaic virus movement protein and coat protein in virus transport. Mol Plant Microbe Interact 14, 1051-1062.

Sánchez-Navarro, J.A., Carmen Herranz, M., Pallás, V. 2006. Cell-to-cell movement of Alfalfa mosaic virus can be mediated by the movement proteins of Ilar-, Bromo-,

Cucumo-, Tobamo- and Comoviruses and does not require virion formation. Virology 346, 66-73.

Sanfaçon, H. 2005. Replication of positive-strand RNA viruses in plants: contact points between plant and virus components. Can J Bot 83, 1529-1549.

Sanfaçon, H. 2015. Plant translation factors and virus resistance. Viruses 7, 3392-3419.

Sanfaçon, H. 2017. Grand challenge in plant virology: Understanding the impact of plant viruses in model plants, in agricultural crops, and in complex ecosystems. Front Microbiol 8, 1-4.

Sarowar, S., Kim, Y. J., Kim, K. D., Hwang, B. K., Ok, S. H., & Shin, J. S. 2009. Overexpression of lipid transfer protein (LTP) genes enhances resistance to plant pathogens and LTP functions in long-distance systemic signaling in tobacco. Plant cell rep, 28, 419-427.

Sasikumar, A. N., Perez, W. B., & Kinzy, T. G. 2012. The many roles of the eukaryotic elongation factor 1 complex. Wiley Interdiscip Rev RNA, 3, 543-555.

Schwanhäusser, B., Busse, D., Li, N., Dittmar, G., Schuchhardt, J., Wolf, J., Chen, W., Selbach, M. 2011. Global quantification of mammalian gene expression control. Nature 473, 337-342.

Seavert, C., Long, L.E. 2007. Financial and economic comparison between establishing a standard and high density sweet cherry orchard in Oregon, USA. Acta Hort 75, 501-504.

Seo, J.-K., Kim, K.-H. 2016. Long-distance movement of viruses in plants, in: Wang, A., Zhou, X. (Eds.), Current research topics in plant virology. Springer International Publishing, Cham, Switzerland, 153-172.

Sharma, N., Sharma, K., Gaur, R., Gupta, V. 2011. Role of chitinase in plant defense. Asian J Biochem 6, 29-37.

Shimura, H., Masuta, C., Yoshida, N., Sueda, K., Suzuki, M. 2013. The 2b protein of Asparagus virus 2 functions as an RNA silencing suppressor against systemic silencing to prove functional synteny with related Cucumoviruses. Virology 442, 180-188.

Shivaprasad, P.V., Chen, H.M., Patel, K., Bond, D.M., Santos, B.a.C.M., Baulcombe, D.C. 2012. A microRNA superfamily regulates nucleotide binding site-leucine-rich repeats and other mRNAs. Plant Cell 24, 859-874.

Snider, J., Kittanakom, S., Curak, J., Stagljar, I. 2010. Split-ubiquitin based membrane yeast two-hybrid (MYTH) system: a powerful tool for identifying protein-protein interactions. J Vis Exp 36, 1-8.

Söding, J., Biegert, A., Lupas, A.N. 2005. The HHpred interactive server for protein homology detection and structure prediction. Nucleic Acids Res 33, 244-248.

Souza, P.F.N., Garcia-Ruiz, H., Carvalho, F.E.L. 2019. What proteomics can reveal about plant–virus interactions? Photosynthesis-related proteins on the spotlight. Theor and Exp Plant Phys 31, 227-248.

Statistics-Canada, 2018. Estimates, production and farm gate value of fresh and processed fruits, in: 32-10-0364-01.
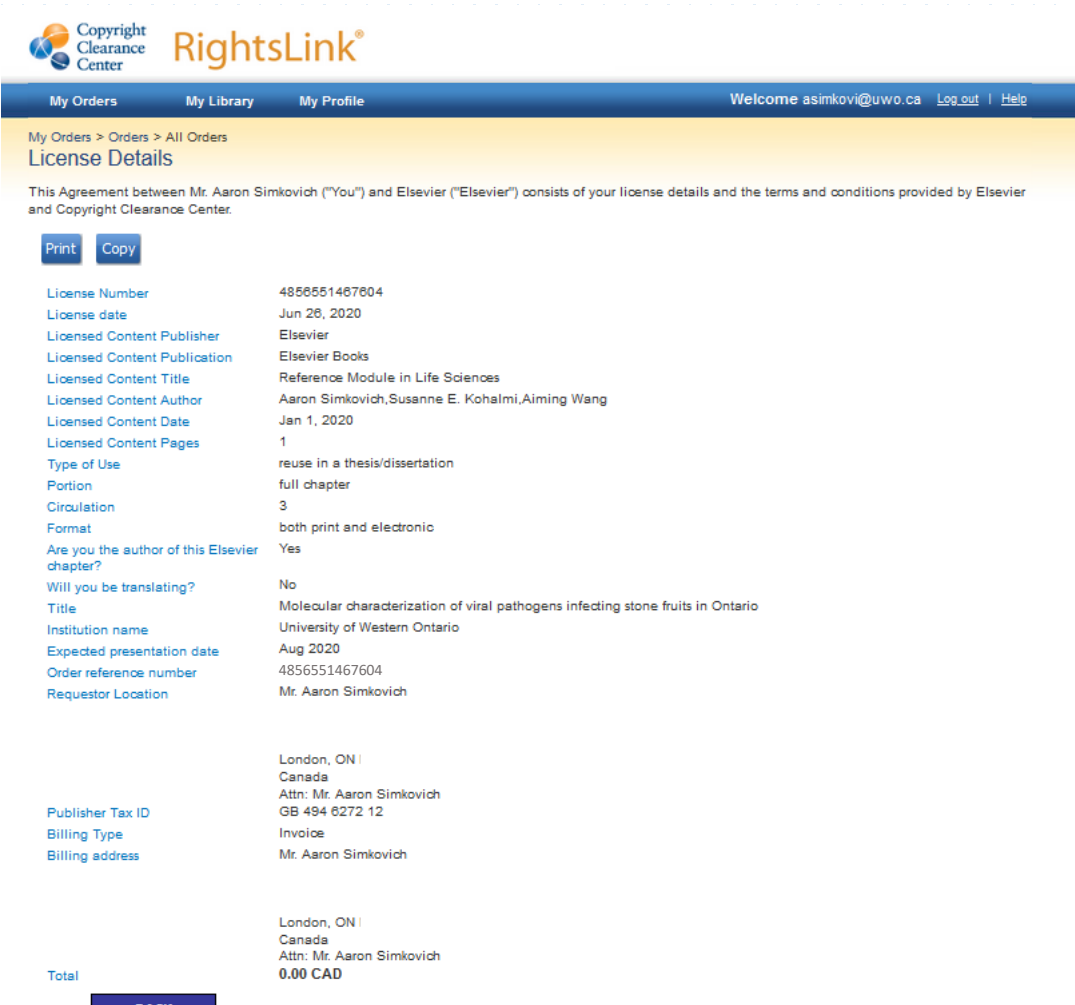
Sun, Y.-D., Folimonova, S.Y. 2019. The p33 protein of Citrus tristeza virus affects viral pathogenicity by modulating a host immune response. New Phytol 221, 2039-2053.

Swanson, M.M., Ansel-Mckinney, P., Houser-Scott, F., Yusibov, V., Loesch-Fries, L.S., Gehrke, L. 1998. Viral coat protein peptides with limited sequence homology bind similar domains of Alfalfa mosaic virus and Tobacco streak virus RNAs. J Virol 72, 3227-3234.

Sztuba-Solińska, J., Bujarski, J.J. 2008. Insights into the single-cell reproduction cycle of members of the family Bromoviridae: Lessons from the use of protoplast systems. J Virol 62, 3581-3588.

Takeshita, D., Tomita, K. 2010. Assembly of qβ viral RNA polymerase with host translational elongation factors Ef-Tu and -Ts. Proc Natl Acad Sci U.S.A. 107, 15733-15738.

Tao, Y.J., Ye, Q. 2010. RNA virus replication complexes. PLoS pathogens 6, 1-3.

Tatineni, S., Bar-Joseph, M., Mawassi, M., Albiach-Marti, M.R., Ayllon, M.A., Gowda, S., Hilf, M.E., Moreno, P., Garnsey, S.M., Dawson, W.O. 2001. Amplification of Citrus tristeza virus from a cDNA clone and infection of citrus trees. Virology 280, 87-96.

Taylor, R.B. 1996. Fruit processing, 1. Chapman & Hali, Frimley, Surrey.

The Uniprot Consortium. 2018. Uniprot: A worldwide hub of protein knowledge, Nucleic Acids Res, pp. 506-515.

Thomas, E.L., Van Der Hoorn, R.a.L. 2018. Ten prominent host proteases in plant-pathogen interactions. Int J Mol Sci 19, 1-12.

Thomas, H.E., Hildebrand, E.M. 1936. A virus disease of prune. Phytopathology 26, 1145-1148.

Topchiiska, M.L. 1982. Effect of Prunus necrotic ringspot virus (PNRV) and Prune dwarf virus (PDV) on some biological properties of peach, 130 Ed. International Society for Horticultural Science (ISHS), Leuven, Belgium, 307-312.

Tyanova, S., Temu, T., Sinitcyn, P., Carlson, A., Hein, M.Y., Geiger, T., Mann, M., Cox, J. 2016. The perseus computational platform for comprehensive analysis of proteomics data. Nat Methods 13, 731-740.

Van Der Heijden, M.W., Carette, J.E., Reinhoud, P.J., Haegi, A., Bol, J.F. 2001. Alfalfa mosaic virus replicase proteins P1 and P2 interact and colocalize at the vacuolar membrane. J Virol 75, 1879-1887.

Van Hoewyk, D., Pilon, M., & Pilon-Smits, E. A. 2008. The functions of NifS-like proteins in plant sulfur and selenium metabolism. Plant Sci 174, 117-123.

Van Vloten-Doting, L. 1975. Coat protein is required for infectivity of Tobacco streak virus: Biological equivalence of the coat proteins of Tobacco streak and Alfalfa mosaic viruses. Virology 65, 215-225.

Villamor, D.E.V., Pillai, S.S., Eastwell, K.C. 2017. High throughput sequencing reveals a novel Fabavirus infecting sweet cherry. Arch Virol 162, 811-816.

Voinnet, O. 2001. RNA silencing as a plant immune system against viruses. Trends Genet 17, 449-459.

Wang, A. 2015. Dissecting the molecular network of virus-plant interactions: the complex roles of host factors. Annu Rev Phytopathol 53, 45-66.

Wang, A., Burch-Smith, T.M., Li, Y. 2020. Focus on cell biology of virus-plant and virus-vector interactions. Mol Plant Microbe Interact 33, 5.

Wang, A., Krishnaswamy, S. 2012. Eukaryotic translation initiation factor 4e-mediated recessive resistance to plant viruses and its utility in crop improvement. Mol Plant Pathol 13, 795-803.

Wang, A., Sanfaçon, H., Stobbs, L.W., James, D., Thompson, D., Svircev, A.M., Brown, D.C.W. 2006. Plum pox virus in Canada: progress in research and future prospects for disease control. Can J Plant Pathol 28, 182-196.

Wang, F., Muto, A., Van De Velde, J., Neyt, P., Himanen, K., Vandepoele, K., Van Lijsebettens, M. 2015. Functional analysis of the *Arabidopsis* tetraspanin gene family in plant growth and development. Plant Phys 169, 2200-2214.

Way, R., Gilmer, R. 1963. Reductions in fruit sets on cherry trees pollinated with pollen from trees with sour cherry yellows. Phytopathology 53, 399-401.

Weigel, D., Glazebrook, J. 2006. Transformation of *Agrobacterium* using electroporation, CSH Protoc, 1-13.

Wieringa-Brants, D.H. 1981. The role of the epidermis in virus-induced local lesions on cowpea and tobacco leaves. J Gen Virol 54, 209-212.

Wu, F.H., Shen, S.C., Lee, L.Y., Lee, S.H., Chan, M.T., Lin, C.S. 2009. Tape-*Arabidopsis* sandwich - a simpler *Arabidopsis* protoplast isolation method. Plant Methods 5, 1-10

Wu, H.-C., Bulgakov, V.P., Jinn, T.-L. 2018. Pectin methylesterases: Cell wall remodeling proteins are required for plant response to heat stress. Front Plant Sci 9, 1-21.

Wu, Q., Luo, Y., Lu, R., Lau, N., Lai, E.C., Li, W.X., Ding, S.W. 2010. Virus discovery by deep sequencing and assembly of virus-derived small silencing RNAs. Proc Natl Acad Sci U.S.A. 107, 1606-1611.

Wu, X., Valli, A., García, J.A., Zhou, X., Cheng, X. 2019. The tug-of-war between plants and viruses: great progress and many remaining questions. Viruses 11, 1-25.

Xiang, C., Han, P., Lutziger, I., Wang, K., Oliver, D.J. 1999. A mini binary vector series for plant transformation. Plant Mol Biol 40, 711-717.

Xin, H.W., Ding, S.W. 2003. Identification and molecular characterization of a naturally occurring RNA virus mutant defective in the initiation of host recovery. Virology 317, 253-262.

Xu, K., Nagy, P.D. 2010. Dissecting virus-plant interactions through proteomics approaches. Curr Proteomics 7, 316-327.

Yokomi, R., Garnsey, S., Permar, T., Lee, R., Youtsey, C. 1991. Natural spread of severe Citrus tristeza virus isolates in citrus preinfected with mild CTV isolates, International Organization of Citrus Virologists Conference Proceedings (1957-2010).

Yuan, C., Lazarowitz, S.G., Citovsky, V. 2016. Identification of a functional plasmodesmal localization signal in a plant viral cell-to-cell-movement protein. mBio 7, 1-10.

Zaltsman, A., Feder, A., Adam, Z. 2005. Developmental and light effects on the accumulation of FTSH protease in *Arabidopsis* chloroplasts–implications for thylakoid formation and photosystem II maintenance. Plant J 42, 609-617.

Zhang, Y. 2008. I-TASSER server for protein 3D structure prediction. BMC Bioinformatics 9, 1-8.

Zhang, Z.-L., Zhang, F.-J., Zheng, P.-F., Xie, Y.-H., You, C.-X., Hao, Y.-J. 2020. Determination of protein interactions among replication components of Apple necrotic mosaic virus. Viruses 12, 1-15.

Zhao, J., Zhang, X., Hong, Y., Liu, Y. 2016. Chloroplast in plant-virus interaction. Front Microbiol 7, 1-20.

Zheng, H., Wang, G., Zhang, L. 1997. Alfalfa mosaic virus movement protein induces tubules in plant protoplasts. Mol Plant Microbe Interact 10, 1010-1014.

Zhou, X., Sun, K., Zhou, X., Jackson, A.O., Li, Z. 2019. The matrix protein of a plant Rhabdovirus mediates superinfection exclusion by inhibiting viral transcription. J Virol 93, 1-18.

Zulauf, M. 1977. Swelling of Brome mosaic virus as studied by intensity fluctuation spectroscopy. J Mol Biol 114, 259-266.

Appendices

Appendix 1 Authorship permission to reuse material in chapter 1

Appendix 2 Primers used in this study

Primer name[a]	Sequence (5' - 3')[b]	Amplicon size (bp)[c]	Melting temperature (°C)
CVA sequencing primers			
CVAsqF1	CAATGGCATTTGTGGCTAAATTCGC	1244	60
CVAsqR1	GAGTTCAGTAATGGCCCTACTGCC		61
CVAsqF2	GAATCATCCTTGGCCAAGCTGAGGCAGC	1095	67
CVAsqR2	CTTCCCTCCAATGTGAATTGCATGC		61
CVAsqF3	GTTGTAAATTCCTGGGATACAGAGTGC	1192	59
CVAsqR3	ATGACGCTGTTGAAGGTGCTTCCTTGTGC		67
CVAsqF4	CAAAAGGTTTGGTTACTTCACTGGC	1063	59
CVAsqR4	GATGAAGAGGAAGATTTCGTTTGTTGGCC		62
CVAsqF5	GTTAAATATATTCCTGAGGAAGGTGCC	1279	57
CVAsqR5	GTTGGATTCATTTGATGCAATGTGGCC		61
CVAsqF6	GAAGGAGGGTTATTTGGGGAGTGTG	1167	61
CVAsqR6	TGAAACTCTGGTCAACACTGACG		59
CVAsqF7	GTACCAGCTCAGTAATCAGAGTACTGC	1242	60
CVAsqR7	GTACACACCCTTGATTGGTGACGG		61
CVA5prGSP1	CTCAAAACGGTTATGCTCAGC	-	55
CVA5prGSP2	ACAAATGCCATTGCACTTGC	-	56
CVA3prGSP1	TAGAGAAGGGAAGAAAGCCG	-	55
CVA3prGSP2	TGTTGCTTAACTGCCAGAGC	-	57
LChV1 sequencing primers			
LChV1sqF1	GAAAAATTTCTTGCATTAGCCGACG	1075	57
LChV1sqR1	CCTTTGGTAAATCCATAGAAACTAAGC		56
LChV1sqF2	CAACTCTGGGAGGACCCTTCG	932	60
LChV1sqR2	GTTTTGTGAATCCCTCAACAATCAGGTCG		62
LChV1sqF3	GTTCTGCTGGTTAGATGCATTTGC	1448	59
LChV1sqR3	GAAAATGAACTTTCTCAGCAAGCCG		59
LChV1sqF4	CTAATTGAGTATTGCGCTAACTGCG	934	58
LChV1sqR4	CATTTCTGAAGTCTTCATCTGAGTCG		57
LChV1sqF5	CTCTTGTTTCGACTGGTTGCG	1073	58
LChV1sqR5	CAAAAATTTGAGCAGCAGCTGTGC		60
LChV1sqF6	GTATTGTATGCCCGTTTGAGCGC	1219	60

Primer name[a]	Sequence (5' - 3')[b]	Amplicon size (bp)[c]	Melting temperature (°C)
LChV1sqR6	GAATTGAATTCTCAACATCACTCACCG		58
LChV1sqF7	GTTGATCATTTGCCTGTTGACGG	1326	58
LChV1sqR7	GAAAGGTCTGTCTTCCAAGATCAAGCTAAATTCG		63
LChV1sqF8	CTTTGACCGGTGTTGCTAACATTCCG	1228	62
LChV1sqR8	CTTTGTACACCAACTCTTCGTAGAGC		59
LChV1sqF9	CAAAACTTGATATGTCTGGTGTCTCCG	1058	59
LChV1sqR9	CTTTAACAGACATCAGATCAACCAAATCG		58
LChV1sqF11	GTTAGTATTATCGACACTGCTGGCG	1503	59
LChV1sqR11	GTAAAAACACAATATGTTCTCAATAGGATATGC		57
LChV1sqF12	GATAAAAATGGAGGACTTGACAATTATGTCGAACG	1032	62
LChV1sqR12	GTCTTTTTCGTCGATGTGATCGC		58
LChV1sqF13	CTTAAAGAGAGTACCAACCATATTATCAAACG	1265	58
LChV1sqR13	GATAGCATGTGCATTTATCAGAGATCG		58
LChV1sqF14	CAACCTATATGGTCAATTCCCAATGC	1264	58
LChV1sqR14	GTTTTATCTACAGCGATACATGTCTCG		57
LChV1sqF15	CTTCATGTTTCGCAAGTATTGGGACCACG	1093	64
LChV1sqR15	CAAGTTATAACACCATTTATTGTGAAGACG		57
LChV1sqF16	GAATCTCATGAGGCTGTCACTTTGTGCG	1294	63
LChV1sqR16	CTTATTCGCTAATGTGCCATCGTGC		60
LChV1sqF17	CTTGTACAGTGGAAGTCTTAGAACTGC	1089	59
LChV1sqR17	GTTCACAAGCACTGTAAGAAATGCC		59
LChV1sqF18	GTACAACAAAGGACGTAGAAACGCC	734	60
LChV1sqR18	CTTTCTTGCTAATCAGTGGATTGGC		58
LChV1-5prGSP1	CATACGCTTGTCATGGACAGC	-	57
LChV1-5prGSP2	GAACGCTGATCTTAGGGGCAGAACG	-	63
LChV1-3prGSP1	CAATCTCGGAAACTGATAGCAACTG	-	58
LChV1-3prGSP2	GAAAATGGTGTGGACATGCTTGC	-	59
PDV sequencing primers			
PDV1sqF1	GATGAGACCACTACCGTCGG	849	60
PDV1sqR1	CAACTCAATCCCAGGTTTATACCCG		59
PDV1sqF2	CAATGCTGTTGATCTAGGTGATGCCG	883	62
PDV1sqR2	CTTAGAAGCAACAAGGGCACGC		60
PDV1sqF3	GATTCTTAACGGGATACATGGAAGTCG	1049	59

Primer name[a]	Sequence (5' - 3')[b]	Amplicon size (bp)[c]	Melting temperature (°C)
PDV1sqR3	GATTGTAGCAGCAGCATATATGCACCC		62
PDV1sqF4	CTCTTGACTTCCAACAGATCTTCTGC	665	59
PDV1sqR4	GATAAAGCCACAAGTCCATGGCAAGC		62
PDV1-5prGSP1	CTTGGACTCATCATGTAGTCCG	-	56
PDV1-5prGSP1	CAAAAGTTCATGGACATTGGCAGC	-	59
PDV1-3prGSP1	CATGAGGTTCAAGGAGGTAGC	-	56
PDV1-3prGSP1	GCTTTATCAAGACACAAGTCGG	-	55
PDV2sqF1	GTTTTTCGGATTTCTTATGATCCGAG	1046	56
PDV2sqR1	CTTCACCAATGGAAATAACGTCTGGC		60
PDV2sqF2	CATTCTCAACACTGTATTGAATGTCG	919	56
PDV2sqR2	GTTCGGTACTGCAACAACTTGC		58
PDV2sqF3	CAAACGTTGCTATGGTGGTTGC	604	59
PDV2sqR3	CAAAATAGATAGTATGGTCATCCACCG		57
PDV2-5prGSP1	GTTGAGCATCAGTAAGTTCAAGATCG	-	58
PDV2-5prGSP1	GAAAAACTGGCACAACGACCTGC	-	61
PDV2-3prGSP1	CTTCTCAGTTTTTGGTTTCGGC	-	56
PDV2-3prGSP1	GAGATAAAAATCCAGATTTACCCATGC	-	56
PDV3sqF1	GTGAAACAATTCTGTGACGTTCG	949	56
PDV3sqR1	CTTTAAGAGGAACAGACTCGGC		56
PDV3sqF2	GATACTCCAGACATTTGCCAAATCACG	905	60
PDV3sqR2	GAATCAGGGATTTCGACTCTCTTAGGC		60
PDV3-5prGSP1	CAATTCAGGAGATAAATCTACGACCG	-	57
PDV3-5prGSP2	CTTCACACTTTGCAAGAAACCTTGC	-	59
PDV3-3prGSP1	CTTGCTCCTACTGACATGACCG	-	58
PDV3-3prGSP2	GAAATATTCGTAGTTGGAGATGCTGC	-	58
Virus detection primers			
CVAdetF	CAAGAGCAGACAAATCAGATTTTGAGC	483	59
CVAdetR	GATTCCACAGCCCGCTGTAAGATATCG		63
PDVdetF	GATACTCCAGACATTTGCCAAATCACG	490	60
PDVdetR	TTTTCACGGGTACATTTGGTCCG		59
LChV1detF	GGAAAGTTAAGTCCAAGTTATGGTAGAGC	787	59
LChV1detR	GGCGTTTCTACGTCCTTTGTTGTAC		60
PDVclnF	GATACTCCAGACATTTGCCAAATCACG	1127	60

Primer name[a]	Sequence (5' - 3')[b]	Amplicon size (bp)[c]	Melting temperature (°C)
PDVclnR	CTTAACTTTTAACGCACGCAGTGC		59
MP amplification and mutagenesis primers			
PDV-MPFWD	GGGGACAAGTTTGTACAAAAAAGCAGGCTTC**ATGGCGTTCTCTGGTGTATCCAGG**	940	62
PDV-MPREV	GGGGACCACTTTGTACAAGAAAGCTGGGTC**ACCAATCGTTACACCAAAAGCTTCC**		60
MPΔ1-14F	GGGGACAAGTTTGTACAAAAAAGCAGGCTTC**ATGGAAGCCAGTGCTAGTTCAGC**	898	61
MPΔ1-44f	GGGGACAAGTTTGTACAAAAAAGCAGGCTTC**ATGATGAAGAACCTTCCAACTAAG**	808	54
MPΔ1-69F	GGGGACAAGTTTGTACAAAAAAGCAGGCTTC**ATGCAATCCAAAGAATCTCGAAGTGC**	733	56
MPΔ279-293r	GGGGACCACTTTGTACAAGAAAGCTGGGTC**AAGAGGAACAGACTCGGCTTCCTTG**	895	62
MPΔ269-293r	GGGGACCACTTTGTACAAGAAAGCTGGGTC**ATCAAGGGAAGATTCGCCC**	865	56
MPΔ252-293r	GGGGACCACTTTGTACAAGAAAGCTGGGTC**TGTTAAAGCCTTTATTGACTCATCAG**	814	55
MPΔ146-293	GGGGACCACTTTGTACAAGAAAGCTGGGTC**TGGCCATCTTGTTACAAAAATAACCGC**	496	60
N48aF	GAAGGCCCTTCCAACTAAGAAATGTTTTTCTTTACAG	-	63
N48aR	GAAGGGCCTTCATCATAGTTTGGGAATAGAAATCATCC	-	65
C54aF	GAAAGCTTTTTCTTTACAGTTGAAGAATGGTGTTCC	-	62
C54aR	GAAAAAGCTTTCTTAGTTGGAAGGTTCTTCATCATAG	-	61
G62aF	GAATGCTGTTCCAATTCAACCCATGAAGTTAC	-	62
G62aR	GAACAGCATTCTTCAACTGTAAAGAAAAACATTTCTTAG	-	61
L59aN61aF	CAGGCGAAGGCTGGTGTTCCAATTCAACCCATG	-	69
L59aN61aR	GAATTGGAACACCAGCCTTCGCCTG	-	64
F140aR143aF	TTGCTGTAACAGCATGGCCAAGAGC	-	64
F140aR143aR	CATGCTGTTACAGCAATAACCGC	-	58
P103aF	CATTGCGACCATTCTGGAAACAACTAGTGGGG	-	66
P103aR	AATGGTCGCAATGTACAACAAGTAGATTATACTATGATGCACG	-	65
V173aG174aF	ATAGCTGCAACTGTTTACCCCTTTTGGG	-	63
V173aG174aR	GTTGCAGCTATCGACGCATGTTTAGC	-	62
R146aF	CCAGCAGCAGTTCATGCCGACGACGG	-	69
R146aR	ACTGCTGCTGGCCATCTTGTTACAAAAATAACCG	-	66
D129aD131aF	ATAGCTACAGCTTCACCGTTGAATGAAGC	-	63
D129aD131aR	GAAGCTGTAGCTATATTAATAGAC	-	50
L70aS72aF	GAAGGCACAAGCCAAAGAATCTCG	-	60
L70aS72aR	TTGGCTTGTGCCTTCATGGGTTG	-	62
Cherry protein coding sequence primers			
TSPAN8F	GGGGACAAGTTTGTACAAAAAAGCAGGCTTC**ATGAAGATCAGCAATAACCTCGTCG**	862	59

Primer name[a]	Sequence (5' - 3')[b]	Amplicon size (bp)[c]	Melting temperature (°C)
TSPAN8R	GGGGACCACTTTGTACAAGAAAGCTGGGTC**ATGCTTCCAATATTCATTGTCCCTCC**		59
TCTP1F	GGGGACAAGTTTGTACAAAAAAGCAGGCTTC**ATGTTGGTTTACCAAGACCTCCTC**	565	58
TCTP1R	GGGGACCACTTTGTACAAGAAAGCTGGGTC**GCACTTGACCTCCTTCAAACCATGAGC**		64
PDV CP coding sequence primers			
PDV-CPF	GGGGACAAGTTTGTACAAAAAAGCAGGCTTC**ATGTCTGGGAAAGCCACTAAATCTGG**	715	61
PDV-CPR	GGGGACCACTTTGTACAAGAAAGCTGGGTC**TCCACTGACTATTTTATCCATTGC**		55
YFP coding sequence primers			
YFP-F	GGGGACAAGTTTGTACAAAAAAGCAGGCTTC**ATGGTGAGCAAGGGCGAGGAGC**	778	65
YFP-R	GGGGACCACTTTGTACAAGAAAGCTGGGTC**CTTGTACAGCTCGTCCATGCCG**		61
Infectious clone primers			
pCB301F	CTTTCGCCAGCTGGCGTAAagcttatcgataccgtcgacctcg	3544	58
pCB301R	CTGCAGGCATGCAAGAAGCTTcactagttctagagcggccgc		62
pCassF	caccgcggtggcggccgctctagaaCTTGCATGCCTGCAGGTCAACATGG	850	66
pCassR	cgaattcctgcagccgatcTACGCCAGCTGGCGAAAGGG		64
PDV1-PromF	*AAGGAAGTTCATTTCATTTGGAGAGG*<u>GGTTTTACGAACGTGGTTGTTCG</u>	3428	58
PDV1-RZR	*CAGGGTATCGGATCCTCTAGAGGTACC*<u>GCATACCTTAAAGGGGCATCCTCAC</u>		61
PDV2-PromF	*AAGGAAGTTCATTTCATTTGGAGAGG*<u>GGTTTTACGAGCGTGGTTGTTCG</u>	2649	60
PDV2-RZR	*CAGGGTATCGGATCCTCTAGAGGTACC*<u>GCATCCCTTAAAGGGGCATCC</u>		59
PDV3-PromF	*GAAGTTCATTTCATTTGGAGAGG*<u>GTTTTTATAATCAAGAGAACTGAATAAATTG</u>	2346	54
PDV3-RZR	*CAGGGTATCGGATCCTCTAGAGGTACC*<u>GCATCCCTTAAAGGGGCATCC</u>		59
R2NarF	TATATAGGCGCCCTCGCATGCCTGCAGGTCAACATGGTGGAGC	3416	62
R2NarR	ATATATGGCGCCCGATCTAGTAACATAGATGACACCGCGC		60

[a] F: forward primer, R: reverse primer, sq: sequencing primer, CVA: Cherry Virus A, LChV1: Little Cherry Virus 1, PDV: Prune Dwarf Virus, det: detection, cln: infectious clone, MP: movement protein, CP: coat protein, YFP: yellow fluoresecent protein, CFP: cyan fluorescent protein, YFP: yellow fluoresecent protein, CFP: cyan fluorescent protein, TCTP1: translationally controlled tumour protein, TET8: tetraspanin 8, 5pr: 5' RACE, 3pr: 3' RACE, GSP: gene specific primer for RACE-PCR, Δ: deletion primer, a: alanine replacement of natural residue, Prom: homology with 35s promoter, RZ: homology with ribozyme

[b] Bolded: coding sequence, Underlined: nucleotide substitution for alanine scanning, Italics: sequence homology to vector PCB301-d35sRZT

[c] Amplicon sizes of RACE primers are unknown as viral 5' and 3' ends are variable

Appendix 3 Proteins with significantly altered accumulation levels associated with PDV infection in cherry

Accession[a]	Protein	Log$_2$ ratio (PDV+/PDV-)	P-value
Pav_sc0001405.1_g1990.1.mk	Chitinase A (CHITA)	5.10	2.48E-05
Pav_sc0000638.1_g680.1.mk	Asparagine synthetase (ASNS)	4.60	7.95E-06
Z84692_9BROM	Viral CP	-	6.35E-06
Pav_sc0000174.1_g1420.1.mk	MLP-like protein 423 (MLP)	4.12	8.53E-03
Pav_sc0000311.1_g1290.1.mk	Blue-copper-binding protein (BCB)	4.11	1.57E-02
Pav_sc0001488.1_g010.1.br	Thaumatin superfamily protein (TLP)	4.10	1.42E-02
Pav_sc0000568.1_g820.1.br	Basic pathogenesis-related protein 1 (PR1)	3.80	1.28E-05
Pav_sc0000044.1_g310.1.mk	Histidine kinase 1 (HK1)	3.73	2.91E-06
Pav_sc0000648.1_g160.1.mk	Lactoylglutathione lyase / glyoxalase I family protein (GLX1)	3.30	8.53E-03
Pav_sc0000354.1_g620.1.mk	DC1 domain-containing protein (Nucleoredoxin 1)	3.29	2.66E-04
Pav_sc0000058.1_g230.1.mk	Pathogenesis-related thaumatin superfamily protein	3.27	3.18E-04
Pav_sc0000174.1_g1620.1.br	MLP-like protein 423 (MLP)	3.23	2.12E-04
Pav_sc0001341.1_g210.1.mk	Ferritin 4	3.12	3.03E-02
Pav_sc0000174.1_g1680.1.br	MLP-like protein 423 (MLP)	3.12	7.08E-03
Pav_sc0001882.1_g020.1.mk	Carbonic anhydrase 2	3.10	8.61E-04
Pav_sc0000418.1_g140.1.mk	Cysteine-rich RLK (RECEPTOR-like protein kinase) 14	3.10	4.26E-04
Pav_sc0000086.1_g050.1.mk	20S proteasome alpha subunit E2	3.09	3.62E-04
Pav_sc0006450.1_g010.1.br	Osmotin 34 (OSM34)	3.03	9.60E-05
Pav_sc0001339.1_g170.1.mk	Glutathione S-transferase family protein (GST)	2.87	1.10E-02
Pav_sc0000418.1_g330.1.mk	Receptor-like protein kinase-related family protein	2.78	4.26E-04
Pav_sc0000675.1_g700.1.br	NAD(P)-binding Rossmann-fold superfamily protein	2.62	7.83E-04
Pav_co4017443.1_g010.1.mk	Peroxidase superfamily protein (PRX)	2.58	3.62E-04
Pav_sc0000072.1_g040.1.mk	Proteasome subunit beta type-1	2.40	3.63E-02
Pav_sc0000396.1_g1220.1.mk	Calcium-binding EF hand family protein	2.32	1.29E-02
Pav_sc0002009.1_g150.1.mk	Polyphenol oxydase	2.30	2.38E-03
Pav_sc0000800.1_g1550.1.mk	Proteasome subunit beta type-6	2.29	2.68E-02
Pav_sc0000058.1_g160.1.mk	Beta-1,3-glucanase 3 (βGluc)	2.25	8.61E-04
Pav_sc0000890.1_g530.1.mk	Hepatoma-derived growth factor-related protein 2	2.22	6.14E-04
Pav_sc0000377.1_g320.1.mk	lysM domain-containing GPI-anchored protein 2 isoform X1	2.16	7.18E-03
Pav_sc0000107.1_g390.1.mk	Glucose-methanol-choline (GMC) oxidoreductase family protein	2.08	2.80E-02

Accession[a]	Protein	Log$_2$ ratio (PDV+/PDV-)	P-value
Pav_sc0000259.1_g240.1.mk	SPFH/Band 7/PHB domain-containing membrane-associated	2.07	2.39E-02
Pav_sc0000652.1_g540.1.mk	Methionine gamma lyase	2.05	1.64E-03
Pav_sc0001545.1_g150.1.mk	C-terminal cysteine residue is changed to a serine 1	2.05	3.50E-03
Pav_sc0001323.1_g700.1.mk	Bifunctional inhibitor/lipid-transfer protein/seed storage 2S albumin superfamily protein (DIR1)	2.04	1.20E-02
Pav_sc0002179.1_g140.1.mk	40S ribosomal protein S8	2.00	4.54E-02
Pav_sc0000597.1_g490.1.mk	20S proteasome beta subunit G1 (PAG1)	1.99	2.29E-02
Pav_sc0000113.1_g820.1.mk	Lysine-ketoglutarate reductase/saccharopine dehydrogenase Bifunctional enzyme	1.83	2.80E-02
Pav_sc0001685.1_g040.1.mk	Dolichyl-diphosphooligosaccharide-protein glycosyltransferase	1.82	1.67E-02
Pav_sc0000624.1_g2200.1.mk	Homolog of carrot EP3-3 chitinase	1.79	2.09E-02
Pav_sc0000195.1_g530.1.br	PDI-like 1-2	1.76	8.79E-04
Pav_co4042821.1_g010.1.br	Pectin methylesterase 3 (PME3)	1.76	1.46E-02
Pav_sc0002009.1_g100.1.mk	Polyphenol oxydase	1.65	6.41E-03
Pav_sc0000567.1_g1160.1.mk	Alpha-xylosidase 1	1.65	2.21E-02
Pav_sc0000174.1_g1690.1.mk	MLP-like protein 423 (MLP)	1.60	1.73E-02
Pav_sc0003894.1_g030.1.mk	General regulatory factor 8	1.58	3.77E-02
Pav_sc0000583.1_g1180.1.mk	Succinate co-enzyme A ligase (SUCLA)	1.54	1.29E-02
Pav_sc0000164.1_g080.1.mk	Heat shock protein 60-3A	1.54	2.41E-02
Pav_sc0000568.1_g580.1.mk	Pyridoxal phosphate (PLP)-dependent transferases superfamily	1.46	6.41E-03
Pav_sc0001461.1_g700.1.mk	Catalase 2 (CAT2)	1.39	3.63E-02
Pav_sc0000045.1_g070.1.mk	Glutathione reductase, cytosolic	1.37	2.09E-02
Pav_sc0000478.1_g500.1.mk	stAR-related lipid transfer protein 7	1.36	2.30E-02
Pav_sc0000119.1_g360.1.mk	60S ribosomal protein L5-2-like	1.35	3.98E-02
Pav_sc0001077.1_g250.1.mk	Dihydrolipoamide succinyltransferase (DLST)	1.31	1.50E-02
Pav_sc0000200.1_g050.1.mk	Nucleoside diphosphate kinase family protein	1.31	2.68E-02
Pav_sc0000164.1_g050.1.mk	26S proteasome regulatory subunit 4 homolog B	1.30	2.56E-02
Pav_sc0001518.1_g200.1.mk	26S protease regulatory subunit S10B homolog B	1.14	4.35E-03
Pav_sc0002009.1_g130.1.mk	Polyphenol oxidase I, chloroplastic-like	1.13	4.54E-02
Pav_sc0000492.1_g630.1.mk	Calmodulin-7-like	1.07	4.22E-02
Pav_sc0000557.1_g950.1.mk	Leucine aminopeptidase 1	1.04	1.94E-02
Pav_sc0000514.1_g280.1.mk	Arginosuccinate synthase family	0.99	1.46E-02

Accession[a]	Protein	Log$_2$ ratio (PDV+/PDV-)	P-value
Pav_sc0000410.1_g390.1.mk	Alanine--tRNA ligase	0.97	8.66E-03
Pav_sc0000119.1_g390.1.mk	Malate dehydrogenase	0.89	2.80E-02
Pav_sc0000212.1_g790.1.mk	NADP-dependent malic enzyme (NADP-ME)	0.85	1.18E-02
Pav_sc0000845.1_g120.1.mk	Peptidyl-prolyl cis-trans isomerase 1 (PPI)	0.77	3.90E-02
Pav_sc0000480.1_g670.1.mk	Cell division control protein 48 homolog D	0.74	1.17E-02
Pav_sc0000037.1_g480.1.mk	Cysteine proteinase COT44-like	0.73	4.44E-02
Pav_sc0001051.1_g070.1.mk	Ribulose bisphosphate carboxylase small chain (RuBisCO_SC)	0.72	1.67E-02
Pav_sc0000290.1_g090.1.mk	Acyl carrier protein 1	0.69	2.29E-02
Pav_sc0000257.1_g150.1.mk	14-3-3-like	0.63	4.54E-02
Pav_sc0001181.1_g610.1.mk	ATP synthase subunit beta (ATPsynβ)	0.57	4.40E-02
Pav_co4011113.1_g010.1.mk	14-3-3 protein 6	0.57	1.17E-02
Pav_sc0002154.1_g060.1.mk	Endoplasmin homolog (HSP90β1)	0.49	1.91E-02
Pav_sc0000052.1_g680.1.mk	Fasciclin-like arabinogalactan protein 1	0.48	3.63E-02
Pav_sc0003032.1_g030.1.mk	ATP synthase 24 kDa subunit, mitochondria	0.45	3.61E-02
Pav_sc0000093.1_g540.1.mk	Glycine rich RNA binding protein	0.28	3.52E-02
Pav_ sc0003747.1_g040.1.mk	Plant protein of unknown function (DUF247)	-5.44	6.41E-03
Pav_ sc0001938.1_g620.1.mk	DEAD box RNA helicase (RH3)	-4.11	6.70E-06
Pav_ sc0000009.1_g390.1.mk	Carbonic anhydrase 1 (CA1)	-3.90	8.45E-03
Pav_ sc0001080.1_g400.1.mk	Vacuolar ATP synthase subunit C (vATPsynC)	-3.79	2.95E-02
Pav_ sc0000037.1_g050.1.mk	magnesium-chelatase subunit ChlI (CHLL)	-3.34	6.35E-06
Pav_ sc0002842.1_g230.1.mk	Alcohol dehydrogenase 1 (ADH1)	-3.29	2.37E-04
Pav_ sc0001289.1_g560.1.mk	Chlorophyll A/B binding protein 1 (LHCB)	-2.97	2.73E-02
Pav_ sc0000174.1_g1650.1.mk	Rieske (2Fe-2S) domain-containing protein	-2.94	2.12E-04
Pav_ sc0000544.1_g100.1.mk	Hemoglobin 1 (HB1)	-2.92	2.51E-05
Pav_ sc0000907.1_g230.1.mk	Haloacid dehalogenase-like hydrolase family protein	-2.78	7.18E-03
Pav_ sc0000568.1_g370.1.mk	Peroxisomal NAD-malate dehydrogenase 1	-2.57	6.31E-03
Pav_ sc0000594.1_g050.1.mk	ATP synthase delta-subunit (ATPsynδ)	-2.48	7.83E-04
Pav_ sc0000044.1_g440.1.mk	Ferredoxin-NADP(+)-oxidoreductase 1	-2.39	2.36E-02
Pav_ sc0000175.1_g100.1.mk	NAD(P)-linked oxidoreductase superfamily protein	-2.33	5.52E-04
Pav_ sc0000370.1_g400.1.mk	Translation elongation factor EFG/EF2 protein	-2.28	2.61E-02
Pav_ sc0000001.1_g020.1.br	Zinc finger MYM-type protein 1-like	-2.28	2.94E-02

Accession[a]	Protein	Log$_2$ ratio (PDV+/PDV-)	P-value
Pav_ sc0000212.1_g390.1.mk	Translation elongation factor 1B (eEF1B)	-2.22	4.86E-02
Pav_ sc0000549.1_g430.1.mk	Chlorophyll A-B binding family protein	-2.19	2.63E-03
Pav_ sc0000910.1_g120.1.mk	Aminomethyltransferase, mitochondrial (AMT)	-2.03	3.92E-02
Pav_ sc0001925.1_g220.1.mk	Aldolase-type TIM barrel family protein	-1.98	2.94E-02
Pav_ sc0000091.1_g450.1.mk	Chlorophyll a-b binding protein, chloroplastic	-1.75	3.77E-02
Pav_ sc0000877.1_g840.1.mk	Pyridine nucleotide-disulphide oxidoreductase (PYROXD)	-1.73	1.46E-02
Pav_ sc0000979.1_g030.1.mk	Sedoheptulose-bisphosphatase	-1.68	2.29E-02
Pav_ sc0000583.1_g750.1.mk	rho-N domain-containing protein 1 (RHON1)	-1.64	7.83E-04
Pav_ sc0000108.1_g030.1.mk	Photosystem II reaction center protein C (PsBC)	-1.59	1.42E-02
Pav_ co4053689.1_g010.1.br	Uracil phosphoribosyltransferase (UPRT)	-1.56	1.17E-02
Pav_ sc0000545.1_g150.1.mk	28 kDa ribonucleoprotein	-1.54	4.88E-03
Pav_ sc0000396.1_g650.1.mk	Rubisco accumulation factor 1 (Raf1)	-1.52	2.57E-02
Pav_ sc0000095.1_g910.1.mk	Aldolase-type TIM barrel family protein	-1.51	1.57E-02
Pav_ sc0000638.1_g010.1.mk	Ribosomal protein L4	-1.50	1.51E-02
Pav_ sc0000554.1_g470.1.mk	Ribulose bisphosphate carboxylase/oxygenase activase, chloroplastic isoform X2	-1.49	4.40E-02
Pav_ sc0000257.1_g200.1.mk	O-fucosyltransferase family protein	-1.32	6.41E-03
Pav_ sc0000563.1_g110.1.mk	Rubisco activase	-1.31	5.47E-05
Pav_ sc0000629.1_g100.1.mk	NAD(P)-binding Rossmann-fold superfamily protein	-1.23	4.40E-02
Pav_ sc0001827.1_g130.1.mk	MLP-like protein 423 (MLP)	-1.18	2.38E-03
Pav_ sc0002360.1_g860.1.mk	Photosynthetic electron transfer C	-1.15	6.41E-03
Pav_ sc0001323.1_g670.1.mk	Light harvesting complex photosystem II subunit 6	-1.14	3.13E-04
Pav_ sc0000877.1_g910.1.mk	Photosystem I light harvesting complex 6 (LHC6)	-1.12	4.69E-02
Pav_ sc0001015.1_g200.1.mk	ATP synthase subunit β (ATPsynβ)	-1.11	3.52E-02
Pav_ sc0001444.1_g150.1.mk	Protein TIC 40, chloroplastic isoform X1	-1.06	4.40E-02
Pav_ sc0000175.1_g270.1.mk	Fructose-bisphosphate aldolase 2	-1.02	5.36E-04
Pav_sc0000700.1_g1850.1.mk	Ribose 5-phosphate isomerase, type A protein	-1.01	1.20E-02
Pav_ sc0000349.1_g020.1.mk	RAB GTPase homolog 1C	-0.97	2.81E-02
Pav_ sc0000800.1_g320.1.mk	Profilin	-0.97	3.63E-02
Pav_ sc0000028.1_g550.1.mk	30S ribosomal protein S1	-0.97	2.60E-03
Pav_ sc0001911.1_g170.1.mk	Phosphoribulokinase	-0.97	4.26E-04
Pav_ sc0000588.1_g060.1.mk	Heat shock protein 90-5	-0.95	2.59E-02
Pav_ sc0001488.1_g320.1.mk	Ribulose bisphosphate carboxylase small chain (RuBisCO_SC)	-0.94	1.30E-03

Accession[a]	Protein	Log$_2$ ratio (PDV+/PDV-)	P-value
Pav_sc0000624.1_g1800.1.mk	Heat shock 70 kDa protein 6 chloroplastic	-0.94	1.74E-02
Pav_ sc0000893.1_g910.1.mk	Clathrin assembly protein	-0.90	2.61E-02
Pav_ sc0000700.1_g670.1.mk	Thylakoid lumen 18.3 kDa protein	-0.90	8.53E-03
Pav_ sc0000775.1_g020.1.mk	GDP-mannose 3,5-epimerase 2-like	-0.77	4.86E-02
Pav_ sc0003681.1_g050.1.mk	ATP-dependent zinc metalloprotease FTSH 2	-0.66	1.29E-02
Pav_ sc0000659.1_g310.1.mk	RuBisCO large subunit-binding protein subunit beta (RuBisCOIβ)	-0.65	8.53E-03
Pav_ sc0000042.1_g030.1.mk	Glutamate-1-semialdehyde 2,1-aminomutase	-0.63	2.80E-02
Pav_ sc0000719.1_g990.1.mk	Fructose-bisphosphate aldolase	-0.63	2.80E-02
Pav_ sc0000711.1_g030.1.mk	Synaptotagmin-3	-0.60	4.44E-02
Pav_ sc0000017.1_g150.1.mk	DNA repair protein RAD51 homolog 3 isoform X1	-0.54	4.40E-02
Pav_ sc0000042.1_g430.1.mk	Chaperone protein ClpC	-0.52	3.52E-02
Pav_ sc0000480.1_g550.1.mk	RuBisCO large subunit-binding protein subunit alpha (RuBisCOIα)	-0.48	2.29E-02

[a] Protein accessions for cucumber encoded proteins were obtained from the Genome Database for Rosaceae, the accession for the viral CP of PDV was obtained from the Uniprot Consortium

Appendix 4 Proteins with significantly altered accumulation levels caused by PDV infection in cucumber

Accession[a]	Protein	Log$_2$ ratio (PDV+/PDV-)	P- Value
A0A0A0L0I0	Peroxidase superfamily protein (PRX)	8.60	1.24E-05
A0A0A0LPJ3	Aspartic proteinase nepenthesin-1 (NEP1)	4.17	1.18E-03
A0A0A0KSQ4	Nucleoredoxin 1 (NRX1)	3.94	2.47E-02
A0A0A0K3Z5	Peroxidase (PRX)	3.06	2.61E-02
A0A0A0L1T4	Peroxidase (PRX)	3.02	4.69E-02
A0A0A0LTR4	Beta-glucosidase 44 (BGLU44)	3.01	3.30E-02
A0A0A0KTH7	WD40 TOPLESS (WD40)	2.85	1.87E-02
A0A0A0LXB9	L-ascorbate oxidase (AO)	2.59	1.84E-02
A0A0A0LFD4	Inhibitor of trypsin and hageman factor (ITHF)	2.52	4.19E-02
A0A0A0KT33	AMP dependent ligase (ADL)	2.48	3.01E-02
A0A0A0L0R0	Catalase 2 (CAT2)	2.23	1.87E-02
A0A0A0LSK4	Eukaryotic translation initiation factor 2c (eIF2C)	2.20	3.33E-02
A0A0A0L835	Glutathione S-transferase (GST)	2.14	3.33E-02
A0A0A0LGD4	Beta-glucosidase 44 (BGLU44)	2.01	2.54E-02
A0A0A0KFX4	Peroxidase (PRX)	2.01	2.61E-02
A0A0A0KDG3	Catalase 2 (CAT2)	1.74	2.74E-02
A0A0A0K2R2	Soluble inorganic pyrophosphatase 6, chloroplastic (PPA6)	1.57	4.67E-02
A0A0A0KDH7	Phosphoprotein ECPP44 (ECPP44)	1.54	3.06E-02
A0A0A0KA68	5'-AMP-activated protein kinase beta-2 subunit (AMPKB)	1.31	4.90E-02
A0A0A0KTZ2	Acetyl-CoA decarbonylase/synthase complex subunit alpha 1 (CdhA1)	1.30	3.33E-02
A0A0A0KDC9	PDI-like 1-2 (PDI)	1.27	3.33E-02
A0A0A0LMA9	Periplasmic beta-glucosidase	1.24	1.01E-02
A0A0A0LXM9	Phosphatidylglycerol/phosphatidylinositol transfer protein DDB (PITP)	1.21	3.69E-02
A0A0A0LZZ9	Cyanogenic beta-glucosidase-like (CBG)	1.21	2.47E-02
Q52UN0	Peptidyl-prolyl cis-trans isomerase (PPI)	1.15	3.14E-02
A0A0A0KC13	Citrate synthase (CS)	1.12	3.59E-02
A0A0A0L5W7	Universal stress protein (USP)	1.09	1.49E-02
A0A0A0LZK4	Aleurain-like protease (ALP)	1.04	2.74E-02
A0A0A0KNX7	Glutathione peroxidase	1.00	1.75E-02
A0A0A0LPH6	DUF642	0.99	4.67E-02
A0A0A0KX90	LRRNT_2 domain-containing protein	0.95	1.84E-02
A0A0A0LTZ1	Tetraspanin 8 (TSPAN8)	0.95	4.51E-02
A0A0A0KIB2	Photosystem II 5 kDa protein	0.91	3.33E-02
A0A0A0L325	Minor allergen Alt a	0.89	3.33E-02
A0A0A0K8E7	30S ribosomal protein 2, chloroplastic	0.89	3.33E-02
A0A0A0KKD9	Luminal-binding protein 5	0.88	1.84E-02
A0A0A0LUA8	Aldehyde dehydrogenase family 2 member B4	0.85	4.76E-02
A0A0A0K6Y0	Post-illumination chlorophyll fluorescence increase	0.84	4.54E-02
A0A0A0LX21	Formate--tetrahydrofolate ligase	0.83	1.87E-02
A0A0A0LF44	Bifunctional inhibitor/lipid-transfer protein/seed storage 2S (DIR1)	0.78	2.31E-02
A0A0A0LUC2	Oxygen-evolving enhancer protein 3-2	0.74	3.33E-02
A0A0A0K8V8	NAD-dependent malic enzyme (NAD-ME)	0.71	2.61E-02
A0A0A0LBI9	Peptidase A1 domain-containing protein	0.71	2.84E-02

Accession[a]	Protein	Log$_2$ ratio (PDV+/PDV-)	P- Value
A0A0A0L917	Translationally-controlled tumor protein homolog (TCTP1)	0.69	4.30E-02
A0A0A0KLU6	2-oxoglutarate dehydrogenase (OGDH)	0.63	4.67E-02
A0A0A0L0Z8	ASPARTIC PROTEASE IN GUARD CELL 2	0.60	2.31E-02
H6WP27	Glutamine synthetase	0.52	4.30E-02
A0A0A0KDF1	Alpha-soluble NSF attachment protein 2	0.48	3.01E-02
A0A0A0KI31	Glyoxysomal fatty acid beta-oxidation multifunctional protein	0.40	3.14E-02
A0A0A0K6Q2	Unknown	0.36	3.01E-02
A0A0A0KGG7	Ribonuclease III domain-containing protein (RNC1)	-1.75	2.61E-02
A0A0A0KTN2	Mitochondrial substrate carrier family protein C (MCF)	-1.65	4.54E-02
A0A0A0KAV8	Aminoacylase-1 (ACY1)	-1.24	4.51E-02
A0A0A0L5T1	3-hydroxy-3-methylglutaryl coenzyme A synthase (HMGCS1)	-1.23	1.87E-02
A0A0A0K5K0	Ribosomal_S7 domain-containing protein (RPS7)	-1.22	3.69E-02
B0F832	Eukaryotic initiation factor iso4E (eIF(iso)4e)	-1.18	3.35E-02
A0A0A0KHX0	tRNase Z (TRZ2)	-1.18	2.25E-02
A0A0A0KYB6	Villin-2 (VLN2)	-1.13	2.09E-02
A0A0A0LC88	Heavy metal associated domain-containing protein (HMA)	-0.98	2.84E-02
A0A0A0M3D4	Inactive ATP-dependent zinc metalloprotease FTSHI 5 (FTSHI5)	-0.97	1.87E-02
A0A0A0KFB8	Ribosomal protein L4 (RPL4)	-0.95	1.87E-02
A0A0A0K8K1	sufE-like protein 1 (SUFE1)	-0.90	2.61E-02
A0A0A0KIM9	60S ribosomal protein L17-2	-0.88	4.19E-02
A0A0A0KWX9	CobW C-terminal domain-containing protein	-0.83	1.49E-02
A0A0A0KKR8	SAL1 phosphatase-like	-0.83	2.61E-02
A0A0A0LJE6	Cyclin	-0.81	3.86E-02
A0A0A0KK51	Reticulon-like protein B2 (RTLNB2)	-0.80	4.89E-02
A0A0A0K952	30S ribosomal protein S17, chloroplastic	-0.79	3.69E-02
A0A0A0LY43	Rubisco accumulation factor 1 (Raf1)	-0.75	1.49E-02
A0A0A0LRP8	Photosynthetic NDH subunit of subcomplex B 4 chloroplastic	-0.74	2.61E-02
A0A0A0L1I7	Magnesium-protoporphyrin IX monomethyl ester [oxidative] cyclase	-0.74	3.86E-02
A0A0A0KL82	40S ribosomal protein S20-2	-0.72	2.31E-02
A0A0A0KJ21	Actin 7	-0.71	4.54E-02
A0A0A0KAU8	RuBisCO large subunit-binding, subunit α (RuBisCOlα)	-0.71	3.14E-02
A0A0A0L5I1	AA_TRNA_LIGASE_II domain-containing protein	-0.68	4.36E-02
A0A0A0LTJ3	Elongation factor Tu (Ef-Tu)	-0.67	3.14E-02
A0A0A0K179	Threonine--tRNA ligase, cytoplasmic	-0.60	4.02E-02
A0A0A0KT42	Chloroplast protein import component Toc159	-0.59	2.61E-02
A0A0A0K7Z3	ATP synthase delta-subunit gene (ATPsynδ)	-0.58	4.51E-02
A0A0A0KXA3	Membrane-associated 30 kDa protein, chloroplastic	-0.55	4.19E-02
A0A0A0LRZ6	Elongation factor Tu (Ef-Tu)	-0.54	3.86E-02
A0A0A0LRI8	Elongation factor 1-delta isoform X1 (EEF1D)	-0.54	3.72E-02
A0A0A0K8H3	Fructose-1,6-bisphosphatase, cytosolic	-0.44	3.72E-02
A0A0A0LDC9	50S ribosomal protein L31	-0.42	4.76E-02
Q96399	Cytosolic ascorbate peroxidase	-0.39	3.33E-02
A0A0A0LTS4	Clustered mitochondria protein homolog	-0.34	4.51E-02
A0A0A0LM10	ATP synthase subunit β (ATPsynβ)	-0.28	1.49E-02

[a] Protein accessions were obtained from the Uniprot Consortium

<div align="center">

Curriculum Vitae

Aaron Joseph Simkovich

</div>

Education

2013-2020	Ph.D. Biology (Cell and Molecular Biology) The University of Western Ontario, London, Ontario, Canada
2008-2013	BSc. Specialization in Biology (Hons.) The University of Western Ontario, London, Ontario, Canada

Awards

2019	Poster presentation award Canadian Association for Plant Biotechnology
2018	Graduate Student Teaching Award of Excellence
2013-2018	Western graduate research scholarship

Work experience

2013-2018	Teaching Assistant, Department of Biology, University of Western Ontario
2013-2020	Research Assistant, Agriculture and Agri-Food Canada

Communications

Simkovich, A.J., Kohalmi, S.E., Wang, A (2021). Ilarviruses (Bromoviridae). Encyclopedia of Virology 4th Edition. Elsevier. (In Press).
DOI: 10.1016/B978-0-12-809633-8.21301-0

Simkovich, A.J., Kohalmi, S.E., Wang, A (2019). "Subcellular localization of prune dwarf virus coat and movement proteins.", Plant Canada 2019, Guelph, Ontario, Canada July 7-10, 2019

Simkovich, A.J., Kohalmi, S.E., Wang, A.M. (2016). "Small RNA Sequencing Leads to the First Report of Cherry Virus A in Ontario, Canada.", 35th Annual Meeting of the American Society for Virology, Blacksburg, Virginia June 18–22, 2016

Simkovich, A.J., Kohalmi, S.E., and Wang, A.M. (2015). "Small RNA sequencing leads to the first report of Cherry virus A in Ontario, Canada.", 34th Annual Meeting of American Society for Virology, London, Ontario, Canada, July 11-15, 2015.